

# Design and Construction of PCC Pavements, Volume III: Improved PCC Performance Models

PB2000-106434



PUBLICATION NUMBER: FHWA/RD-98-113

JANUARY 1999



REPRODUCED BY:  
U.S. Department of Commerce  
National Technical Information Service  
Springfield, Virginia 22161

**NTIS**



U.S. Department of Transportation  
**Federal Highway Administration**

Research and Development  
Turner-Fairbank Highway Research Center  
6300 Georgetown Pike  
McLean, VA 22101-2296

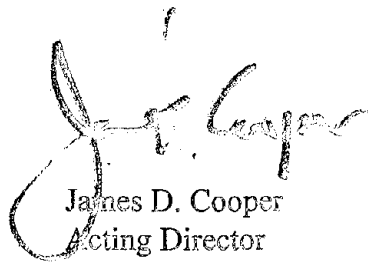


## FOREWORD

This report documents the process of model development and the final models developed for the prediction of key portland cement concrete (PCC) pavement distress types and roughness. The models were developed using Long-Term Pavement Performance (LTPP) data. Mechanistic-empirical models were developed for the following distress types: transverse joint faulting, transverse joint spalling, transverse cracking, and corner breaks. The roughness models developed were empirical.

The positive outcome of this study was the development of mechanistic-based performance models for use in pavement design and management. This is expected to provide expanded capabilities for considering the effect of load- and climate-related stresses on PCC pavement performance. The development of mechanistic-based models reflects current trends of upgrading the pavement design and evaluation process through the use of mechanistic-based design methods.

This report is important to everyone who designs, constructs, and manages pavements.



James D. Cooper  
Acting Director  
Office of Engineering  
Research and Development

## NOTICE

This document is disseminated under the sponsorship of the Department of Transportation in the interest of information exchange. The United States Government assumes no liability for its contents or use thereof. This report does not constitute a standard, specification, or regulation.

The United State Government does not endorse products or manufacturers. Trade and manufacturers' names appear in this report only because they are essential to the object of the document.

| 1. Report No.<br>FHWA-RD-98-113   |                | 2. Government Accession No.   |  | 3. Recipient's Catalog No.  |           |                 |                |                    |                |   |   |                |    |   |
|---|----------------|---|--|---|-----------|-----------------|----------------|--------------------|----------------|---|---|----------------|----|---|
| 4. Title and Subtitle<br><b>DESIGN AND CONSTRUCTION OF PCC PAVEMENTS</b><br><b>Volume III: Improved PCC Performance Models</b>  |                |   |  | 5. Report Date<br>January 1999  |           |                 |                |                    |                |   |   |                |    |   |
|   |                |   |  | 6. Performing Organization Code                                       |           |                 |                |                    |                |   |   |                |    |   |
|   |                |   |  | 8. Performing Organization Report No.                                 |           |                 |                |                    |                |   |   |                |    |   |
| 7. Author(s)<br>L. Titus-Glover, E. B. Owusu-Antwi, and M. I. Darter  |                |   |  | 10. Work Unit No. (TRAIS)<br>C6B                                      |           |                 |                |                    |                |   |   |                |    |   |
| 9. Performing Organization Name and Address<br>ERES Consultants, Inc.<br>505 W. University Avenue<br>Champaign, IL 61820-3915   |                |   |  | 11. Contract or Grant No.<br>DTFH61-94-C-00218                        |           |                 |                |                    |                |   |   |                |    |   |
|   |                |   |  | 13. Type of Report and Period Covered<br>Final Report<br>1994 to 1998 |           |                 |                |                    |                |   |   |                |    |   |
| 12. Sponsoring Agency Name and Address<br>Office of Engineering R&D<br>Federal Highway Administration<br>6300 Georgetown Pike<br>McLean, Virginia 22101-2296  |                |   |  | 14. Sponsoring Agency Code  |           |                 |                |                    |                |   |   |                |    |   |
| 15. Supplementary Notes<br><br>FHWA Contracting Officer's Technical Representative (COTR): Cheryl A. Richter, HNR-30  |                |   |  |   |           |                 |                |                    |                |   |   |                |    |   |
| 16. Abstract<br><br><p>This study was conducted to evaluate and analyze portland cement concrete (PCC) pavements in order to develop recommendations for the design and construction of long-lived concrete pavements. It involved a detailed evaluation and analysis of the PCC pavement data in the Long-Term Pavement Performance (LTPP) database using a variety of methods to determine the design features and practices that have beneficial effects on long-term performance. Emphasis was placed on identifying those specific design features that can be included during design to improve the performance of PCC pavements under various combinations of environmental and traffic loading conditions, and for different subgrade support conditions. The study focused on the development of practical recommendations that can be implemented by highway agencies to increase pavement life.</p> <p>This volume describes and provides information on improved pavement distress and roughness prediction models that were developed as part of the study. A key focus was to develop distress and roughness prediction models that incorporate mechanistic principles but are still practical for use by State highway agencies.</p> <p>This report is the third in a series of three volumes on the study. The other volumes are as follows:</p> <table border="1"> <thead> <tr> <th><u>FHWA No.</u></th> <th><u>Vol No.</u></th> <th><u>Short Title</u></th> </tr> </thead> <tbody> <tr> <td>FHWA-RD-98-052</td> <td>I</td> <td>Summary of Design Features and Construction Practices That Influence Performance of Pavements</td> </tr> <tr> <td>FHWA-RD-98-127</td> <td>II</td> <td>Design Features and Practices That Influence Performance of PCC Pavements</td> </tr> </tbody> </table> |                |   |  |   |           | <u>FHWA No.</u> | <u>Vol No.</u> | <u>Short Title</u> | FHWA-RD-98-052 | I | Summary of Design Features and Construction Practices That Influence Performance of Pavements | FHWA-RD-98-127 | II | Design Features and Practices That Influence Performance of PCC Pavements |
| <u>FHWA No.</u>   | <u>Vol No.</u> | <u>Short Title</u>  |  |   |           |                 |                |                    |                |   |   |                |    |   |
| FHWA-RD-98-052  | I              | Summary of Design Features and Construction Practices That Influence Performance of Pavements |  |   |           |                 |                |                    |                |   |   |                |    |   |
| FHWA-RD-98-127  | II             | Design Features and Practices That Influence Performance of PCC Pavements                     |  |   |           |                 |                |                    |                |   |   |                |    |   |
| 17. Key Words<br>Concrete pavement, design, construction, faulting, spalling, transverse cracking, corner breaks, roughness, mechanistic analysis, pavement evaluation.   |                |   | 18. Distribution Statement<br>No restrictions. This document is available to the public through the National Technical Information Service, Springfield, Virginia 22161. |   |           |                 |                |                    |                |   |   |                |    |   |
| 19. Security Classif. (of this report)<br>Unclassified  |                | 20. Security Classif. (of this page)<br>Unclassified  |  | 21. No of Pages<br>231  | 22. Price |                 |                |                    |                |   |   |                |    |   |

# SI\* (MODERN METRIC) CONVERSION FACTORS

## APPROXIMATE CONVERSIONS FROM SI UNITS

| Symbol   | When You Know              | Multiply By             | To Find                     | Symbol            | When You Know               | Multiply By | To Find                    | Symbol              |
|--|----------------------------|-------------------------|-----------------------------|-------------------|-----------------------------|-------------|----------------------------|---------------------|
| <b>LENGTH</b>  |                            |                         |                             |                   |                             |             |                            |                     |
| in   | inches                     | 25.4                    | millimeters                 | mm                | millimeters                 | 0.039       | inches                     | in                  |
| ft   | feet                       | 0.305                   | meters                      | m                 | meters                      | 3.28        | feet                       | ft                  |
| yd   | yards                      | 0.914                   | meters                      | m                 | meters                      | 1.09        | yards                      | yd                  |
| mi   | miles                      | 1.61                    | kilometers                  | km                | kilometers                  | 0.621       | miles                      | mi                  |
| <b>AREA</b>  |                            |                         |                             |                   |                             |             |                            |                     |
| in <sup>2</sup>  | square inches              | 645.2                   | square millimeters          | mm <sup>2</sup>   | square millimeters          | 0.0016      | square inches              | in <sup>2</sup>     |
| ft <sup>2</sup>  | square feet                | 0.093                   | square meters               | m <sup>2</sup>    | square meters               | 10.764      | square feet                | ft <sup>2</sup>     |
| yd <sup>2</sup>  | square yards               | 0.836                   | square meters               | m <sup>2</sup>    | square meters               | 1.195       | square yards               | yd <sup>2</sup>     |
| ac   | acres                      | 0.405                   | hectares                    | ha                | hectares                    | 2.47        | acres                      | ac                  |
| mi <sup>2</sup>  | square miles               | 2.59                    | square kilometers           | km <sup>2</sup>   | square kilometers           | 0.386       | square miles               | mi <sup>2</sup>     |
| <b>VOLUME</b>  |                            |                         |                             |                   |                             |             |                            |                     |
| fl oz  | fluid ounces               | 29.57                   | milliliters                 | mL                | milliliters                 | 0.034       | fluid ounces               | fl oz               |
| gal  | gallons                    | 3.785                   | liters                      | L                 | liters                      | 0.264       | gallons                    | gal                 |
| ft <sup>3</sup>  | cubic feet                 | 0.028                   | cubic meters                | m <sup>3</sup>    | cubic meters                | 35.71       | cubic feet                 | ft <sup>3</sup>     |
| yd <sup>3</sup>  | cubic yards                | 0.765                   | cubic meters                | m <sup>3</sup>    | cubic meters                | 1.307       | cubic yards                | yd <sup>3</sup>     |
| NOTE: Volumes greater than 1000 l shall be shown in m <sup>3</sup> . |                            |                         |                             |                   |                             |             |                            |                     |
| <b>MASS</b>  |                            |                         |                             |                   |                             |             |                            |                     |
| oz   | ounces                     | 28.35                   | grams                       | g                 | grams                       | 0.035       | ounces                     | oz                  |
| lb   | pounds                     | 0.454                   | kilograms                   | kg                | kilograms                   | 2.202       | pounds                     | lb                  |
| T  | short tons (2000 lb)       | 0.907                   | megagrams (or "metric ton") | Mg (or "t")       | megagrams (or "metric ton") | 1.103       | short tons (2000 lb)       | T                   |
| <b>TEMPERATURE (exact)</b>   |                            |                         |                             |                   |                             |             |                            |                     |
| °F   | Fahrenheit temperature     | 5(F-32)/9 or (F-32)/1.8 | Celcius temperature         | °C                | Celcius temperature         | 1.8C + 32   | Fahrenheit temperature     | °F                  |
| <b>ILLUMINATION</b>  |                            |                         |                             |                   |                             |             |                            |                     |
| fc   | foot-candles               | 10.76                   | lux                         | lx                | lux                         | 0.0929      | foot-candles               | fc                  |
| fl   | foot-Lamberts              | 3.426                   | candela/m <sup>2</sup>      | cd/m <sup>2</sup> | candela/m <sup>2</sup>      | 0.2919      | foot-Lamberts              | fl                  |
| <b>FORCE and PRESSURE or STRESS</b>                                  |                            |                         |                             |                   |                             |             |                            |                     |
| lbf  | poundforce                 | 4.45                    | newtons                     | N                 | newtons                     | 0.225       | poundforce                 | lbf                 |
| lbf/in <sup>2</sup>  | poundforce per square inch | 6.89                    | kilopascals                 | kPa               | kilopascals                 | 0.145       | poundforce per square inch | lbf/in <sup>2</sup> |

\* SI is the symbol for the International System of Units. Appropriate rounding should be made to comply with Section 4 of ASTM E380.

(Revised September 1993)



## TABLE OF CONTENTS

| Section  | Page |
|--|------|
| <b>1. INTRODUCTION</b> .....                                     | 1    |
| Background .....   | 1    |
| Project Objectives and Scope .....                               | 1    |
| Research Approach .....  | 2    |
| Sequence of Report .....   | 2    |
| <b>2. OVERVIEW OF LTPP DATA USED FOR MODEL DEVELOPMENT</b> ..... | 3    |
| Introduction .....   | 3    |
| Overview of the LTPP Data .....                                  | 3    |
| Summary .....  | 5    |
| <b>3. MODEL DEVELOPMENT METHODS</b> .....                        | 7    |
| Introduction .....   | 7    |
| Model Types .....  | 9    |
| Developing Practical Prediction Models .....                     | 9    |
| <b>4. FAULTING MODEL FOR JOINTED CONCRETE PAVEMENTS</b> .....    | 15   |
| Introduction .....   | 15   |
| Faulting Mechanism .....   | 15   |
| Evaluation of Existing Faulting Models .....                     | 16   |
| Faulting Model Development Approach .....                        | 20   |
| Determination of Differential Elastic Deformation Energy .....   | 23   |
| Data Preparation and Evaluation .....                            | 29   |
| Erodibility Scaling Factor .....                                 | 31   |
| Faulting Model Formulation .....                                 | 34   |
| Faulting Model Calibration .....                                 | 36   |
| Final Faulting Prediction Model .....                            | 37   |
| Sensitivity Analysis .....                                       | 39   |
| Summary .....  | 49   |
| Implications and Recommendations .....                           | 49   |


## TABLE OF CONTENTS (continued)

| Section   | Page |
|---|------|
| <b>5. TRANSVERSE JOINT SPALLING</b> .....   | 51   |
| <b>Introduction</b> .....   | 51   |
| <b>Spalling Mechanism</b> .....   | 51   |
| <b>Evaluation of Existing Spalling Models</b> .....                               | 53   |
| <b>Spalling Model Development Approach</b> .....                                  | 56   |
| <b>Mechanistic-Empirical Spalling Model Formulation</b> .....                     | 65   |
| <b>Determination of Empirical Scaling Variables</b> .....                         | 67   |
| <b>Calibration of Mechanistic-Empirical Joint Spalling Models</b> .....           | 75   |
| <b>Sensitivity Analysis for Mechanistic-Empirical Spalling Models</b> .....       | 84   |
| <b>Summary</b> .....  | 92   |
| <b>Implications and Recommendations</b> .....                                     | 93   |
| <b>6. TRANSVERSE CRACKING AND CORNER BREAKS OF JPCP</b> ...                       | 95   |
| <b>Introduction</b> .....   | 95   |
| <b>Transverse Cracking and Corner Break Mechanisms</b> .....                      | 95   |
| <b>Evaluation of Existing Transverse Cracking and Corner Break Models</b> .....   | 96   |
| <b>Fatigue Cracking Modeling Approach</b> .....                                   | 98   |
| <b>Application of Fracture Mechanics Principles</b> .....                         | 99   |
| <b>Development of Empirical Scaling Factors</b> .....                             | 105  |
| <b>Calibration Procedure for Transverse Cracking and Corner Break Models</b> .... | 105  |
| <b>Final Corner Breaks Model</b> .....  | 111  |
| <b>Final Transverse Cracking Model</b> .....                                      | 114  |
| <b>Sensitivity Analysis</b> .....   | 117  |
| <b>Summary</b> .....  | 126  |
| <b>Implications and Recommendations</b> .....                                     | 127  |
| <b>7. ROUGHNESS MODELS</b> .....  | 129  |
| <b>Introduction</b> .....   | 129  |
| <b>Roughness Measure</b> .....  | 129  |
| <b>Progression of Roughness</b> .....   | 130  |
| <b>Evaluation of Existing Roughness Models</b> .....                              | 132  |
| <b>Roughness Model Forms</b> .....  | 135  |
| <b>Preliminary Data Analysis</b> .....  | 136  |
| <b>Final IRI Prediction Models</b> .....  | 146  |
| <b>Sensitivity Analysis</b> .....   | 153  |
| <b>Summary</b> .....  | 165  |
| <b>Implications and Recommendations</b> .....                                     | 168  |

## TABLE OF CONTENTS (continued)

| <b>Section</b>   | <b>Page</b> |
|--|-------------|
| <b>8. APPLICATION OF DISTRESS PERFORMANCE MODELS</b> .....               | 169         |
| <b>Introduction</b> .....  | 169         |
| <b>Faulting of JPCP</b> .....  | 169         |
| <b>Transverse Joint Spalling for JPCP and JRCP</b> .....                 | 172         |
| <b>Transverse Cracking for JPCP</b> .....                                | 177         |
| <b>Corner Breaks for JPCP</b> .....                                      | 180         |
| <b>Roughness for JPCP, JRCP, and CRCP</b> .....                          | 181         |
| <b>Suitability of Prediction Models</b> .....                            | 184         |
| <b>Examples of Application of Performance Models</b> .....               | 184         |
| <b>Checking the Design of New Pavements with Prediction Models</b> ..... | 185         |
| <b>Comparing Cost-Effectiveness of Alternative Designs</b> .....         | 187         |
| <b>Summary</b> .....   | 190         |
| <b>9. CONCLUSIONS AND RECOMMENDATIONS</b> .....                          | 193         |
| <b>Conclusions</b> .....   | 193         |
| <b>Recommendations</b> .....   | 193         |
| <b>Recommendations for Future Research</b> .....                         | 194         |
| <b>APPENDIX A. CALIBRATION OF PREDICTION MODELS</b> .....                | 203         |
| <b>Data Preparation and Selection of Independent Variables</b> .....     | 203         |
| <b>Model Development and Verification</b> .....                          | 206         |
| <b>Model Evaluation and Verification</b> .....                           | 212         |
| <b>REFERENCES</b> .....  | 215         |

*PROTECTED UNDER INTERNATIONAL COPYRIGHT  
ALL RIGHTS RESERVED  
NATIONAL TECHNICAL INFORMATION SERVICE  
U.S. DEPARTMENT OF COMMERCE*

Reproduced from  
best available copy. 

## LIST OF FIGURES

| Figure   | Page |
|--|------|
| 1 Flow chart for developing distress models for rigid pavements .....  | 10   |
| 2 Finite element model .....   | 26   |
| 3 Plot of mean joint faulting versus significant variables for jointed PCC pavement .....  | 33   |
| 4 Plot of predicted versus measured faulting .....   | 39   |
| 5 Plot of residuals versus predicted faulting .....  | 40   |
| 6 Influence of dowel and dowel size on predicted faulting .....  | 42   |
| 7 Influence of base or subbase type on predicted faulting .....  | 43   |
| 8 Influence of PCC slab thickness on predicted faulting .....  | 44   |
| 9 Influence of modulus of subgrade reaction on predicted faulting .....  | 45   |
| 10 Influence of joint spacing on predicted faulting .....  | 46   |
| 11 Influence of drainage coefficient on predicted faulting .....   | 47   |
| 12 Influence of number of wet days (precipitation >12.7 mm) on predicted faulting .....  | 48   |
| 13 Schematic diagram of spalling mechanism for tensile mode of failure in jointed<br>concrete pavement .....                         | 58   |
| 14 Finite element model for estimating spall stress .....  | 60   |
| 15 Sensitivity plot of tensile stress versus height of sealant .....   | 62   |
| 16 Sensitivity plot of tensile stress versus modulus of subgrade reaction .....  | 63   |
| 17 Sensitivity plot of tensile stress versus sealant modulus .....   | 63   |
| 18 Sensitivity plot of tensile stress versus PCC slab thickness .....  | 64   |
| 19 Sensitivity plot of tensile stress versus PCC slab modulus .....  | 64   |
| 20 Plot of percentage of joint spalling versus significant variables for JPCP .....  | 71   |
| 21 Plot of percentage of joint spalling versus significant variables for JRCP .....  | 74   |
| 22 Predicted percentage of spalled joints versus the actual percentage of spalled<br>joints for JPCP .....                           | 79   |
| 23 Plot of residuals versus the predicted percentage of spalled joints for JPCP .....  | 79   |
| 24 Predicted percentage of spalled joints versus the actual percentage of spalled<br>joints for JRCP .....                           | 83   |
| 25 Plot of residuals versus the predicted percentage of spalled joints for JRCP .....  | 83   |
| 26 Sensitivity plot of percentage of JPCP joint spalling versus average daily<br>temperature range .....                             | 85   |
| 27 Sensitivity plot of percentage of JPCP spalling versus mean relative humidity during<br>month of construction .....               | 85   |
| 28 Sensitivity plot of percentage of JPCP spalling versus number of freeze-thaw cycles ..  | 87   |
| 29 Sensitivity plot of percentage of JPCP spalling versus elongation .....   | 87   |
| 30 Sensitivity plot of percentage of JPCP spalling versus ESAL's .....   | 88   |
| 31 Plot of percentage of joint spalling versus age .....   | 89   |
| 32 Effect of freezing index on percentage of JRCP joints spalled .....   | 89   |
| 33 Plot of percentage of JRCP joints spalled versus ESAL's .....   | 90   |
| 34 Influence of traffic tensile stresses on percentage of JRCP joints spalled .....  | 90   |
| 35 Influence of different ELONG (joint movement) values from temperature<br>gradients on the percentage of JRCP joints spalled ..... | 91   |

## LIST OF FIGURES (continued)

| Figure   | Page |
|--|------|
| 36 Influence of k-value on percentage of JRCP joints spalled .....   | 92   |
| 37 Pavement deformation with wheel load placed directly over the plane with the crack .  | 103  |
| 38 Pavement deformation with wheel load placed at the corner of the slab .....   | 103  |
| 39 Plot of percentage of slabs with corner breaks versus significant variables for JPCP ..   | 108  |
| 40 Plot of percentage of transverse cracking versus significant variables for JPCP .....   | 110  |
| 41 Measured versus predicted percentage of slabs with corner breaks .....  | 113  |
| 42 Plot of residuals versus predicted percentage of slabs with corner breaks .....   | 113  |
| 43 Measured versus predicted percentage of slabs with transverse cracking .....  | 116  |
| 44 Plot of residuals versus predicted percentage of slabs with transverse cracking .....   | 116  |
| 45 Plot of percentage of slabs with corner breaks versus pavement age .....  | 118  |
| 46 Plot of percentage of slabs with corner breaks versus cumulative ESAL's .....   | 118  |
| 47 Plot of percentage of slabs with corner breaks versus cumulative ESAL's<br>for different slab thicknesses .....                                   | 119  |
| 48 Plot of percentage of slabs with corner breaks versus cumulative ESAL's<br>for different levels of joint spacing .....                            | 120  |
| 49 Plot of percentage of slabs with corner breaks versus cumulative ESAL's<br>for different levels of freeze-thaw cycles .....                       | 120  |
| 50 Plot of percentage of slabs with transverse cracking versus pavement age .....  | 122  |
| 51 Plot of percentage of slabs with transverse cracking versus cumulative ESAL's .....   | 123  |
| 52 Plot of percentage of slabs with transverse cracking versus cumulative ESAL's<br>for different slab thicknesses .....                             | 124  |
| 53 Plot of percentage of slabs with transverse cracking versus cumulative ESAL's<br>for different levels of freeze-thaw cycles .....                 | 124  |
| 54 Plot of percentage of slabs with transverse cracking versus cumulative ESAL's<br>for different annual number of wet days .....                    | 125  |
| 55 Plot of percentage of slabs with transverse cracking versus cumulative ESAL's<br>for different number of days with temperatures above 32 °C ..... | 125  |
| 56 IRI model form A .....  | 131  |
| 57 IRI model form B .....  | 131  |
| 58 IRI model form C .....  | 132  |
| 59 Plots of IRI versus significant variables for JPCP .....  | 140  |
| 60 Plots of IRI versus significant variables for JRCP .....  | 141  |
| 61 Plots of IRI versus significant variables for CRCP .....  | 142  |
| 62 Plot of predicted versus actual IRI for JPCP .....  | 148  |
| 63 Plot of residual versus predicted IRI for JPCP .....  | 148  |
| 64 Plot of predicted versus actual IRI for JRCP .....  | 150  |
| 65 Plot of residual versus predicted IRI for JRCP .....  | 150  |
| 66 Plot of predicted versus actual IRI for CRCP .....  | 152  |
| 67 Plot of residual versus predicted IRI for CRCP .....  | 152  |
| 68 Influence of annual number of wet days on IRI of JPCP .....   | 154  |
| 69 Influence of climate (freeze or no-freeze) on IRI of JPCP .....   | 154  |



## LIST OF FIGURES (continued)

| Figure |   | Page |
|--------|---|------|
| 70     | Influence of subgrade type on IRI of JPCP .....                                   | 156  |
| 71     | Influence of dowels and dowel diameter on IRI of JPCP .....                       | 156  |
| 72     | Influence of design steel content on JRCP IRI .....                               | 157  |
| 73     | Influence of subgrade type on JRCP IRI .....                                      | 158  |
| 74     | Influence of edge drains on JRCP IRI .....  | 159  |
| 75     | Influence of precipitation on JRCP IRI .....                                      | 161  |
| 76     | Influence of design steel content on CRCP IRI .....                               | 162  |
| 77     | Influence of subgrade support on CRCP IRI .....                                   | 163  |
| 78     | Influence of climatic region on CRCP IRI .....                                    | 164  |
| 79     | Influence of hot weather on CRCP IRI .....  | 167  |
| 80     | Schematic diagram of pavement design practice with emphasis on cost-effectiveness | 189  |
| 81     | Flow chart for developing distress models .....                                   | 204  |
| 82     | Typical functional forms used for pavement distress modeling .....                | 207  |
| 83     | Variation in $C_p$ with MSE and $R^2$ .....                                       | 211  |

## LIST OF TABLES

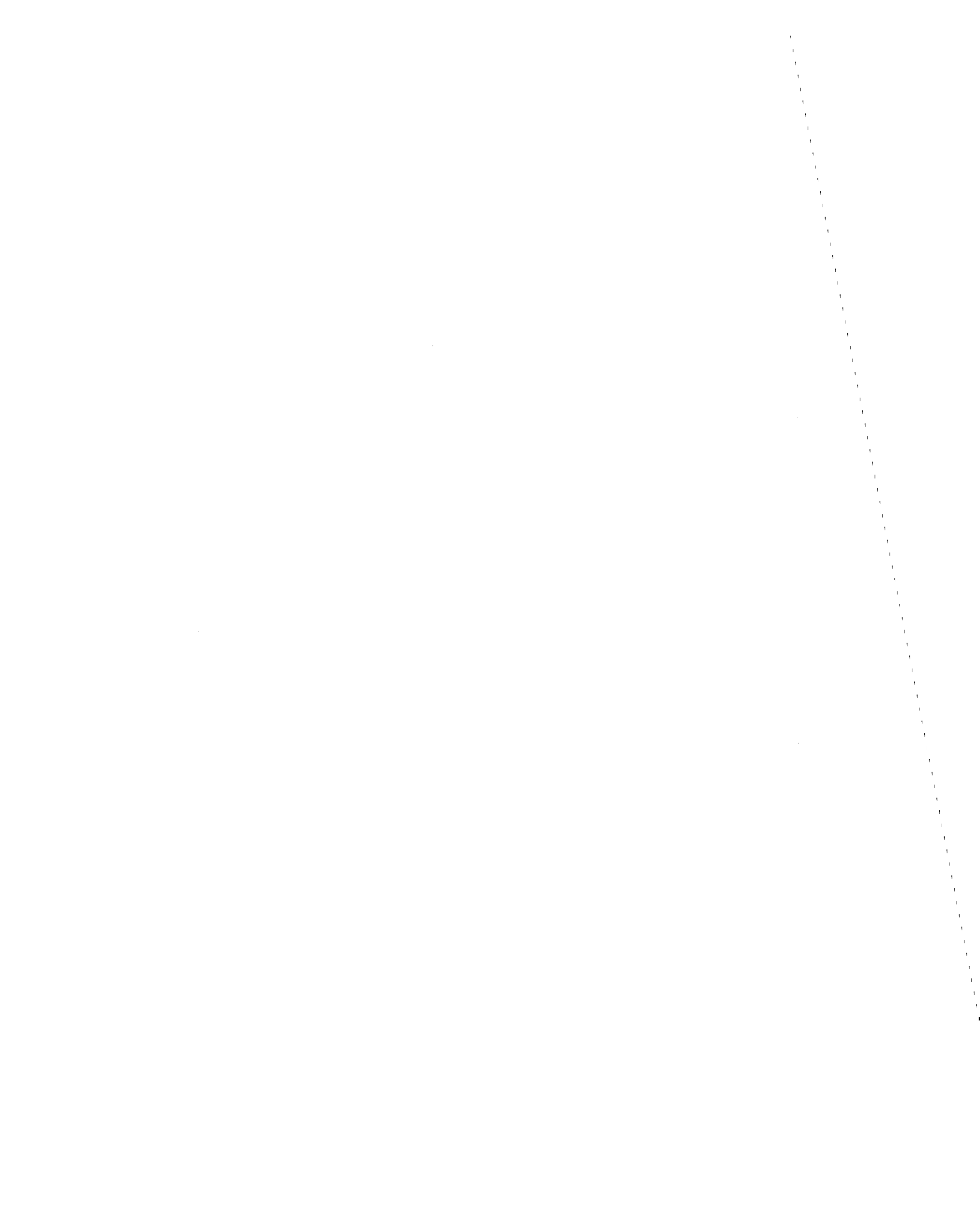
| Table   | Page |
|---|------|
| 1 Model and corresponding source of GPS data . . . . .  | 5    |
| 2 Independent variables significant to the key distress types . . . . .   | 8    |
| 3 Pavement parameters and range of values used in corner deflection model<br>development . . . . .                    | 26   |
| 4 Correlation matrix for selected variables for jointed PCC pavement faulting . . . . .                               | 30   |
| 5 Definitions of selected variables significant to joint faulting of JCP . . . . .                                    | 31   |
| 6 Matrix for selection of the overall drainage coefficient, $C_d$ . . . . .   | 35   |
| 7 Factorial of traffic and pavement properties used to develop model for predicting<br>traffic spall stress . . . . . | 61   |
| 8 Summary of inputs and results of sensitivity analyses of traffic tensile stress model . . .                         | 62   |
| 9 Correlation matrix for variables for JPCP transverse joint spalling model . . . . .                                 | 69   |
| 10 Definitions of selected variables significant to spalling of JPCP . . . . .  | 70   |
| 11 Correlation matrix for selected variables for JRCP transverse joint spalling model . . .                           | 72   |
| 12 Definition of selected variables significant to spalling of JRCP . . . . .   | 73   |
| 13 Approximate relationship between shrinkage and indirect tensile strength . . . . .                                 | 77   |
| 14 Recommended values of thermal coefficient . . . . .  | 77   |
| 15 Adjusted sealant modulus for JPCP . . . . .  | 77   |
| 16 Adjusted sealant modulus for JRCP . . . . .  | 81   |
| 17 Correlation matrix for selected variables for JPCP corner break model . . . . .                                    | 107  |
| 18 Correlation matrix for selected variables for JPCP transverse cracking model . . . . .                             | 109  |
| 19 Variables identified for use in the development of roughness models . . . . .                                      | 138  |
| 20 Summary of correlation analysis for significant variables versus IRI for JPCP . . . . .                            | 143  |
| 21 Summary of correlation analysis for significant variables versus IRI for JRCP . . . . .                            | 144  |
| 22 Summary of correlation analysis for significant variables versus IRI for CRCP . . . . .                            | 145  |
| 23 Summary of variables required for estimating faulting . . . . .  | 170  |
| 24 Summary of variables required for estimating JPCP joint spalling . . . . .   | 174  |
| 25 Summary of variables required for estimating JRCP joint spalling . . . . .   | 175  |
| 26 Summary of variables required for estimating JPCP transverse cracking . . . . .                                    | 179  |
| 27 Summary of variables required for estimating JPCP corner breaks . . . . .  | 182  |
| 28 Variables required for predicting IRI for JPCP, JRCP, and CRCP . . . . .   | 183  |
| 29 Suggested critical values for key performance indicators . . . . .   | 186  |
| 30 Comparison of cost-effectiveness of two alternate pavement designs . . . . .                                       | 191  |
| 31 Effect of key pavement design features and site condition factors on transverse<br>joint faulting . . . . .        | 195  |
| 32 Effect of key pavement design features and site condition factors on transverse<br>joint spalling . . . . .        | 196  |
| 33 Effect of key pavement design features and site condition factors on JRCP<br>transverse joint spalling . . . . .   | 197  |
| 34 Effect of key pavement design features and site condition factors on JPCP<br>corner breaks . . . . .               | 198  |

## LIST OF TABLES (continued)

| Table |   | Page |
|-------|---|------|
| 35    | Effect of key pavement design features and site condition factors on JPCP transverse cracking ..... | 199  |
| 36    | Effect of key pavement design features and site condition factors on JPCP roughness .....           | 200  |
| 37    | Effect of key pavement design features and site condition factors on JRCP roughness .....           | 201  |
| 38    | Effect of key pavement design features and site condition factors on CRCP roughness .....           | 201  |
| 39    | Diagnostic statistics and corresponding critical values .....                                       | 210  |

## LIST OF ACRONYMS AND ABBREVIATIONS

|        |  |
|--------|--|
| AASHO  | American Association of State Highway Officials                    |
| AASHTO | American Association of State Highway and Transportation Officials |
| AC     | asphalt concrete   |
| ANOVA  | analysis of variance   |
| $C_d$  | drainage coefficient   |
| CESAL  | cumulative equivalent single-axle load                             |
| CRCP   | continuously reinforced concrete pavement                          |
| DE     | differential elastic deformation energy                            |
| DOWDIA | dowel diameter   |
| ESAL   | equivalent single-axle load  |
| FHWA   | Federal Highway Administration                                     |
| FI     | freezing index   |
| FWD    | falling weight deflectometer                                       |
| GPS    | general pavement studies   |
| IMS    | information management system                                      |
| IRI    | international roughness index                                      |
| IRRE   | International Road Roughness Experiment                            |
| JCP    | jointed concrete pavements   |
| JPCP   | jointed plain concrete pavement                                    |
| JRCP   | jointed reinforced concrete pavement                               |
| JTSP   | joint spacing or PCC slab length                                   |
| k      | modulus of subgrade reaction                                       |
| LFM    | linear fracture mechanics  |
| LTE    | load transfer efficiency   |
| LTPP   | Long-Term Pavement Performance                                     |
| NIMS   | National Information Management System                             |
| PCA    | Portland Cement Association  |
| PCC    | portland cement concrete   |
| PMARP  | Purdue Method for Analysis of Rigid Pavements                      |
| PSI    | present serviceability index                                       |
| PSR    | present serviceability rating                                      |
| $R^2$  | coefficient of determination                                       |
| SEE    | standard error of estimate   |
| SHA    | State highway agency   |
| SHRP   | Strategic Highway Research Program                                 |
| SMP    | seasonal monitoring program  |
| SPS    | specific pavement studies  |





# 1. INTRODUCTION

## Background

The Long-Term Pavement Performance (LTPP) study began in 1987 with the goal of determining ways of increasing pavement life through improvements in design, construction, and other pavement practices. This is being achieved through the investigation of various designs of pavement structures that use different materials and experience different loads, environments, subgrade soils, and maintenance practices. This is emphasized in two of the six objectives established for the LTPP study in 1985, by the Pavement Advisory Committee of the Strategic Highway Research Program (SHRP), which are as follows:

- Determine the effects of loading, environment, material properties and variability, construction quality, and maintenance levels on pavement distress and performance.
- Determine the effects of specific design features on pavement performance.

By investigating the performance of in-service pavement sections, specific information can be obtained on the various factors and design features that influence pavement deterioration. In addition, mathematical prediction models that relate the various factors and specific design features to pavement performance provide a means for quantifying the effects of the specific design features on long-term performance. The results from such investigations and evaluations can be used to develop recommendations for improving the design and construction of new and reconstructed pavements.

This study was instituted to evaluate portland cement concrete (PCC) pavements to develop recommendations to meet the needs of the States. It involved an evaluation and analysis of the PCC pavement data in the LTPP database, using a variety of means to determine the design features and practices that have beneficial effects on long-term performance. Emphasis was placed on identifying those specific features that can be selected during design to improve the performance of PCC pavements under various combinations of environmental and traffic loading conditions, and for different subgrade support conditions. The study focused on the development of practical recommendations that can be implemented easily by highway agencies to increase pavement life.

## Project Objectives and Scope

The specific objectives of this study are as follows:

- Examine and analyze the LTPP data for PCC pavements to determine the pavement design features and construction practices that have a beneficial effect on their performance.
- Develop improved PCC pavement performance models.
- Develop specific recommendations for improving the design and construction of PCC pavements.

Although all types of PCC pavement were considered, special emphasis was placed on jointed plain concrete pavement (JPCP), since it is the pavement type that is constructed most often in the United States.

### **Research Approach**

To maximize the results obtained from this study, a three-part systematic research approach was adopted. It involved taking advantage of the knowledge from past studies and building on it using the pavement engineering knowledge obtained from current analysis of the LTPP data. The first part of the study consisted of an evaluation of the LTPP database using a variety of techniques to determine the beneficial effects of various pavement design features and practices on long-term performance.

In the second part of the study, improved pavement prediction models were developed, using the information obtained from a thorough evaluation of the database and the results from recent studies. A key focus was to develop distress prediction models that incorporate mechanistic principles to the greatest extent possible but that are still practical for use by State highway agencies.

The third part of the study used the results obtained from this study to develop comprehensive recommendations for design and construction of PCC pavements.

### **Sequence of Report**

This report is the third of a three-volume report on this study and consists of nine chapters. Chapter 2 provides an overview of the LTPP data used for model development and analysis. This includes information on the data processing and reduction techniques used and the strengths and weaknesses of the data. Chapter 3 provides background information on the different methods and techniques that were used to develop the prediction models. Chapters 4 through 7 discuss the background and techniques used to develop models for predicting transverse joint faulting, transverse joint spalling, transverse cracking, corner breaks, and roughness of PCC pavements. Chapter 8 presents examples of the application of the models developed for design and construction of long-lived PCC pavements. It includes comprehensive guidance on use of the models to check new designs and in pavement management systems. Finally, chapter 9 summarizes the results of this study and provides recommendations for further research to improve the models. A detailed description of the statistical techniques used in model development is presented in appendix A.

## 2. OVERVIEW OF LTPP DATA USED FOR MODEL DEVELOPMENT

### Introduction

The data used for this study were obtained from the LTPP National Information Management System (NIMS). The NIMS contains pavement inventory information and performance histories for over 2,400 in-service and specially constructed pavements. The data include information on design features, climatic conditions, traffic loads, materials, maintenance, and rehabilitation.<sup>(1, 3, 4)</sup> This chapter provides background information on the LTPP data that were used to develop distress and roughness prediction models for PCC pavements. The data were obtained from the NIMS at the beginning of this study (1993) but were updated frequently to take advantage of ongoing improvements made to the database. As a result, the study was able to take advantage of the most comprehensive data on concrete pavements that have ever been available from the LTPP database. For brevity, the discussion in this chapter is limited to the approximately 300 General Pavement Studies (GPS) concrete pavement sections that were used in this study. Additional information on the data can be found in volume II.

To guide researchers who use the data in the LTPP database, several sources of information that describe how to access and use the database were very useful to this study.<sup>(5)</sup> Key sources of information that are recommended include the *Data Collection Guide for Long-Term Pavement Performance Studies*, which provides data collection instructions and data sheets for the LTPP program.<sup>(6)</sup> The *SHRP Database Structure Reference Manual* is also highly recommended for users of the LTPP data.<sup>(7)</sup> It includes the LTPP IMS schema that defines the various tables and fields in the NIMS. The schema describes the data structure and also identifies the key fields (variables) and data types in each table. Other parts of the *SHRP Database Structure Reference Manual* are a data dictionary that provides a more detailed description of each field in the LTPP database and tables that define all the codes used in the database.

### Overview of the LTPP Data

The LTPP data represent the most comprehensive pavement performance data that have ever been assembled. Currently, the LTPP database is the world's largest pavement performance database and has enormous potential for the development of products that will significantly improve pavement technology. The database includes close to 800 flexible and concrete pavement sections located across North America as part of the GPS. The GPS sections are made up of in-service pavement sections, and the data from the concrete pavements in this group offer an opportunity to refine and improve upon existing PCC pavement performance models.

### Advantages

Some of the advantages of the database include the even distribution of pavement sections across the four climatic zones in the United States and Canada, defined as wet-freeze, wet-no freeze, dry-freeze, and dry-no freeze. Also, with the exception of a few sections, the LTPP experiments are replicated in all four environmental zones. Extensive design, materials, climatic, traffic, distress, and roughness information is available on each of the sections.

The LTPP database also offers some time-series performance data. The time-series data allow monitoring of the rate of progression of the key distresses for individual pavement sections. These data also provide a method for evaluating the accuracy and reliability of the data on a section-by-section basis, which is valuable information for developing and validating performance models.

Clearly, the LTPP database offers enormous potential for the development of performance prediction models that can be used to address the key issues of concrete pavement analysis, design, and construction. As a result, a major objective of this project was to develop prediction models for the key PCC pavement distress types and roughness. This follows previous efforts in the SHRP P-020 LTPP Data Analysis project.<sup>(3, 4, 11)</sup> In that study, prediction models were developed for several distress types; however, the usefulness of these models was limited because of the unavailability of data at that time from a majority of the pavement sections. Since then, the database has grown considerably and data are available for many more sections.

#### Data Available for This Study

The LTPP study consists of nine different experiments. The specific experiments used in this study were as follows:

- GPS 3 Jointed plain concrete pavement (JPCP).
- GPS 4 Jointed reinforced concrete pavement (JRCP).
- GPS 5 Continuously reinforced concrete pavement (CRCP).

All subsequent discussion of the database will focus on the three pavement types listed. Overall, data from 123 GPS 3, 69 GPS 4, and 85 GPS 5 LTPP pavement sections were available for this study. For each of the pavement types in the LTPP database, data were available for the following 10 categories:

- Inventory.
- Materials and laboratory testing.
- Traffic.
- Distress.
- Profile.
- Deflection.
- Friction.
- Environment.
- Maintenance.
- Rehabilitation.

Typical LTPP pavement sections evaluated in this study are 150-m sections with 3.65-m-wide traffic lanes and either asphalt concrete (AC) or tied PCC shoulders.

The data were downloaded from the NIMS and imported into a local Microsoft Access® database for sorting. Because the LTPP data are provided in several different tables, several software packages were used for merging and organizing the data. This approach is recommended because the software also allows exporting of different combinations of the data

into spreadsheets for further analysis. For this study, following a thorough checking of the data for consistency and accuracy, spreadsheets were created for development of prediction models for each of the key distress types.

Additional information on the LTPP data used in this study is contained in volume II. Table 1 shows the sources of the data that were used for the development of models for four key distress types and roughness.

Initially, there were plans to include data collected from the LTPP Specific Pavement Studies (SPS) in this study. The SPS include pavement sections specifically designed and constructed through a cooperative effort with the State highway agencies (SHA) and that are being observed over their entire lives. However, although data from the SPS sections are currently available in the NIMS, they were not available for analysis during this study. It is anticipated that some of the SPS data will be available during the next round of LTPP data analyses and can be used to check and improve upon the results obtained in this study. A summary of the basic statistics such as mean, median, and standard deviation of the GPS data used in this analysis is presented in appendix A of volume II of this report.

### Summary

The data used in this study to develop models for predicting key distresses and roughness of concrete pavements include comprehensive design, materials, traffic loading, and climatic data from the LTPP database. Specifically, data from the GPS 3, 4, and 5 pavement sections were used to develop models for faulting, spalling, transverse cracking, corner breaks, and roughness. The data were checked thoroughly and prepared for the subsequent analyses. Additional information on all the LTPP concrete pavement sections obtained for analyses can be found in appendix A of volume II of this report.

Table 1. Model and corresponding source of GPS data.

| <b>Model</b>        | <b>Source of Data</b> |
|---------------------|-----------------------|
| Faulting            | GPS 3                 |
| Spalling            | GPS 3 and 4           |
| Transverse cracking | GPS 3                 |
| Corner breaks       | GPS 3                 |
| Roughness           | GPS 3, 4, and 5       |





### 3. MODEL DEVELOPMENT METHODS

#### Introduction

In the past, several attempts have been made to develop performance models and recommendations for concrete pavement design and construction.<sup>(3, 4, 8, 9, 10, 11, 12)</sup> These have included studies that have used the LTPP database.<sup>(3, 4, 11, 12)</sup> To a large extent, these studies have all added to the knowledge on the development of predictive models for the key concrete pavement distress types and roughness. However, it is necessary to improve upon these models continuously to obtain further insights into the factors that affect the occurrence of the key distress types and roughness, so that further improvements can be made in design and construction of long-lived pavements. This chapter reviews the approach used in this study to develop models for predicting distresses using the LTPP database.

The results from past model development efforts were investigated, including independent and dependent variables, interaction of variables, mechanistic clusters, and model functional forms used. This included extensive evaluation of the LTPP database to uncover any possible relationships suggested by the data collected from pavements in service. Table 2 shows the explanatory variables that were found to be significant to the various PCC distresses in the first of the LTPP concrete pavement data analysis studies and other studies on the performance of PCC pavements.<sup>(3)</sup>

The best predictive models are those that are first formulated using the principles of mechanics and then calibrated using field data. Therefore, a considerable amount of time was spent identifying the fundamental mechanisms that cause the distresses being modeled. Once the underlying principles behind the development of the key distress types were understood, appropriate mechanistic functional forms were selected for investigation and for development of the most feasible prediction model for each distress type.

Using modern statistical and mathematical techniques, the engineering-based model forms selected were calibrated using the LTPP database to obtain the best prediction model for each distress type. This included using the various approaches for optimization, limiting errors, and maximizing model accuracy. The predictive models were tested in several ways to identify any weaknesses. The limitations identified were remedied using both statistical techniques and engineering analysis. Finally, each model was further evaluated by using it to determine the effect of key design, traffic, and environmental features on performance and for predicting future pavement deterioration.

Table 2. Independent variables significant to the key distress types.<sup>(3)</sup>

| Data Element                      | Joint Faulting | Joint Spalling | Transverse Cracking | Corner Breaks | Roughness |
|-----------------------------------|----------------|----------------|---------------------|---------------|-----------|
| Pavement Age                      | ✓              | ✓              | ✓                   | ✓             | ✓         |
| Slab Thickness                    | ✓              | ✓              | ✓                   | ✓             | ✓         |
| Joint Spacing                     | ✓              | ✓              | ✓                   | ✓             | ✓         |
| Drainage                          | ✓              |                |                     |               |           |
| Base Type                         | ✓              |                | ✓                   |               | ✓         |
| Cumulative ESAL's                 | ✓              | ✓              | ✓                   | ✓             | ✓         |
| Joint Opening                     | ✓              | ✓              |                     |               |           |
| Corner Deflection                 | ✓              |                |                     |               |           |
| Freezing Index                    | ✓              | ✓              | ✓                   |               | ✓         |
| Edge Support                      | ✓              |                |                     | ✓             | ✓         |
| Subgrade Type                     | ✓              |                | ✓                   | ✓             | ✓         |
| Pumping                           | ✓              |                | ✓                   | ✓             | ✓         |
| Annual Precipitation              | ✓              | ✓              | ✓                   | ✓             | ✓         |
| Bearing Stress                    | ✓              |                |                     |               |           |
| Dowel Diameter                    | ✓              |                |                     | ✓             |           |
| Slab Stress                       |                |                | ✓                   |               | ✓         |
| PCC Modulus of Rupture            |                | ✓              | ✓                   | ✓             | ✓         |
| PCC Elastic Modulus               | ✓              | ✓              |                     | ✓             | ✓         |
| PCC Compressive Strength          | ✓              |                |                     |               |           |
| Average Monthly Temperature Range | ✓              | ✓              | ✓                   | ✓             | ✓         |
| Thornthwaite Index                | ✓              | ✓              | ✓                   |               | ✓         |
| Static k-value                    | ✓              |                | ✓                   | ✓             | ✓         |
| Steel Percentage                  |                |                | ✓                   |               | ✓         |
| Imcompressibles in Joint          |                | ✓              |                     |               |           |
| D-cracking                        |                | ✓              |                     |               | ✓         |
| Reactive Aggregate                |                | ✓              |                     |               | ✓         |
| Joint Sealant Type                |                | ✓              |                     |               |           |
| Sealant Damage                    |                | ✓              |                     |               | ✓         |
| Load Transfer Type                | ✓              | ✓              | ✓                   | ✓             |           |
| Freeze-Thaw Cycles                |                | ✓              |                     |               | ✓         |

## **Model Types**

Generally, two types of prediction models can be developed: empirical and mechanistic-empirical. Empirical models are developed using statistical regression methods and basic engineering analysis and judgment; however, they do not explain or model basic mechanisms of the distress. They are simply the best relationship that allows prediction of an explanatory or dependent variable from a set of independent variables based on the available data. The model obtained may not necessarily signify a cause-and-effect relationship between the independent variables and the dependent variable. However, the analyst can use the knowledge available from past observations and experimental results to improve this empirical aspect of the model.

Mechanistic-empirical models, on the other hand, attempt to incorporate mechanistic principles that account for the cause-and-effect relationship between the explanatory (dependent) variable and independent variables. Based on the mechanistic principles behind the cause of a particular distress, a model can be formulated that attempts to describe both the occurrence and progression of the distress. The model is then calibrated using field data (e.g., LTPP data) and standard statistical and optimization techniques. Perhaps the most important benefit of a mechanistic-empirical model is its potential to extrapolate beyond the limits of the data used in its development.

For these reasons, the approach adopted in this study was to develop mechanistic-empirical models for the key distress types. Empirical models were used only in those cases where it was not possible to develop mechanistic-empirical models, such as for roughness. Roughness is highly correlated to the development of distress, so there is no single mechanism for modeling roughness.

A systematic approach was adopted that utilized knowledge accumulated over the years.<sup>(4, 8, 9, 10, 12)</sup> An essential step in this approach was a thorough investigation to uncover the actual mechanism responsible for the occurrence and propagation of each distress type. This involved an evaluation of previous studies and an examination of the data available for specific sections. An attempt to model distress was made only after achieving an understanding of the engineering mechanism that causes the distress. Using this approach, it was possible to obtain mechanistic-based prediction models for the distress types analyzed in this study.

## **Developing Practical Prediction Models**

The basic steps that were followed to develop prediction models are summarized in the flow chart shown in figure 1. This approach, which has been used numerous times in previous studies, has been continuously improved and provides practical prediction models for implementation as design checks and for use in pavement management.<sup>(3, 4, 8, 9, 10, 12)</sup> Following are the key elements in the application of this approach to develop models for predicting pavement distress and roughness.

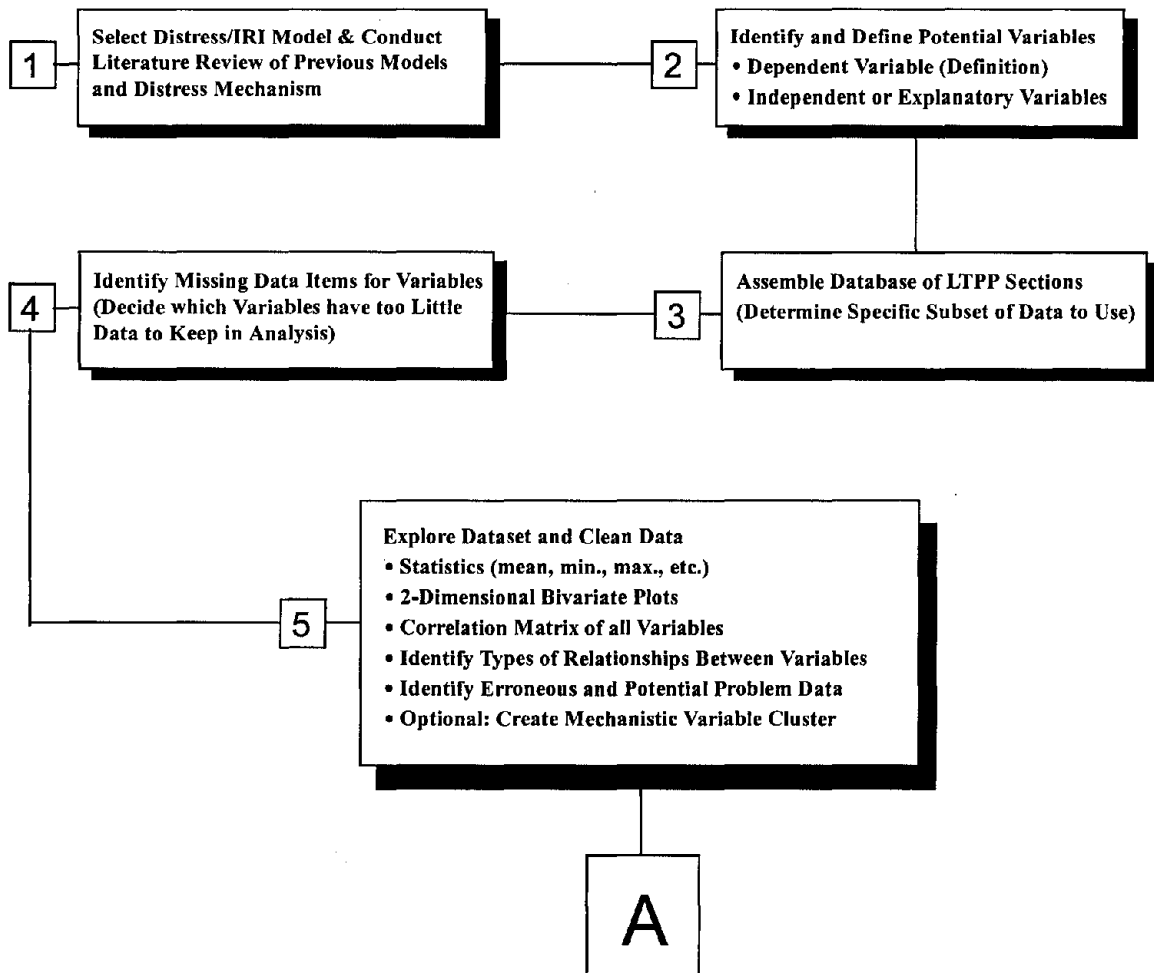


Figure 1. Flow chart for developing distress models for rigid pavements.



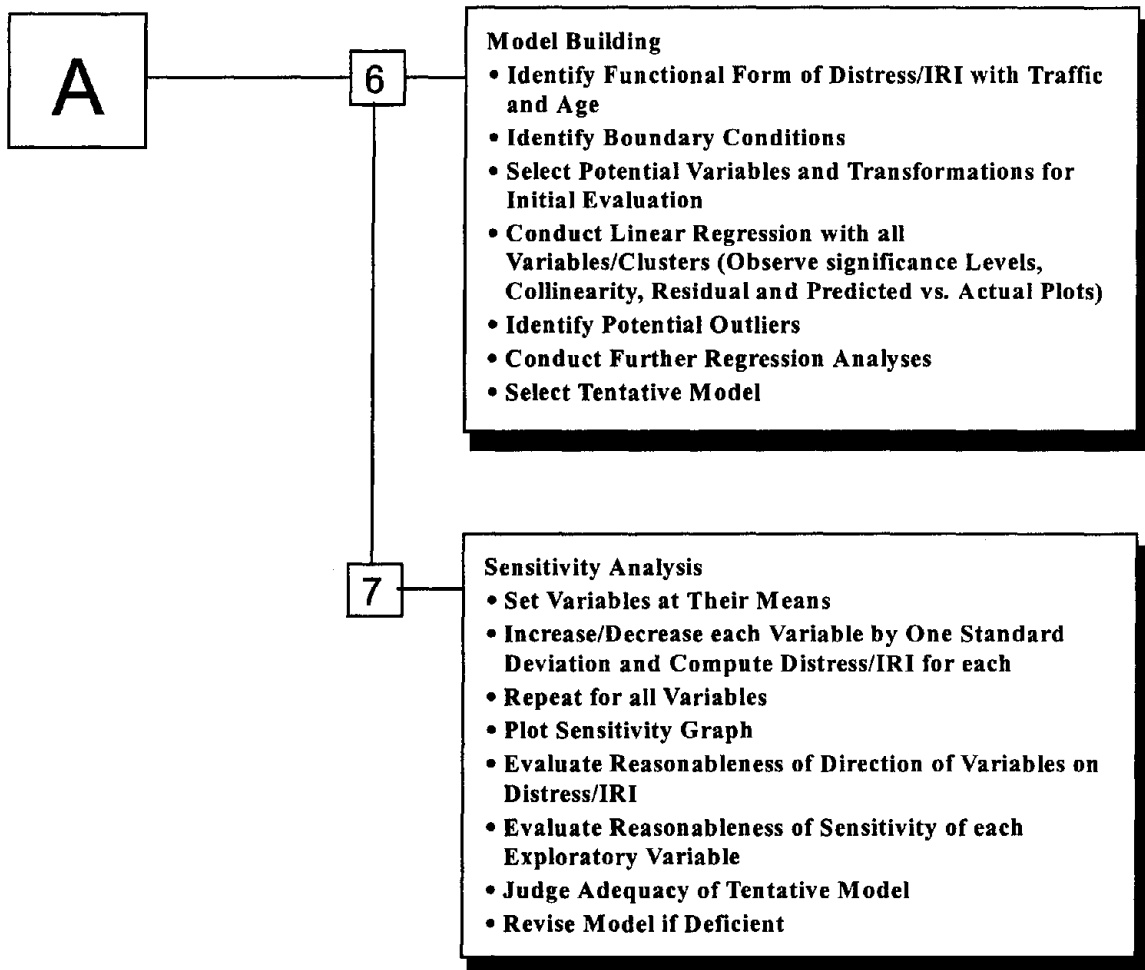


Figure 1. Flow chart for developing distress models for rigid pavements (continued).

### Step 1: Literature Review- Establish Cause of Distress

This first step involves a comprehensive literature search, review of past studies, and brainstorming by the research team to establish the cause of the distress to be modeled. Past models for predicting distress and roughness were also evaluated to determine significant variables.

The goals are to learn as much as possible about the mechanism of the distresses, the model forms previously used to model both distresses and roughness, and the independent variables that were found to influence the key distress types and roughness in past studies. Also, the form in which the response variable or distress/roughness was best represented in the models can be established from a review of previous models. The results of this review were used to determine possible shortcomings in the current prediction models and to recommend improvements to the models.

### Step 2: Identify and Define Potential Independent Variables and Clusters

The next important step involves further in-depth investigations to identify and define the potential independent variables to use in the models for predicting distress or roughness. Of particular importance are any mechanistic-based independent variables that significantly explain the cause of the distresses. By building on past knowledge, it is possible to identify or develop a mathematical cluster of mechanistic parameters relevant to pavement performance prediction, also called mechanistic clusters, that can be incorporated into models to improve their accuracy and practicality.

Because such cluster variables are based on mechanistic principles, they offer the advantage of reducing the data requirements for developing good prediction models. Using these principles, a systematic process based on both statistical analysis and engineering judgment was used to determine the independent variables necessary for effective model development. Table 2 shows the variables that were identified in this study for the development of each prediction model.

### Step 3: Assemble Database for Each Model

With the dependent and independent variables for each distress type and roughness established, the next step is the process of assembling the data required for each model. Table 1 lists the sources of data that were used to develop the various prediction models in this study. Because of the structure of the LTPP database in the NIMS, a key step in this study was to organize the data to facilitate its quick retrieval into the unique analysis data sets used for developing the prediction models. A local Microsoft Access<sup>®</sup> database proved to be very effective for organizing the LTPP data.

### Step 4: Identify Missing/Erroneous Data Items

Each data set had to be examined thoroughly to identify gaps and erroneous data. In this study, the LTPP database was examined to determine if data were not available for certain key variables. In some cases, data were not available because they had not yet been processed into the NIMS. Some pavements simply did not have data available for certain design features.

Therefore, the database was checked closely for anomalies, and appropriate measures were taken to correct any erroneous data.

#### Step 5: Explore and Clean Data

For both empirical and mechanistic-empirical models, a very important step in the process is exploration of the data set for each model to examine the general properties of the data, clean the data, and get it ready for further analysis. Basic univariate statistics for the variables are used to determine if the data set is representative of the inference space of the expected model. Also the variables are examined using univariate and bivariate analysis methods (e.g., histograms, scatter plots, and correlations) to identify extreme outliers, erroneous data, and possible transformations, strong interactions, possible mechanistic clusters, and to determine the relationships between the distress and explanatory variables. Prior knowledge and expertise should be applied to screen independent variables and to identify possible transformations, interactions, and specific mechanistic clusters to consider.

#### Step 6: Select Model Form

Following the selection of a large pool of independent variables, transformed variables, interactions, and cluster variables to consider, the model building process begins with the selection of the functional form that best describes the path of progression of the key distresses or roughness. Various functional forms available for modeling pavement distresses and roughness are described in appendix A. Several statistical procedures are available for selecting the subset of independent variables, including transformations, interactions, and cluster variable, to include in the model form for further investigation. They include forward and backward selection methods, stepwise regression, and other linear regression-based methods that use a variety of criteria to select the independent variables and the forms of the variables to include in a model.

#### Step 7: Develop and Verify Prediction Model

Following the preliminary investigations to determine the best model form to use, multiple linear regression analysis is conducted on all of the variables and clusters to produce the parameter estimates and summary statistics for the selected model. Optimization techniques can also be used to improve this process. The model obtained should then be verified for accuracy of the regression coefficients, reasonableness of the regression function, and ability to generalize inferences drawn from the regression analysis. Appendix A includes some of the diagnostic statistics used in this study to establish the suitability of the models developed. If the results obtained are not satisfactory, remedial measures should be taken and further regression and optimization analysis conducted as necessary to obtain the best tentative model for predicting the distress under investigation.

#### Step 8: Verification of Model

Following step 7, a robust and reliable model should be available. An extremely important and final step that should not be neglected is verification of the model. This is necessary to check the

predictive capability of the model outside of the data used to develop it. The only reliable approach is to use data obtained from independent sources to verify the model. However, several other statistical methods can be used to partially verify models, including the following:

- Sensitivity analyses.
- Statistical diagnostic tests.
- Data splitting (i.e., using part of the data that is held back to check the model's predictive ability).

A sensitivity analysis involves using the model to evaluate the effect of various inputs on the predicted distress and comparing those results with empirical and theoretical observations. A comprehensive sensitivity analysis of the selected model can be performed as follows:

- Except for the variables of interest (the independent and a dependent variable), set all other variables in the model to their means.
- With all the other variables set at their means, vary the variables of interest over their typical ranges and observe the variation in the response variable or predicted distress. Use of plots to observe these variations is highly recommended.
- Compare the results obtained with empirical observations and theoretical results.

## 4. FAULTING MODEL FOR JOINTED CONCRETE PAVEMENTS

### Introduction

Faulting is a major distress that occurs in jointed concrete pavements (JCP). It is the difference in elevation between the adjacent slabs across a transverse joint or crack. Excessive faulting will greatly reduce the serviceability of a JCP because the increase in roughness caused by the faulted joints and cracks appreciably increases user discomfort. Therefore, in the design of jointed concrete pavements, faulting is one of the major distress types that must be prevented. For existing pavements, forecasting the occurrence of the distress is important to ensure a good riding surface and user safety. Rehabilitation of faulted joints must be performed as soon as possible in JCP.

Diamond grinding of the joints is an effective way to eliminate faulting, provided the faulting is not excessive. However, unless the fundamental causes of faulting are addressed, it is likely that the pavement will continue to fault. Alternatively, faulting can be remedied with a thick overlay. In either case, the rehabilitation of pavements with faulting is costly and time consuming. Therefore, it is more effective to prevent faulting during design. Some of the design features that can be used to reduce faulting include dowel bars, nonerrodible bases, and positive drainage. <sup>(3, 8, 10, 13, 14)</sup> This chapter describes the development of a model for predicting joint faulting of JCP. The model can be used as a design check to ensure that the appropriate measures have been taken to limit faulting. For pavements already in service, the model also provides a means for predicting the occurrence of faulting. This information can be used to plan rehabilitation as part of an overall pavement management system. To provide a model that is most suitable for all these uses, the model incorporates mechanistic principles that explain the occurrence of faulting.

### Faulting Mechanism

Faulting is the result of a combination of poor load transfer across a joint or crack, heavy axle loads, free moisture beneath the pavement, and pumping of the supporting base, subbase, or subgrade material from underneath the slab. <sup>(3, 8, 10, 13, 14)</sup> It is primarily caused by erosion of the supporting material from underneath the leave slab and a buildup of the loose material under the approach slab at a joint or crack. The erosion of material from underneath the leave slab is caused by the phenomenon of pumping. Therefore, it is important to understand pumping in order to understand the mechanism that leads to faulting.

Pumping is a phenomenon that has been observed on concrete pavements since the advent of large trucks with heavy axle loads. <sup>(13, 15, 16, 17, 18, 19, 20, 21, 22)</sup> Four elements must be present for pumping and, therefore, faulting to occur. There must be free water in the pavement, an erodible underlying or supporting material, heavy truck traffic, and differential deflections due to inadequate load transfer.

When these elements are present, as a heavy wheel load approaches a joint or crack, the approach slab deflects and forces water trapped under the slab to transport fine material underneath the leave slab. As the wheel load crosses the joint or crack, the sudden vertical pressure on the leave slab causes pumping or ejection of the water and loose material from beneath the slab through the joint or crack. A large part of the fine material that is eroded from beneath the leave slab is

deposited under the approach slab. Repeated cycles of this phenomenon, which occurs with each wheel load application, can be in the millions. Eventually, this leads to measurable faulting at the joint or crack because of a lift up of the approach slab and a depression of the leave slab.

Although this is the basic mechanism of pumping that leads to faulting, several other factors can exacerbate the distress and need to be taken into account. Field results show that the reduced support from upward curling or warping of the slab at the joint or crack will increase pumping pressures because of the higher deflections experienced.<sup>(24)</sup> The potential for faulting of a pavement is at a minimum in the summer months when the joints are closed due to thermal expansion.<sup>(24)</sup> Also, faulting increases in the other seasons when the joint width is widest and the underlying materials typically have a higher moisture content.<sup>(24, 25)</sup>

The impact of a heavy wheel load as it crosses the joint or crack is far more pronounced if there is inadequate load transfer. The higher differential deflections that occur at the joint or crack will lead to more pumping and faulting. However, it is important to note that, even for a pavement with 100 percent load transfer, deflections at the joint or crack can be abnormally high and result in horizontal pumping.<sup>(13)</sup> This was observed at the American Association of State Highway Officials (AASHTO) Road Test, where the joints with dowels used for load transfer showed extensive pumping but no faulting in the 2-year period of the study.<sup>(19)</sup> Laboratory and empirical evidence show that the loss of support caused by horizontal pumping will eventually lead to more pumping.<sup>(12, 23)</sup> This will increase corner deflections and lead to faulting as the magnitude of the deflections increases. In addition, the loss of support at the joints and slab edge caused by pumping will also increase the stress in the slab and can eventually lead to corner cracking.

Based on the mechanism described, it is clear that the following conditions must exist for pumping and faulting to occur:

- Significant joint differential deflections brought on by several factors, including heavy wheel loads, inadequate load transfer, and loss of support.
- A high percentage of fines in the underlying base, subbase, or subgrade material that is erodible.
- Saturation or a high moisture content of the underlying base, subbase, or subgrade material.

These factors must be considered in the development of a model for predicting joint faulting.

### **Evaluation of Existing Faulting Models**

To determine the factors that should be considered in the development of a model for predicting faulting, several existing doweled and nondoweled faulting models were reviewed. These models included empirical and mechanistic-empirical models.

## Empirical Models

An early empirical faulting model based on distress surveys from six States is shown below.<sup>(8)</sup> The model predicts faulting for both doweled and nondoweled pavements.

$$\text{FAULT} = \text{ESAL}^{0.144} \left[ -0.298 + 0.2671/(\text{THICK}^{0.3184}) - 0.0285*\text{BTYP} + 0.00406(\text{FI} + 1)^{0.3598} - 0.0462*\text{EDSUP} + 0.2384*(\text{PUMP}+1)^{0.0109} - 0.0340*\text{DOW}^{2.0587} \right] \quad (1)$$

where

|       |   |  |
|-------|---|--|
| FAULT | = | mean transverse joint faulting, in                               |
| ESAL  | = | accumulated 18-kip single-axle loads, millions                   |
| THICK | = | slab thickness, in   |
| BTYP  | = | 0 for granular and 1 if treated                                  |
| FI    | = | freezing index   |
| EDSUP | = | 0 for AC shoulders and 1 for tied PCC shoulder                   |
| PUMP  | = | 0 if no pumping and 1, 2, or 3 for low, medium, or high severity |
| DOW   | = | diameter of dowel bar in inches and 0 if no dowel bars present   |

The unique aspect of this model is the inclusion of shoulder type and a pumping factor. The pumping factor is similar to an erosion factor, which recognizes the effect pumping has on faulting. The pumping factor is calculated from traffic, soil type, slab thickness, precipitation, and freezing index. It was realized from this study that tied shoulders reduce faulting by about 50 percent. It was also one of the first models to relate dowel diameter to faulting.

In the first attempt to develop prediction models using the LTPP data, the following faulting models were also developed for doweled and nondoweled pavements:<sup>(3, 4)</sup>

$$\begin{aligned} \text{FAULTD} = \text{CESAL}^{0.25} * & \left[ 0.0238 + 0.0006 * \left( \frac{\text{JTSPACE}}{10} \right)^2 \right. \\ & + 0.0037 * \left( \frac{100}{\text{KSTATIC}} \right)^2 + 0.0039 * \left( \frac{\text{AGE}}{10} \right)^2 \\ & \left. - 0.0037 * \text{EDGESUP} - \frac{2.18 * \text{DOWDIA}}{100} \right] \quad (2) \end{aligned}$$

where

|         |   |   |
|---------|---|---|
| FAULTD  | = | mean transverse doweled joint faulting, in            |
| CESAL   | = | cumulative 18,000-lb ESAL's in traffic lane, millions |
| JTSPACE | = | mean transverse joint spacing, ft                     |
| KSTATIC | = | mean backcalculated static k-value, psi/in            |

AGE = age since construction, yr  
 EDGESUP = edge support (1 for tied concrete shoulder and 0 for other shoulder types)  
 DOWDIA = diameter of dowels in transverse joints, in

$$\text{FAULTND} = \text{CESAL}^{0.25} * [ - 0.0757 + 0.0251 * \sqrt{\text{AGE}} + 0.0000012 \text{ FI} * \text{PRECIP} - 0.0378 \text{ DRAIN} + 0.000013 \text{ PRECIP}^2 \quad (3)$$

where

FAULTND = mean transverse nondoweled joint faulting, in  
 CESAL = cumulative 18,000-lb ESALs in traffic lane, millions  
 AGE = age since construction, yr  
 PRECIP = mean annual precipitation, in  
 FI = mean freeze index, degree-days  
 DRAIN = drainage type, 1=longitudinal subdrainage exists; 0=otherwise

For the nondoweled pavement, the significant variables include traffic loading, dowel diameter, edge support, joint spacing, and subgrade support. Environmental factors that influence the erodibility of the underlying materials and joint width were significant.

Faulting models were also developed recently in the Federal Highway Administration (FHWA) jointed concrete pavement study, commonly referred to as RIPPER, for both doweled and nondoweled concrete pavements.<sup>(10)</sup>

$$\text{FAULTND} = \text{CESALS}^{0.25} * [0.2347 - 0.1516 * C_d - 0.00025 * \text{Slabthick}^2 / \text{Jtspace}^{0.25} - 0.0115 * \text{Basetype} + 0.7784 * 10^{-7} * \text{FI}^{1.5} * \text{Precip}^{0.25} - 0.002478 * \text{Days90} - 0.0415 * \text{Widenlane}] \quad (4)$$

$$\text{FAULTD} = \text{CESALS}^{0.25} * [0.0628 - 0.0628 * C_d + 0.3673 * 10^{-8} * \text{Bstress}^2 + 0.4116 * 10^{-5} * \text{Jtspace}^2 + 0.7466 * 10^{-9} * \text{FI}^2 * \text{Precip}^{0.5} - 0.009503 * \text{Basetype} - 0.01917 * \text{Widenlane} + 0.0009217 * \text{Age}] \quad (5)$$

where

FAULTND = mean transverse nondoweled joint faulting, in  
 CESALS = cumulative 18-kip ESAL's, millions  
 C<sub>d</sub> = drainage coefficient  
 Slabthick = slab thickness, in  
 Jtspace = joint spacing, ft  
 Basetype = stabilized or unstabilized base  
 FI = freezing index



|           |   |  |
|-----------|---|--|
| Precip    | = | annual precipitation, in                   |
| Days90    | = | days temperature is above 90°F             |
| Widenlane | = | presence of a widenlane or not             |
| FAULTD    | = | mean transverse doweled joint faulting, in |
| Bstress   | = | maximum dowel/concrete bearing stress, psi |
| Age       | = | pavement age, yr                           |

Much like the previous faulting models, these models show that a combination of variables that influence the level of differential deflection at the joint, erodibility of the underlying material, and the availability of free water have a significant effect on faulting.

### Mechanistic-Empirical Models

In 1993, a mechanistic-empirical faulting model developed by the Portland Cement Association (PCA) introduced the concept of erodibility as one of the important parameters to consider directly in a model for predicting faulting.<sup>(26)</sup> The PCA model defines the rate of work or power of each axle pass at the corner of a slab as follows:

$$P = 268.7 * p^2/t/k^{0.73} \tag{6}$$

where

|   |   |  |
|---|---|--|
| P | = | power (rate of work)                       |
| p | = | pressure at slab-foundation interface, psi |
| t | = | slab thickness, in                         |
| k | = | modulus of subgrade reaction, psi/in       |

For each axle, the number of allowable axle load applications for the pavement was calculated as follows:

$$\log N = 14.524 - 6.777 * (C_1 * P - 9.0)^{0.103} \tag{7}$$

where

|                |   |   |
|----------------|---|---|
| N              | = | allowable axle load repetitions to end of design period |
| C <sub>1</sub> | = | 1 - (k/2000*4/t) <sup>2</sup>                           |
| P              | = | power   |

Using Miner's damage equation, erosion damage at the slab corner was calculated with the following equation:

$$EROSION = 100 * n_1 * (C_2/N_i) \tag{8}$$

where

|                |   |  |
|----------------|---|--|
| EROSION        | = | percent erosion damage                                       |
| n <sub>i</sub> | = | expected number of axle load repetitions for each axle group |

- $C_2$  = 0.06 for pavements without a shoulder and 0.94 for pavements with a tied concrete shoulder  
 $N_i$  = allowable number of repetitions for each axle group

The erosion damage calculated in this fashion was used as a cluster variable to develop the following models for predicting faulting of doweled and nondoweled jointed concrete pavements:

$$\text{FAULTND} = \text{EROSION}^{0.25} [9.75873 \times 10^{-4} * (\text{Precip})^{0.91907} + 0.0060291 * \text{JS}^{0.54428} - 0.016799 * \text{DRAIN}] \quad (9)$$

$$\text{FAULTD} = \text{EROSION}^{0.25} [0.0038332 * (\text{Precip}/10)^{1.84121} + 0.0057763 * \text{JS}^{0.38274}] \quad (10)$$

where

- $\text{FAULTND}$  = mean faulting at nondoweled transverse pavement joints, in  
 $\text{EROSION}$  = calculated accumulated erosion  
 $\text{Precip}$  = annual precipitation, in  
 $\text{JS}$  = joint spacing, ft  
 $\text{DRAIN}$  = dummy variable for the presence of edge drains  
 $\text{FAULTD}$  = mean faulting at doweled transverse pavement joints, in

Other mechanistic-empirical faulting models have been developed based on the concept of damage estimated from the pavement's corner deflection. Equations 11 and 12 are examples of some of the models developed to estimate the allowable number of load repetitions:<sup>(27)</sup>

$$\text{Log } N_d = 0.5064 / (D_f)^{0.312} \quad (D_f = w^2 / hk^{-1.27} > 1.862 \times 10^{-4}) \quad (11)$$

$$\text{Log } N_d = 3.749 \times 10^{-22} / (D_f)^{5.96} \quad (D_f = w^2 / hk^{-1.27} < 1.862 \times 10^{-4}) \quad (12)$$

where

- $N_d$  = number of load repetitions before critical damage  
 $D_f$  = damage index  
 $w$  = corner deflection  
 $h$  = pavement thickness  
 $k$  = subgrade reaction modulus

### Faulting Model Development Approach

Based on the review of literature and previous models, an approach similar to the PCA procedure was adopted for development of a mechanistic-empirical model for predicting faulting.<sup>(26, 27)</sup> It involved the identification of a mechanistic parameter that could be related to the damage that causes faulting. The mechanistic parameter that was selected is the differential elastic deformation energy (DE) imposed on the underlying base, subbase, or subgrade at the slab corner.<sup>(22, 28, 29, 30)</sup>

The differential elastic deformation energy imposed on the underlying material by traffic loads is related to the differential deflection at the joint. The pore water pressure generated by the differential energy imposed on the slabs is responsible for the erosion and ejection of fine material from underneath the slab. The differential elastic deformation energy was used as a mechanistic response parameter for predicting the allowable number of cycles of 80-kN equivalent single axle load (ESAL) applications to failure. This approach was used successfully to develop similar models for predicting faulting for cost allocation purposes.<sup>(12)</sup>

### Preliminary Model Form

With DE selected as the mechanistic parameter to relate to faulting, it is possible to use Miner's linear damage hypothesis to determine the total damage that is accumulated by a pavement from repeated 80-kN ESAL load applications. However, in recognition of the effect of other non-load factors such as the pumping potential of the underlying material and the environment, the following general model form was selected for consideration as a faulting model:

$$\text{FAULT} = (\text{FDAMAGE})^\beta C \quad (13)$$

where

|         |   |  |
|---------|---|--|
| FAULT   | = | mean joint faulting, mm  |
| C       | = | erodibility scaling factor related to the pumping potential of the underlying material and the environment |
| $\beta$ | = | regression coefficient   |
| FDAMAGE | = | accumulated faulting damage = $\sum n/N_f$   |
| n       | = | actual number of 80-kN ESAL's  |
| $N_f$   | = | allowable number of 80-kN ESAL's to failure related to the differential elastic deformation energy, DE     |

Although this model assumes that the faulting damage ( $\text{FDAMAGE} = \sum n/N_f$ ) due to load applications accumulates linearly with the number of 80-kN ESALs, there is a non-linear relationship between the total damage and predicted faulting. The scaling factor, C, accounts for the interaction between the load causes of faulting and the other non-load-related factors described previously that contribute to faulting. This model form meets the boundary conditions for faulting; faulting is equal to zero when there are no load applications, and faulting increases early in the life of the pavement and levels off after early load applications.

### Mechanistic Response Parameter

A procedure for calculating DE for pavements was developed for use in the development of the faulting model. The concept of a deflection-based deformation energy criterion has been used several times in the past for pavement research.<sup>(22, 28, 29, 30)</sup> The Purdue Method for Analysis of Rigid Pavements (PMARP) to compute the volume of materials pumped from beneath a loaded slab was developed in 1984.<sup>(22)</sup> The volume of pumped materials was defined as a function of the deformation energy imposed on the pavement by a load, which was defined as follows:

$$DE = \sum_{i=1}^n k_i A_i \Delta_i^2 \quad (14)$$

where

- DE = deformation energy imposed by an axle load, kN mm  
 $k_i$  = modulus of subgrade reaction, kN/mm<sup>3</sup>  
 $A_i$  = area associated with node i, mm<sup>2</sup>  
 $\Delta_i$  = deflection at node i, mm

In this model, only those nodes within the finite element mesh with deflections over 0.5 mm are considered significant to pumping. However, there is ample empirical and laboratory evidence to suggest that even lesser deflections can lead to pumping and faulting.<sup>(13, 23, 25)</sup>

As a wheel load crosses a joint, the difference in the elastic deformation energy between the loaded (leave) slab and the unloaded (approach) slab is directly related to the pore water pressure generated and the resultant volume of material that is pumped from beneath the load slab. Therefore, a response parameter that can be related to pumping and faulting is the difference between the elastic deformation energy per unit area imposed on the loaded and unloaded slabs, defined as follows:

$$DE = E_L - E_{UL} \quad (15)$$

where

- DE = differential elastic deformation energy per unit area between the loaded and unloaded slab, kN/mm  
 $E_L$  = elastic deformation energy per unit area imposed on the loaded slab, kN/mm  
 $E_{UL}$  = elastic deformation energy imposed on the unloaded slab, kN/mm

The elastic deformation energy in equation 15 is defined as follows:

$$E = \frac{1}{2} w p \quad (16)$$

where

- E = elastic deformation energy per unit area, kN/mm  
w = slab's deflection at the joint, mm  
p = pressure at the slab-foundation interface at the joint, kN/mm<sup>2</sup>

If the underlying material is modeled as a Winkler foundation, the pressure at the slab-foundation interface can be determined from the following equation:

$$p = k w \quad (17)$$

where

$p$  = pressure at the slab-foundation interface,  $\text{kN/mm}^2$   
 $k$  = modulus of subgrade reaction,  $\text{kN/mm}^3$

Substituting equation 17 into equation 16 results in the following relationship:

$$E = \frac{1}{2} k w^2 \quad (18)$$

Therefore, DE can be defined as follows:

$$DE = 1.84k (w_L^2 - w_{UL}^2) \quad (19)$$

The validity of relating DE to faulting can be checked by examining the following form of equation 19:

$$DE = 1.84k (w_L + w_{UL})(w_L - w_{UL}) \quad (20)$$

The term  $(w_L - w_{UL})$  is the differential corner deflection between the loaded and unloaded slabs. It represents the relative movement between the loaded and unloaded slabs and is an indication of the amount of load transfer present at the joint. The higher the difference (i.e., inadequate load transfer), the higher the joint faulting will be. Without any differential deflections at the corner (perfect load transfer), there will be no faulting. The term  $(w_L + w_{UL})$  is equivalent to the free-edge corner deflection  $w_{fe}$  and is defined as follows:

$$w_{fe} = w_L + w_{UL} \quad (21)$$

It represents the total flexibility of the slab at the joint. The higher the slab's flexibility, the higher the potential for joint deterioration and faulting. This increases the resulting differential corner deflections. These observations support use of the differential elastic deformation energy as a response parameter to model faulting.

### **Determination of Differential Elastic Deformation Energy**

The corner deflections of the loaded and unloaded slabs at the joint are required to calculate the differential elastic deformation energy. These corner deflections are dependent on pavement design features such as the load transfer at the joint, material strength properties, saturation level of the underlying materials, and the applied loads. Finite element analysis presents the best approach for calculating these required deflections. However, since it is impractical to use finite element analysis every time the model is used, simple deflection prediction equations were developed for use in calculating the deflections.

#### **Loaded and Unloaded Corner Deflections**

Following is a general equation for calculating the free-edge corner deflection for a load placed along the joint based on Westergaard's free corner deflection equation:<sup>(31)</sup>

$$w_{fe} = w_L + w_{UL} = \alpha * P / k \ell^2 \quad (22)$$

where

|          |   |  |
|----------|---|--|
| $w_{fe}$ | = | free corner deflection, mm                       |
| $\alpha$ | = | nondimensional scale factor                      |
| $P$      | = | applied load, kN                                 |
| $k$      | = | modulus of subgrade reaction, kN/mm <sup>3</sup> |
| $\ell$   | = | radius of relative stiffness, mm                 |

This equation takes the applied load, modulus of subgrade reaction, and radius of relative stiffness into consideration for calculation of the corner deflection. The nondimensional scale factor takes into account factors such as the distance of the load from the corner and the type and configuration of the load.

Another parameter critical to faulting is the load transfer at the corner, which is defined as follows:

$$LTE = w_{UL} / w_L \quad (23)$$

where

|          |   |                                 |
|----------|---|---------------------------------|
| LTE      | = | corner load transfer efficiency |
| $w_{UL}$ | = | unloaded slab corner deflection |
| $w_L$    | = | loaded slab corner deflection   |

For any pavement, if the free-edge corner deflection and the load transfer across the joint of a pavement at the corner are known, the unloaded corner deflection can be calculated as follows:

$$w_{UL} = w_{fe} * (LTE) / (1 + LTE) \quad (24)$$

The loaded corner deflection can then be calculated from the corner LTE and the unloaded corner deflection in the following manner:

$$w_L = w_{UL} / LTE \quad (25)$$

Therefore, if equations are available for calculating the free-edge corner deflection and the corner load transfer, both the unloaded and loaded corner deflections can be calculated. This was accomplished by developing prediction equations for calculating the free-edge corner deflection and the corner load transfer efficiency. The results from finite element runs for a factorial of pavement design features that cover a wide range of field conditions were used to develop the models.

### Finite Element Analysis

The finite element analysis program ILLI-SLAB was used in the analysis of a factorial of pavement design features to develop the regression equations for calculating the free-edge corner deflection and corner load transfer efficiency. The factorial was designed to cover the range of

pavement parameters covered by the GPS 3 sections, as well as those expected to be encountered in the field. Additionally, two nondimensional parameters,  $L/\ell$  and  $AGG/k\ell$ , were used to minimize the number of cases that had to be analyzed. The  $L/\ell$  ratio gives an indication of the effect of slab size on the corner deflection, where  $L$  is the joint spacing and  $\ell$  is the radius of relative stiffness.  $AGG/k\ell$  and  $\ell$  are defined as follows:

$$AGG/k\ell = AGG_0 \exp[1 + aD^\alpha - b(L/\ell)] \quad (26)$$

$$\ell^4 = E \cdot h^3 / [12 \cdot k(1 - \mu^2)] \quad (27)$$

where

|                       |   |                                      |
|-----------------------|---|--------------------------------------|
| AGG                   | = | load transfer factor, kPa            |
| D                     | = | dowel diameter, mm                   |
| L                     | = | joint spacing, m                     |
| $\ell$                | = | radius of relative thickness, mm     |
| $AGG_0, a, b, \alpha$ | = | regression coefficients              |
| E                     | = | modulus of PCC slab, kPa             |
| h                     | = | slab thickness, mm                   |
| k                     | = | modulus of subgrade reaction, kPa/mm |
| $\mu$                 | = | Poisson's ratio                      |

$AGG/k\ell$  is essentially a nondimensional load transfer factor that is directly related to the joint load transfer efficiency. Following a review of the LTPP database, the pavement parameters and ranges given in table 3 were selected for use in the factorial analysis. The basic model used for the finite element analysis is shown in figure 2 and consisted of four adjacent slabs in the longitudinal direction. Slabs in the transverse direction were used in the analysis because the finite element analysis showed that, even when loaded, they did not significantly affect the pavement's corner deflections. However, the analysis showed that all the wheels on an axle influenced corner deflection; therefore, the entire axle was considered in the analysis.

Table 3. Pavement parameters and range of values used in corner deflection model development.

| Variable                             | Range of Values   |
|--------------------------------------|-------------------|
| Load, kN                             | 80-kN ESAL        |
| Load transfer factor, kPa            | 185 to 400        |
| Outer wheel distance from corner, mm | 0 to 915          |
| Slab length, mm                      | 4600              |
| Slab width, mm                       | 3600              |
| AGG/ $k\ell$                         | 0.0171 to 3701    |
| $L/\ell$                             | 3.1 to 6.7        |
| Modulus of concrete, kPa             | $34.5 \cdot 10^6$ |
| Modulus of subgrade reaction, kPa/mm | 27                |
| Poisson's ratio                      | 0.15              |

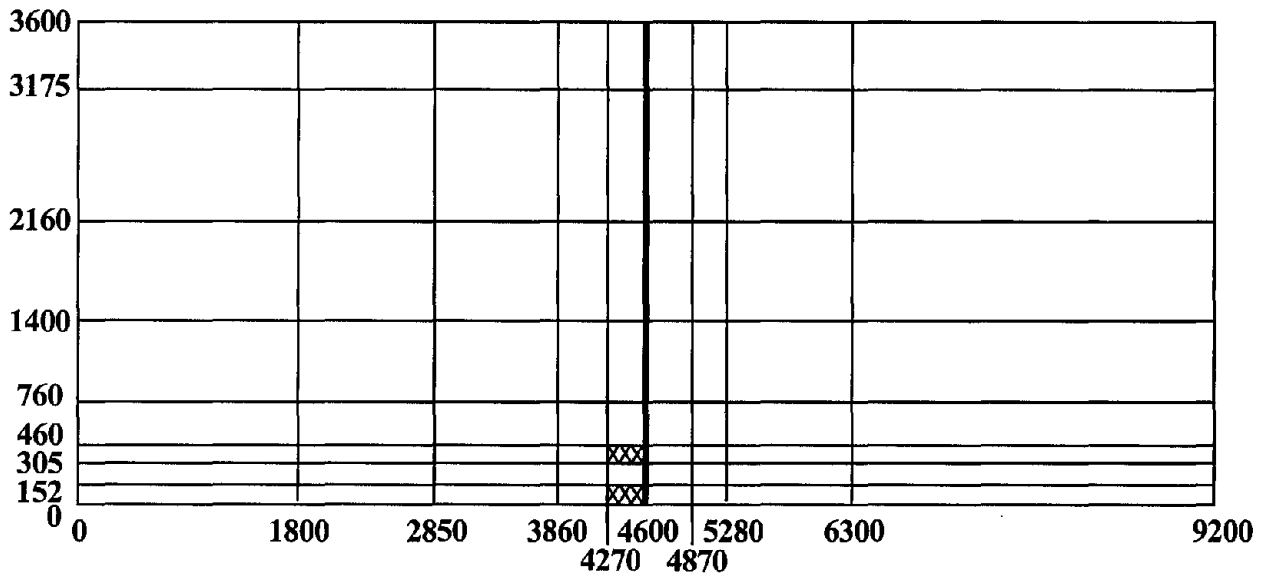


Figure 2. Finite element model.



## Free-Edge Corner Deflection Model

The highest deflection at the corner of a slab occurs when the load is placed at the outside edge of a pavement without edge support or tied shoulders. As the load is placed at increasing distances inward from the unsupported pavement edge, the magnitude of stress and deflection at the corner decreases.

Studies on pavement encroachment show that most trucks are driven with the outside wheels placed about 460 to 610 mm from the edge, and only approximately 6 percent of trucks run with their wheels placed at the edge.<sup>(32)</sup> To take this distribution into account, it was decided to develop models for predicting deflections for loads placed along the joint anywhere between 0 and 915 mm from the edge.

From the results obtained, the following equations were developed for calculating the free-edge corner deflection for an 80-kN ESAL placed at the corner (i.e., 0 mm from the corner) and 915 mm from the corner, respectively:

$$w_{fe, x=0} = (0.1051 \ell^2 + 87.18 \ell + 231473)/k\ell^2 \quad (28)$$

$$w_{fe, x=915} = (0.078 \ell^2 + 123.6 \ell - 19993)/k\ell^2 \quad (29)$$

where

|          |   |                                      |
|----------|---|--------------------------------------|
| $w_{fe}$ | = | free-edge corner deflection, mm      |
| $k$      | = | modulus of subgrade reaction, kPa/mm |
| $\ell$   | = | radius of relative stiffness, mm     |

Regression analysis of the results obtained from these models and those from finite element analysis runs showed that the models estimated deflections with reasonable accuracy.

## Load Transfer Efficiency Models

As noted, equations 28 and 29 calculate the free-edge corner deflections for pavements with no load transfer. However, for most pavements, there is some load transfer across adjacent slabs, either through aggregate interlock or by the provision of dowels. The free-edge corner deflections calculated should therefore be corrected for the effect of load transfer. This requires knowledge of the load transfer across the pavement slabs.

Several studies have developed models from finite element analysis for calculating load transfer for wheel loads placed close to the corner of a pavement slab. Two such equations are provided as equations 30 and 31. Equation 30 was developed for calculating load transfer efficiency (LTE) for a load placed at the corner of a slab, and equation 31 was developed for calculating the LTE for a load placed 915 mm from the slab corner.<sup>(2, 3)</sup>

$$LTE_{x=0} = 1/[1 + 1.2*(AGG/K\ell)^{-0.849}] \quad (30)$$

$$LTE_{x=915} = 1/[1 + 0.3483*(AGG/K\ell)^{-1.13677}] \quad (31)$$

where

LTE = load transfer efficiency, percent  
x = distance of load from corner, mm  
AGG/kℓ = nondimensional load transfer factor

A linear relationship exists between the load transfer calculated for loads placed between 0 and 915 mm from the corner of a slab. Therefore, equations 30 and 31 can be used to calculate the corner LTE for any load placed between 0 and 915 mm from the slab corner by linear interpolation between  $LTE_{x=0}$  and  $LTE_{x=915}$ .

#### Calculation of Corner Deflections for Loaded and Unloaded Slabs

Using equations 28 through 31, the unloaded corner deflection for an 80-kN ESAL placed at a distance of 0 or 915 mm from the corner can be calculated as follows:

$$w_{UL} = w_{fe, x=0 \text{ or } 915 \text{ mm}} * (LTE_{x=0 \text{ or } 915 \text{ mm}}) / (1 + LTE_{x=0 \text{ or } 915 \text{ mm}}) \quad (32)$$

The unloaded corner deflection for an axle load placed at any distance between 0 and 915 mm from the corner can be determined by interpolating between the results obtained for  $x = 0$  and  $x = 915$  mm. This result was verified using the results obtained from finite element analysis. The loaded corner deflection can then be calculated from the unloaded corner deflection and the corner LTE as follows:

$$w_L = w_{UL} / LTE \quad (33)$$

#### Calculation of Differential Elastic Deformation Energy

On the basis of equations developed in the preceding section, following is a procedure that was used to obtain estimates of the differential elastic deformation energy for the LTPP sections for use in the model development. In this study, an axle load with the outer wheel placed 305 mm from the corner was considered. This procedure is also required for calculating the differential elastic deformation energy, DE, for use in the final model that was developed.

1. Calculate the nondimensional load transfer factor,  $AGG/k\ell$ , using equation 26 (use its final form, equation 39, for the final model).
2. Using equations 28 and 29, calculate the deflections,  $w_{fe}$ , using the values of  $\ell$  and  $k$  for the pavement and with the load,  $P$ , placed at  $x = 0$  and  $x = 915$  mm.
3. Calculate LTE at  $x = 0$  and  $x = 915$  mm using equations 30 and 31 and the value of  $AGG/k\ell$  from step 1.

4. Correct the free-edge deflections,  $w_{fe}$ , for corner LTE at  $x = 0$  and 915 mm to obtain the unloaded slab corner deflections,  $w_{UL}$ , at  $x = 0$  and  $x = 915$  mm using equation 32.
5. Calculate  $w_{UL}$  at  $x = 305$  mm by interpolating between the unloaded slab deflections at  $x = 0$  and 915 mm.
6. Calculate the loaded corner deflection,  $w_L$ , at  $x = 305$  mm using equation 33.
7. With  $w_{UL}$  and  $w_L$  at 305 mm, calculate the differential elastic deformation energy, DE, for an 80-kN axle placed 305 mm from the corner using equation 19.

### **Data Preparation and Evaluation**

The next step in the model development was preparation and evaluation of the data available from the GPS 3 sections in order to determine the plausibility of the preliminary model form and to gain further insight about the variables that influence faulting. The database of GPS 3 pavement sections that was created was checked thoroughly for gross errors, cleaned, and prepared for analysis. A comprehensive statistical analysis of the cleaned data was conducted to evaluate the preliminary relationships between the measured faulting and several explanatory variables.

Table 4 is a correlation table that shows the strength of the relationships between the explanatory variables and faulting, as well as the relationship between the variables themselves. The definitions of the variables in table 4 are provided in table 5. Although the results do not show very strong relationships between the independent variables and faulting, several interesting trends are evident. The variables with the highest positive correlations to faulting are cumulative ESAL's and age.

Table 4. Correlation matrix for selected variables for jointed PCC pavement faulting.\*

|         | HPCC     | k-value  | JTSP     | DOWDIA   | DT       | FI       | PRECIP   | WTDYS    | MEANT    | AGE      | ESAL     | EPCC     | LTC      | Cd       | BT       | ST       | FAULT    |
|---------|----------|----------|----------|----------|----------|----------|----------|----------|----------|----------|----------|----------|----------|----------|----------|----------|----------|
| HPCC    | 1        | 0.20058  | 0.04567  | 0.16603  | 0.04809  | -0.14939 | -0.04082 | -0.18801 | 0.03885  | -0.09302 | 0.0706   | 0.02911  | -0.24665 | -0.04158 | 0.0478   | -0.19419 | -0.18126 |
| k-value | 0.20058  | 1        | 0.02185  | -0.01931 | 0.10616  | -0.32218 | 0.07737  | 0.05085  | 0.34421  | -0.23584 | 0.04577  | -0.05402 | -0.08062 | 0.33438  | 0.18896  | 0.24932  | 0.04164  |
| JTSP    | 0.04567  | 0.02185  | 1        | 0.30383  | 0.20279  | -0.37042 | 0.5018   | 0.28681  | 0.34266  | 0.3585   | 0.43957  | -0.26813 | -0.22995 | -0.02778 | 0.10025  | -0.09234 | 0.12074  |
| DOWDIA  | 0.16603  | -0.01931 | 0.30383  | 1        | 0.10763  | -0.12995 | 0.40269  | 0.26912  | 0.08382  | -0.16885 | -0.04356 | -0.16687 | -0.90703 | -0.37105 | -0.02979 | -0.28474 | -0.27488 |
| DT      | 0.04809  | 0.10616  | 0.20279  | 0.10763  | 1        | -0.05898 | 0.13129  | 0.21816  | 0.0227   | -0.08369 | 0.24234  | -0.19285 | -0.0931  | 0.17399  | 0.07708  | -0.03085 | 0.0149   |
| FI      | -0.14939 | -0.32218 | -0.37042 | -0.12995 | -0.05898 | 1        | -0.40791 | -0.06858 | -0.86655 | -0.23369 | -0.26391 | -0.06718 | 0.21947  | -0.30104 | -0.40403 | -0.0306  | -0.16442 |
| PRECIP  | -0.04082 | 0.07737  | 0.5018   | 0.40269  | 0.13129  | -0.40791 | 1        | 0.7998   | 0.53686  | 0.20402  | 0.30838  | -0.1409  | -0.32447 | -0.13718 | -0.0112  | -0.00776 | 0.1984   |
| WTDYS   | -0.18801 | 0.05085  | 0.28681  | 0.26912  | 0.21816  | -0.06858 | 0.7998   | 1        | 0.25122  | 0.16788  | 0.25769  | -0.00947 | -0.19399 | -0.22116 | -0.21582 | 0.08471  | 0.26939  |
| MEANT   | 0.03885  | 0.34421  | 0.34266  | 0.08382  | 0.0227   | -0.86655 | 0.53686  | 0.25122  | 1        | 0.12936  | 0.29552  | 0.07864  | -0.12578 | 0.39311  | 0.3522   | 0.15304  | 0.22041  |
| AGE     | -0.09302 | -0.23584 | 0.3585   | -0.16885 | -0.08369 | -0.23369 | 0.20402  | 0.16788  | 0.12936  | 1        | 0.4926   | -0.07957 | 0.21124  | -0.18921 | -0.2184  | -0.1231  | 0.23186  |
| ESAL    | 0.0706   | 0.04577  | 0.43957  | -0.04356 | 0.24234  | -0.26391 | 0.30838  | 0.25769  | 0.29552  | 0.4926   | 1        | -0.17086 | 0.05907  | -0.01568 | -0.12794 | -0.04847 | 0.1522   |
| EPCC    | 0.02911  | -0.05402 | -0.26813 | -0.16687 | -0.19285 | -0.06718 | -0.1409  | -0.00947 | 0.07864  | -0.07957 | -0.17086 | 1        | 0.21413  | 0.1227   | -0.02004 | 0.17256  | 0.03083  |
| LTC     | -0.24665 | -0.08062 | -0.22995 | -0.90703 | -0.0931  | 0.21947  | -0.32447 | -0.19399 | -0.12578 | 0.21124  | 0.05907  | 0.21413  | 1        | 0.295    | -0.03455 | 0.28067  | 0.27485  |
| Cd      | -0.04158 | 0.33438  | -0.02778 | -0.37105 | 0.17399  | -0.30104 | -0.13718 | -0.22116 | 0.39311  | -0.18921 | -0.01568 | 0.1227   | 0.295    | 1        | 0.54272  | 0.69938  | 0.15073  |
| BT      | 0.0478   | 0.18896  | 0.10025  | -0.02979 | 0.07708  | -0.40403 | -0.0112  | -0.21582 | 0.3522   | -0.2184  | -0.12794 | -0.02004 | -0.03455 | 0.54272  | 1        | 0.17969  | -0.09411 |
| ST      | -0.19419 | 0.24932  | -0.09234 | -0.28474 | -0.03085 | -0.0306  | -0.00776 | 0.08471  | 0.15304  | -0.1231  | -0.04847 | 0.17256  | 0.28067  | 0.69938  | 0.17969  | 1        | 0.09891  |
| FAULT   | -0.18126 | 0.04164  | 0.12074  | -0.27488 | 0.0149   | -0.16442 | 0.1984   | 0.26939  | 0.22041  | 0.23186  | 0.1522   | 0.03083  | 0.27485  | 0.15073  | -0.09411 | 0.09891  | 1        |

\*See table 5 for definitions.

Table 5. Definitions of selected variables significant to joint faulting of JCP.

| Symbol    | Potential Independent Variable                                |
|-----------|---|
| $H_{PCC}$ | PCC slab thickness, mm  |
| k-value   | Static backcalculated k-value, kPa/mm                         |
| JTSP      | Mean transverse joint spacing, m                              |
| DOWDIA    | Dowel diameter, mm  |
| DT        | Presence of edge drain, 0=no edge drain, 1=edge drain present |
| FI        | Freezing index, degree-days ( $^{\circ}$ C) below freezing    |
| PRECIP    | Average annual precipitation, mm                              |
| WTDYS     | Number of days precipitation > 12.7 mm in a year              |
| MEANT     | Average mean daily temperature, $^{\circ}$ C                  |
| AGE       | Time since pavement construction, yr                          |
| ESAL      | Cumulative equivalent 80-kN single axle load                  |
| $E_{PCC}$ | PCC slab modulus of elasticity, kPa                           |
| LTC       | AASHTO load transfer coefficient, J-Factor                    |
| Cd        | Time since pavement construction, yr                          |
| BT        | Base type, 0=erodible and 1=nonerodible                       |
| ST        | Subbase type, 0=fine and 1=coarse                             |
| FAULT     | Mean edge joint faulting, mm                                  |

Faulting is, of course, strongly related to the number of heavy axle loads passing over a joint that cause differential deflections. The number of wet days and precipitation level are also positively correlated to faulting, supporting the empirical evidence that higher levels of moisture in the pavement will result in more faulting. There is also an indication that base type and dowel diameter are negatively correlated to faulting; that is, a nonerodible base and larger dowel diameter will result in less faulting. A pictorial representation of some of these trends is shown in the bivariate plots in figure 3.

### Erodibility Scaling Factor

The scaling factor, C, in equation 13 accounts for important factors that interact with the differential elastic deformation energy at the joint to cause pumping and faulting, but that cannot yet be fully described with mechanistic response parameters. The factors include the type and

erodibility of the underlying pavement layers, the environment, drainage, and other pavement features. Mainly, these factors influence the pumping potential of the base, subbase, or subgrade beneath the PCC slab and are collectively represented by the erodibility factor.

The degree to which the underlying materials pump or erode when subjected to heavy wheel loads depends on the material type, physical properties, and level of saturation. The level of saturation of the pavement materials depends on the environment and the drainage provided. Therefore, the challenge is to select the components of the scaling factor that account for these effects as much as possible. Several model forms and variables were selected to be used for defining the erodibility factor. Based on the results of past studies and evaluation of the data for the GPS 3 concrete pavements from the correlation analysis and stepwise regression, the following model form and variables were selected as the most promising for defining the erodibility factor:

$$C = \beta_0 + \beta_1 \text{WETDAYS} - \beta_2 \text{DOWDIA} - \beta_3 C_d (\beta_4 + \text{BASE}) \quad (34)$$

where

|   |   |  |
|---|---|--|
| C   | = | erodibility scaling factor                             |
| WETDAYS                                       | = | number of days with precipitation greater than 12.7 mm |
| DOWDIA  | = | dowel diameter, mm                                     |
| $C_d$   | = | drainage coefficient                                   |
| BASE  | = | base or subbase type, 0=erodible, 1=nonerodible        |
| $\beta_0, \beta_1, \beta_2, \beta_3, \beta_4$ | = | regression constants                                   |

For all types of pavement materials, pumping and faulting can be magnified by environmental factors such as the amount of precipitation, freeze-thaw damage, depth of frost penetration, thermal expansion of the slab, and daytime slab curling.

Evaluation of the GPS 3 data showed that the number of days with precipitation greater than 12.7 mm was relatively highly correlated with faulting, and was therefore selected to account for the general effect of the environment in the scaling factor. Past results show a similar significant effect of precipitation on faulting.<sup>(3, 10)</sup> Another variable included in the scaling factor is dowel diameter. Although dowel diameter is considered in the calculation of the load transfer parameter in equation 26, there is strong evidence from past models that dowels are significant to faulting.<sup>(3,</sup>

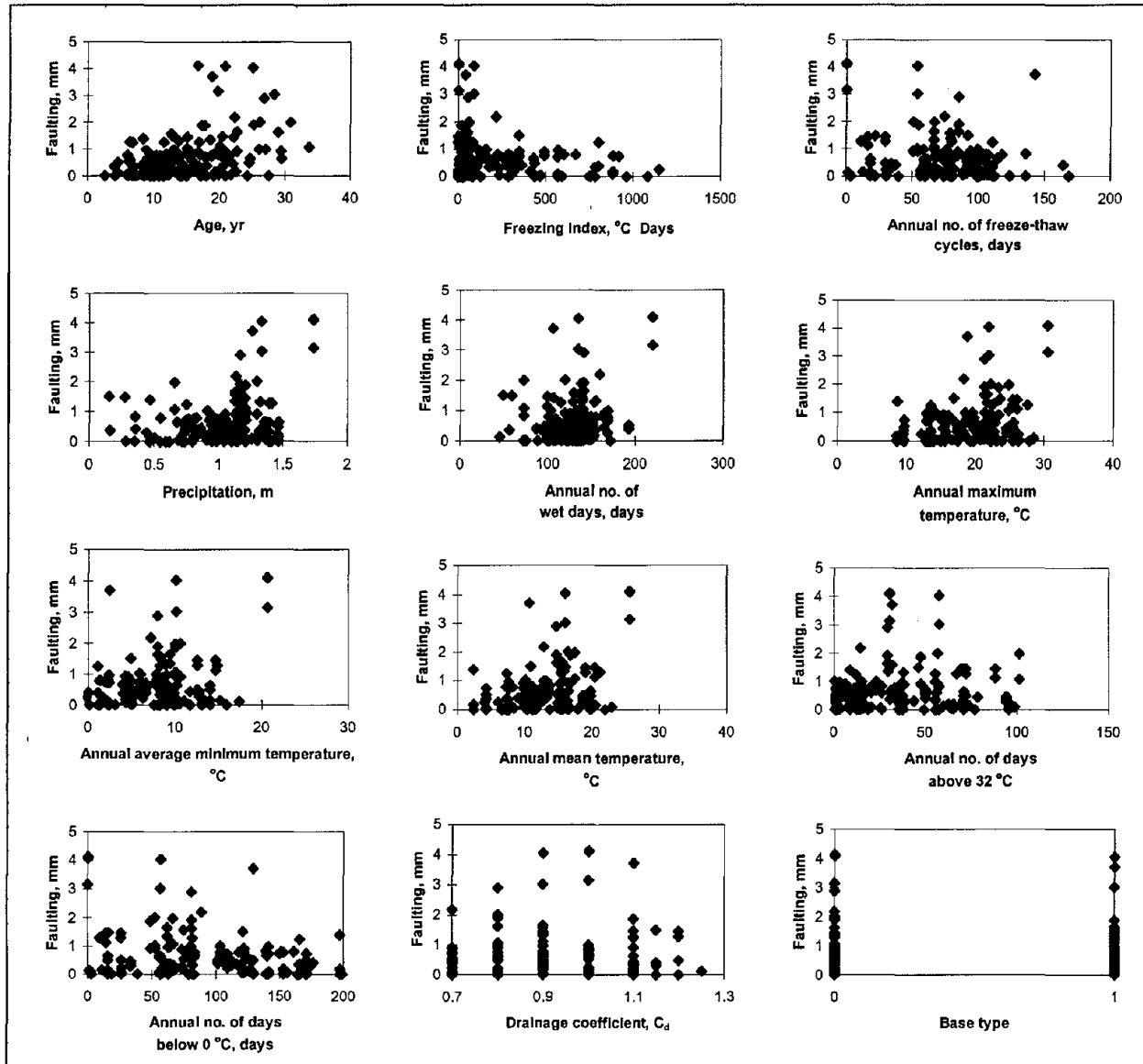


Figure 3. Plot of mean joint faulting versus significant variables for jointed PCC pavement.

The results from the correlation studies also show that dowel diameter is very significant to faulting. Consequently, dowel diameter was also included.

The drainage coefficient,  $C_d$ , used in the scaling factor is a modified version of the American Association of State Highway and Transportation Officials (AASHTO) drainage coefficient introduced in the AASHTO rigid pavement design procedure in 1986.<sup>(33)</sup> It accounts for the pavement's ability to drain excessive moisture from within the structure, as well as the pavement's potential to be exposed to near-saturated conditions. It considers precipitation, base and underlying soil type, permeability of the underlying material, and the presence of edge drains. This makes it possible for factors that are not included directly in the faulting model to be accounted for. For this study, the drainage coefficients for the GPS 3 pavement sections were determined from the simplified matrix presented in table 6.<sup>(10)</sup> This matrix is based on the

original AASHTO drainage coefficients and several additional recommendations that account for the base type and other material properties.

The type of base or subbase has a strong influence on faulting. A nonerrodible base increases the resistance of the pavement structure to erosion. In unbound granular materials such as dense-graded aggregates, pore water pressure buildup is the main factor that causes horizontal and vertical movement of materials.<sup>(34, 35, 36, 37)</sup> In stabilized materials such as lean concrete, cement-treated base (CTB), or soil-cement subbases, surface erosion of the material is of main concern. For all base types, degradation, aggregate abrasion and fracture resistance, and stability under repeated loads are some of the other factors that influence pumping and faulting. Therefore, a variable was also included in the scaling factor to account for the type of base. Because of the strong interaction between the drainage coefficient and base type, it was considered important to model the interaction between those two variables in the scaling factor.

It is recognized that the factors selected for inclusion in equation 34 are not exhaustive. For example, it was found that vehicle speed affects the pore water pressure under a slab.<sup>(23, 38)</sup> Similar analysis and results showed that the use of skewed joints and an increase in joint opening decrease the water expulsion velocity under the slab and, therefore, reduce pumping and faulting.<sup>(39)</sup> Paradoxically, a larger joint opening will increase joint deterioration and increase the potential for faulting. Such additional factors can be considered in future improvements of the faulting model.

### **Faulting Model Formulation**

From the results of the analysis conducted, the final model form for predicting joint faulting that was selected for calibration consisted of the following key parts:

- A model for calculating the allowable number of load applications to reach a critical level of faulting as a function of DE.
- A model for predicting faulting.



Table 6. Matrix for selection of the overall drainage coefficient,  $C_d$ .<sup>(10)</sup>

| Edge Drains | Precipitation Level | Fine-Grained Soils |                | Coarse-Grained Soils |                |
|-------------|---------------------|--------------------|----------------|----------------------|----------------|
|             |                     | Nonpermeable Base  | Permeable Base | Nonpermeable Base    | Permeable Base |
| No          | Wet                 | 0.70-0.90          | 0.85-0.95      | 0.75-0.95            | 0.90-1.00      |
|             | Dry                 | 0.90-1.10          | 0.95-1.10      | 0.90-1.15            | 1.00-1.15      |
| Yes         | Wet                 | 0.75-0.95          | 1.00-1.10      | 0.90-1.10            | 1.05-1.15      |
|             | Dry                 | 0.95-1.15          | 1.10-1.20      | 1.10-1.20            | 1.15-1.20      |

Notes: 1. Fine-grained = A-1 through A-3 classes  
 2. Coarse-grained = A-1 through A-3 classes  
 3. Permeable base =  $k = 300$  m/day or  $C_U < 6$   
 4. Wet climate = Precipitation  $> 635$  mm/yr  
 5. Dry climate = Precipitation  $\leq 635$  mm/yr  
 6. Select midpoint of range and use other drainage features to adjust upward or downward.

#### Allowable Number of Load Repetitions

The allowable number of load repetitions to failure,  $N_p$ , is a function of the differential elastic deformation energy, DE. DE is calculated from equation 19 and requires the determination of the corner deflections and the load transfer efficiency using equations 28 through 33. This, in turn, requires calculation of the nondimensional load transfer factor, given as follows:

$$AGG/k\ell = AGG_0 \exp[1 + aD^\alpha - b(L/\ell)] \quad (35)$$

where

AGG = load transfer factor, kPa  
 D = dowel diameter, mm  
 L = joint spacing, m  
 $\ell$  = radius of relative thickness, mm  
 AGG<sub>0</sub>, a,  $\alpha$ , b = regression coefficients

To determine the model form to use for estimating  $N_p$ , several model forms were obtained from the literature and were tested for their suitability for fitting the available data.<sup>(40)</sup> The model form with the best fit for estimating the number of allowable axle passes a slab can endure before reaching critical faulting that was selected is as follows:<sup>(3)</sup>

$$\text{Log } N = \alpha_1 - \alpha_2 * \text{Log}(DE + 1) \quad (36)$$

where

N = allowable number of 80-kN axle loads  
 DE = differential elastic deformation energy calculated from equation 19  
 $\alpha_1, \alpha_2$  = regression coefficients

According to the functional form, as DE increases, the allowable number of repetitions decreases. Furthermore, if DE is zero, the allowable number of repetitions practically approaches an infinite number of 80-kN load applications and faulting damage will not occur. Although this model is not unique, on the basis of the mechanistic understanding of faulting, it provides a logical equation for calculating N.

### Faulting Prediction Model

From the results of the analysis presented, the final model form selected for predicting joint faulting is as follows:

$$\text{FAULT} = \text{FDAM}^{\beta} [\beta_0 + \beta_1 \text{WETDAYS} - \beta_2 \text{DOWDIA} - \beta_3 C_d (\beta_4 + \text{BASE})] \quad (37)$$

where

FAULT = mean joint faulting, mm  
 FDAM = accumulated faulting damage =  $\sum n/N$   
 n = actual number of 80-kN ESAL's  
 $N_f$  = allowable number of 80-kN ESAL's calculated from equation 35  
 WETDAYS = number of days with precipitation greater than 0.254 mm  
 DOWDIA = dowel diameter, mm  
 $C_d$  = drainage coefficient  
 BASE = base or subbase type, 0=erodible, 1=nonerodible  
 $\beta, \beta_0, \beta_1, \beta_2, \beta_3, \beta_4$  = regression constants

### Faulting Model Calibration

Calibration of equations 35 through 37 using the LTPP data for GPS 3 was the final step in development of the prediction model for JPCP faulting. A combination of optimization techniques and nonlinear regression analysis was used to determine the values of the parameters in those equations that provide the best fit for the LTPP data. The criterion used was minimization of the error between the actual field faulting and the predicted faulting. The procedure that was used is as follows:

1. For nonlinear regression analysis, initial values were assigned to the load transfer factor parameters ( $AGG_0$ , a, b, and  $\alpha$  in equation 35) to calculate the nondimensional load transfer factor,  $AGG/k\ell$ .
2. With the calculated  $AGG/k\ell$ , the LTE,  $W_L$ ,  $W_{UL}$ , and DE were calculated for each section.

3. For nonlinear regression analysis, initial values were assigned to  $\alpha_1$  and  $\alpha_2$  in equation 36 and the number of load applications to failure,  $N_p$ , was calculated for every section.
4. From the actual traffic load level and the corresponding number of load applications to failure,  $N_p$ , the accumulated damage,  $n/N_p$ , corresponding to the faulting level measured on each section was calculated.
5. For the assigned values of the aggregate interlock (equation 35) and damage model (equation 36) parameters  $AGG_0$ ,  $a$ ,  $b$ ,  $\alpha$ ,  $\alpha_1$  and  $\alpha_2$ , nonlinear regression analysis was performed to find the values of the faulting model (equation 37) parameters  $\beta$ ,  $\beta_0$ ,  $\beta_1$ ,  $\beta_2$ ,  $\beta_3$ , and  $\beta_4$  that minimize the following objective function:

$$\text{Minimize} = \Sigma (\text{Measured}_{\text{Fault}} - \text{Predicted}_{\text{Fault}})^2 \quad (38)$$

6. For different assigned values of the aggregate interlock parameters ( $AGG_0$ ,  $a$ ,  $b$ , and  $\alpha$ ) and damage model parameters ( $\alpha_1$  and  $\alpha_2$ ), steps 1 through 5 were repeated until the corresponding faulting model regression parameters  $\beta$ ,  $\beta_0$ ,  $\beta_1$ ,  $\beta_2$ ,  $\beta_3$ , and  $\beta_4$  were found that did not change the minimum value of equation 38. Step 6 is essential to ensure that the final regression constants obtained are not those for a local minima.

### Final Faulting Prediction Model

The final faulting model obtained consists of the following models:

#### Load Transfer Factor Model

$$\frac{AGG}{k\ell} = 0.25 e^{\left(1 + 0.0992D^{0.1} - 99.93 \frac{L}{\ell}\right)} \quad (39)$$

where

|             |   |  |
|-------------|---|--|
| $AGG/k\ell$ | = | nondimensional load transfer factor                |
| $D$         | = | dowel diameter, mm ( $D=0$ if nondoweled pavement) |
| $L$         | = | slab length, m                                     |
| $\ell$      | = | radius of relative stiffness, mm                   |

#### Allowable Number of Load Repetitions

$$\text{Log}_e N_f = 5.5 \text{Log}_{10} (0.005706 DE + 1) \quad (40)$$

where

|       |   |  |
|-------|---|--|
| $N_f$ | = | allowable number of load repetitions     |
| $DE$  | = | differential elastic deformation energy  |
|       | = | $0.5 * k * (W_L + W_{UL})(W_L - W_{UL})$ |
| $k$   | = | modulus of subgrade reaction, kPa/mm     |

$W_L$  = deflection of loaded slab, mm  
 $W_{UL}$  = deflection of unloaded slab, mm

#### Faulting Prediction Model

$$\text{Fault} = \text{FDAM}^{0.3} [1.25 + 0.00102\text{WETDAYS} - 2.5 \cdot 10^{-3}\text{DOWDIA} - 0.625C_d(0.5 + \text{BASE})] \quad (41)$$

where

$\text{FDAM}$  =  $n/N_f$   
 $n$  = number of 80-kN ESAL applications, in thousands  
 $N_f$  = allowable number of 80-kN ESAL applications, in thousands  
 $\text{WETDAYS}$  = number of wet days in the year  
 $\text{DOWDIA}$  = dowel diameter, mm  
 $C_d$  = drainage coefficient  
 $\text{BASE}$  = base or subbase type, 0=erodible 1=nonerodible

Statistics:

$N$  = 120  
 $R^2$  = 0.56  
 $\text{SEE}$  = 0.762 mm  
 $p\text{-value}$  < 0.0001 (level of significance of model)

A plot of the predicted and measured faulting is shown in figure 4. A plot of the residuals (predicted - actual faulting) against the predicted faulting is shown in figure 5. The overall accuracy of the faulting model is reflected by the  $R^2$  of 0.56, which is the proportion of variation of faulting explained by the variables included in the model. A test of hypothesis was performed to determine the significance of the variables used in the model for predicting faulting. The null and alternate hypotheses were as follows:

$H_0$ : all model parameters are zero (variables are not significant)  
 $H_A$ : all model parameters are not zero

The F-test statistic used for the hypothesis test was calculated as the ratio of the mean square for the model divided by the mean square of the error. For this study the null hypothesis will be rejected if the level of significance is less than 5 percent (0.05). A level of significance (p-value) of less than 0.0001 implies a rejection of the null hypothesis. This shows that the variables in the model are highly significant. Also, individual t-tests were conducted to test if the individual parameter estimates are equal to zero.

The p-values for this test ranged from 0.0001 to 0.01. The results show that all the parameter estimates had values other than zero; therefore, the variables in the model were significant. Prediction accuracy of faulting in absolute units is reflected by the standard error of estimate (SEE = 0.762 mm). The overall effectiveness of the model should be judged on all of the diagnostic statistics, the residual plots, and the results from the sensitivity analysis to follow. The

diagnostic statistics obtained for the faulting model show that the model can predict transverse faulting with reasonable accuracy for the LTPP database utilized.

### Sensitivity Analysis

The final step in the model-building process is the verification of the selected regression model. For the faulting model developed, model verification was limited to a comprehensive sensitivity analysis that involved the comparison of results with theoretical expectations, earlier empirical results, and simulated results reported in previously published literature. The sensitivity analysis involved using the model to determine the effect of each variable on faulting when the other variables were held at their mean values.

Plots were prepared to show these results. The plots were examined and the results compared with theoretical expectations and empirical results from earlier research studies. There were relatively limited data for model development, so a comprehensive validation of the model was not possible. However, with more data being collected as part of the LTPP GPS and SPS, data should be available soon for additional model validation. The plots and discussions on the results from the sensitivity analysis are discussed in the following sections.

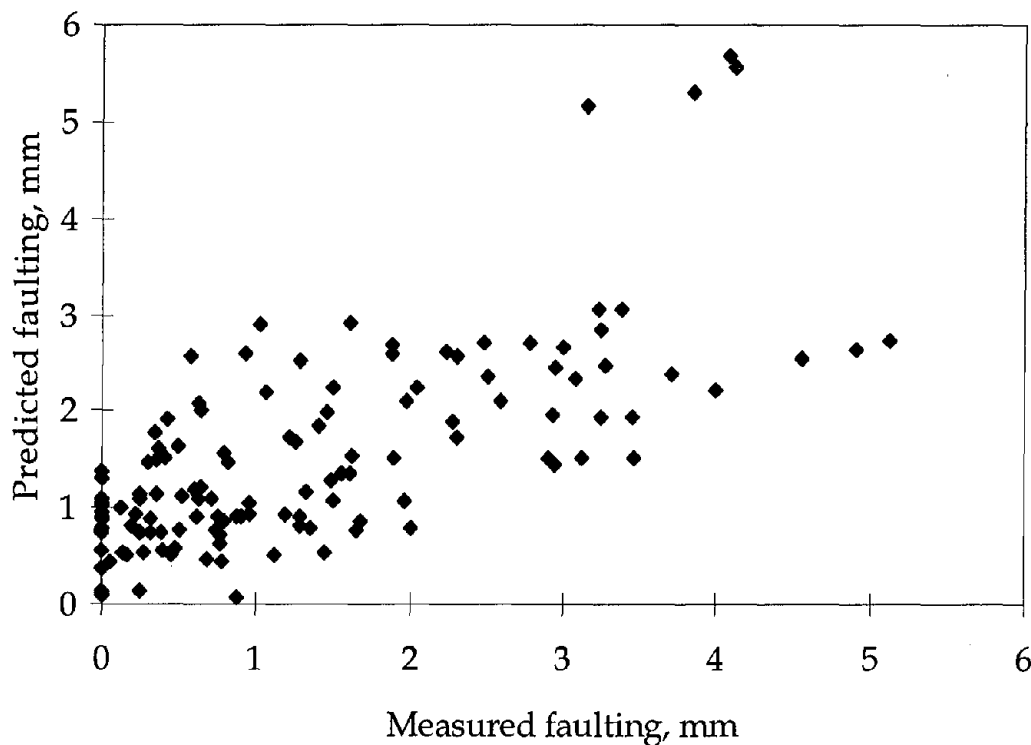


Figure 4. Plot of predicted versus measured faulting.

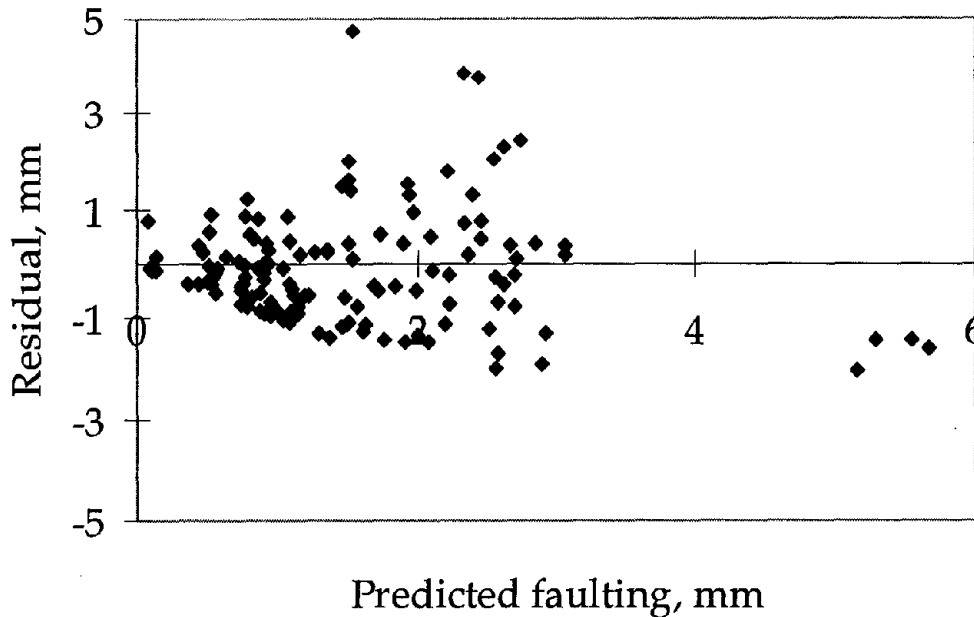


Figure 5. Plot of residuals versus predicted faulting.

#### *Effect of Traffic Loading*

Figures 6 through 12 illustrate the effect of traffic loading on the predicted joint faulting for different conditions. Clearly, in all cases, the predicted faulting increases rapidly in the beginning with increasing traffic loading and then levels off. This agrees with previous observations of faulting of jointed concrete pavements in the field. It shows that the model form selected and approach used to develop the model are both plausible from an engineering sense.

#### *Effect of Pavement Design Features*

For further verification of the models, the effect of key pavement design features on the faulting predicted by the model was checked against empirical and theoretical observations. Figure 6 shows a plot of the predicted faulting for different dowel diameters. It clearly shows that dowels of a minimum size of 25.4 mm greatly decrease faulting of jointed concrete pavements. Increasing the dowel diameter further reduces faulting. However, the small difference in faulting predicted for pavements using 25.4- and 38.1-mm-diameter dowels does not agree with the results of previous research studies.

The influence of the type of base (or subbase) used underneath the PCC slab is shown in figure 7. The results confirm that there is a tremendous reduction in faulting from the use of a nonerrodible base such as lean concrete. The rate of progression and magnitude of faulting is far less for pavements with a nonerrodible base in comparison to those with errodible bases. The effects of PCC slab thickness and subgrade support on the predicted faulting are shown in figures 8 and 9, respectively. According to the model, an increase in stiffness provided by either an increase in slab thickness or an increase in subgrade support results in less faulting. Increased slab thickness reduces joint deflection regardless of load transfer. The increase in subgrade stiffness, by

contributing to a reduction in deflections at the joints, is believed to be responsible for the reduction in faulting. Figure 10 shows the effect of joint spacing on faulting and shows that shorter joint spacing results in less faulting. Longer joint spacing results in more expansion and contraction, and wider joint widths, which lead to an increase in differential deflections.

### *Effect of the Environment*

Two important variables in the model that deal with the effect of environmental factors on the predicted faulting are  $C_d$  and number of wet days. Figures 11 and 12 show the effect of drainage coefficient and annual number of wet days on faulting. The plots clearly show that a higher  $C_d$  will reduce faulting. Fewer rainfall events, which will generally cause an increase in  $C_d$ , will also result in less faulting.

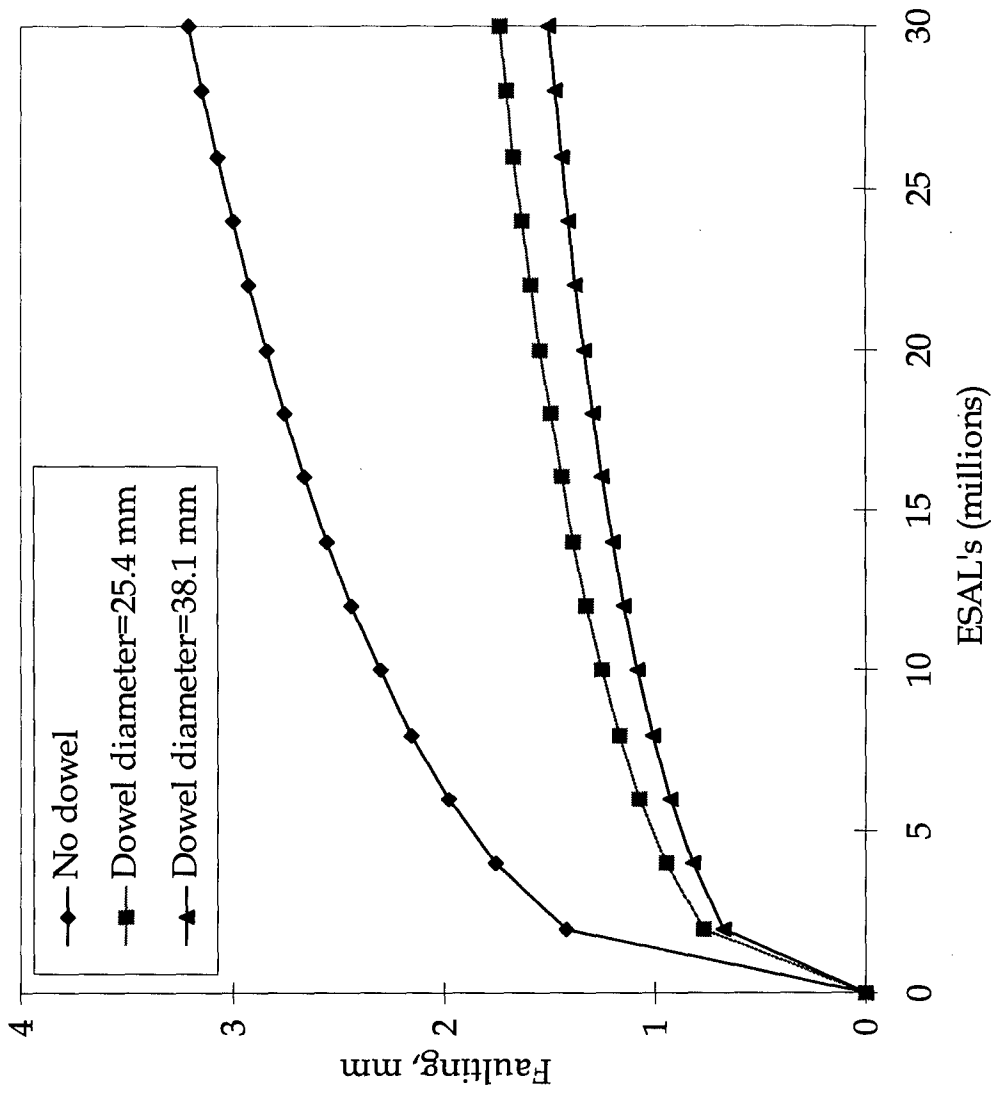


Figure 6. Influence of dowel and dowel size on predicted faulting.



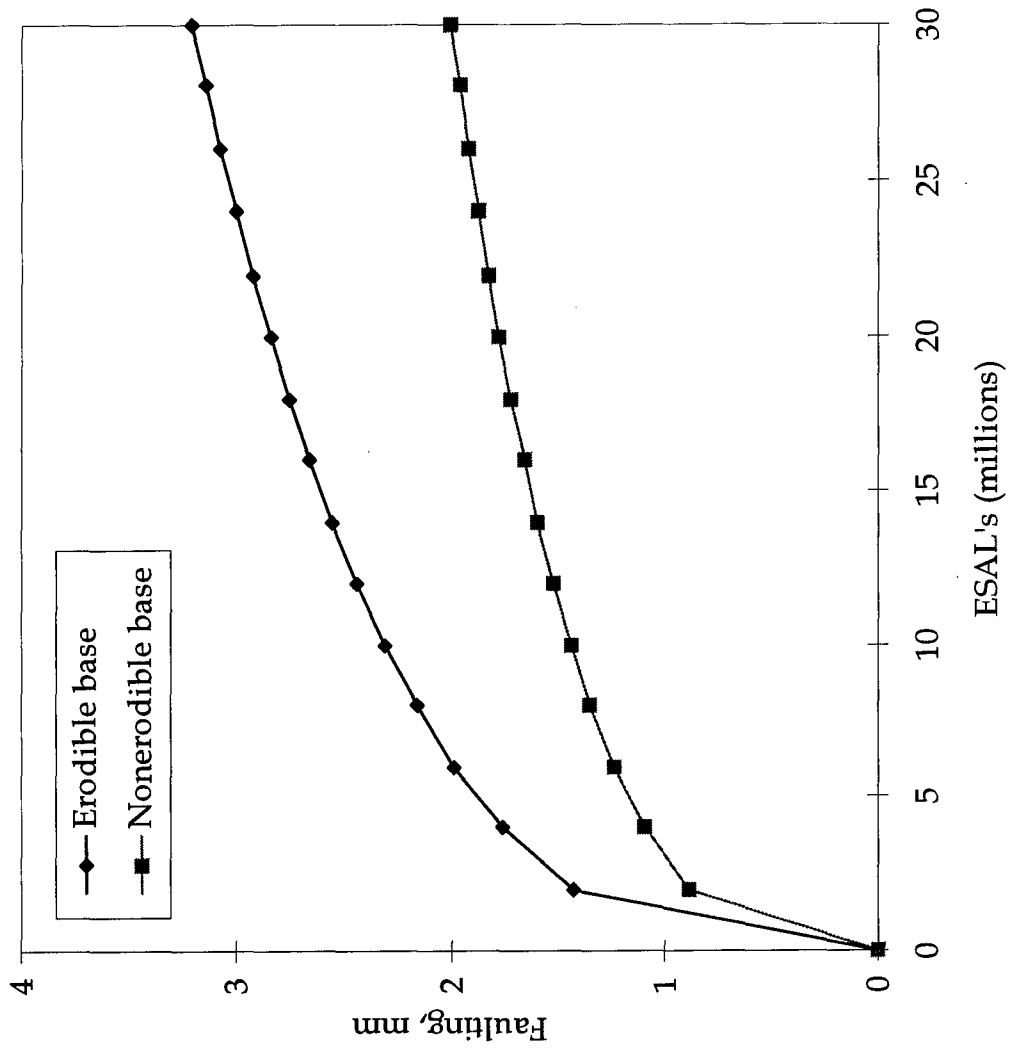


Figure 7. Influence of base or subbase type on predicted faulting.

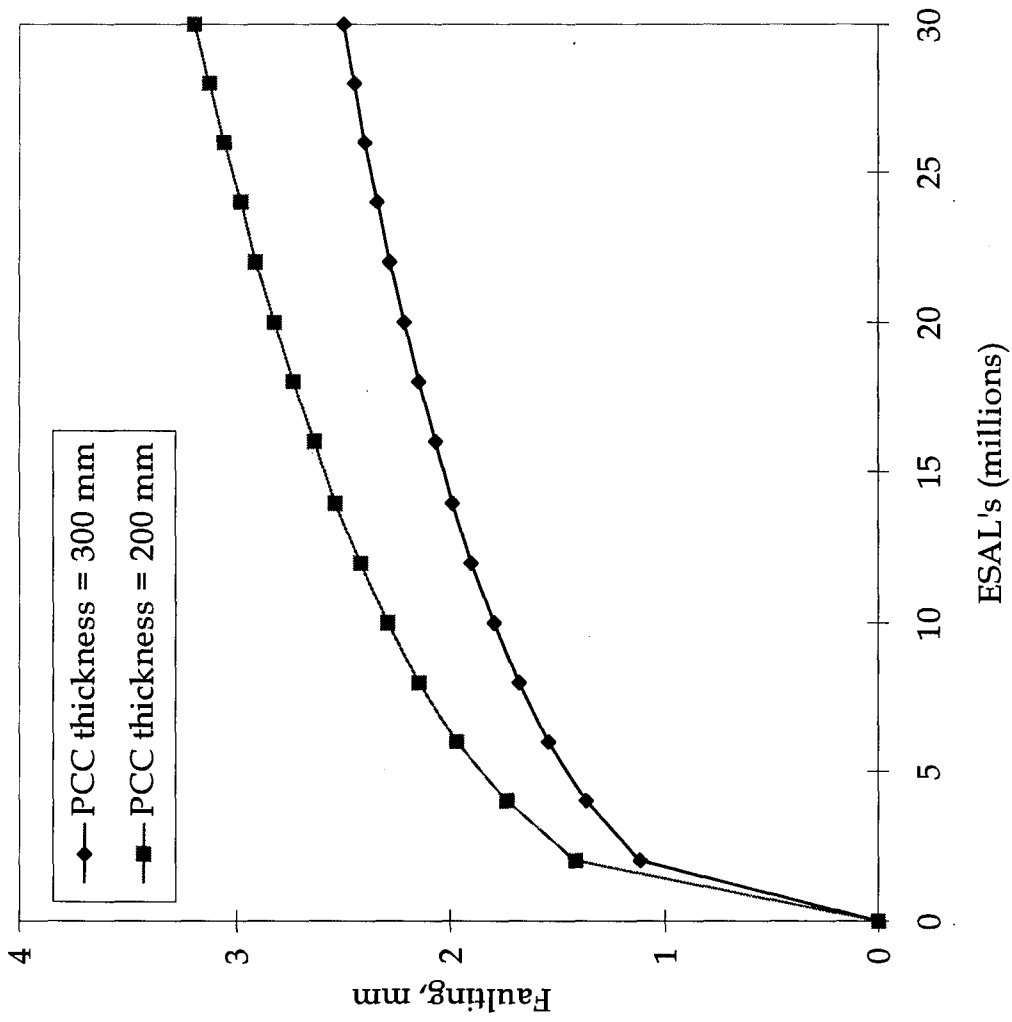


Figure 8. Influence of PCC slab thickness on predicted faulting.

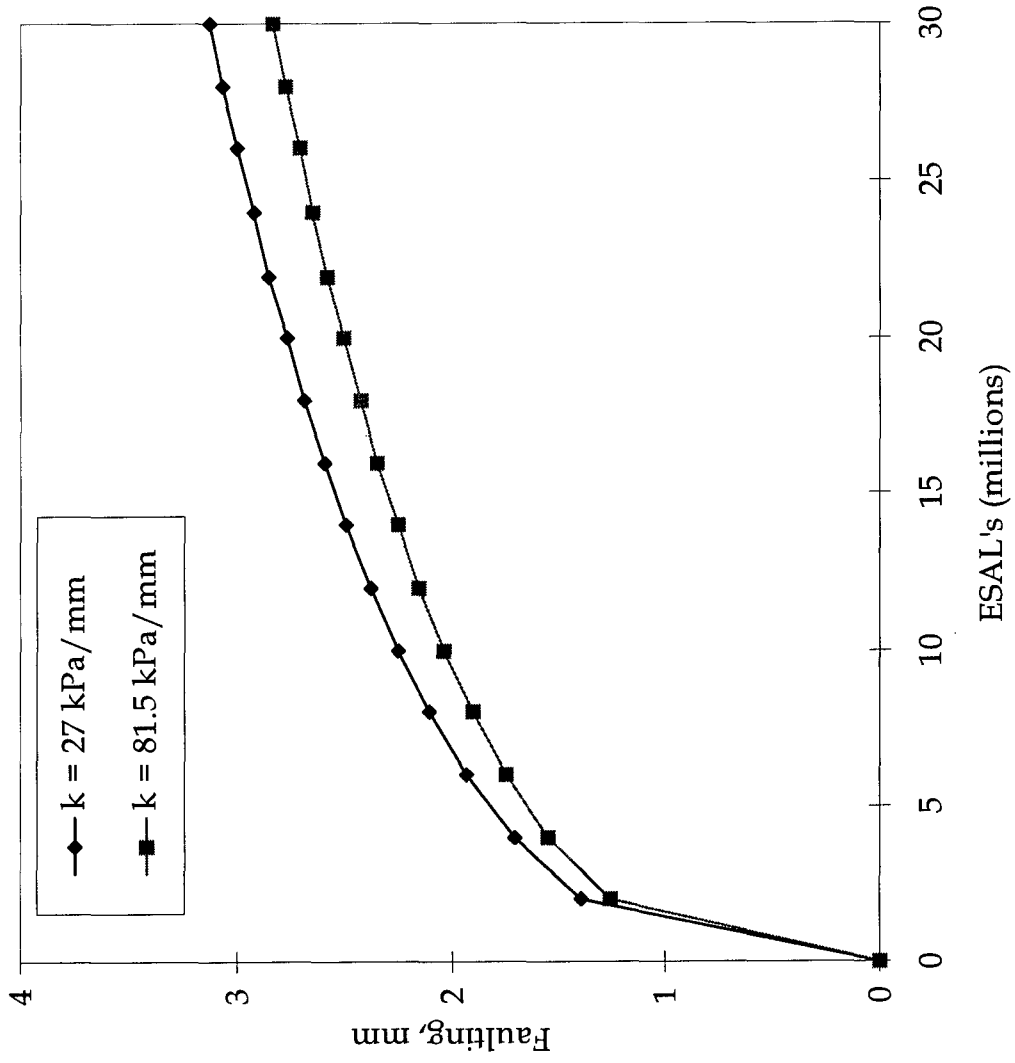


Figure 9. Influence of modulus of subgrade reaction on predicted faulting.

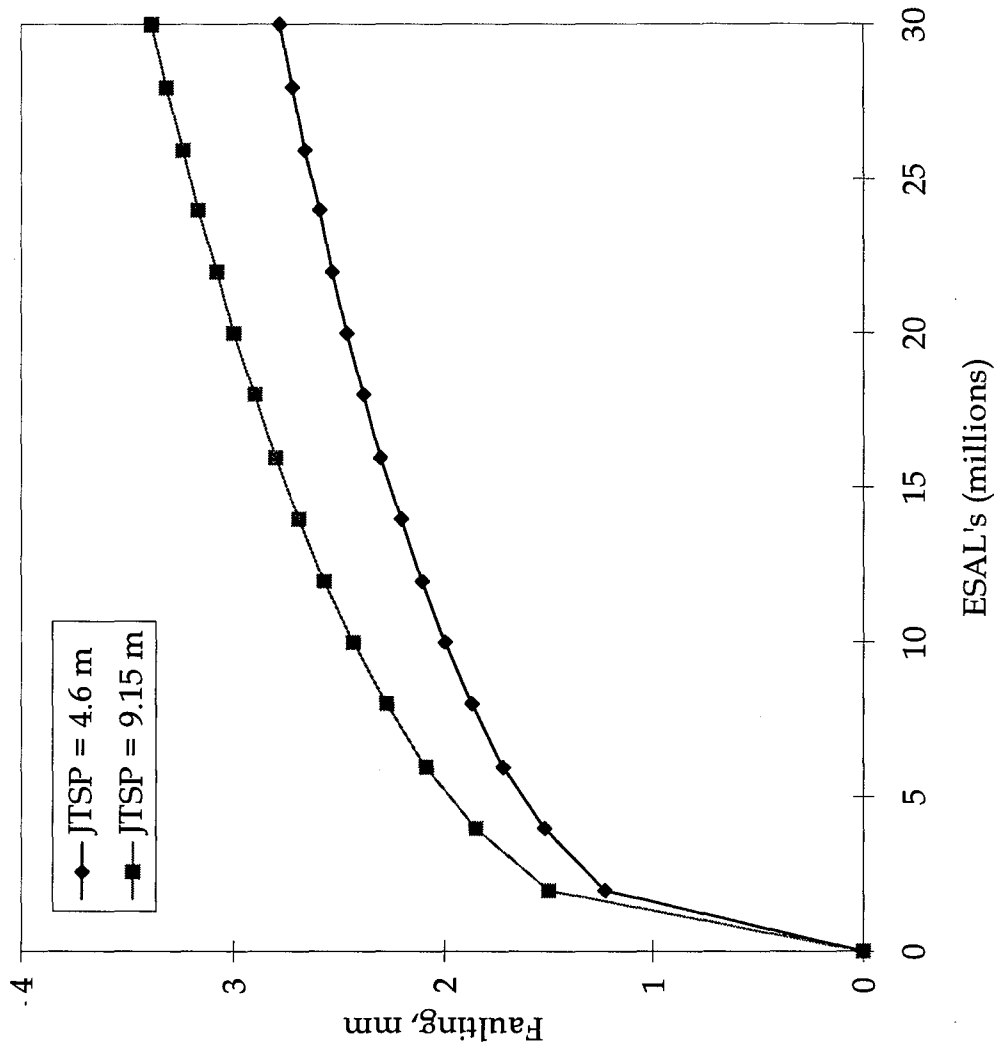


Figure 10. Influence of joint spacing on predicted faulting.

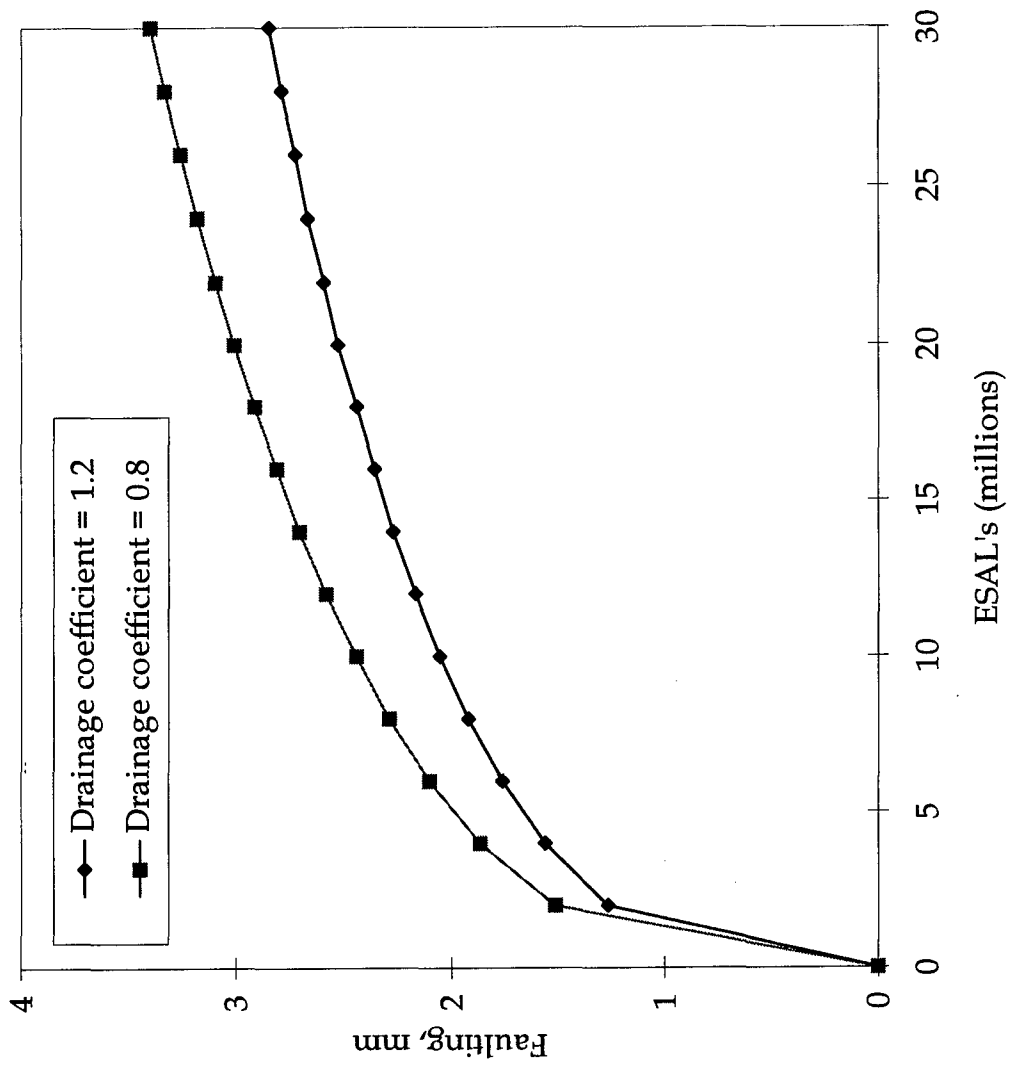


Figure 11. Influence of drainage coefficient on predicted faulting.

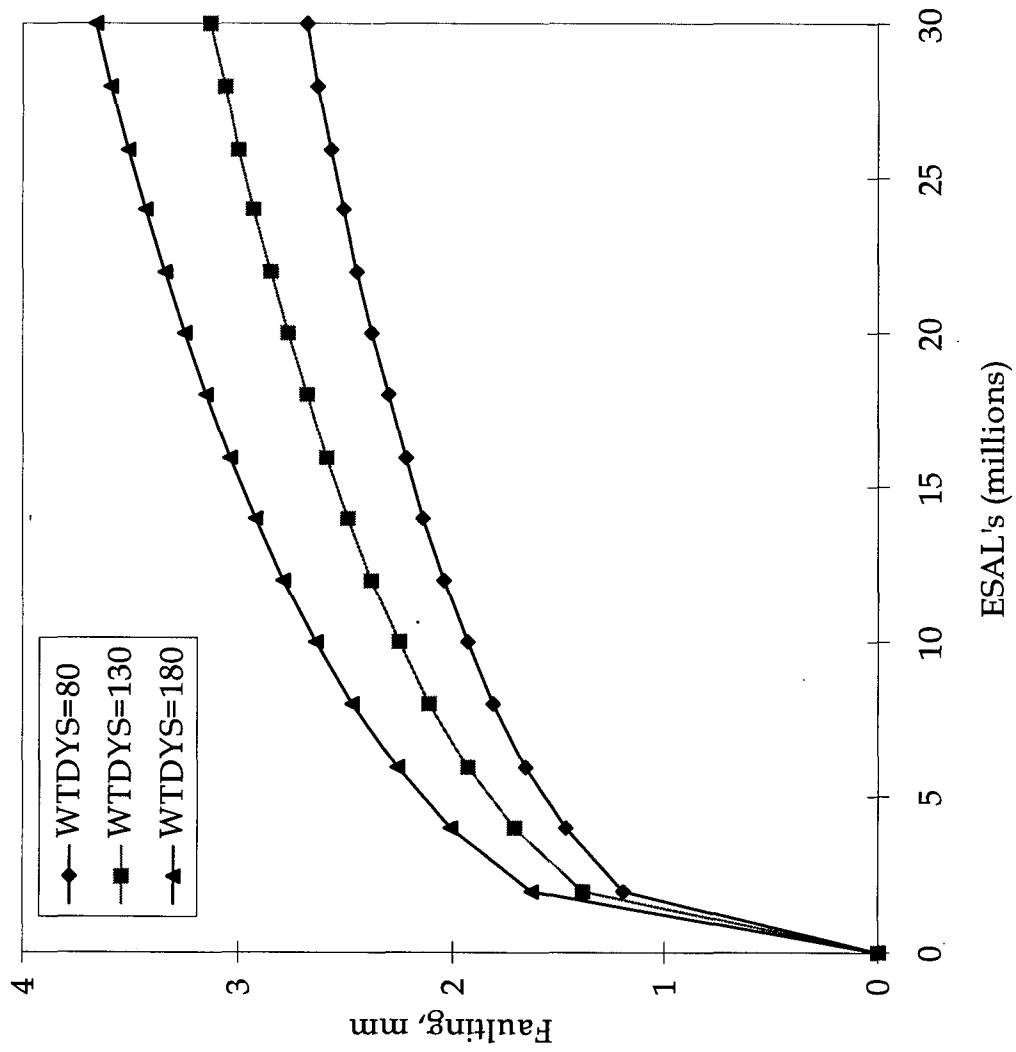


Figure 12. Influence of number of wet days (precipitation > 12.7 mm) on predicted faulting.

## Summary

The following can be summarized about the faulting model:

- Fifty-six percent of the total variation of faulting can be explained by the included variables.
- Some of the unexplained variation may be due to errors in the independent variables used to develop the model, such as the traffic estimates.
- The “average” residual in predicting faulting is 0.762 mm.
- There are no discernible patterns in the residuals. This means that there was little or no serial correlation in the data used for model development.
- Data from a large number of pavement sections from all over the United States were used to develop the model (N = 120).
- Each independent variable was significant at the  $p < 0.05$  level, and the overall model was highly significant with a p-value of less than 0.0001.
- The sensitivity analysis shows that all of the explanatory variables have a plausible effect on faulting that agrees with theoretical expectations and previous empirical field results.

## Implications and Recommendations

The model developed for predicting faulting uses the differential elastic deformation energy concept. The differential elastic deformation imposed by traffic loading is postulated to be directly related to the pore water pressure that is generated underneath a PCC slab and that leads to faulting. The model obtained clearly indicates that the incorporation of pavement design features that reduce the differential deflections at the joints of PCC pavements will decrease faulting. For example, the use of dowels that are at least 25.4 mm in diameter will decrease faulting appreciably.

According to the model, a stiffer pavement obtained by increasing the PCC slab thickness, higher subgrade support, use of a nonerodible base such as lean concrete, and shorter joint spacing will all combine to decrease the average faulting. From the results of sensitivity analyses conducted, each of these features by itself has an influence on faulting. Therefore, they will together have a tremendous influence on the progression of faulting.

The model obtained also shows that measures taken to reduce moisture in the pavement will reduce faulting. Higher drainage coefficients, which imply less saturation of the underlying material and shorter periods of exposure to moisture, cause a reduction in faulting. Similarly, less faulting was predicted for pavements in locations with a lower frequency of days during which the precipitation is in excess of 12.7 mm.

An important finding is the interacting effect of  $C_d$  with a nonerodible base. According to the model, a nonerodible base will increase the effect of the drainage coefficient on faulting about threefold. Therefore, a nonerodible base used in conjunction with other measures taken to increase the drainage coefficient will reduce faulting significantly.



## 5. TRANSVERSE JOINT SPALLING

### Introduction

The SHRP *Distress Identification Manual for the Long-Term Pavement Performance Studies* describes spalling as the breakdown or disintegration of a PCC slab's edges at joints or cracks or directly over the reinforcement steel, usually resulting in the removal of sound concrete.<sup>(41)</sup> Spalls are generally categorized by their length and depth. The same manual classifies spalling into three levels of severity: low, medium, and high. Spalling is measured both numerically (number of spalled cracks/joints and length of cracks/joints spalled) and qualitatively (low-, medium-, or high-severity).

Several field studies have observed that joint spalling may be due to infiltration of incompressibles into pavement joints, the deterioration of the concrete material from environmental factors, or the exposure of the slab's joint to a sudden and massive tensile stress. Spalling caused by a sudden force is usually of low severity and does not progress or deteriorate with time. However, spalling caused by incompressibles, repeated high tensile stress at the slab edges (fatigue), or concrete deterioration is more significant. It increases in severity with time and eventually causes pavement joint deterioration. It also results in the deterioration of load transfer devices such as dowels through corrosion and the loss of cover. Spalling eventually causes an increase in the roughness of the pavement, resulting in a decrease in serviceability of the pavement and costly rehabilitation.

Therefore, spalling is an important distress to PCC pavements. Monitoring and predicting the occurrence of spalling is important for pavement design and management. The development of sound prediction models for use in pavement design and management will provide engineers with an efficient tool for budgeting and planning, resulting in savings for State highway agencies throughout the United States. This chapter describes the development of mechanistic-empirical models for predicting joint spalling. The concepts used have been applied successfully to develop mechanistic-empirical models for spalling.<sup>(12)</sup>

### Spalling Mechanism

Research into spalling of concrete pavements has been ongoing since the early 1960s. The mechanism of spalling is yet to be fully understood. However, spalling is believed to be caused by several interacting mechanisms, including stresses imposed on the pavement by both traffic and environmental forces and inadequate quality control during construction.

Some primary causes of spalling identified from past research are as follows:<sup>(42)</sup>

- Entrapment of incompressibles in cracks, which causes a buildup of stress at the PCC slab joint when the pavement is subjected to temperature stresses and a combination of shear and tensile stress under the wheel load.
- Poor concrete at the slab surface due to poor construction practices.

The findings summarize the interacting forces that result in spalling and have been confirmed by other researchers.<sup>(42)</sup> Finite element analyses also showed that spalling results from incompressible material lodged in the pavement's joints or cracks.<sup>(43)</sup> They indicated that stiffer materials in a pavement's joint or crack restrain the pavement slab from volumetric changes when subjected to temperature gradients. This results in high stress concentrations at the slab joints and, hence, spalling. Some researchers have suggested that the use of joint filler would retard the development of crack or joint spalling by inhibiting edge raveling, admission of incompressible material, and corrosion of reinforcement.<sup>(44)</sup>

A study of two projects in Minnesota noted that spalls generally occurred in the wheel path.<sup>(45)</sup> It was also realized that a majority of deep spalls were caused by the corrosion of the reinforcement in the PCC slab by the chloride in the concrete. Studies at the University of Illinois also reported that the loss of bending stiffness at the transverse crack is related to spalling in CRCP. The analysis indicated that considerable stresses, both shear and normal, are created at the face of the transverse crack and result in a high potential for spalls to develop. The study also reported that loss of pavement support significantly increases stresses at the pavement joints and, hence, spalling.<sup>(46)</sup>

Researchers at the Texas Transportation Institute and Texas A&M University reported that poor construction practices can result in spalling later in the pavement's life. They reported that several planes of weakness develop during the early age of the pavement from differential shrinkage in the concrete and an inadequate aggregate cement paste bond. The addition of traffic and temperature stresses, shrinkage, and incompressible materials in the joints later in the pavement's life increases tensile stresses around the joint. These stresses acting on the already weakened planes from construction and environmental effects at the time of construction result in spalling.<sup>(47)</sup>

It can therefore be concluded that factors that cause an increase in tensile stresses at the edge of joints and cracks significantly influence the occurrence of spalling. Only recently has mechanistic modeling of spalling been investigated. CRCP spalling models based on traffic and environmental loading conditions have been developed by several researchers.<sup>(46, 47)</sup> The mechanistic analysis considered the following:

- The development of microcracks at or near the joint in the early age of the concrete.
- Microcracks develop primarily at the aggregate-cement paste interface.
- Microcracks grow into delaminations as a result of early age shrinkage, temperature curling, or excessive tensile stresses at or near the joint due to the infiltration of incompressibles in the pavement joint.
- The composition of the concrete mix is very important in determining the amount of microcracking and eventual delamination in the concrete.
- Delamination near the joint eventually spalls off as a result of continuing cyclic temperature, shrinkage, and traffic stresses.

On the basis of the preceding information, the mechanism of spalling can be summarized as follows:

- It is caused by a stress concentration at the edge of a slab joint or crack.
- The stress concentration can be attributed to any combination of the following:
  - Traffic stress imposed on the pavement.
  - Environmental stress imposed on the pavement by temperature variations and shrinkage.
  - The stiffness of the material in the pavement joint, which ranges from moderately soft materials such as regular joint sealing material (e.g., asphalt concrete, low modulus silicone, and preformed sealants) to very stiff incompressibles such as aggregates that fill up the joint with no joint sealant.

Current empirical models do not address all these variables; therefore, they cannot predict the percentage of joints spalled with precision and accuracy. The introduction of a mechanistic-empirical spalling model will allow better representation of the phenomenon of spalling in concrete pavements. Such a model should include mechanistic clusters that take into consideration these causes of spalling.

### **Evaluation of Existing Spalling Models**

A lot of empirical knowledge has been accumulated from past development of empirical models. These models were reviewed as a means of bringing expert knowledge into the model development process at an early stage. The review was used to select potential variables to consider in calibrating a final mechanistic spalling model. A lot of attention was paid to the engineering significance of the variables. The models reviewed were from the SHRP P-020 and RIPPER studies.<sup>(4, 10)</sup>

#### **SHRP P-020**

The following is a model developed using the LTPP data available in 1992 for predicting joint spalling in JPCP:<sup>(4)</sup>

$$SPALLJP = 9.79 + 10.09[-1.227 + 0.0022*(0.985AGE + 0.1709FT)^2] \quad (42)$$

where

SPALLJP = predicted percentage of joints spalled (all severities) expressed as a percentage of the total number of joints  
AGE = pavement age, yr  
FT = mean annual number of air freeze-thaw cycles

The model relates spalling to the pavement age and the mean annual number of air freeze-thaw cycles. This model suggests that joint spalling increases with age, and that stress cycles generated within the pavement while undergoing freezing and thawing contribute to spalling. Freezing and thawing of concrete also result in the expansion of water in the pores of the concrete, creating additional stresses that weaken the concrete.

The following similar model was developed for predicting spalling for JRCP:

$$SPALLJR = -79.0 + 0.604*AGE^{1.5} + 0.129*TRANGE^{1.5} \quad (43)$$

where

SPALLJR = predicted percentage of transverse joint spalling (all severities)  
 AGE = pavement age, yr  
 TRANGE = mean monthly temperature range, °F

For this model, the rate of increase in spalling is also dependent on the age of the pavement. The magnitude of spalling depends on the temperature range (i.e., the difference between the mean maximum and minimum annual temperatures) at the location of the pavement. This model, like the previous one, is based on environmental factors. Also, the age variable in both models represents several factors. These include factors such as slab curling, warping, and temperature cycles due to daily and seasonal temperature variations that result in joint movements. The joint movements increase joint openings and allow for the infiltration of incompressibles into the joints. Traffic loading is also represented, since older pavements are expected to have carried more traffic.

The models indicate that spalling generally increases slowly during the first few years of the pavement's life and then increases more rapidly after several years. This is logical because it takes some time for incompressibles in the pavement's joints or cracks to accumulate and increase the stress concentrations at the pavement joint. It also takes time for damage to the pavement to accumulate. However, both models include only two of the variables that are known to cause spalling. Therefore, it can be expected that the addition of other variables and clusters that account directly for the effect of traffic and construction practices will improve the model's accuracy.

#### RIPPER Study

The RIPPER study undertook a detailed examination of several past models.<sup>(10)</sup> It resulted in a comprehensive list of explanatory variables that can be used in exploratory analysis for model development. The explanatory variables are as follows:

AGE: time since pavement was constructed  
 CESAL: cumulative 18-kip (80-kN) ESAL's in the traffic lane  
 JTSP: mean transverse joint spacing  
 THICK: PCC slab thickness  
 C<sub>d</sub>: AASHTO drainage coefficient  
 JTOPEN: joint opening

JTWIDTH: mean joint width  
 $E_{PCC}$ : elastic modulus of the PCC slab  
 Kvalue: mean backcalculated modulus of subgrade reaction  
 MI: Thornthwaite moisture index  
 JTSEAL: joint sealant type

These explanatory variables were used to develop two models for JPCP and JRCP pavements using the RIPPER database:

$$SPALLJP = AGE^2 * 10^{-6} * JTSP * (551.6 - 847.3 * [LIQSEAL + PREFSEAL] + 0.936 * Days90^3 * 10^{-3} + 364 * DOWELCOR + [2.783 - 1.400 * LIQSEAL - 2.368 * PREFSEAL - 0.676 * SILSEAL] * FI) \quad (44)$$

$$SPALLJR = AGE^3 * JTSP * (1.94 * DOWELCOR + 8.819 * BASE * (1 - PREFSEAL) + 0.00701 * FI) * 10^{-5} \quad (45)$$

where

SPALLJP = percentage medium- and high-severity spalled joints in JPCP  
 SPALLJR = percentage medium- and high-severity spalled joints in JRCP  
 AGE = pavement age, yr  
 JTSP = mean joint spacing, ft  
 LIQSEAL = 0, if no liquid sealant exists  
           1, if liquid sealant exists  
 PREFSEAL = 0, if no preformed sealant exists  
           1, if preformed sealant exists  
 Days90 = mean number of days in the year with temperature above 32 °C  
 DOWELCOR = 0, if no dowels exist, or dowels are protected from corrosion  
           1, if dowels are not protected from corrosion  
 SILSEAL = 0, if no silicone sealant exists  
           1, if silicone sealant exists  
 FI = mean annual freezing index, °F days  
 BASE = 0, if nonstabilized base  
        1, if stabilized base

The models are more comprehensive because they take into account more variables related to spalling. Also, the variables can be divided into two distinct groups— environmental and design-related variables.

The environment-related variables include age (cycles of climate changes such as opening and closing of joints), annual number of days with temperature above 32 °C, and freezing index. The annual number of days with temperature above 32 °C is indicative of the magnitude of expansion or contraction to which the PCC slab is subjected. Since pavements located in areas with a high annual number of days with temperature above 32 °C generally undergo a lot of expansion, this can result in the generation of high stresses in the PCC slab and joint that result in more spalling. Older pavements and those subjected to a higher freezing index are subjected to prolonged cycles

of frozen water within the pores of the PCC slab and deterioration of the concrete material. This generally results in the disintegration of the concrete slab material at the slab surfaces and joints and, hence, spalling.

The design-related variables include joint spacing, liquid sealant, preformed sealant, silicone sealant, coated or uncoated dowels, and base type. The joint spacing is highly correlated to the degree of joint movement. Longer slabs expand more when subjected to cyclic temperature variations and create higher stresses at the joint when restrained by the presence of incompressibles. The base type is an indication of the support condition of the pavement. Pavements on firm supports are likely to experience smaller deflections and, hence, less stresses. Spalling can also be caused by the corrosion of the dowel bar by the chlorides and other chemicals in PCC. Protecting the dowels from corrosion therefore reduces spalling. The final design variable considered in the models is the joint sealant type. The role of joint sealants in minimizing spalling is to prevent the intrusion of incompressibles into the joint. Incompressibles restrain the slab joints from moving and, in the process, increase stresses around the pavement joint, increasing spalling. The RIPPER study suggests that the use of preformed sealants in both JPCP and JRCP resulted in the lowest level of spalling for all sealed and unsealed joints. Preformed sealants are particularly effective in minimizing the intrusion of incompressibles into pavement joints.

### **Spalling Model Development Approach**

Most of the models developed in the past, like the SHRP P-020 and RIPPER models, have been empirical models that did not attempt to account directly for the mechanism of spalling described. This is because previous attempts to use mechanistic principles to describe spalling have not been very successful. However, these empirical models have been used successfully to identify the environmental and design factors that have an effect on spalling (see table 2). Recent research work has resulted in considerable progress in the application of mechanistic principles for modeling spalling, and this made it possible to develop mechanistic-based models for predicting spalling for both JPCP and JRCP.<sup>(47)</sup>

#### Application of Mechanistic Principles to Spalling

To determine the mechanistic-based response to use in modeling spalling, the mechanism of spalling previously described was evaluated in detail. The key concepts investigated concerned the mechanism that causes tensile stresses across the face of joints and cracks in PCC pavements. Spalling initially begins as microcracks and delaminations that exist at the joint interface early in the life of a pavement because of stresses from temperature variations and shrinkage from bad construction practices.<sup>(47)</sup> These delaminations are continuous flaws parallel to the pavement surface and usually occur at a depth of not more than 25.4 mm.

Traffic load and additional temperature and shrinkage tensile stresses will tend to enlarge and propagate the microcracks and delaminations within the concrete slab. Even though the occurrence of tensile stresses in this part of the PCC slab will eventually transform the delaminations into spalls, not all of the delaminated portion of the slab edge will necessarily spall off. However, tensile stresses of higher magnitude can create new cracks within the pavement and at the joint interface. With the initiation of new cracks or the transformation of existing

construction defects into cracks, the tensile stresses propagate these cracks from the joint interface to the slab surface and result in spalling.

This mode of spall initiation and propagation is known as the tensile mode of spalling of PCC pavements.<sup>(47)</sup> The tensile stress within the slab at the joint interface and along the path of crack growth is the mechanistic parameter that was used to model spalling. It is called the tensile or spall stress,  $\sigma_t$ , and can be used to estimate the allowable number of stress cycles the pavement slab will withstand before spalling occurs.

### Determining the Tensile Spall Stress

Figure 13 is a free body diagram that illustrates the stresses that occur at the joint interface of a jointed concrete pavement because of both traffic and environmental loads.<sup>(47)</sup> An analysis of the free body diagram showed that the tensile spall stresses are dependent on the normal and shear stresses caused by traffic and environmental loading and the properties of the joint sealant. Resolving all forces for equilibrium in the horizontal direction and solving provides the following equation for estimating the spall stress:<sup>(47)</sup>

$$\sigma_t = (\tau - \tau_f) \frac{l}{t} + \frac{q\mu}{\tan \theta} - \sigma_{js} \quad (46)$$

where

|               |   |  |
|---------------|---|--|
| $\tau$        | = | vehicle tire shear stress, kPa                   |
| $\tau_f$      | = | friction stress = $q\mu$ , kPa                   |
| $l$           | = | tire pressure load length, mm                    |
| $t$           | = | depth of spall delamination, mm                  |
| $q$           | = | normal tire pressure, kPa                        |
| $\mu$         | = | concrete friction coefficient                    |
| $\theta$      | = | orientation angle of principal stresses, degrees |
| $\sigma_{js}$ | = | joint sealant or incompressibles stress, kPa     |

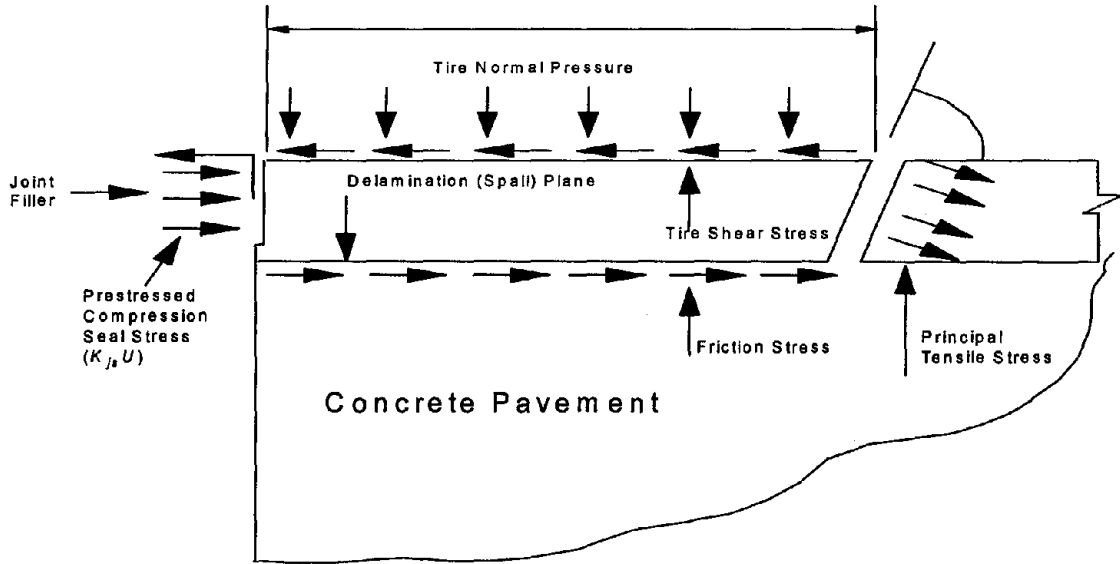


Figure 13. Schematic diagram of spalling mechanism for tensile mode of failure in jointed concrete pavement.<sup>(47)</sup>

The last part of equation 46,  $\sigma_{js}$ , represents the stress exerted by the joint sealant or incompressibles, if present. It can be determined using the following equation:

$$\sigma_{js} = k_{js}u/t = k_{js}CL(\alpha\Delta T + e)/2t \quad (47)$$

where

- $k_{js}$  = spring coefficient of joint sealant or incompressibles in the joint, kPa
- $u$  = displacement of spalled concrete, mm
- $t$  = depth of spall delamination, mm
- $C$  = subbase friction factor
- $L$  = joint spacing, mm
- $\alpha$  = concrete thermal expansion
- $\Delta T$  = thermal gradient in the slab
- $e$  = concrete drying shrinkage strain

Equation 47 represents the spall stress caused by environmental loading. An assumption of a unit value for the depth of spall delamination,  $t$ , is reasonable for most cases. Additionally,  $\sigma_{js}$  can be used to represent the stress caused by incompressibles that have infiltrated into the joint if an equivalent  $k_{js}$  is used. If a sealant is used, the stress  $\sigma_{js}$  can be positive if the joint sealant maintains a compressive stress (e.g., preformed compression seals) across the whole face of the joint. This will decrease the spall stress given by equation 46. For other sealants and incompressibles,  $\sigma_{js}$  may be negative or zero and will increase or not change the spall stress.

The remaining portions of equation 46 represent the stresses due to traffic loads. This part of the equation may be difficult to implement for everyday use because some of the inputs are not



readily available. Therefore, a series of finite element runs were conducted to develop a regression model for estimating the traffic spall stress,  $\sigma_{tr}$ , defined as follows:

$$\sigma_{tr} = (\tau - q\mu) \frac{l}{t} + \frac{q\mu}{\tan \theta} \quad (48)$$

### Traffic Load Tensile Stress Model

Since calculation of the tensile stress using equation 48 requires inputs that may not be readily available, a simple equation for determining the traffic spall stress was developed. This was accomplished by modeling the tensile stresses that occur at a PCC slab joint using the three-dimensional finite element program ABAQUS.<sup>(48)</sup> A two-dimensional model (assuming plane strain conditions) was used in ABAQUS to analyze a PCC slab over a subgrade subjected to traffic loads, to determine and examine the tensile stress distribution within the PCC slab and to identify the occurrence of peak stresses at the joint surface. The finite element configuration consisted of 450 nodes and 200 elements. The finite element model and boundary conditions used in the analysis are shown in figure 14.

Joint sealants and incompressibles were modeled as an elastic material with different moduli corresponding to the different joint sealant types and incompressibles in the joint. Preliminary analysis showed that the end conditions (fixed or simply supported) of the PCC slab joint had little or no influence on the analysis. The foundation was modeled as a Winkler foundation, with the elastic-spring constant of the foundation corresponding to the modulus of subgrade reaction,  $k$ , of the subgrade. The PCC slab was assumed to be a homogeneous elastic material, and the aggregate interlock and load transfer across the joint were modeled using vertical springs of varying spring constants to reflect different levels of load transfer.

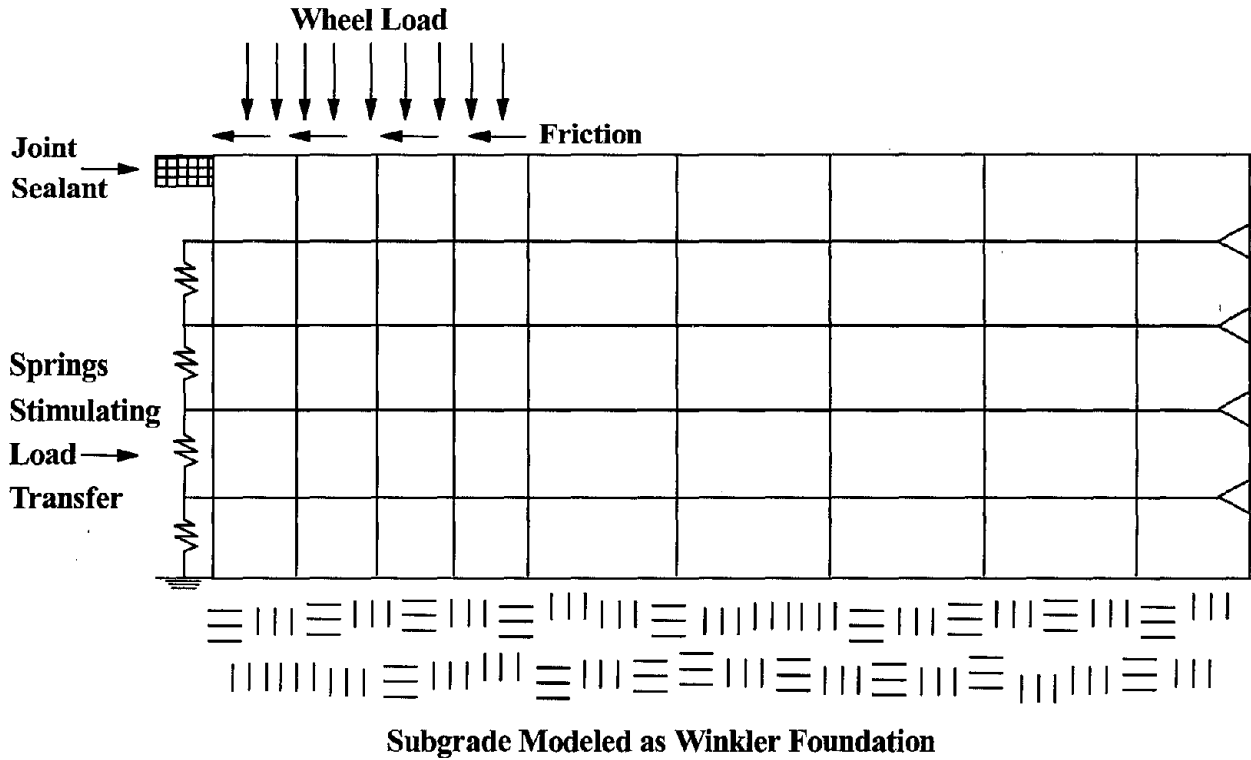


Figure 14. Finite element model for estimating spall stress.<sup>(14)</sup>

A factorial of different material properties and design features was used to obtain the maximum tensile stress that occurs at the face of the joint or crack for different pavement conditions. The variables and the range of values used in the factorial are shown in table 7. An 80-kN axle load was used in this instance, but it is important to note that a regression equation can be obtained that can be used for different load levels by varying the load level. The results from the ABAQUS factorial runs were used to develop the following regression model for predicting the maximum traffic load tensile stress:<sup>(3)</sup>

$$\begin{aligned} \sigma_{tr} = & 305.5 + 48.563h_s - 23.62k_v + 0.000757 k_s - 0.17728h_p h_s \\ & + 0.0888h_p k_v - 1.89 \cdot 10^{-6} h_p k_s - 1.889 \cdot 10^{-7} h_s E_p \\ & + 1.98 \cdot 10^{-6} h_s k_s - 1.32 \cdot 10^{-6} k_v k_s \end{aligned} \quad (49)$$

where

|               |   |  |
|---------------|---|--|
| $\sigma_{tr}$ | = | maximum tensile stress at crack or joint surface from traffic loading, kPa |
| $h_s$         | = | depth of sealant, mm   |
| $k_v$         | = | modulus of subgrade reaction, kPa/mm                                       |
| $k_s$         | = | modulus of sealant material, kPa   |
| $h_p$         | = | PCC slab thickness, mm   |
| $E_p$         | = | modulus of PCC slab, kPa   |

Statistics:

N = 340  
R<sup>2</sup> = 0.74  
SEE = 250 kPa

Sensitivity Analysis of Traffic Load Tensile Stress Model

Sensitivity analyses were conducted to verify whether equation 49 was in agreement with results from mechanistic and finite element analysis. Other checks, such as analyzing the diagnostic statistics results and plots of the predicted tensile stress versus the independent variables, were also made to test the suitability of the model. The primary input parameters of interest were the PCC slab thickness, sealant depth, sealant or incompressible modulus, and PCC elastic modulus. The ranges of values used and the results obtained are presented in table 8.

The effects of the different design features on the estimated traffic tensile stress for an 80-kN axle load are illustrated in figures 15 through 19. The sensitivity analysis indicates that, in all cases, the model provides results in line with engineering expectations.

Table 7. Factorial of traffic and pavement properties used to develop model for predicting traffic spall stress.<sup>(3)</sup>

| <b>Pavement/Traffic Variable</b>                | <b>Range of Values Used in Finite Element Analysis</b> |
|---|--|
| PCC slab modulus, kPa                           | 27.6*10 <sup>6</sup> to 55.2*10 <sup>6</sup>           |
| Modulus of joint sealant or incompressible, kPa | 1.4*10 <sup>6</sup> to 5.5*10 <sup>6</sup>             |
| Modulus of subgrade reaction, kPa/mm            | 27 to 136  |
| PCC slab thickness, mm                          | 100 to 300   |
| Single axle load, kN                            | 80   |
| Sealant depth, mm                               | 12.7 to 115  |

Table 8. Summary of inputs and results of sensitivity analyses of traffic tensile stress model.<sup>(3)</sup>

| Variable                             | Inputs            |                   |                   | Spall Stress, kPa |      |
|--------------------------------------|-------------------|-------------------|-------------------|-------------------|------|
|                                      | Mean              | Min.              | Max.              | Min.              | Max. |
| Slab thickness, mm                   | 300               | 100               | 300               | 2350              | 380  |
| Sealant depth, mm                    | 64                | 12.7              | 115               | 830               | 1070 |
| PCC slab modulus, kPa                | $31 \cdot 10^6$   | $14 \cdot 10^6$   | $62 \cdot 10^6$   | 1240              | 790  |
| Modulus of subgrade reaction, kPa/mm | 95                | 27                | 163               | 1240              | 450  |
| Sealant/incompressibles modulus, kPa | $3.45 \cdot 10^6$ | $1.38 \cdot 10^6$ | $5.52 \cdot 10^6$ | 276               | 1450 |

#### Calculating Total Tensile Spall Stress

The total tensile spall stress can be calculated using equations 47 and 49 to account for the tensile stress due to environmental loading and traffic loads, respectively. These models are simple to use and were used to estimate the total spall stress for each of the GPS 3 and 4 sections. This was the mechanistic parameter used for developing a model for predicting spalling in this study.

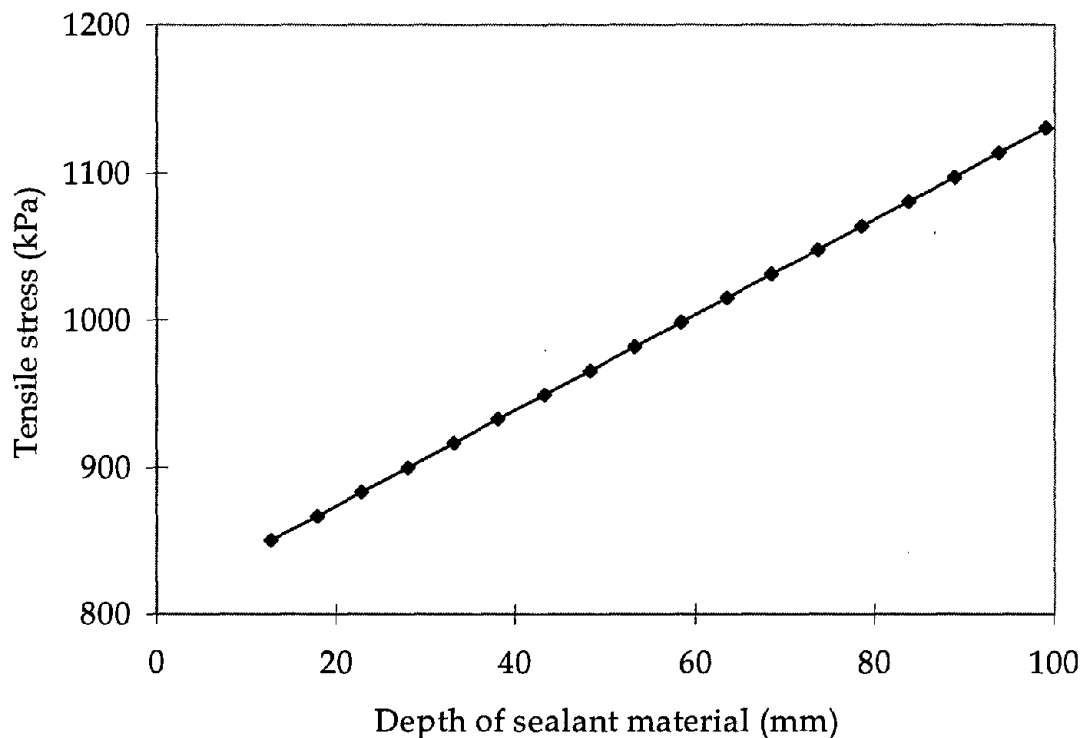


Figure 15. Sensitivity plot of tensile stress versus height of sealant.<sup>(3)</sup>

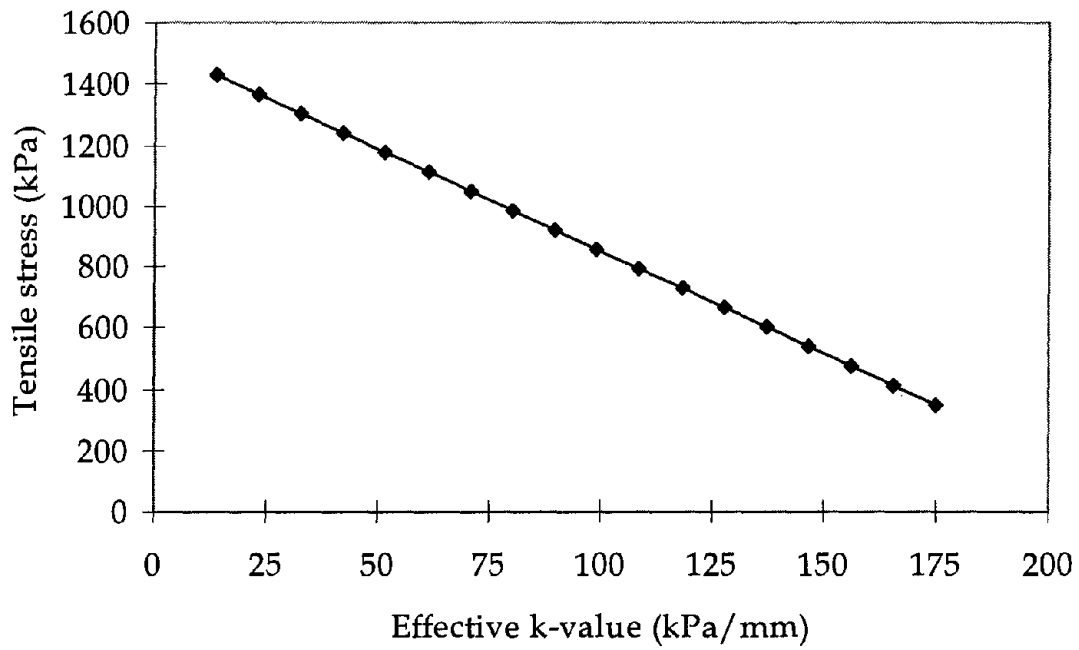


Figure 16. Sensitivity plot of tensile stress versus modulus of subgrade reaction.

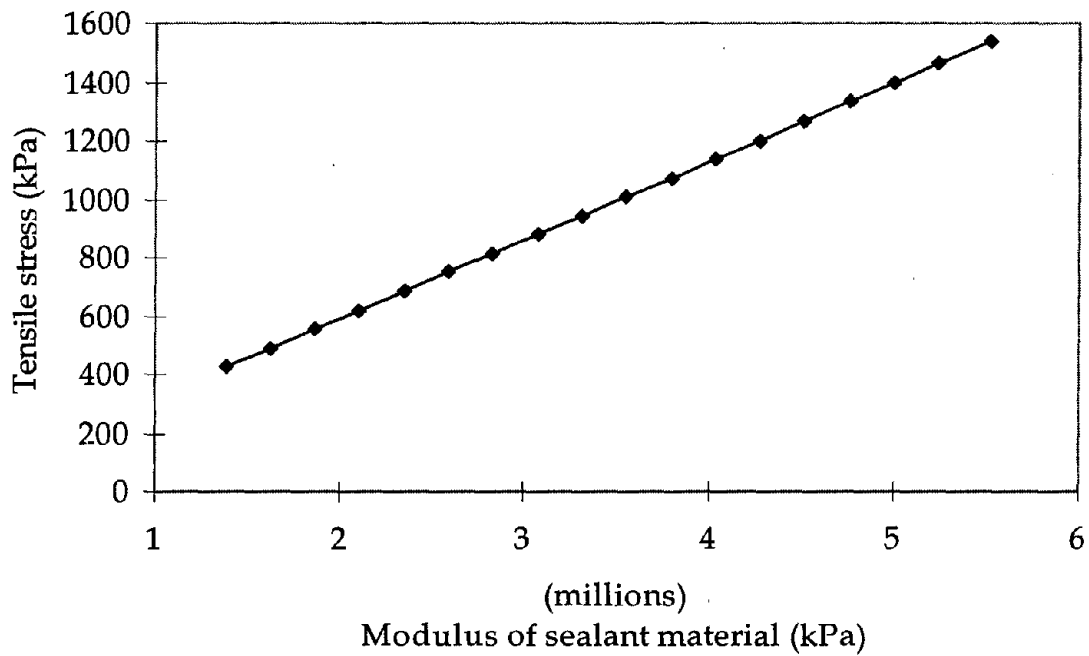


Figure 17. Sensitivity plot of tensile stress versus sealant modulus.<sup>(3)</sup>

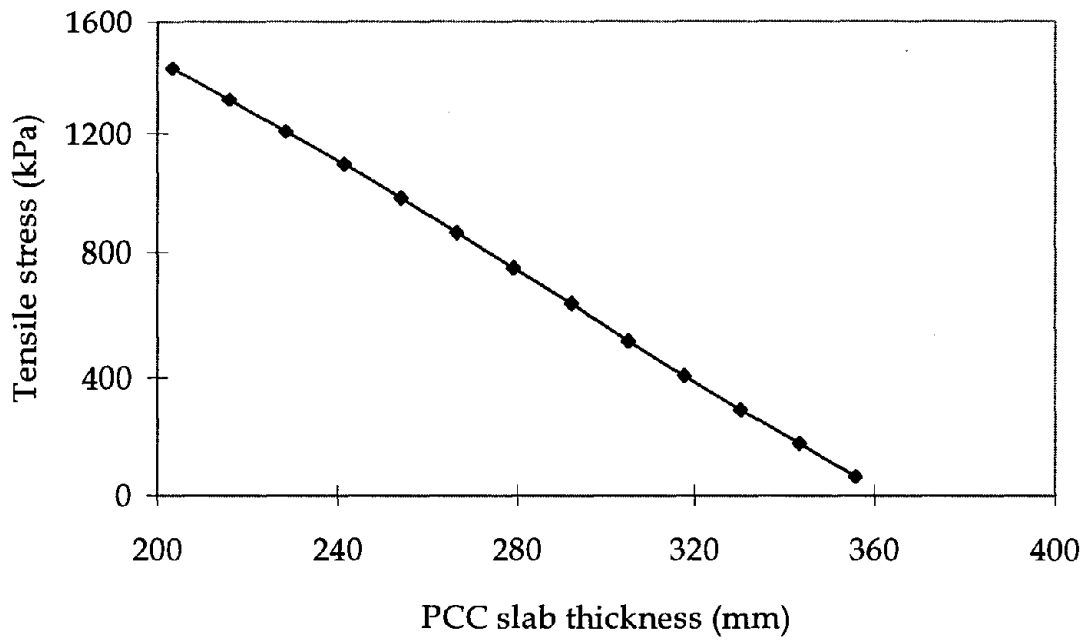


Figure 18. Sensitivity plot of tensile stress versus PCC slab thickness.<sup>(3)</sup>

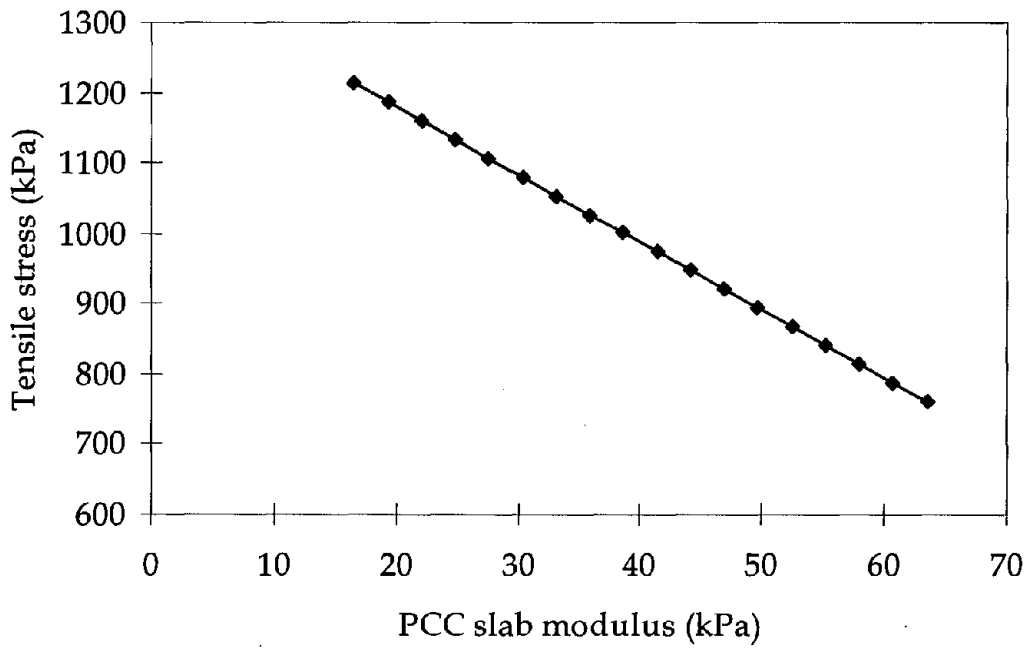


Figure 19. Sensitivity plot of tensile stress versus PCC slab modulus.<sup>(3)</sup>

## Mechanistic-Empirical Spalling Model Formulation

Using the equations developed for calculating the total spall stress, it is possible to develop mechanistic-empirical models for predicting joint spalling of JPCP and JRCP using Miner's damage accumulation approach.<sup>(49)</sup> The three key parts of the model are as follows:

- A damage accumulation model that is used to accumulate the damage caused by individual traffic and environmental load applications.
- A model for calculating the allowable number of traffic and environmental spall stress applications to failure.
- A model for predicting the percentage of joints spalled from the damage accumulation.

### Spalling Damage Accumulation

If the spalling damage caused by traffic and environmental loading is assumed to be additive, the following equation based on Miner's hypothesis can be used to calculate the total damage:<sup>(49)</sup>

$$\text{Damage} = \alpha_1 \sum_i^k \frac{n_{iT}}{N_T} + \alpha_2 \sum_i^k \frac{n_{iE}}{N_E} \quad (50)$$

where

|                      |   |   |
|----------------------|---|---|
| $n_{iT}$             | = | number of cycles of traffic loads                     |
| $n_{iE}$             | = | number of environmental stress cycles                 |
| $N_T$                | = | allowable number of cycles for traffic loading        |
| $N_E$                | = | allowable number of cycles for environmental stresses |
| $\alpha_1, \alpha_2$ | = | regression constants                                  |

The number of cycles of traffic loads is essentially equal to the cumulative number of 80-kN ESAL applications. Since the number of cycles of environmental stresses is also a function of the pavement age, equation 50 can be rewritten as follows:

$$\text{Damage} = \alpha_1 \frac{\text{KESAL}}{N_T} + \alpha_2 \frac{\text{AGE}}{N_E} \quad (51)$$

where

|       |   |  |
|-------|---|--|
| KESAL | = | cumulative number of 80-kN ESAL's, thousands |
| AGE   | = | pavement age, yr                             |

## Allowable Number of Traffic and Environmental Stress Repetitions

The estimated allowable number of traffic load spall stress repetitions to failure,  $N_T$ , and the allowable number of environmental spall stress repetitions to failure,  $N_E$ , are required to use equation 51. To develop models for predicting  $N_T$  and  $N_E$ , several model forms were evaluated for their suitability for predicting the number of load cycles to failure. A typical model form that relates the allowable number of load repetitions,  $N$ , to the calculated tensile stress in concrete pavements is as follows:<sup>(50)</sup>

$$N = k_1 \left( \frac{1}{\sigma_t} \right)^{k_2} \quad (52)$$

where

$\sigma_t$  = tensile stress that causes spalling, kPa  
 $k_1, k_2$  = regression constants

This model form, which is used in fatigue analysis of concrete pavements, is in accordance with basic engineering principles and was selected for use. According to the model, an increase in tensile stress decreases the allowable number of cycles to failure, and a decrease in tensile stress increases the allowable number of cycles to failure.

For spalling caused by the traffic load stress,  $\sigma_t$  can be replaced with  $\sigma_r$  from equation 49 to obtain the following appropriate model form:

$$N_T = k_1 \left( \frac{1}{\sigma_r} \right)^{k_2} \quad (53)$$

Replacing  $\sigma_t$  in equation 52 with the joint sealant stress from equation 47,  $\sigma_{js}$ , the following model can be used to estimate the number of environmental spall stress cycles to failure, assuming a unit thickness of depth of spall delamination:

$$N_E = k_3 \left( \frac{1}{k_{js} \text{ELONG}} \right)^{k_4} \quad (54)$$

where

$K_{js}$  = modulus of the sealant material or incompressibles, kPa/mm  
 ELONG = a factor estimating the horizontal movement of the slab, m  
 =  $CL(\alpha\Delta T + e)$   
 L = slab length or joint spacing, m  
 $\Delta T$  = thermal gradient in the slab, °C



|            |   |                                  |
|------------|---|----------------------------------|
| e          | = | concrete drying shrinkage strain |
| $\alpha$   | = | concrete thermal expansion, / °C |
| C          | = | subbase friction factor          |
| $k_3, k_4$ | = | regression constants             |

### Mechanistic-Empirical Spalling Prediction Model Form

Using the damage calculated from equation 51 and based on an examination of the progression of spalling with traffic loading and pavement age for the LTPP pavements, the following form was selected for the development of models for predicting transverse joint spalling for JPCP and JRCP:

$$\%Spall = \frac{\text{Damage}^m}{(1 + \text{Damage})^n} \text{ (Scaling Factor)} \quad (55)$$

where

|                |   |  |
|----------------|---|--|
| %Spall         | = | the percentage of joints with low-, medium-, or high-severity spalls |
| Damage         | = | the total damage due to traffic and environmental stresses           |
| Scaling Factor | = | scaling factor used to calibrate the model to field conditions       |
| m, n           | = | regression parameters  |

This model form assumes that the percentage of joints with spalls is a function of the interaction between the damage caused by traffic and environmental stresses and a scaling factor. The scaling factor accounts for all the other factors that are not directly considered in the mechanistic portion of the model.

### Determination of Empirical Scaling Variables

An essential part of equation 55 is the scaling factor that is applied to calibrate the model to field conditions. An exhaustive evaluation of the LTPP GPS 3 and 4 data was conducted to determine the best scaling factor to use. This included using the knowledge obtained from the review of past models and statistical analyses of the GPS 3 and 4 data. The objective was to use the results to identify potential variables for inclusion in the model.

#### Jointed Plain Concrete Pavement

Table 9 presents a summary of the correlation analysis results for the potential variables selected for development of a JPCP spalling model. It shows the strength of the relationships between several significant variables and spalling. The definitions of the variables are presented in table 10. Figure 20 shows a plot of those independent variables against the percentage of JPCP joints with low-, medium-, or high-severity spalling in the LTPP database. These results were analyzed to evaluate the independent variables that show an influence on spalling for possible use in developing the model. The results confirm that an increase in traffic loading and age (which are related) results in more spalling and that these are important variables to consider in a spalling

model for JPCP. Also, of the variables selected for evaluation, several environmental variables were comparatively more correlated to spalling. The number of wet days, the average relative humidity during the month of construction, and annual precipitation are all negatively correlated to spalling, with increasing values of those factors resulting in less spalling. Conversely, higher values of the mean monthly temperature range and number of air freeze-thaw cycles result in more spalling. The design features that were relatively highly correlated to spalling were the mean joint spacing and the type of joint sealant.

Table 9. Correlation matrix for variables for JPCP transverse joint spalling model.\*

|         | RH       | TRANGE   | HPCC     | BTHICK   | K        | JTSP     | ST       | FI       | FTCYC    | PRECIP   | WTDYS    | AGE      | ESAL     | PSPALL           |
|---------|----------|----------|----------|----------|----------|----------|----------|----------|----------|----------|----------|----------|----------|------------------|
| RH      | 1        | -0.39738 | -0.00177 | -0.24465 | -0.08145 | 0.40414  | -0.11217 | -0.19846 | -0.38549 | 0.53343  | 0.45624  | 0.08518  | -0.19678 | -0.312 RH        |
| TRANGE  | -0.39738 | 1        | 0.08987  | -0.02222 | 0.02256  | -0.2113  | 0.11469  | -0.04922 | 0.39865  | -0.53464 | -0.56232 | 0.02027  | 0.11601  | 0.29578 TRANGE   |
| HPCC    | -0.00177 | 0.08987  | 1        | -0.09364 | 0.14486  | 0.13208  | 0.03054  | 0.00229  | 0.11117  | -0.00142 | -0.05859 | -0.10402 | 0.05562  | -0.15785 HPCC    |
| BTHICK  | -0.24465 | -0.02222 | -0.09364 | 1        | 0.00075  | -0.22472 | 0.24054  | -0.09388 | -0.12418 | 0.09575  | 0.23869  | -0.34868 | -0.16771 | 0.045 BTHICK     |
| k-value | -0.08145 | 0.02256  | 0.14486  | 0.00075  | 1        | -0.09458 | 0.17845  | -0.37952 | -0.14078 | 0.01048  | -0.00819 | -0.11041 | -0.00504 | -0.01219 k-value |
| JTSP    | 0.40414  | -0.2113  | 0.13208  | -0.22472 | -0.09458 | 1        | -0.25111 | -0.23863 | -0.14154 | 0.53154  | 0.32552  | 0.2899   | 0.1594   | -0.21851 JTSP    |
| ST      | -0.11217 | 0.11469  | 0.03054  | 0.24054  | 0.17845  | -0.25111 | 1        | -0.41399 | -0.18469 | -0.02482 | -0.16453 | -0.06583 | 0.04793  | 0.20583 ST       |
| FI      | -0.19846 | -0.04922 | 0.00229  | -0.09388 | -0.37952 | -0.23863 | -0.41399 | 1        | 0.48967  | -0.34727 | -0.10239 | -0.19996 | -0.24355 | -0.04915 FI      |
| FTCYC   | -0.38549 | 0.39865  | 0.11117  | -0.12418 | -0.14078 | -0.14154 | -0.18469 | 0.48967  | 1        | -0.41372 | -0.29057 | -0.04611 | -0.0275  | 0.15023 FTCYC    |
| PRECIP  | 0.53343  | -0.53464 | -0.00142 | 0.09575  | 0.01048  | 0.53154  | -0.02482 | -0.34727 | -0.41372 | 1        | 0.82875  | 0.14309  | 0.02319  | -0.28214 PRECIP  |
| WTDYS   | 0.45624  | -0.56232 | -0.05859 | 0.23869  | -0.00819 | 0.32552  | -0.16453 | -0.10239 | -0.29057 | 0.82875  | 1        | 0.08088  | -0.04418 | -0.36436 WTDYS   |
| AGE     | 0.08518  | 0.02027  | -0.10402 | -0.34868 | -0.11041 | 0.2899   | -0.06583 | -0.19996 | -0.04611 | 0.14309  | 0.08088  | 1        | 0.39556  | 0.1742 AGE       |
| ESAL    | -0.19678 | 0.11601  | 0.05562  | -0.16771 | -0.00504 | 0.1594   | 0.04793  | -0.24355 | -0.0275  | 0.02319  | -0.04418 | 0.39556  | 1        | 0.22992 ESAL     |
| PSPALL  | -0.312   | 0.29578  | -0.15785 | 0.045    | -0.01219 | -0.21851 | 0.20583  | -0.04915 | 0.15023  | -0.28214 | -0.36436 | 0.1742   | 0.22992  | 1 PSPALL         |

\* See table 10 for definitions.

Table 10. Definitions of selected variables significant to spalling of JPCP.

| Symbol | Potential Independent Variable                                     |
|--------|--|
| RH     | Mean relative humidity during month of construction, percent       |
| TRANGE | Mean monthly temperature range, °C                                 |
| HPCC   | PCC slab thickness, mm   |
| BTHICK | Base thickness, mm   |
| K      | Static backcalculated k-value, kPa/mm                              |
| JTSP   | Mean transverse joint spacing, mm                                  |
| ST     | Sealant type   |
| FI     | Freezing index, degree-days (°C) below freezing                    |
| FTCYC  | Yearly number of air freeze-thaw cycles                            |
| PRECIP | Average annual precipitation, mm                                   |
| WTDYS  | Number of wet days in a year, days                                 |
| AGE    | Time since pavement construction, yr                               |
| ESAL   | Cumulative equivalent 80-kN single axle load                       |
| PSPALL | Percentage of joints with low-, medium-, or high-severity spalling |

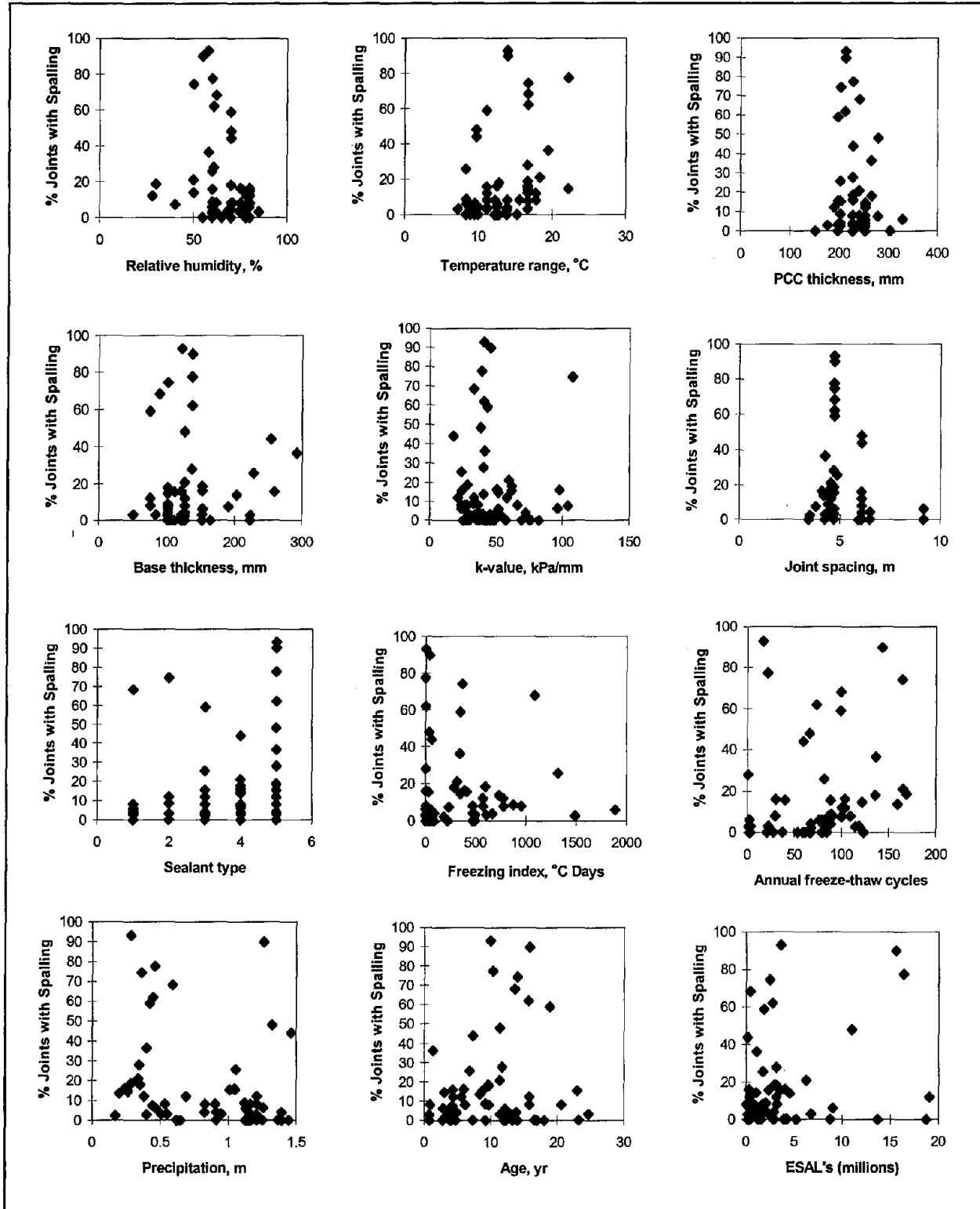


Figure 20. Plot of percentage of joint spalling versus significant variables for JPCP.

Table 11. Correlation matrix for selected variables for JRCP transverse joint spalling model.\*

|         | FI | FTCYC   | PRECIP   | WTDYS    | MAXT     | MINT    | MEANT    | D90      | JTSP     | HPCC     | EPCC     | ESAL     | AGE      | BTHICK   | BTYPE   | Cd       | k-value  | PSPALL   |         |
|---------|----|---------|----------|----------|----------|---------|----------|----------|----------|----------|----------|----------|----------|----------|---------|----------|----------|----------|---------|
| FI      | 1  | 0.57991 | -0.74212 | -0.03719 | -0.89006 | -0.8824 | -0.89017 | -0.77309 | -0.46041 | -0.41858 | -0.01902 | 0.02284  | 0.00474  | -0.09942 | -0.5767 | -0.46159 | -0.37244 | -0.24593 | FI      |
| FTCYC   |    | 1       | -0.81893 | -0.00997 | -0.80147 | -0.8538 | -0.83184 | -0.79381 | -0.18328 | -0.46474 | -0.16779 | 0.13122  | -0.18318 | -0.13859 | -0.4015 | -0.42369 | -0.17988 | -0.05075 | FTCYC   |
| PRECIP  |    |         | 1        | 0.19078  | 0.80481  | 0.83679 | 0.8248   | 0.7104   | 0.35478  | 0.41184  | 0.09325  | 0.04284  | 0.24926  | 0.23176  | 0.37458 | 0.32675  | 0.25818  | -0.0394  | PRECIP  |
| WTDYS   |    |         |          | 1        | -0.16577 | -0.0768 | -0.12104 | -0.35508 | 0.15484  | 0.29129  | 0.01827  | 0.22645  | 0.1207   | 0.27547  | -0.3514 | -0.39467 | -0.06923 | -0.00579 | WTDYS   |
| MAXT    |    |         |          |          | 1        | 0.98212 | 0.99535  | 0.9545   | 0.3693   | 0.40402  | 0.02191  | -0.05428 | 0.08585  | 0.08135  | 0.64368 | 0.56878  | 0.36552  | 0.16011  | MAXT    |
| MINT    |    |         |          |          |          | 1       | 0.99569  | 0.91242  | 0.36377  | 0.49087  | 0.07765  | -0.07447 | 0.08379  | 0.13827  | 0.60155 | 0.5463   | 0.32641  | 0.1741   | MINT    |
| MEANT   |    |         |          |          |          |         | 1        | 0.93725  | 0.36809  | 0.45021  | 0.05055  | -0.0649  | 0.08518  | 0.10982  | 0.62504 | 0.55984  | 0.34715  | 0.16798  | MEANT   |
| D90     |    |         |          |          |          |         |          | 1        | 0.27871  | 0.28123  | -0.01334 | -0.11472 | 0.0649   | 0.00147  | 0.62835 | 0.57072  | 0.34526  | 0.13082  | D90     |
| JTSP    |    |         |          |          |          |         |          |          | 1        | 0.04951  | -0.17453 | 0.37116  | 0.35035  | -0.09127 | 0.00282 | 0.00807  | -0.07957 | -0.00827 | JTSP    |
| HPCC    |    |         |          |          |          |         |          |          |          | 1        | 0.3628   | 0.03391  | -0.07105 | 0.1667   | 0.15603 | 0.13792  | 0.01732  | 0.31903  | HPCC    |
| EPCC    |    |         |          |          |          |         |          |          |          |          | 1        | 0.14583  | -0.05375 | -0.03553 | 0.00829 | 0.17392  | -0.13616 | -0.12035 | EPCC    |
| ESAL    |    |         |          |          |          |         |          |          |          |          |          | 1        | 0.47839  | 0.1062   | -0.2121 | -0.14971 | -0.14787 | -0.09871 | ESAL    |
| AGE     |    |         |          |          |          |         |          |          |          |          |          |          | 1        | -0.07076 | -0.1657 | -0.09605 | 0.0071   | -0.25296 | AGE     |
| BTHICK  |    |         |          |          |          |         |          |          |          |          |          |          |          | 1        | -0.0575 | -0.27232 | 0.1944   | 0.24687  | BTHICK  |
| BTYPE   |    |         |          |          |          |         |          |          |          |          |          |          |          |          | 1       | 0.79679  | 0.56174  | 0.07514  | BTYPE   |
| Cd      |    |         |          |          |          |         |          |          |          |          |          |          |          |          |         | 1        | 0.38795  | -0.12729 | Cd      |
| k-value |    |         |          |          |          |         |          |          |          |          |          |          |          |          |         |          | 1        | 0.08321  | k-value |
| PSPALL  |    |         |          |          |          |         |          |          |          |          |          |          |          |          |         |          |          | 1        | PSPALL  |

\* See table 12 for definitions.

Table 12. Definition of selected variables significant to spalling of JRCP.

| Symbol  | Potential Independent Variable                                     |
|---------|--|
| FI      | Freezing index, degree-days (°C) below freezing                    |
| FTCYC   | Yearly number of air freeze-thaw cycles                            |
| PRECIP  | Average annual precipitation, mm                                   |
| WTDYS   | Number of wet days in a year, days                                 |
| MAXT    | Average maximum daily temperature, °C                              |
| MINT    | Average minimum daily temperature, °C                              |
| MEANT   | Average mean daily temperature, °C                                 |
| D90     | Number of days maximum temperature is greater than 32°C            |
| JTSP    | Mean transverse joint spacing, mm                                  |
| HPCC    | PCC slab thickness, mm   |
| EPCC    | Elastic modulus, kPa   |
| ESAL    | Cumulative equivalent 80-kN single axle load, thousands            |
| AGE     | Time since pavement construction, yr                               |
| BTHICK  | Base thickness, mm   |
| BTYPE   | Type of base, 0=erodible and 1=nonerodible                         |
| Cd      | Drainage coefficient   |
| k-value | Backcalculated static k-value, kPa/mm                              |
| PSPALL  | Percentage of joints with low-, medium-, or high-severity spalling |

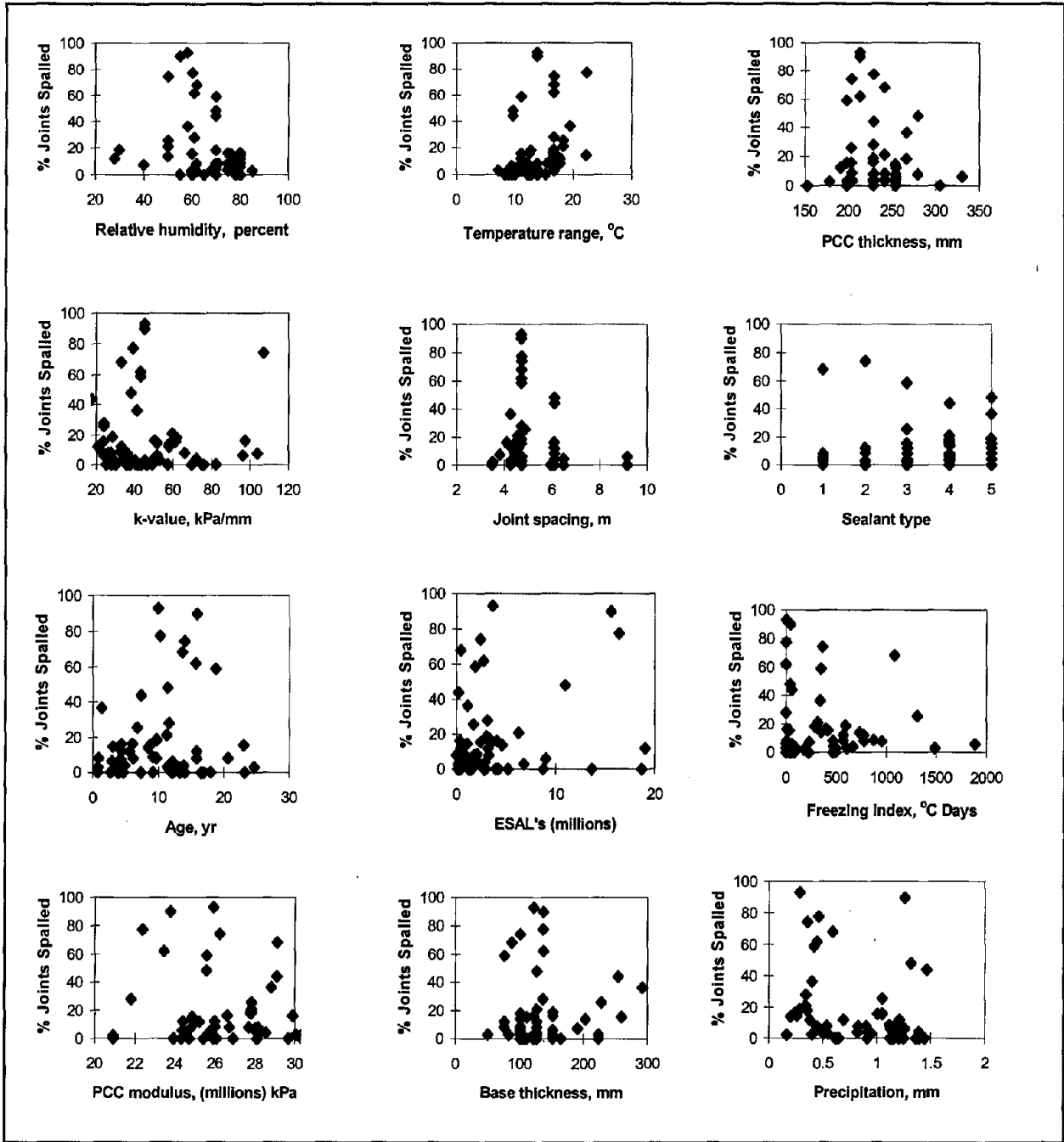


Figure 21. Plot of percentage of joint spalling versus significant variables for JRCP.



## Jointed Reinforced Concrete Pavement

The results of correlation analysis that show the strength of the relationships between selected variables and JRCP spalling are shown in table 11. The definitions of the variables in table 11 are presented in table 12. Figure 21 is a plot of those independent variables versus the percentage of joints with low-, medium-, or high-severity spalling in the LTPP database for JRCP. These results were analyzed to evaluate the independent variables that show a strong influence on JRCP spalling.

From the results, the variables that were relatively highly correlated to JRCP joint spalling were the thicknesses of the PCC slab and base, pavement age, and freezing index. Unlike the results obtained for JPCP spalling, however, the results of the correlation analysis showed some unexpected trends. Traffic loading and age both turned out to be negatively correlated with spalling, with the younger and less trafficked GPS 4 sections showing more spalling than the older sections. Other variables that were relatively significantly correlated to spalling included environmental variables such as the average maximum, minimum, and mean monthly temperatures and the number of days with temperature greater than 32 °C.

### Calibration of Mechanistic-Empirical Joint Spalling Models

The final step in the development of the prediction models was calibration of the models formulated with the LTPP data for the GPS 3 and 4 pavement sections. Mechanistic-empirical models were developed for joint spalling of JPCP and JRCP. This was accomplished using optimization and regression analysis techniques similar to those described previously for the other models developed in this study. The procedure involved determining the best-fit parameters ( $\alpha_1$ ,  $\alpha_2$ ,  $K_1$ ,  $K_2$ ,  $K_3$ ,  $K_4$ ,  $m$ , and  $n$ ) in equations 51, 53, 54, and 55.

#### JPCP Spalling Model

The mechanistic-empirical model for predicting JPCP spalling developed using the LTPP GPS 3 database consists of three parts. They include equations for estimating the allowable number of traffic and environmental load applications to failure, a spalling damage accumulation model, and a model for calculating the percentage of joints with spalling of all severities. Following are the models that were developed.

#### *Allowable Number of Traffic ( $N_T$ ) and Environment ( $N_E$ ) Load Applications*

The equations for calculating  $N_T$  and  $N_E$  for JPCP are as follows:

$$N_T = 199252 \left( \frac{1}{\sigma_t} \right)^{0.15} \quad (56)$$

where

$\sigma_t$  = tensile stress, kPa (calculated from equation 49)

$$N_E = 650162 \left( \frac{t}{k_{js} \text{ELONG}} \right)^{0.85} \quad (57)$$

|            |   |  |
|------------|---|--|
| $k_{js}$   | = | modulus of the sealant material or incompressibles, kPa    |
| ELONG      | = | a factor estimating the horizontal movement of the slab, m |
|            | = | $3.28CL(3.24\alpha\Delta T + e)$                           |
| L          | = | slab length or joint spacing, m                            |
| $\Delta T$ | = | thermal gradient in the slab, °C                           |
| e          | = | concrete drying shrinkage strain                           |
| $\alpha$   | = | concrete thermal expansion, per °C                         |
| C          | = | subbase friction factor                                    |
| t          | = | 1 mm   |

Tables 13 through 15 provide estimates for shrinkage, e, concrete thermal coefficient,  $\alpha$ , and the sealant and incompressible modulus if they cannot be obtained from field or laboratory tests. The type of aggregates used in the PCC, the indirect tensile strength, and the sealant type are available in most databases, including the LTPP database.

#### *Damage Accumulation Model*

The final model for calculating the total damage from traffic and environmental loading for JPCP is as follows:

$$\text{Damage} = \left( \frac{\text{KESAL}}{N_T} \right) + \left( \frac{\text{AGE}^{0.145}}{N_E} \right) \quad (58)$$

where

|       |   |  |
|-------|---|--|
| KESAL | = | 80-kN ESAL's in thousands                                |
| AGE   | = | pavement age in years                                    |
| $N_T$ | = | allowable number of cycles due to traffic stresses       |
| $N_E$ | = | allowable number of cycles due to environmental stresses |

Table 13. Approximate relationship between shrinkage and indirect tensile strength.<sup>(33)</sup>

| <b>Indirect Tensile Strength</b> | <b>Shrinkage mm/mm</b> |
|----------------------------------|------------------------|
| 300 or less                      | 0.0008                 |
| 400                              | 0.0006                 |
| 500                              | 0.00045                |
| 600                              | 0.0003                 |
| 700 or greater                   | 0.0002                 |

Table 14. Recommended values of thermal coefficient.<sup>(33)</sup>

| <b>Type of Coarse Aggregate</b> | <b>Concrete Thermal Coefficient (<math>10^{-6}/^{\circ}\text{C}</math>)</b> |
|---------------------------------|---|
| Quartz                          | 3.66  |
| Sandstone                       | 3.61  |
| Gravel                          | 3.33  |
| Granite                         | 2.94  |
| Basalt                          | 2.66  |
| Limestone                       | 2.11  |

Table 15. Adjusted sealant modulus for JPCP.

| <b>Sealant Type</b> | <b>Adjusted Sealant Modulus (<math>10^6</math> kPa)</b> |
|---------------------|---|
| Preformed           | 1.405   |
| Low modulus asphalt | 1.396   |
| Silicone            | 2.529   |
| Others              | 2.300   |
| Incompressibles     | 5.290   |

### *JPCP Spalling Model*

The final model for predicting the percentage of spalled joints for JPCP is as follows:

$$\text{Spall}_{\text{JPCP}} = \frac{100 \text{Damage}^{2.1}}{1 + \text{Damage}^{2.5}} (0.344 \text{TRANGE} - 0.042 \text{RH} + 0.0318 \text{FTCYC}) \quad (59)$$

where

|                       |   |  |
|-----------------------|---|--|
| Spall <sub>JPCP</sub> | = | percentage of JPCP joints with spalling of all severities  |
| TRANGE                | = | average daily temperature range, °C  |
| RH                    | = | average daily range of relative humidity during the month of construction that can be obtained from the National Oceanic and Atmospheric Administration (NOAA) tables, percent |
| FTCYC                 | = | number of freeze-thaw cycles   |
| Damage                | = | damage from traffic and environmental stresses (equation 58)   |

Statistics:

|                |   |                                |
|----------------|---|--------------------------------|
| N              | = | 52                             |
| R <sup>2</sup> | = | 0.61                           |
| SEE            | = | 12 percent                     |
| p-value        | < | 0.0001 (significance of model) |

A plot of the predicted and measured percentage of spalled joints is shown in figure 22. A plot of the residuals (predicted - actual percentage of joints spalled) against the predicted percentage of joints spalled is shown in figure 23. Figure 22 does not show very good fit of the LTPP data with the model. However, the overall accuracy of the spalling model is reflected by the R<sup>2</sup> of 0.61, which is the proportion of variation of spalling explained by the variables included in the model. A test of hypothesis was performed to determine the significance of the variables used in the model for predicting spalling. The null and alternate hypothesis were as follows:

|                  |   |
|------------------|---|
| H <sub>0</sub> : | all model parameters are zero (variables are not significant) |
| H <sub>A</sub> : | all model parameters are not zero                             |

The F-test statistic used for the hypothesis test was calculated as the ratio of the mean square for the model divided by the mean square of the error. For this study the null hypothesis will be rejected if the level of significance is less than 5 percent (0.05). A level of significance (p-value) of less than 0.0001 implies a rejection of the null hypothesis. This shows that the variables in the model are highly significant.

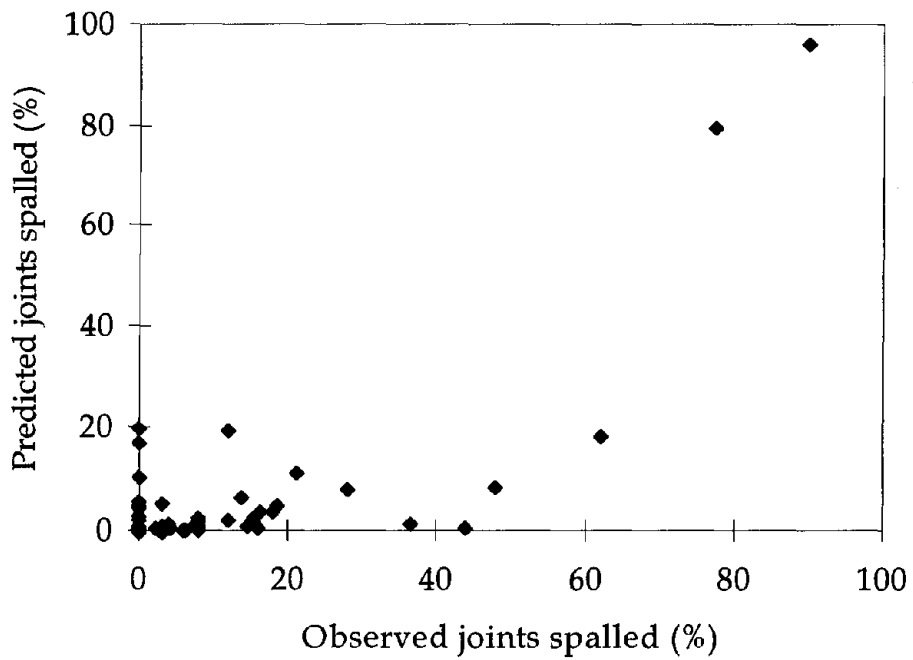


Figure 22. Predicted percentage of spalled joints versus the actual percentage of spalled joints for JPCP.

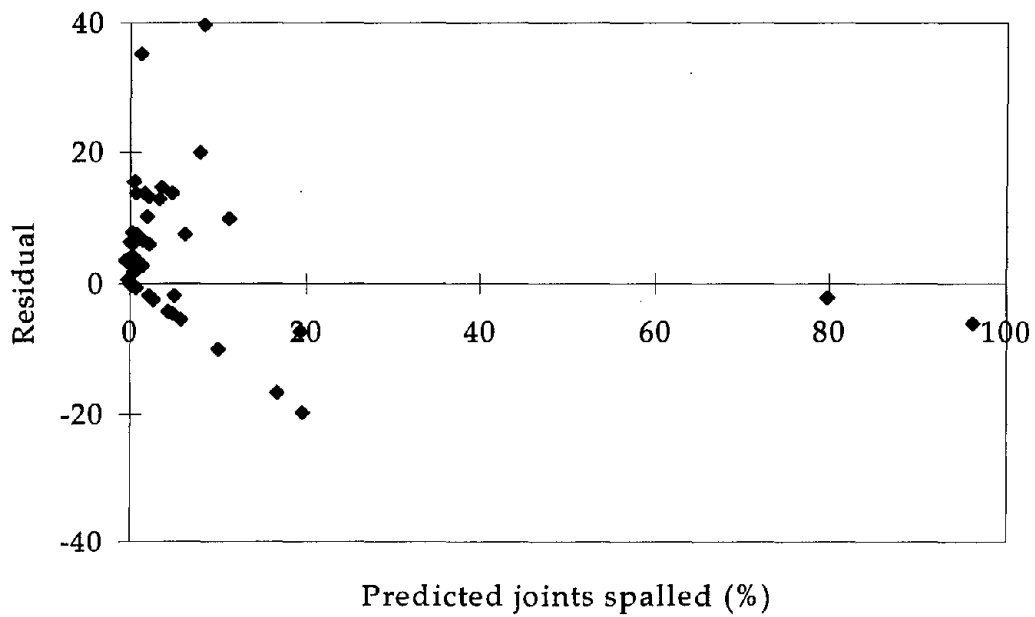


Figure 23. Plot of the residuals versus the predicted percentage of spalled joints for JPCP.

Also, individual t-tests were conducted to test if the individual parameter estimates are equal to zero. The p-values for this test ranged from 0.0002 to 0.016. The results show that all the parameter estimates had values other than zero; therefore, the variables in the model were significant. Prediction accuracy of the percentage of spalled joints in absolute units is reflected by the standard error of estimate (SEE = 12 percent). The overall effectiveness of the model should be judged on all of the diagnostic statistics, the residual plots, and the results from the sensitivity analysis to follow. The diagnostic statistics obtained for the JPCP spalling model show that the model can predict transverse joint spalling with reasonable accuracy for the LTPP database utilized.

### JRCP Spalling Model

The mechanistic-empirical model for predicting JRCP spalling developed using the LTPP GPS 4 database also consists of three parts. Following are the different parts of the model.

#### *Allowable Number of Traffic ( $N_T$ ) and Environment ( $N_E$ ) Load Applications*

The equations for calculating  $N_T$  and  $N_E$  for JRCP obtained are as follows:

$$N_T = \left( \frac{26841 k^2 + 28.9 k h_{PCC}}{\sigma_t} \right) \quad (60)$$

$$N_E = \left( \frac{868 h_{PCC}^2 + 83800 k h_{PCC}}{k_{js} \text{ELONG}} \right) \quad (61)$$

where

|            |   |   |
|------------|---|---|
| $\sigma_t$ | = | tensile stress, kPa (calculated from equation 49)                 |
| $k_{js}$   | = | modulus of the sealant material or incompressibles, kPa           |
| ELONG      | = | an estimate of the horizontal movement defined for equation 57, m |
| k          | = | modulus of subgrade reaction, kPa/mm                              |
| $h_{PCC}$  | = | PCC thickness, mm   |

The recommended values for elastic moduli of the sealants or incompressible,  $k_{js}$ , for JRCP are given in table 16.

Table 16. Adjusted sealant modulus for JRCP.

| Sealant Type       | Adjusted Sealant Modulus (10 <sup>6</sup> kPa) |
|--------------------|--|
| Preformed          | 9.00   |
| Rubberized asphalt | 17.78  |
| Silicone           | 0.069  |
| Asphalt            | 0.069  |
| Incompressibles    | 22.84  |

*Damage Accumulation Model*

The final model for JRCP for calculating the total damage from traffic and environmental loading is as follows:

$$\text{Damage} = \frac{0.0667 * \text{KESAL}}{N_T} + \frac{5.667 * \text{AGE}}{N_E} \quad (62)$$

where

- KESAL = number of 80-kN ESAL's in thousands
- AGE = pavement age in years
- N<sub>T</sub> = allowable number of cycles due to traffic stresses
- N<sub>E</sub> = allowable number of cycles due to environmental stresses

*JRCP Spalling Model*

The final model for predicting the percentage of spalled joints for JRCP is as follows:

$$\text{Spall}_{\text{JRCP}} = 100 \text{DAM}^{0.85} (1.764 * 10^{-5} \text{FI} + 6.348 * 10^{-8} E_{\text{PCC}} - 0.02714 k) \quad (63)$$

where

- Spall<sub>JRCP</sub> = percentage of joints with spalling of all severities
- FI = mean annual freezing index, °C days
- E<sub>PCC</sub> = PCC elastic modulus, kPa
- k = modulus of subgrade reaction, kPa/mm
- DAM = damage due to traffic and environmental stresses

Statistics:

|                |   |                               |
|----------------|---|-------------------------------|
| N              | = | 68                            |
| R <sup>2</sup> | = | 0.43                          |
| SEE            | = | 5.06 percent                  |
| p-value        | < | 0.002 (significance of model) |

A plot of the predicted and measured percentage of spalled joints is shown in figure 24. A plot of the residuals (predicted - actual percentage of spalled joints) against the predicted percentage of spalled joints is shown in figure 25. The overall accuracy of the JRCP spalling model is reflected by the R<sup>2</sup> of 0.43, which is the proportion of variation of JRCP spalling explained by the variables included in the model. A test of hypothesis was performed to determine the significance of the variables used in the model for predicting spalling. The null and alternate hypothesis were as follows:

- H<sub>0</sub>: all model parameters are zero (variables are not significant)
- H<sub>A</sub>: all model parameters are not zero

The F-test statistic used for the hypothesis test was calculated as the ratio of the mean square for the model divided by the mean square of the error. For this study the null hypothesis will be rejected if the level of significance is less than 5 percent (0.05). A level of significance (p-value) of less than 0.002 implies a rejection of the null hypothesis. This shows that the variables in the model are significant. Also, individual t-tests were conducted to test if the individual parameter estimates are equal to zero. The p-values for this test ranged from 0.001 to 0.03.

The results show that all the parameter estimates had values other than zero; therefore, the variables in the model were significant. Prediction accuracy of percentage of spalled joints in absolute units is reflected by the standard error of estimate (SEE = 5.06 percent). The overall effectiveness of the model should be judged on all of the diagnostic statistics, the residual plots, and the results from the sensitivity analysis to follow. The diagnostic statistics obtained for the JRCP spalling model show that the model can predict transverse joint spalling for JRCP with reasonable accuracy for the LTPP database utilized.



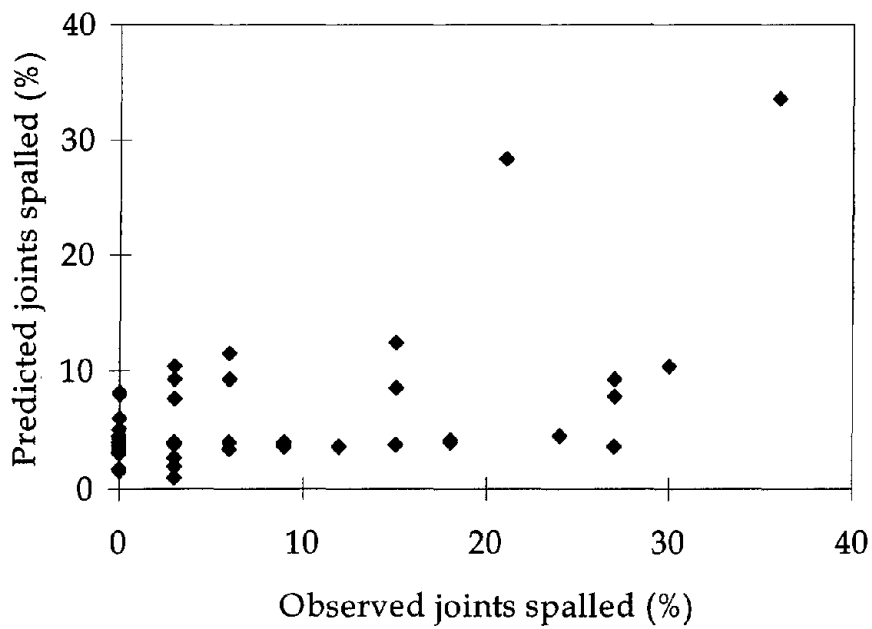


Figure 24. Predicted percentage of spalled joints versus the actual percentage of spalled joints for JRCP.

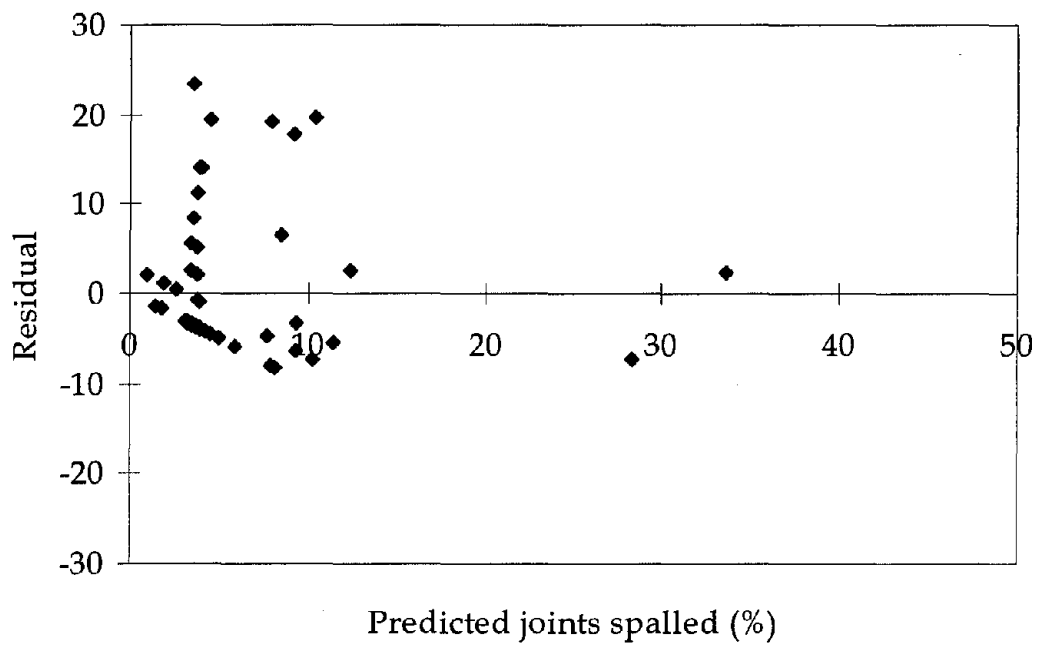


Figure 25. Plot of residuals versus the predicted percentage of spalled joints for JRCP.

## **Sensitivity Analysis for Mechanistic-Empirical Spalling Models**

The final step in the model-building process is the verification of the selected regression model. For the JPCP and JRCP spalling models developed, model verification was limited to a comprehensive sensitivity analysis that involved the comparison of results with theoretical expectations, earlier empirical results, and simulated results reported in previously published literature. The sensitivity analysis involved using the model to determine the effect of each variable on percentage of joints spalled when the other variables in the model were held at their mean values. Plots were prepared to show these results. The plots were examined and the results compared with theoretical expectations and empirical results from earlier research studies. There were relatively limited data for model development, so a comprehensive validation of the model was not possible. The plots and results from the sensitivity analysis are discussed in the following sections.

### JPCP Mechanistic-Empirical Model

The effects of three key groups of factors on JPCP spalling were checked using the mechanistic-empirical model. The factors investigated included environmental effects, traffic loading, and sealants and incompressibles.

#### *Effect of Environmental Factors*

The key environmental variables that were found to have an influence on joint spalling of JPCP were the average daily temperature range, the mean monthly relative humidity during the month of construction, and the number of annual freeze-thaw cycles. The model also shows the influence of the type of sealant, or lack thereof, in relation to all these factors.

Figure 26 shows the significance of the daily temperature range and type of joint sealant on spalling. A high daily temperature range results in more spalling regardless of the type of sealant used. It is believed that the higher temperature range may result in higher restrained thermal stresses. Early in the life of the pavement, this may result in more microcracks and delaminations that contribute to more spalling. Preformed sealants seem to decrease these stresses and cause less spalling, whereas joints without any sealants and that are probably filled with incompressibles experience more spalling. As shown in figure 27, a high relative humidity during the month of construction reduces the occurrence of spalling. A possible explanation is that, by aiding the curing process because of the reduced rate at which moisture leaves the PCC slab, a high relative humidity may increase strength gain and reduce shrinkage. This can reduce the magnitude of early age stresses and the occurrence of delaminations and microcracks that lead to spalling.

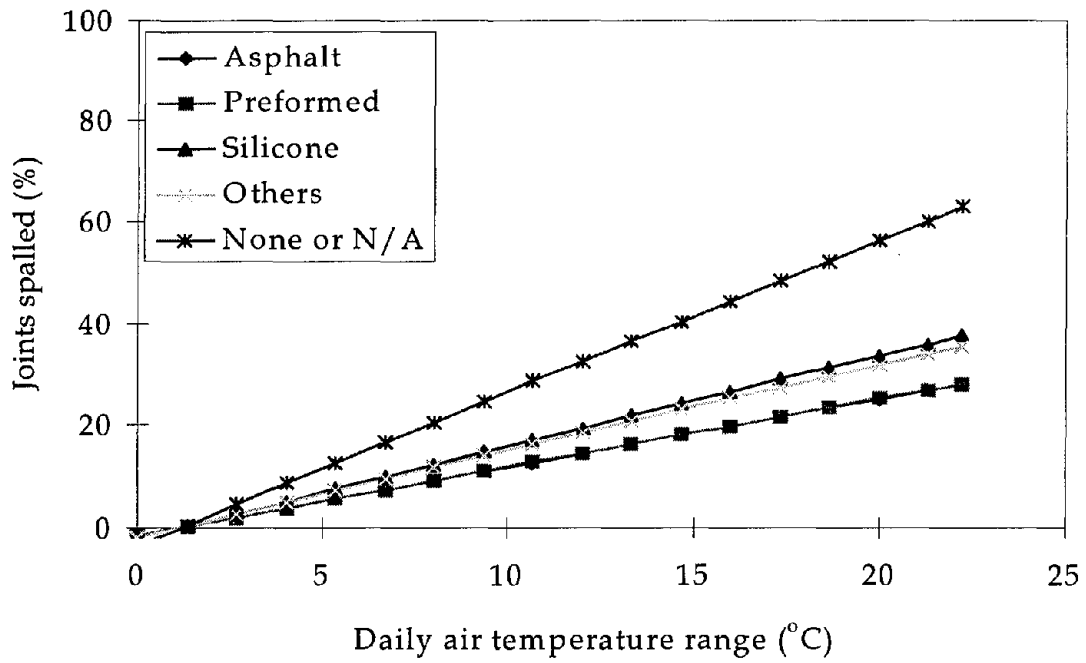


Figure 26. Sensitivity plot of percentage of JPCP joint spalling versus average daily temperature range.

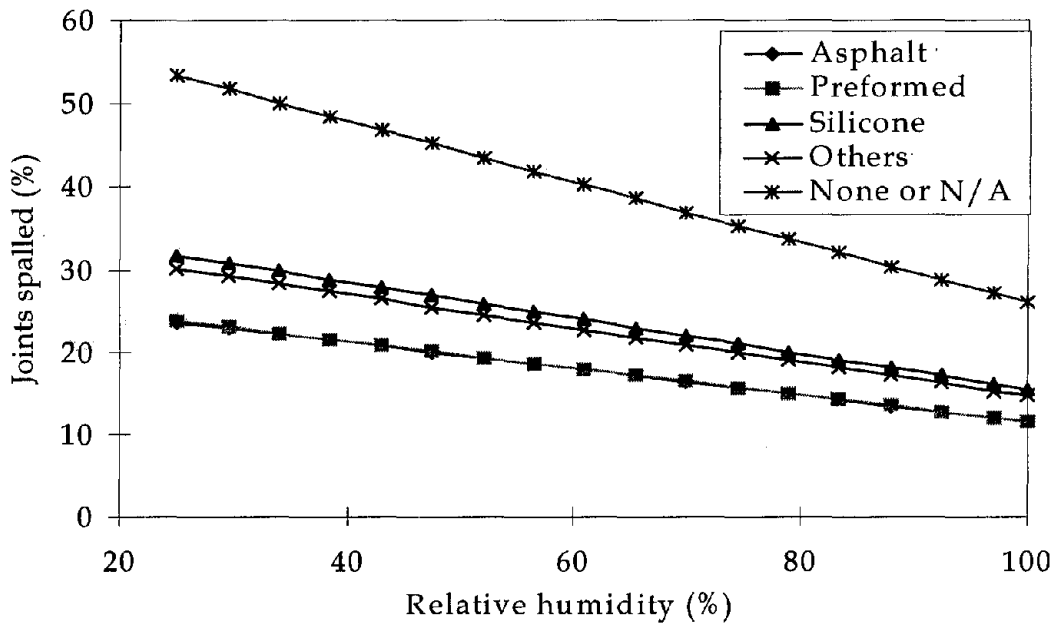


Figure 27. Sensitivity plot of percentage of JPCP spalling versus mean relative humidity during month of construction.

The influence of freeze-thaw cycles is shown in figure 28. The higher the number of freeze-thaw cycles, the greater the chance for durability damage of the concrete. This will lead to more spalling. Finally, figure 29 shows the effect of the horizontal movement or elongation of the PCC slab on joint spalling. As expected, such movement increases spalling because this causes an increase in the pressure or reaction to the joint surface to sealants and incompressibles, as well as from actual contact of the two concrete slab surfaces.

#### *Effect of Traffic Loads*

The influence of traffic loading on joint spalling of JPCP as depicted by the model is shown in figure 30. An increase in traffic load applications increases spalling, as expected. The rate of increase of spalling is quite rapid and is greatest for joints with no sealants. Joints with preformed sealant perform the best in terms of joint spalling.

#### *Effect of Joint Sealant and Incompressibles*

The tremendous influence of sealants on joint spalling is illustrated by the sensitivity plots shown in figures 26 through 30. In all cases, the greatest spalling was for joints without any sealants (presumably filled up with incompressibles). For those pavements with sealed joints, there is also an appreciable effect of the type of sealant used and the amount of spalling that occurs. Preformed sealants are far better at reducing joint spalling than the other types of sealants. Because of the relatively uniform compression on the surface of the joint provided by preformed sealants or because they keep out incompressibles, it seems that they somewhat reduce the tensile stresses that cause microcracks and delaminations at the joint to spall off. The performance of the other types of sealants is comparable.

#### JRCP Mechanistic-Empirical Model

A similar sensitivity analysis was conducted for the mechanistic-empirical model for predicting joint spalling of JRCP. Following are the results that were obtained that show the significance of the environment, traffic loading, joint sealant, and other factors on the predicted percentage of joints spalled.

#### *Effect of Environmental Factors*

The influence of the environment was less prominent for the mechanistic-empirical model developed for predicting joint spalling of JRCP. The only environmental variable that was found to be mildly significant was freezing index. However, the pavement age, which is related to the cyclic effect of the environment, has a significant effect on joint spalling of JRCP, according to the model. Figure 31 is a plot of percentage of joints spalled versus age. The influence of the type of sealant used is also shown by the plot. The clear trend of the percentage of spalled joints increasing with age confirms the validity of the model. The plot also shows that the different sealant types influence spalling appreciably.

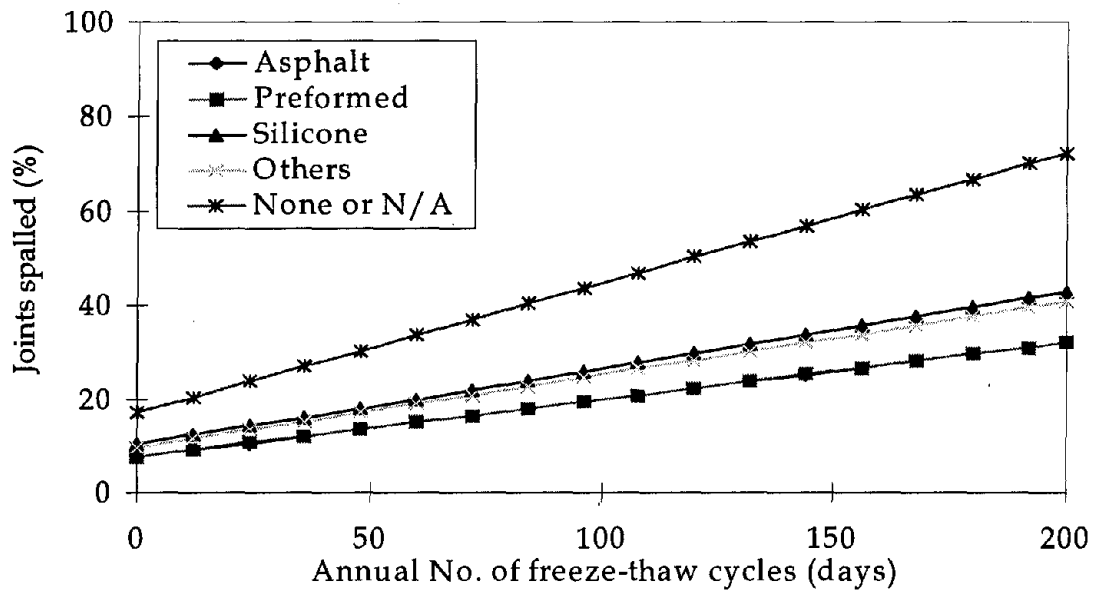


Figure 28. Sensitivity plot of percentage of JPCP spalling versus number of freeze-thaw cycles.

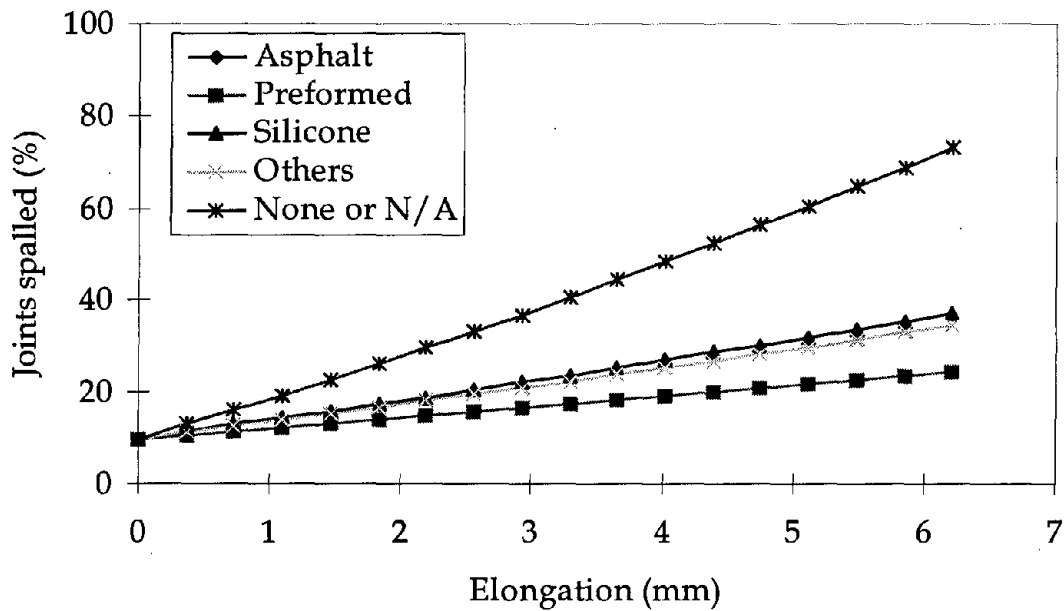


Figure 29. Sensitivity plot of percentage of JPCP spalling versus elongation.

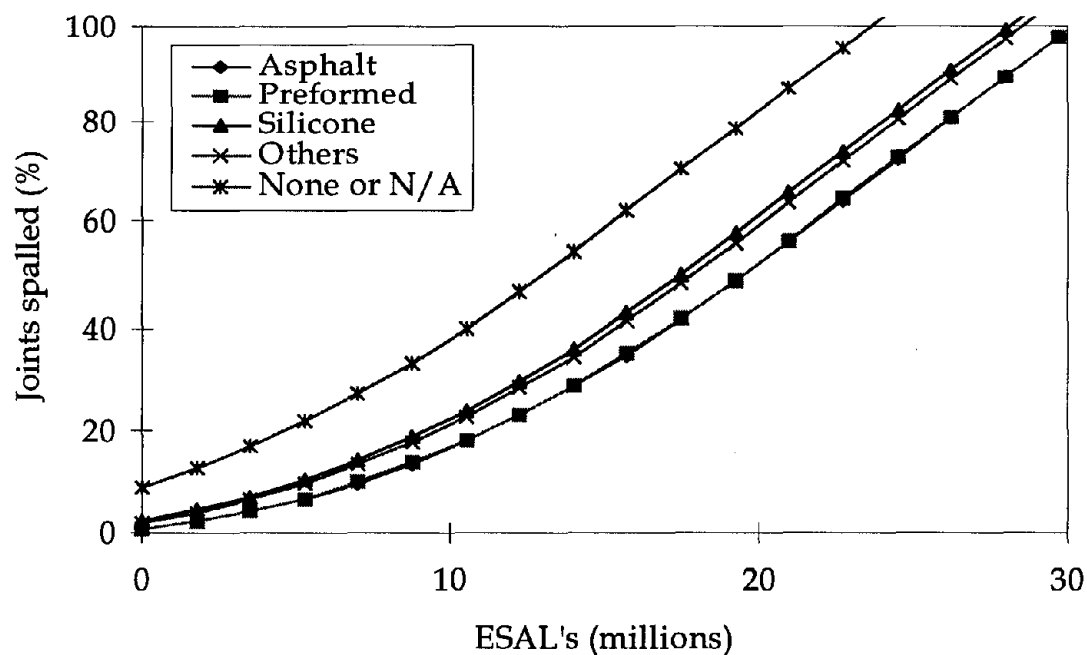


Figure 30. Sensitivity plot of percentage of JPCP spalling versus ESAL's.

Figure 32 shows the effect of freezing index on spalling. The higher the freezing index, the higher the percentage of spalled joints predicted by the model. This is reasonable, because concrete material will deteriorate more in the colder regions of the country since they experience prolonged freezing and freeze-thaw cycles that result in the disintegration of the concrete material and increase spalling.

#### *Effect of Traffic Loading*

An increase in the number of load applications shows the same trend as that for age and increases the percentage of JPCP joints spalled, as shown in figure 33. Figures 34 and 35 are plots of the percentage of joints spalled versus age for a pavement with a preformed sealant and different traffic stress values and elongation due to temperature gradients within the pavement. The figures show that there is more spalling as the traffic and temperature stresses increase. This is in agreement with the mechanistic causes of spalling outlined in earlier sections of this chapter. An increase in tensile stresses around the PCC slab joint helps to propagate existing cracks or develop new ones.

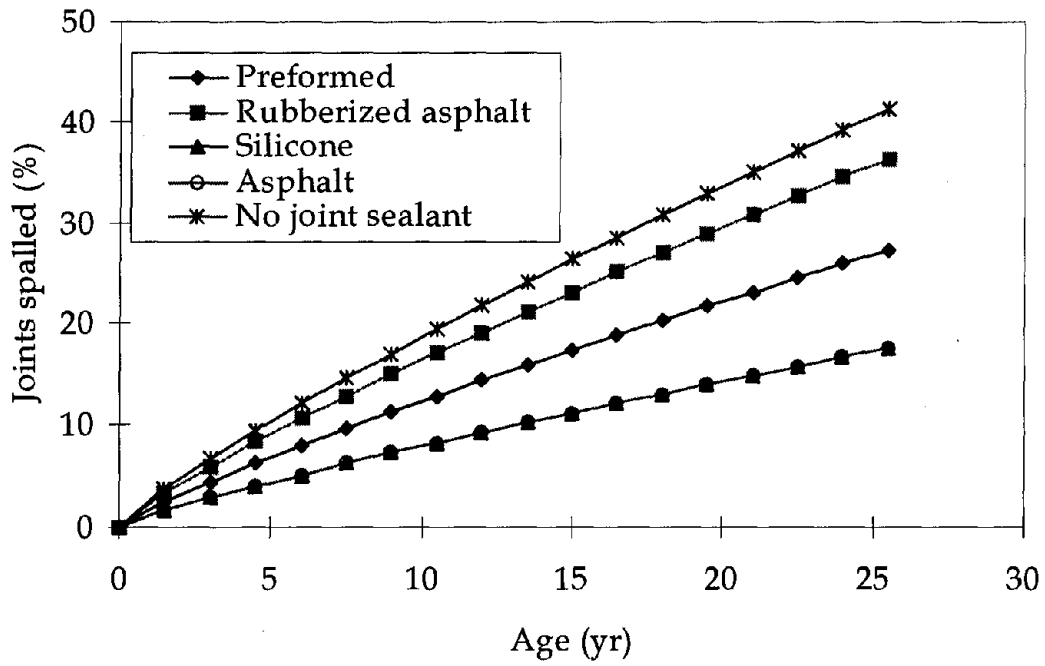


Figure 31. Plot of percentage of joint spalling versus age.

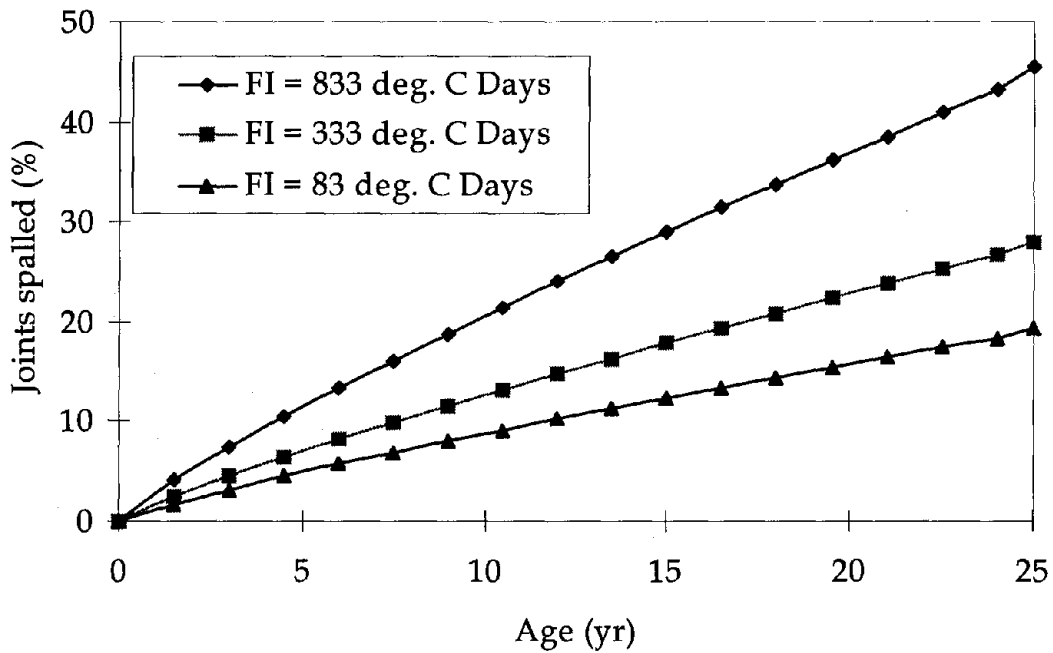


Figure 32. Effect of freezing index on percentage of JRC joints spalled.

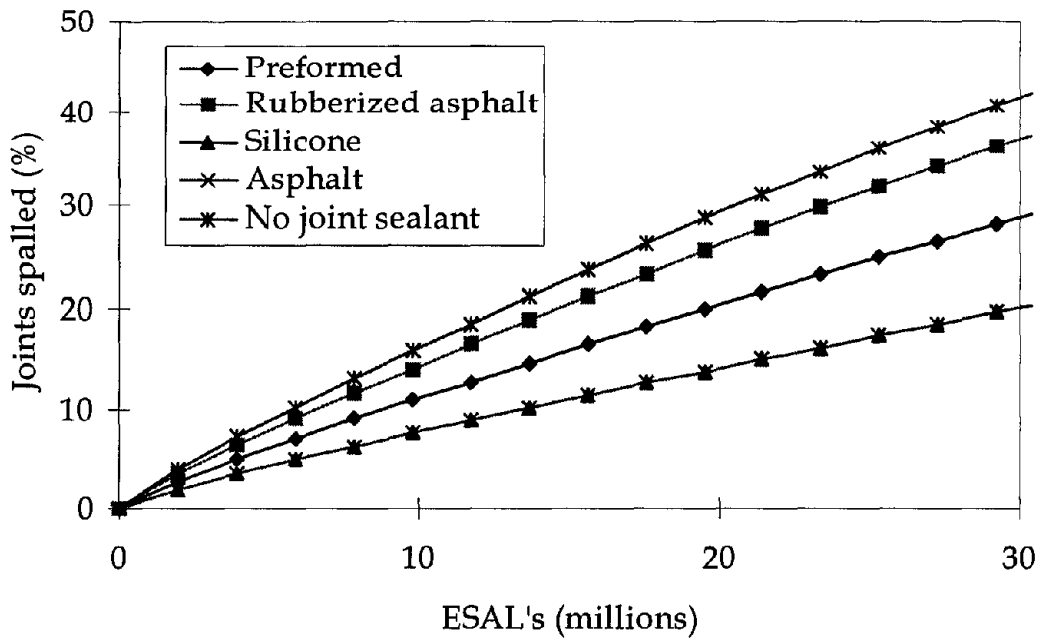


Figure 33. Plot of percentage of JRCP joints spalled versus ESAL's.

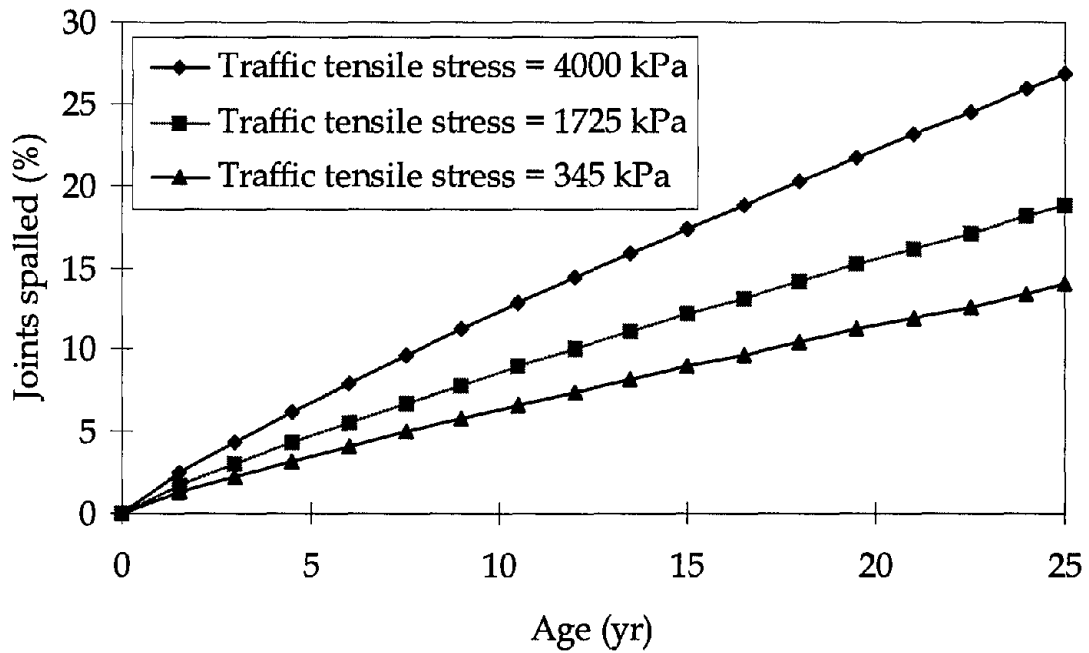


Figure 34. Influence of traffic tensile stresses on percentage of JRCP joints spalled.



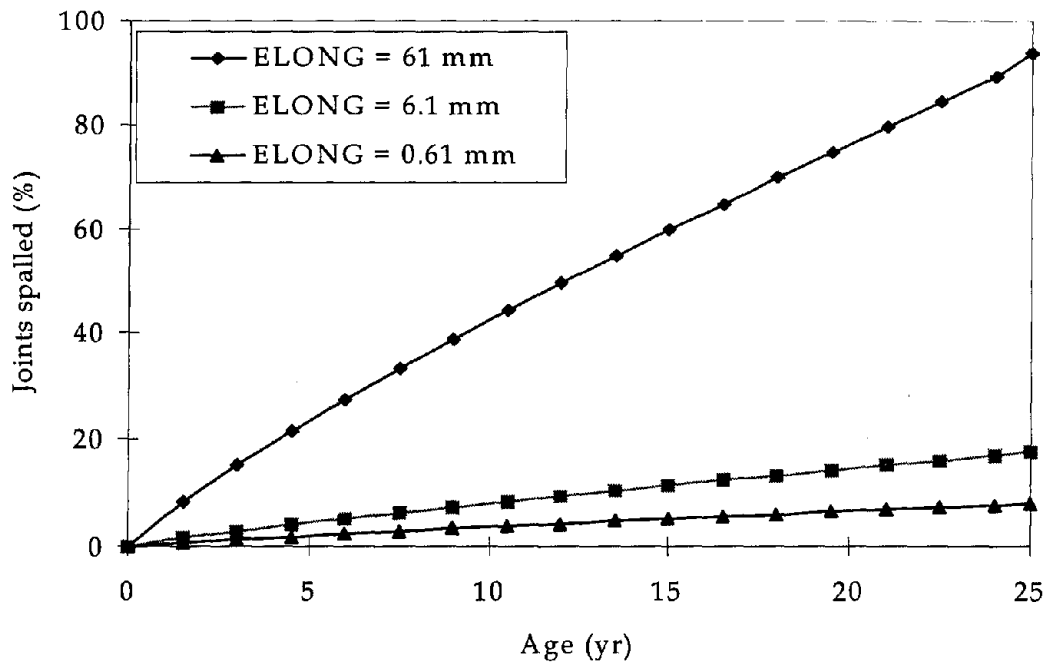


Figure 35. Influence of different ELONG (joint movement) values from temperature gradients on the percentage of JRCP joints spalled.

#### *Effect of Joint Sealant*

The effect of the different types of sealants on joint spalling of JRCP was not very different from that observed for the JPCP model. Figures 29 and 32 both illustrate the influence of the different joint sealant conditions. For JRCP, unsealed joints were also found to spall more, and the type of sealant used has an influence on spalling. However, silicone sealants seem to provide the best protection against spalling, followed by preformed sealants. Joints with rubberized asphalt sealants do not perform as well and seem not to be much better than unsealed joints.

#### *Effect of Modulus of Subgrade Reaction*

Figure 36 is a plot of percentage of joints spalled versus age for a pavement with a preformed sealant and different subgrade k-values. The figure shows that there is less spalling as the k-value of subgrade strength increases. This is reasonable because stronger subgrades reduce deflections at the pavement joints, thus reducing spalling stresses.

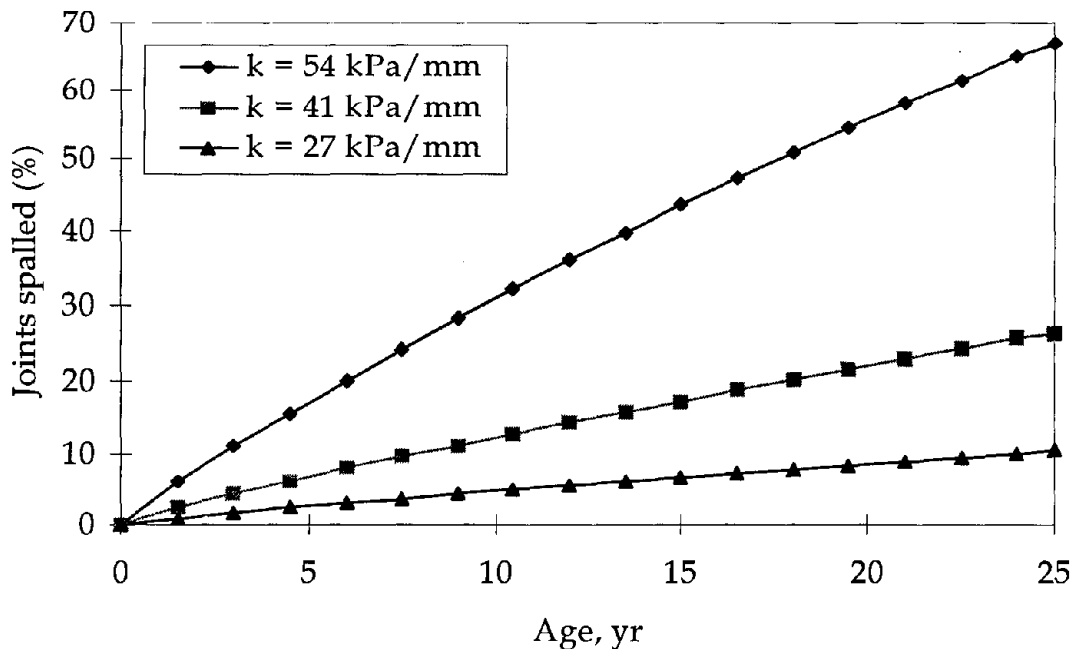


Figure 36. Influence of k-value on percentage of JRCP joints spalled.

## Summary

### JPCP Spalling

The following can be summarized about the JPCP spalling model:

- Sixty-one percent of the total variation of spalling can be explained by the included variables.
- Some of the unexplained variation may be due to errors in the independent variables used to develop the model, such as the traffic estimates.
- The “average” error in predicting JPCP spalling is 12 percent.
- There are no discernible patterns in the residuals. This means that the data used in model development had little or no serial correlation.
- Data from 52 pavement sections from all over the United States were used to develop the model (N = 52).
- Each independent variable and the overall model was found to be significant.
- The sensitivity analysis shows that all of the explanatory variables have a plausible effect on spalling that agrees with theoretical expectations and previous empirical field results.

## JRCP Spalling

The following can be summarized about the JRCP spalling model:

- Forty-three percent of the total variation of spalling can be explained by the included variables.
- Some of the unexplained variation may be due to errors in the independent variables used to develop the model, such as the traffic estimates.
- The “average” error in predicting JRCP spalling is 5 percent.
- There are no discernible patterns in the residuals.
- Data from 68 pavement sections from all over the United States were used to develop the model (N = 68).
- Each of the independent variables and the overall model was significant at a level of significance of 5 percent.
- The sensitivity analysis shows that all of the explanatory variables have a plausible effect on spalling that agrees with theoretical expectations and previous empirical field results.

## Implications and Recommendations

The mechanistic-empirical models presented were successfully developed through a combination of applying the knowledge available about the mechanism of spalling and analytical methods currently available. The models show that this approach can be used to develop models that reasonably predict joint spalling of JPCP and JRCP. The mechanistic analysis for both types of jointed concrete pavements shows that spalling is a function of tensile stresses generated from both traffic and environmentally imposed stresses.

Although both models show that the environment has a strong influence on joint spalling, for the data set used, the influence was more significant for JPCP. The models indicate that the environmental factors that influence the durability of the concrete and the restrained thermal stresses within the pavement influence spalling. These results are in line with empirical evidence from the field. Also, the model for JPCP indicates that the conditions that exist during construction of the pavement influence the amount of spalling, possibly because of their effect on the occurrence of early microcracks and delaminations.

Both models show the influence of joint sealing on spalling, probably through differences in incompressibles infiltrating into the joints. There is strong evidence that sealing of joints will greatly decrease the occurrence of spalling. The models predict that the most spalling will occur if joints are not sealed and incompressibles get into the joint. Preformed sealants and silicone sealants were found to be most effective for JPCP and JRCP, respectively.



## 6. TRANSVERSE CRACKING AND CORNER BREAKS OF JPCP

### Introduction

Transverse cracks can occur at the midslab of JPCP slabs parallel to the joint. Typically, midslab cracks initiate as a single crack at the edge of the slab that propagate through the entire slab and across the slab. Transverse cracks can also occur close to the joint, and they can propagate across the slab or cut diagonally from the edge to the transverse joint and become corner breaks. Both transverse cracks and corner breaks in JPCP can be measured by counting the number of cracks and corner breaks that exist in the original PCC pavement.

Transverse cracks and corner breaks will increase the roughness of the pavement as the cracks fault and spall and there is a general breakup of the pavement. This decreases serviceability and results in costly rehabilitation. Transverse cracks, especially when they are badly spalled, also cause surface runoff from rainfall to infiltrate the pavement structure. This normally results in the weakening and erosion of the base course, increasing deflections and resulting in increased cracking and faulting. Transverse cracks and corner breaks must be avoided as much as possible. Models developed for predicting transverse cracks and corner breaks can be used as design checks to avoid their occurrence. These models are also useful in pavement management for predicting the occurrence of transverse cracks and corner breaks so that needed rehabilitation can be scheduled properly.

### Transverse Cracking and Corner Break Mechanisms

The mechanisms for transverse cracking and corner breaks are similar, and for this study a similar mechanism for crack initiation and propagation was used to model both transverse cracking and corner breaks. The occurrence of cracking in concrete pavements can be attributed to early age cracking, fatigue failure of the concrete, or both. Early age cracking is usually material- and construction-related. Fatigue cracking, however, is caused by the repeated application of traffic and environmental stresses to the pavement at both the midsection and corner. These stresses are typically less than the ultimate failure stress of the PCC slab; they do not result in the sudden breakup of the concrete, but rather open up new or existing microcracks that develop into the main cracks that propagate through the PCC slab.

#### Transverse Cracking Mechanism

There are two modes of crack development for transverse fatigue cracking: top down cracking and bottom up cracking. Top down cracking occurs from the application of traffic loads on a slab that is in a severely curled-up position due to a negative temperature differential and drying shrinkage at the slab surface. These cracks typically occur close to the joint. Bottom up cracking occurs from the application of loads on a pavement that is in a curled-down position as a result of a positive temperature differential that causes the slab to lose support at the midslab. The crack typically occurs at the midslab location, starts from the edge of the outer lane, and propagates transversely through the slab.

The first model described in this chapter was based on the assumption that most transverse cracks observed on JPCP are the result of fatigue failure initiated at the slab bottom (bottom up

failure). This assumption is reasonable if nighttime temperature curling combined with shrinkage and moisture warping are not significant and dowel bars are used at the joints. This is a typical mode of failure that has been observed in the field for JPCP in most parts of the United States. The goal was to develop a fatigue cracking model based on the repeated maximum stress due to both traffic and temperature loading at the critical location of the PCC slab.

### Corner Breaks

Corner breaks are initiated from the top of the PCC slab (i.e., top down cracking). Top down crack initiation and progression occur in situations where the pavement support is weak or erosion has occurred, load transfer across the joint is poor, the slab is curled up at the corner, and the pavement corners are subjected to heavy wheel loads. This results in excessive deflection of the slab corners and a corresponding increase in the tensile stresses at the top of the PCC slab corner. The tensile stresses cause the initiation of microcracks. Repeated loading propagates these cracks through the PCC slab and results in corner breaks. Corner breaks start at the edge of the PCC slab joint but do not propagate transversely across the slab. Rather, they cut across diagonally to the joint.

### Evaluation of Existing Transverse Cracking and Corner Break Models

A lot of empirical and mechanistic knowledge has been accumulated over the years in modeling cracking of PCC pavements. Several existing models were reviewed to evaluate the potential variables for model development.

#### SHRP P-020 Study

The following is a mechanistic model developed for predicting transverse cracking in JPCP using the LTPP data available in 1992:<sup>(4)</sup>

$$\text{PCRK} = \frac{1}{0.01 + 10 * 100^{-\log_{10} \text{FD}}} \quad (64)$$

where

|          |   |  |
|----------|---|--|
| PCRK     | = | percentage of slabs cracked  |
| FD       | = | fatigue damage = n/N   |
| n        | = | expected number of applied edge stress   |
| N        | = | allowable number of applied edge stress = $10^{[2.13 * (1/\text{Ratio})^{1.2}]}$   |
| Ratio    | = | stress/strength  |
| Stress   | = | $f(E_{\text{pcc}}, \text{Thick}, \text{Poisson's ratio}, K_{\text{static}})$ , psi |
| Strength | = | mean 28-day flexural strength, psi   |

Sensitivity analysis of this model showed that, by far, slab thickness had the greatest effect on transverse cracking. This was followed by the flexural strength of the concrete at 28 days. Although the model was developed using limited data, it provides useful insights into the potential variables that can be used to develop a model for transverse cracking of JPCP.

## RIPPER Study

Following is a similar model that was developed in the FHWA research study commonly referred to as RIPPER, using data from concrete pavement sections surveyed as part of the study.<sup>(10)</sup>

$$\text{PCRK} = \frac{100}{1 + 1.41 \text{FD}^{-1.66}} \quad (65)$$

where

|          |   |  |
|----------|---|--|
| PCRK     | = | percentage of slabs cracked  |
| FD       | = | accumulated fatigue damage = n/N   |
| n        | = | expected number of applied edge stress   |
| N        | = | allowable number of applied edge stress = $10^{[2.13*(1/\text{Ratio})1.2]}$                      |
| Ratio    | = | stress/strength  |
| Stress   | = | $f(E_{\text{pcc}}, \text{Thick}, \text{Poisson's ratio}, K_{\text{static}})$ , edge support, psi |
| Strength | = | mean 28-day flexural strength, psi   |

Sensitivity analysis of this model showed that increasing the thickness of the PCC slab decreases cracking. According to the model, shorter joint spacing will reduce transverse cracking, as will a tied PCC shoulder in comparison to an AC shoulder. Bonding between the PCC slab and an underlying stabilized base and stronger support in terms of a higher k-value were also found to decrease cracking. As expected, the effect of modulus of rupture was very significant, with a higher modulus of rupture resulting in an appreciable decrease in cracking.

## NAPCOM Cost Allocation Model

Following is another model developed recently for cost allocation purposes using concepts similar to the previous models.<sup>(3)</sup>

$$\text{Percent Cracking} = \frac{100 \text{FD}^{1.52}}{1 + \text{FD}^{1.52}} \quad (66)$$

where

|    |   |   |
|----|---|---|
| FD | = | accumulated fatigue damage = n/N        |
| n  | = | expected number of applied edge stress  |
| N  | = | allowable number of applied edge stress |

The allowable number of the combined traffic and temperature edge stress repetitions to failure is calculated using the following equation:

$$N = \frac{1}{1 - R} 10^{0.531 + 2.13 \left( \frac{\sigma_{\text{max}}}{M_R} \right)^{-1.2}} \quad (67)$$

where

$$\begin{aligned} R &= \sigma_{\text{temp}} / \sigma_{\text{max}} \\ \sigma_{\text{temp}} &= \text{curling stress (stress in the slab when no axle loading is applied), psi} \end{aligned}$$

A unique feature about this model is that equations were developed for calculating the maximum edge stress,  $\sigma_{\text{max}}$ , for different axle loads and types as follows:

$$\sigma_{\text{max}} = \left[ 1 + (0.08 \text{ TANDEM} + 0.012 \text{ TRIDEM}) \frac{S}{\ell} \right] \sigma_{\text{combined}} \quad (68)$$

where

$$\begin{aligned} \text{TANDEM} &= \text{code for tandem axle type, 1=tandem, 0=otherwise} \\ \text{TRIDEM} &= \text{code for tridem axle type, 1=tridem, 0=otherwise} \\ S &= \text{axle spacing, in} \\ \ell &= \text{radius of relative stiffness, in} \\ \sigma_{\text{combined}} &= \text{bending stress induced in the pavement from combined axle loading and temperature curling stress, psi} \end{aligned}$$

Sensitivity analyses of the model provided similar results as for the previous model. However, it was also possible to use this model to determine the effect of axle load level and configuration.

### Fatigue Cracking Modeling Approach

The approach used to develop the cracking model in this study is similar to that used to develop the previous models. It is based on the fatigue damage approach and requires determination of the allowable number of load applications to failure. In the models presented, the number of allowable load repetitions to failure,  $N$ , is determined as the ratio of the maximum bending stress to the modulus of rupture. In this study, it was decided to investigate the use of linear fracture mechanics (LFM) principles to estimate the number of load applications to failure.

The approach used is based on extensive investigation of the mechanism of crack propagation using LFM principles. These studies confirmed that stress intensity factor at the crack tip as the crack propagates through the PCC slab can be used effectively to estimate fatigue damage to JPCP. The stress concentration at the crack tip is induced by the traffic and environmental loads applied to the pavement. If the stress intensity factor can be determined, it can be used to estimate the allowable number of load repetitions using Paris's law.<sup>(51)</sup>

Consequently, a major need of this approach was calculating accurately the stress intensity factor caused by traffic load and temperature stresses. It was important to account for the effect of the interaction between traffic loading factors, temperature curling, and design factors (i.e., joint spacing, slab thickness, concrete and foundation elastic properties) on the calculated stress intensity factor. The stress intensity factor obtained was used to calculate the allowable number of load applications to failure and, consequently, the accumulated fatigue damage. The procedure for calculating stress intensity factor is presented in later sections of this chapter. Using information from the LTPP database, accumulated damage for pavements from both traffic- and



environmental-related stresses was calculated. The distress observed in the field was used to calibrate the following model form for predicting fatigue transverse cracking:

$$\text{Percent Cracking} = \alpha_1 \text{FD}_T^m C_1 + \alpha_2 \text{FD}_E^n C_2 \quad (69)$$

where

|                            |   |  |
|----------------------------|---|--|
| $\text{FD}_T$              | = | accumulated fatigue damage from traffic-related stress     |
| $\text{FD}_E$              | = | accumulated fatigue damage from temperature-related stress |
| $\alpha_1, \alpha_2, m, n$ | = | regression constant  |
| $C_1, C_2$                 | = | scaling variables that account for unexplained effects     |

The fatigue damage in equation 66 is based on Miners law and is defined as follows:

$$\text{FD} = \sum_{i=1}^k \frac{n_i}{N_i} \quad (70)$$

where

|     |   |   |
|-----|---|---|
| $n$ | = | actual number of load cycles                |
| $N$ | = | allowable number of load cycles to fracture |

### **Application of Fracture Mechanics Principles**

Current mechanistic-empirical design procedures for JPCP estimate fatigue life of uncracked pavements as a function of the ratio of the maximum bending stress to the modulus of rupture of the concrete. The equations to describe the fatigue life of concrete slabs are derived empirically from laboratory and field performance data. Fatigue cracking (transverse cracking or corner breaks) can also be analyzed using the principles of crack propagation and fracture mechanics. Several researchers have used such fracture mechanics principles and beam-on-elastic foundation theory to develop theoretical mechanistic models for crack growth analysis.

In general, the fracture mechanics approach is applicable to homogeneous materials with continuous crack growth. Crack growth in most materials, including concrete, is not continuous. Also, because concrete is not homogeneous, the accurate application of fracture mechanics principles requires complicated three-dimensional finite element analysis that can take this into account. However, in spite of these limitations, linear fracture mechanics principles can be used to develop practical models for predicting cracking in pavements.<sup>(3)</sup> Following is a description of the approach that was used in this study.

### **Application of Stress Intensity Factor in Damage Analysis**

Several studies have shown that Paris's crack growth law can be used to model crack propagation in pavement materials such as PCC. It is stated mathematically as follows:<sup>(3, 51)</sup>

$$\frac{dc}{dN} = A K^n \quad (71)$$

where

$dc/dN$  = rate of crack propagation through pavement material  
 $K$  = stress intensity factor  
 $A, n$  = fracture properties of the pavement material

Integrating equation 71 yields equation 72, which can be used to estimate the number of repeated stress applications it will take for the crack to propagate through the PCC slab. The number of repeated stress applications is also called the allowable number of load applications to failure, that is, the number of cycles it will take for a crack to propagate through the PCC slab.

$$N_i = \frac{1}{A} \int_{C_0}^{C_f} \frac{dc}{K^n} \quad (72)$$

where

$N_i$  = number of load cycles to failure  
 $C_0$  = initial crack length, 0 mm  
 $C_f$  = final crack length, slab thickness, mm  
 $K$  = stress intensity factor, kPa/mm<sup>2</sup>  
 $A, n$  = fracture properties of the materials

The stress intensity factor is required to use equation 72. It can be determined using a modified version of the ILLISLAB finite element analysis program.<sup>(52)</sup> However, since this modified ILLISLAB program is not yet readily available, it was necessary to develop mathematical expressions for calculating the integral of the stress intensity factors.

#### Determination of Stress Intensity Factor

Figures 37 and 38 show a PCC slab subjected to wheel and temperature stresses at the midsection and corners of the slab, respectively. The mode of crack propagation of interest at these locations is bending, or mode I crack propagation. A modified version of ILLISLAB, a two-dimensional finite element program, was used to model the stresses and cracks at the midsection and the corners of a PCC slab.<sup>(52)</sup>

The finite element analysis approach used is as follows:

- The PCC slab was modeled as a plain strain elastic material.
- The pavement foundation was modeled as a Winkler foundation with k-values represented by equivalent spring constants.

- The JPCP slab was assumed to have no load transfer.
- An 80-kN axle load placed at the PCC slab corner and midsection was used to model stress applied by traffic loading.
- A temperature gradient from 3 to 11 °C was used to model the effects of temperature differentials through the pavement, depending on the PCC slab thickness.

Following is the procedure used to analyze the ILLISLAB output to obtain the stress intensity factor:<sup>(52)</sup>

1. A finite element model was developed to calculate stresses, strains, and moments with a given PCC pavement structure with a partial crack. The elements at the zone around the crack tip were modified to take the effect of singularity into account when estimating the stress intensity factor at the crack tip.
2. Calculate the moment, stress, rotation, and displacement for the nodes of the finite element model around the crack tip. This will be done for different crack positions, or crack length to PCC slab thickness ratios ( $a/h$ ). Note that for  $a/h = 0$ , the PCC slab has no crack present; for  $a/h = 1$ , the slab is fully cracked.
3. The stress intensity factor at the tip of the crack can then be determined using the equation shown below:

$$K_I = \frac{1}{\sqrt{h}} \left[ P f_t \left( \frac{a}{h} \right) + \frac{M}{h} f_b \left( \frac{a}{h} \right) \right] \quad (73)$$

where

- $K_I$  = mode I stress intensity factor from the crack tip,  $\text{kPa}/\text{mm}^2$   
 $h$  = PCC slab thickness, mm  
 $P$  = stress due to restraint at the slab edges, kPa  
 $f_t, f_b$  = geometric functions that are a function of  $a/h$   
 $a$  = crack depth, mm  
 $M$  = bending moment in the slab from imposed stresses, kN-m

The geometric functions,  $f_t$  and  $f_b$ , are defined as follows:

$$f_t \left( \frac{a}{h} \right) = \frac{\sqrt{2 \tan \left( \frac{\pi a}{2h} \right)}}{\cos \left( \frac{\pi a}{2h} \right)} \left[ 0.752 + 2.02 \left( \frac{a}{h} \right) + 0.37 \left( 1 - \sin \left( \frac{\pi a}{2h} \right)^3 \right) \right] \quad (74)$$

$$f_b \left( \frac{a}{h} \right) = \frac{6 \sqrt{2 \tan \left( \frac{\pi a}{2h} \right)}}{\cos \left( \frac{\pi a}{2h} \right)} \left[ 0.923 + 0.199 \left( 1 - \sin \left( \frac{\pi a}{2h} \right)^4 \right) \right] \quad (75)$$

where

$a/h$  = ratio of crack length to slab thickness  
 $\pi$  = 3.142  
 $h$  = PCC slab thickness, mm

Using this approach, the stress intensity factor was calculated for each pavement section in the LTPP database. The finite element model accounted for both traffic-imposed stresses and positive and negative (daytime and nighttime) temperature gradient curling. The variables used in calculating stresses at the edge and midsections of the PCC slab include slab thickness, modulus of elasticity, Poisson's ratio, slab length, coefficient of expansion of concrete, and subgrade k-value.

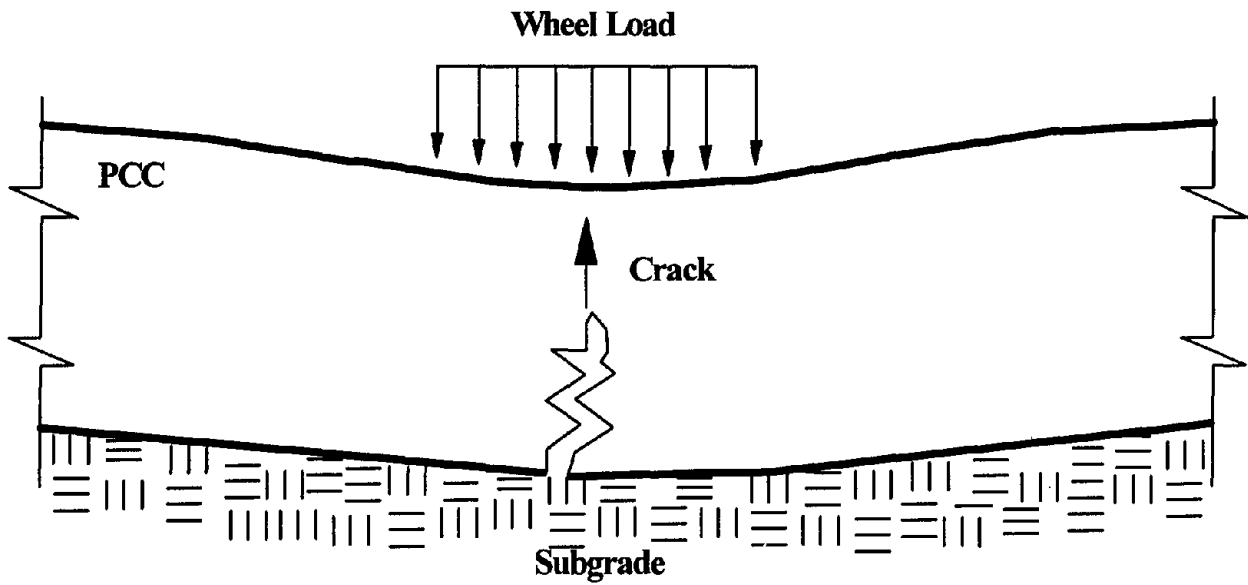


Figure 37. Pavement deformation with wheel load placed directly over the plane with the crack.

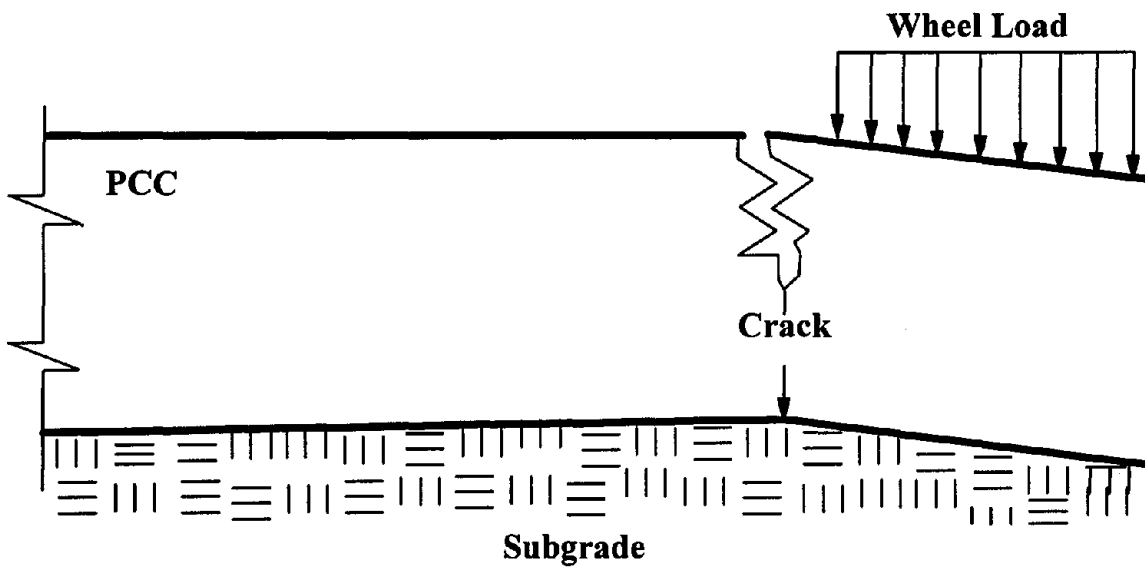


Figure 38. Pavement deformation with wheel load placed at the corner of the slab.

## Development of Stress Intensity Factor Models

This section describes the method used to obtain a database of stress intensity factors, crack tip locations, and other pavement properties that were then used to develop models for predicting the stress intensity factors at both the midsections and corners of PCC slabs. The model development and integration procedure is summarized as follows:

1. Use the database of pavement properties and stress intensity factor from the ILLISLAB runs to develop models for determining stress intensity factor of the following form:

$$K_i = f(a/h, \text{pavement properties}) \quad (76)$$

2. Numerically integrate the stress intensity factor equation in the form  $(dc/K^n=AN)$  for  $a/h = 0$  to 1 to obtain values for the factorial of pavements. In this study,  $n$  values ranging from 1 to 3 were used to obtain the integral of the stress intensity factor for the factorial.
3. Using the results obtained, develop an empirical model that can be used to determine the integral of stress intensity factor for the database of pavement properties in the LTPP database.

Note that from Paris's law the integral of  $(dc/K^n)$  is related to the number of allowable load repetitions as follows:

$$AN_i = \int_{c_0}^{c_r} \frac{dc}{K^n} = f(\text{pavement properties}) \quad (77)$$

Therefore,  $AN_i$  can be related to the model for determining the integral of stress intensity factor as follows:

$$AN_i = f(\text{pavement properties}) \quad (78)$$

The model for estimating the allowable number of load repetitions can therefore be determined as follows:

$$N_i = \beta_0 f(\text{pavement properties}) \quad (79)$$

where

$$\begin{aligned} N_i &= \text{allowable number of load repetitions} \\ \beta_0 &= 1/A \end{aligned}$$

## Allowable Load Repetitions Models

Using the approach outlined above, models for estimating the allowable number of load repetitions, which is the product of  $\beta = 1/A$ , the fracture properties of the material, and the integral of  $dc/K^n$ , were developed for corner breaks and transverse cracking. Following are the equations that were developed:

### Corner Breaks

$$N_i = \beta_E(-0.02 + 5.507*10^{-9}E_{PCC} + 1.5063*10^{-4}h_{PCC} - 4.564*10^{-12}E_{PCC}h_{PCC} + 1.0082*10^{-5}E_{PCC}^2) \quad (80)$$

### Transverse Cracking

$$N_i = \beta_{TC}(0.0056 + 8.7*10^{-11}E_{PCC} - 4.724*10^{-5}h_{PCC} - 1.7117*10^{-13}E_{PCC}h_{PCC} + 1.056*10^{-6}h_{PCC}^2) \quad (81)$$

where

$E_{PCC}$  = elastic modulus of PCC pavement, kPa  
 $h_{PCC}$  = PCC slab thickness, mm  
 $\beta_i$  = 1/A

### Development of Empirical Scaling Factors

The empirical scaling factors to be used in model calibration were selected from the LTPP database on the basis of a review of existing cracking models. The data for development of corner breaks and transverse cracking models for JPCP were obtained from the GPS 3 sections. The database was evaluated thoroughly to check for gross errors, cleaned, and prepared for analysis. A comprehensive statistical analysis of the cleaned data was conducted to evaluate the preliminary relationships between the measured transverse cracking and the explanatory variables, including cluster variables. Tables 17 and 18 are correlation tables that show the strength of the relationships between the independent variables and corner breaks for JPCP, the relationships between the independent variables and transverse cracks for JPCP, and the relationship between the variables themselves. Figures 39 and 40 are bivariate plots of the distress versus the potential independent variables for transverse cracking and corner breaks, respectively.

### Calibration Procedure for Transverse Cracking and Corner Break Models

In the previous sections, the model forms for estimating the allowable number of 80-kN equivalent axle load repetitions and the final cracking model form were selected. Calibration was accomplished using the LTPP database and optimization techniques to find values for the regression parameters that best match field data. The calibration procedure is summarized as follows:

1. Select initial starting values and variables for the parameters,  $\alpha_1$ ,  $\alpha_2$ ,  $\beta$ ,  $m$ ,  $n$ , and  $C = f(\text{climate variables})$ .
2. For the 80-kN ESAL load, calculate the number of load applications to failure.
3. Estimate total damage using the model based on Miner's damage equation (equation 70).

4. For the given set of the cracking and damage data, perform nonlinear regression or optimization analysis to determine the values of the cracking model parameters  $\alpha_1$ ,  $\alpha_2$ ,  $\beta$ ,  $n$ , and  $C$  that minimize the error function given below:

$$ERR(\alpha_1, \alpha_2, A, n, C) = \sum_j (\text{Predicted}_{\text{Distress}} - \text{Measured}_{\text{Distress}})^2 \quad (82)$$

5. Repeat steps 2, 3, and 4 until the regression parameters that minimize the error function are obtained.



Table 17. Correlation matrix for selected variables for JPCP corner break model.

|        | FI       | FTCYC    | PRECIP   | WTDYS    | MAXT     | MINT     | MTEMP    | D90      | D32      | EPCC     | JTSP     | HPCC     | HB       | EB       | Cd       | Kvalue   | KESAL    | AGE      | CB       |
|--------|----------|----------|----------|----------|----------|----------|----------|----------|----------|----------|----------|----------|----------|----------|----------|----------|----------|----------|----------|
| FI     | 1        | 0.12891  | -0.30987 | -0.10834 | -0.61918 | -0.55818 | -0.59389 | -0.44905 | 0.50446  | 0.12714  | -0.19632 | -0.00485 | -0.0809  | -0.27989 | -0.30367 | -0.40043 | -0.15367 | -0.10516 | 0.06936  |
| FTCYC  | 0.12891  | 1        | -0.61932 | -0.57251 | -0.75339 | -0.84469 | -0.80856 | -0.69399 | 0.88922  | 0.13766  | -0.35459 | 0.12129  | -0.32083 | -0.00551 | -0.24247 | -0.19671 | -0.10811 | -0.08101 | -0.02442 |
| PRECIP | -0.30987 | -0.61932 | 1        | 0.80856  | 0.63192  | 0.74007  | 0.69456  | 0.41471  | -0.68036 | 0.00719  | 0.58853  | -0.09631 | 0.16193  | 0.07879  | -0.00319 | 0.11511  | -0.08188 | -0.00806 | 0.10098  |
| WTDYS  | -0.10834 | -0.57251 | 0.80856  | 1        | 0.40854  | 0.58877  | 0.5062   | 0.16329  | -0.5032  | 0.09215  | 0.37037  | -0.20513 | 0.23031  | -0.17289 | -0.04768 | 0.0849   | -0.20666 | -0.15485 | 0.00916  |
| MAXT   | -0.61918 | -0.75339 | 0.63192  | 0.40854  | 1        | 0.95913  | 0.98919  | 0.89573  | -0.95294 | -0.34259 | 0.45366  | -0.02888 | 0.23518  | 0.26349  | 0.44367  | 0.39097  | 0.17258  | 0.11283  | 0.08185  |
| MINT   | -0.55818 | -0.84469 | 0.74007  | 0.58877  | 0.95913  | 1        | 0.99025  | 0.82878  | -0.97037 | -0.21722 | 0.44025  | -0.01777 | 0.28268  | 0.18187  | 0.32812  | 0.37175  | 0.09347  | 0.0704   | 0.02299  |
| MEANT  | -0.59389 | -0.80856 | 0.69456  | 0.5062   | 0.98919  | 0.99025  | 1        | 0.87033  | -0.97188 | -0.28124 | 0.45148  | -0.02344 | 0.26226  | 0.22392  | 0.3884   | 0.38503  | 0.13341  | 0.09205  | 0.0522   |
| D90    | -0.44905 | -0.69399 | 0.41471  | 0.16329  | 0.89573  | 0.82878  | 0.87033  | 1        | -0.83644 | -0.3656  | 0.34464  | 0.08135  | 0.16168  | 0.34147  | 0.47126  | 0.49402  | 0.13503  | 0.07687  | -0.01756 |
| D32    | 0.50446  | 0.88922  | -0.68036 | -0.5032  | -0.95294 | -0.97037 | -0.97188 | -0.83644 | 1        | 0.23447  | -0.43953 | 0.04592  | -0.29883 | -0.19396 | -0.34258 | -0.34619 | -0.21288 | -0.16009 | -0.05403 |
| EPCC   | 0.12714  | 0.13766  | 0.00719  | 0.09215  | -0.34259 | -0.21722 | -0.28124 | -0.3656  | 0.23447  | 1        | -0.22497 | 0.12909  | -0.00314 | -0.14677 | -0.50245 | -0.16991 | -0.21131 | -0.02259 | -0.35674 |
| JTSP   | -0.19632 | -0.35459 | 0.58853  | 0.37037  | 0.45366  | 0.44025  | 0.45148  | 0.34464  | -0.43953 | -0.22497 | 1        | 0.02662  | -0.06332 | 0.0201   | 0.1123   | 0.13188  | 0.01631  | 0.18986  | 0.23111  |
| HPCC   | -0.00485 | 0.12129  | -0.09631 | -0.20513 | -0.02888 | -0.01777 | -0.02344 | 0.08135  | 0.04592  | 0.12909  | 0.02662  | 1        | 0.06334  | 0.37325  | -0.16222 | 0.03189  | 0.16657  | 0.13369  | -0.26215 |
| HB     | -0.0809  | -0.32083 | 0.16193  | 0.23031  | 0.23518  | 0.28268  | 0.26226  | 0.16168  | -0.29883 | -0.00314 | -0.06332 | 0.06334  | 1        | -0.1128  | -0.0719  | 0.04313  | -0.11654 | -0.00607 | -0.09276 |
| EB     | -0.27989 | -0.00551 | 0.07879  | -0.17289 | 0.26349  | 0.18187  | 0.22392  | 0.34147  | -0.19396 | -0.14677 | 0.0201   | 0.37325  | -0.1128  | 1        | 0.22586  | 0.17771  | 0.20109  | -0.07446 | -0.02849 |
| Cd     | -0.30367 | -0.24247 | -0.00319 | -0.04768 | 0.44367  | 0.32812  | 0.3884   | 0.47126  | -0.34258 | -0.50245 | 0.1123   | -0.16222 | -0.0719  | 0.22586  | 1        | 0.40539  | 0.06043  | -0.23663 | 0.03059  |
| Kvalue | -0.40043 | -0.19671 | 0.11511  | 0.0849   | 0.39097  | 0.37175  | 0.38503  | 0.49402  | -0.34619 | -0.16991 | 0.13188  | 0.03189  | 0.04313  | 0.17771  | 0.40539  | 1        | -0.12238 | -0.10809 | -0.0851  |
| KESAL  | -0.15367 | -0.10811 | -0.08188 | -0.20666 | 0.17258  | 0.09347  | 0.13341  | 0.13503  | -0.21288 | -0.21131 | 0.01631  | 0.16657  | -0.11654 | 0.20109  | 0.06043  | -0.12238 | 1        | 0.56372  | 0.32454  |
| AGE    | -0.10516 | -0.08101 | -0.00806 | -0.15485 | 0.11283  | 0.0704   | 0.09205  | 0.07687  | -0.16009 | -0.02259 | 0.18986  | 0.13369  | -0.00607 | -0.07446 | -0.23663 | -0.10809 | 0.56372  | 1        | 0.4479   |
| CB     | 0.06936  | -0.02442 | 0.10098  | 0.00916  | 0.08185  | 0.02299  | 0.0522   | -0.01756 | -0.05403 | -0.35674 | 0.23111  | -0.26215 | -0.09276 | -0.02849 | 0.03059  | -0.0851  | 0.32454  | 0.4479   | 1        |

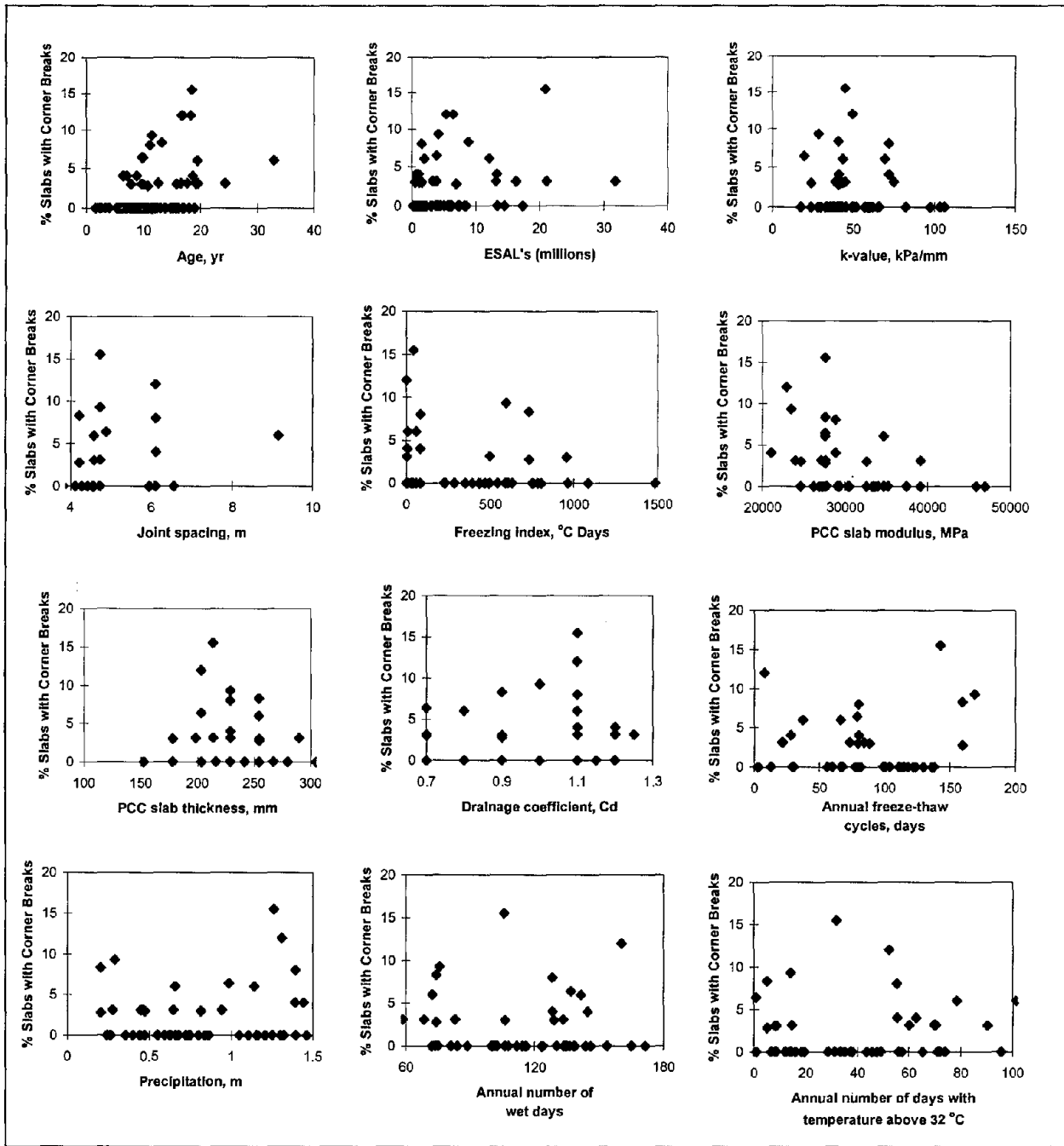


Figure 39. Plot of percentage of slabs with corner breaks versus significant variables for JPCP.

Table 18. Correlation matrix for selected variables for JPCP transverse cracking model.

|        | FI      | FTCYC   | PRECIP  | WTDYS   | MAXT    | MINT    | MEANT   | D90     | D32     | JTSP    | HPCC    | EPCC    | HB      | KESAL   | AGE     | CD      | Kvalue  | TC      |
|--------|---------|---------|---------|---------|---------|---------|---------|---------|---------|---------|---------|---------|---------|---------|---------|---------|---------|---------|
| FI     | 1       | 0.13982 | -0.3171 | -0.0845 | -0.6175 | -0.5546 | -0.5912 | -0.4442 | 0.50483 | -0.2522 | 0.03989 | 0.2136  | 0.08901 | -0.1206 | -0.1173 | -0.2631 | -0.3778 | -0.1181 |
| FTCYC  | 0.13982 | 1       | -0.6559 | -0.5476 | -0.751  | -0.8556 | -0.8129 | -0.6912 | 0.88802 | -0.3357 | -2E-05  | 0.2062  | -0.4112 | -0.0583 | -0.0099 | -0.2297 | -0.1425 | -0.0656 |
| PRECIP | -0.3171 | -0.6559 | 1       | 0.78913 | 0.63895 | 0.74183 | 0.69882 | 0.40997 | -0.6962 | 0.66681 | -0.1141 | -0.1808 | 0.22045 | -0.1185 | -0.1468 | 0.05191 | 0.1538  | 0.07909 |
| WTDYS  | -0.0845 | -0.5476 | 0.78913 | 1       | 0.34869 | 0.52063 | 0.44133 | 0.07311 | -0.4591 | 0.37199 | -0.2757 | -0.1995 | 0.26624 | -0.2378 | -0.3033 | 0.09892 | 0.10001 | 0.06874 |
| MAXT   | -0.6175 | -0.751  | 0.63895 | 0.34869 | 1       | 0.95938 | 0.98928 | 0.89062 | -0.9559 | 0.43065 | 0.03074 | -0.2957 | 0.34519 | 0.2214  | 0.08244 | 0.36674 | 0.41848 | 0.1962  |
| MINT   | -0.5546 | -0.8556 | 0.74183 | 0.52063 | 0.95938 | 1       | 0.9903  | 0.83233 | -0.9793 | 0.43034 | 0.02075 | -0.2727 | 0.34644 | 0.13077 | 0.03578 | 0.28808 | 0.34587 | 0.17338 |
| MEANT  | -0.5912 | -0.8129 | 0.69882 | 0.44133 | 0.98928 | 0.9903  | 1       | 0.86963 | -0.9779 | 0.43499 | 0.02588 | -0.2869 | 0.34948 | 0.17681 | 0.05913 | 0.32981 | 0.38518 | 0.18645 |
| D90    | -0.4442 | -0.6912 | 0.40997 | 0.07311 | 0.89062 | 0.83233 | 0.86963 | 1       | -0.8349 | 0.2667  | 0.1708  | -0.1776 | 0.34627 | 0.22488 | 0.12826 | 0.31901 | 0.43481 | 0.18221 |
| D32    | 0.50483 | 0.88802 | -0.6962 | -0.4591 | -0.9559 | -0.9793 | -0.9779 | -0.8349 | 1       | -0.4332 | -0.0396 | 0.29169 | -0.3662 | -0.1749 | -0.0904 | -0.3074 | -0.334  | -0.1311 |
| JTSP   | -0.2522 | -0.3357 | 0.66681 | 0.37199 | 0.43065 | 0.43034 | 0.43499 | 0.2667  | -0.4332 | 1       | 0.01526 | -0.3945 | -0.0943 | 0.07407 | 0.09979 | 0.04123 | 0.19848 | 0.1756  |
| HPCC   | 0.03989 | -2E-05  | -0.1141 | -0.2757 | 0.03074 | 0.02075 | 0.02588 | 0.1708  | -0.0396 | 0.01526 | 1       | 0.21021 | -0.0885 | 0.32944 | 0.14587 | -0.1444 | 0.06101 | 0.29021 |
| EPCC   | 0.2136  | 0.2062  | -0.1808 | -0.1995 | -0.2957 | -0.2727 | -0.2869 | -0.1776 | 0.29169 | -0.3945 | 0.21021 | 1       | 0.01797 | -0.1786 | -0.1061 | -0.2202 | -0.0952 | -0.3424 |
| HB     | 0.08901 | -0.4112 | 0.22045 | 0.26624 | 0.34519 | 0.34644 | 0.34948 | 0.34627 | -0.3662 | -0.0943 | -0.0885 | 0.01797 | 1       | 0.15259 | -0.1066 | 0.11341 | 0.14518 | -0.0532 |
| KESAL  | -0.1206 | -0.0583 | -0.1185 | -0.2378 | 0.2214  | 0.13077 | 0.17681 | 0.22488 | -0.1749 | 0.07407 | 0.32944 | -0.1786 | 0.15259 | 1       | 0.60192 | 0.04439 | -0.0756 | 0.57422 |
| AGE    | -0.1173 | -0.0099 | -0.1468 | -0.3033 | 0.08244 | 0.03578 | 0.05913 | 0.12826 | -0.0904 | 0.09979 | 0.14587 | -0.1061 | -0.1066 | 0.60192 | 1       | -0.2625 | -0.1585 | 0.09209 |
| CD     | -0.2631 | -0.2297 | 0.05191 | 0.09892 | 0.36674 | 0.28808 | 0.32981 | 0.31901 | -0.3074 | 0.04123 | -0.1444 | -0.2202 | 0.11341 | 0.04439 | -0.2625 | 1       | 0.5457  | 0.19523 |
| Kvalue | -0.3778 | -0.1425 | 0.1538  | 0.10001 | 0.41848 | 0.34587 | 0.38518 | 0.43481 | -0.334  | 0.19848 | 0.06101 | -0.0952 | 0.14518 | -0.0756 | -0.1585 | 0.5457  | 1       | 0.03543 |
| TC     | -0.1181 | -0.0656 | 0.07909 | 0.06874 | 0.1962  | 0.17338 | 0.18645 | 0.18221 | -0.1311 | 0.1756  | 0.29021 | -0.3424 | -0.0532 | 0.57422 | 0.09209 | 0.19523 | 0.03543 | 1       |

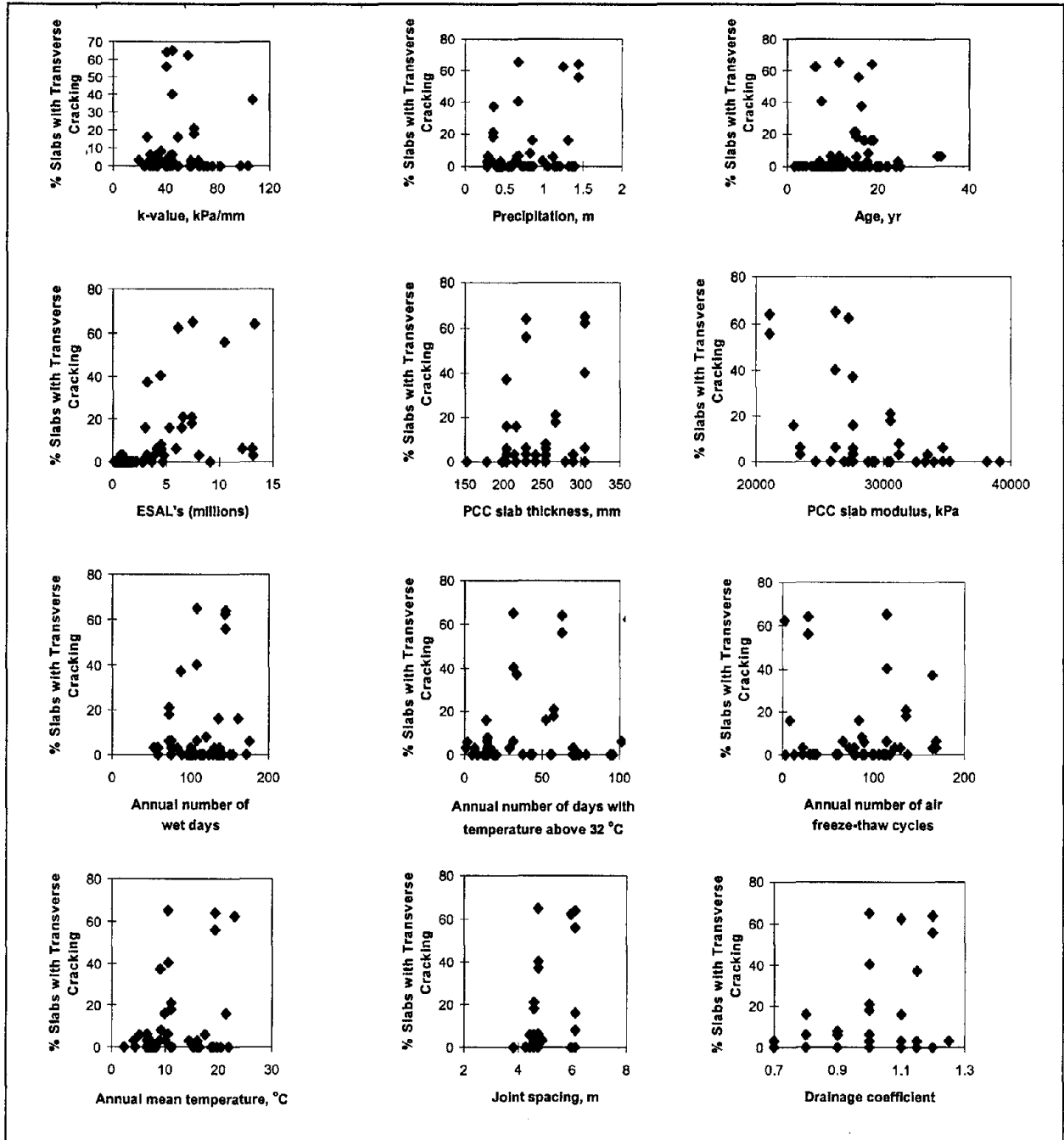


Figure 40. Plot of percentage of transverse cracking versus significant variables for JPCP.

## Final Corner Breaks Model

### Estimating Damage Due to Temperature and Traffic Loading

Damage to the pavement from the imposed stresses was calculated using Miner's cumulative damage equation (equation 70). The damage for both traffic and temperature stresses was calculated as follows:

$$DAM_{TRCB} = \left( \frac{KESAL}{N_{TRCB}} \right)^{0.75} \quad (83)$$

$$DAM_{TECB} = \left( \frac{AGE}{N_{TECB}} \right)^{0.25} \quad (84)$$

where

KESAL = cumulative number of ESAL's/1000  
 AGE = pavement age in years  
 $N_i$  = allowable number of load repetitions

### Allowable Number of Load Repetitions Model

The final model for estimating  $N_i$  for traffic was as follows:

$$N_{TRCB} = \frac{(5.6 + 8.7 \cdot 10^{-8} E_{PCC} - 4.724 \cdot 10^{-2} h_{PCC} - 1.7 \cdot 10^{-10} E_{PCC} h_{PCC} + 1.056 \cdot 10^{-3} h_{PCC}^2)^{2.93}}{DAM_{TRCB}} \quad (85)$$

The final model for estimating  $N_i$  for temperature was as follows:

$$N_{TECB} = \frac{(5.6 + 8.7 \cdot 10^{-8} E_{PCC} - 4.724 \cdot 10^{-2} h_{PCC} - 1.7 \cdot 10^{-10} E_{PCC} h_{PCC} + 1.056 \cdot 10^{-3} h_{PCC}^2)^{8.8}}{DAM_{TECB}} \quad (86)$$

where

$E_{PCC}$  = PCC slab modulus, kPa  
 $h_{PCC}$  = PCC slab thickness, mm

### Final Form of Corner Breaks Model

The final model for predicting the occurrence of corner breaks is as follows:

$$SWCB = 100 \cdot (24.26JTSP + 2.236AGE - 9.95 \cdot 10^{-7} E_{PCC}) DAM_{TECB} + 100 \cdot (3.08 \cdot 10^{-3} FTCYC - 3.78 \cdot 10^{-3} C_d) DAM_{TRCB} \quad (87)$$

where

|              |   |  |
|--------------|---|--|
| SWCB         | = | percentage of slabs with corner breaks |
| JTSP         | = | pavement joint spacing, m              |
| AGE          | = | pavement age, yr                       |
| $E_{PCC}$    | = | elastic modulus of PCC, kPa            |
| $DAM_{TECB}$ | = | damage due to temperature stresses     |
| FTCYC        | = | annual number of freeze-thaw cycles    |
| $C_d$        | = | drainage coefficient                   |
| $DAM_{TRCB}$ | = | damage due to traffic stresses         |

Statistics:

|         |   |                                |
|---------|---|--------------------------------|
| $R^2$   | = | 0.69                           |
| N       | = | 92                             |
| SEE     | = | 9 percent                      |
| p-value | < | 0.0001 (significance of model) |

A plot of the predicted and measured percentage of joints with corner breaks is shown in figure 41. A plot of the residuals (predicted - actual percentage of joints with corner breaks) against the predicted percentage of joints with corner breaks is shown in figure 42. The overall accuracy of the corner breaks model is reflected by the  $R^2$  of 0.69, which is the proportion of variation of corner breaks explained by the variables included in the model. A test of hypothesis was performed to determine the significance of the variables used in the model for predicting corner breaks. The null and alternate hypotheses were as follows:

- $H_o$ : all model parameters are zero (variables are not significant)
- $H_A$ : all model parameters are not zero

The F-test statistic used for the hypothesis test was calculated as the ratio of the mean square for the model divided by the mean square of the error. For this study, the null hypothesis will be rejected if the level of significance is less than 5 percent (0.05). A level of significance (p-value) of less than 0.0001 implies a rejection of the null hypothesis. This shows that the variables in the model are highly significant. Also, individual t-tests were conducted to test if the individual parameter estimates are equal to zero. The p-values for this test ranged from 0.0001 to 0.001. The results shows that all the parameter estimates had values other than zero; therefore, the variables in the model were significant. Prediction accuracy of corner breaks in absolute units is reflected by the standard error of estimate (SEE = 9 percent). This value was found to be reasonable. The overall effectiveness of the model should be judged on all the diagnostic statistics, the residual plots, and the results from the sensitivity analysis to follow. The diagnostic statistics obtained for the corner breaks model show that the model can predict corner breaks with reasonable accuracy for the LTPP data utilized.

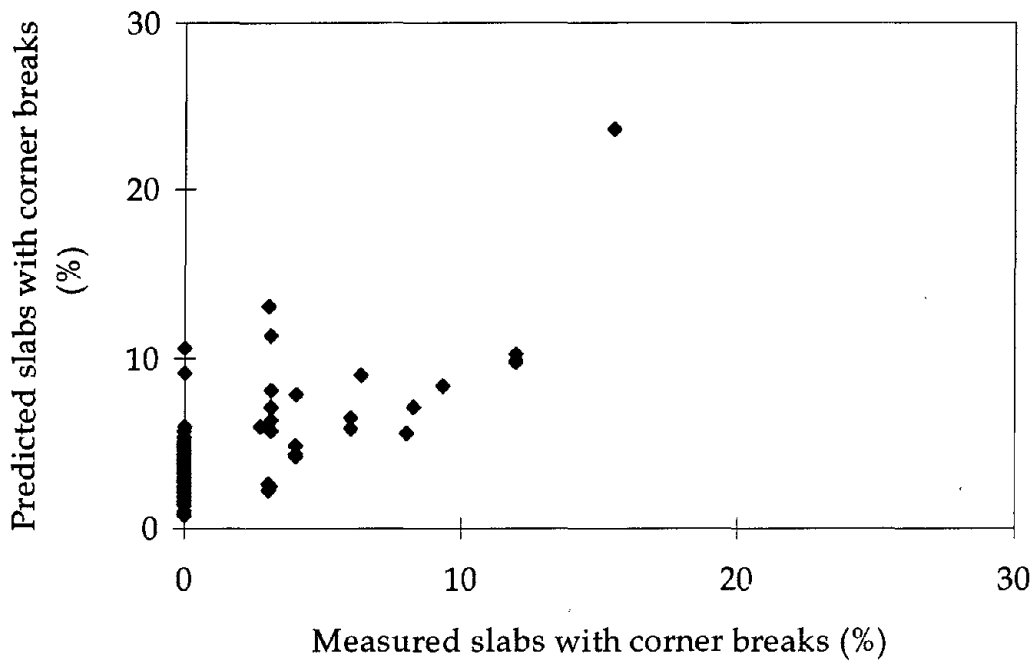


Figure 41. Measured versus predicted percentage of slabs with corner breaks.

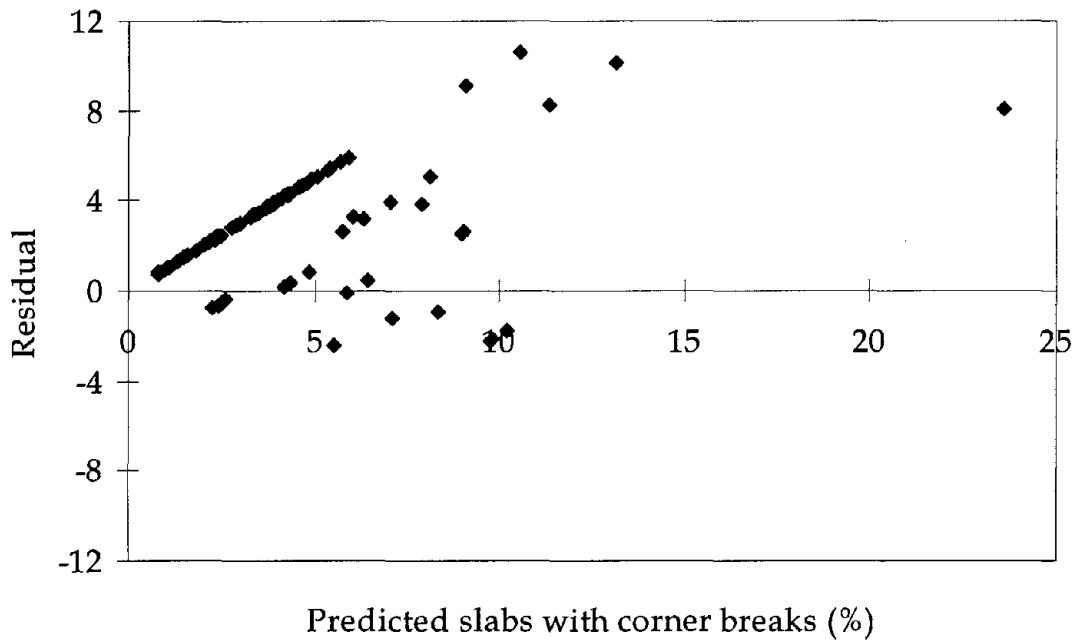


Figure 42. Plot of residuals versus predicted percentage of slabs with corner breaks.

## Final Transverse Cracking Model

### Estimating Damage Due to Temperature and Traffic Loading

The damage to the pavement from the imposed stresses can be calculated using a modified form of Miner's cumulative damage equation. The modified damage equations for estimating both traffic and temperature stresses are as follows:

$$DAM_{TRTC} = \left( \frac{KESAL}{N_{TRTC}} \right)^{0.5} \quad (88)$$

$$DAM_{TETC} = \left( \frac{AGE}{N_{TETC}} \right)^{0.75} \quad (89)$$

where

|            |   |  |
|------------|---|--|
| KESAL      | = | cumulative number of ESAL's, thousands                         |
| AGE        | = | pavement age, yr   |
| $N_{TRTC}$ | = | allowable number of load repetitions for traffic loads         |
| $N_{TETC}$ | = | allowable number of load repetitions for climate-related loads |

### Allowable Number of Load Repetitions Model

The final model for estimating  $N_i$  for traffic is as follows:

$$N_{TRTC} = \frac{(-2.0 \cdot 10^4 + 5.507 \cdot 10^{-3} E_{PCC} + 150.63 h_{PCC} + 4.564 \cdot 10^{-6} E_{PCC} h_{PCC} + 0.744 h_{PCC}^2)^{1.33}}{1} \quad (90)$$

The final model for estimating  $N_i$  for temperature is as follows:

$$N_{TETC} = \frac{(-2.0 \cdot 10^4 + 5.507 \cdot 10^{-3} E_{PCC} + 150.63 h_{PCC} + 4.564 \cdot 10^{-6} E_{PCC} h_{PCC} + 0.744 h_{PCC}^2)^2}{1} \quad (91)$$

where

|           |   |                        |
|-----------|---|------------------------|
| $E_{PCC}$ | = | PCC slab modulus, kPa  |
| $h_{PCC}$ | = | PCC slab thickness, mm |

### Final Form of Transverse Cracking Model

The final model for predicting transverse cracking is given as follows:

$$TC = 100 \cdot (50.8FTCYC - 3.2 \cdot 10^{-5} E_{PCC}) DAM_{TETC} + 100 \cdot (0.274WTDYS + 0.432D32) DAM_{TRTC} \quad (92)$$



where

|              |   |  |
|--------------|---|--|
| TC           | = | percentage of slabs with transverse cracks         |
| FTCYC        | = | annual number of freeze-thaw cycles                |
| $E_{PCC}$    | = | elastic modulus of PCC, kPa                        |
| $DAM_{TETC}$ | = | damage caused by temperature stresses              |
| WTDYS        | = | annual number of wet days                          |
| D32          | = | annual number of days with temperature above 32 °C |
| $DAM_{TRTC}$ | = | damage caused by traffic stresses                  |

Statistics:

|         |   |                                |
|---------|---|--------------------------------|
| $R^2$   | = | 0.64                           |
| N       | = | 92                             |
| SEE     | = | 12                             |
| p-value | < | 0.0001 (significance of model) |

A plot of the predicted and measured percentage of slabs with transverse cracking is shown in figure 43. A plot of the residuals (predicted - actual percentage of slabs with transverse cracking) against the predicted percentage of slabs with transverse cracking is shown in figure 44. The overall accuracy of the transverse cracking model is reflected by the  $R^2$  of 0.64, which is the proportion of variation of transverse cracking explained by the variables included in the model. A test of hypothesis was performed to determine the significance of the variables used in the model for predicting transverse cracking. The null and alternate hypotheses were as follows:

- $H_o$ : all model parameters are zero (variables are not significant)
- $H_A$ : all model parameters are not zero

The F-test statistic used for the hypothesis test was calculated as the ratio of the mean square for the model divided by the mean square of the error. For this study the null hypothesis will be rejected if the level of significance is less than 5 percent (0.05). A level of significance (p-value) of less than 0.0001 implies a rejection of the null hypothesis. This shows that the variables in the model are highly significant. Also, individual t-tests were conducted to test if the individual parameter estimates are equal to zero. The p-values for this test ranged from 0.001 to 0.035.

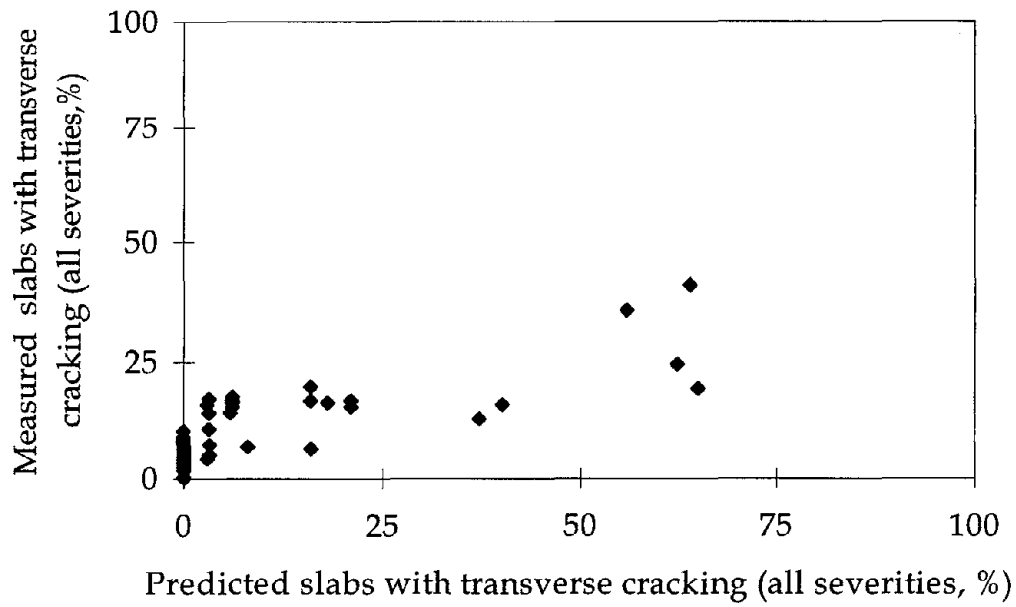


Figure 43. Measured versus predicted percentage of slabs with transverse cracking.

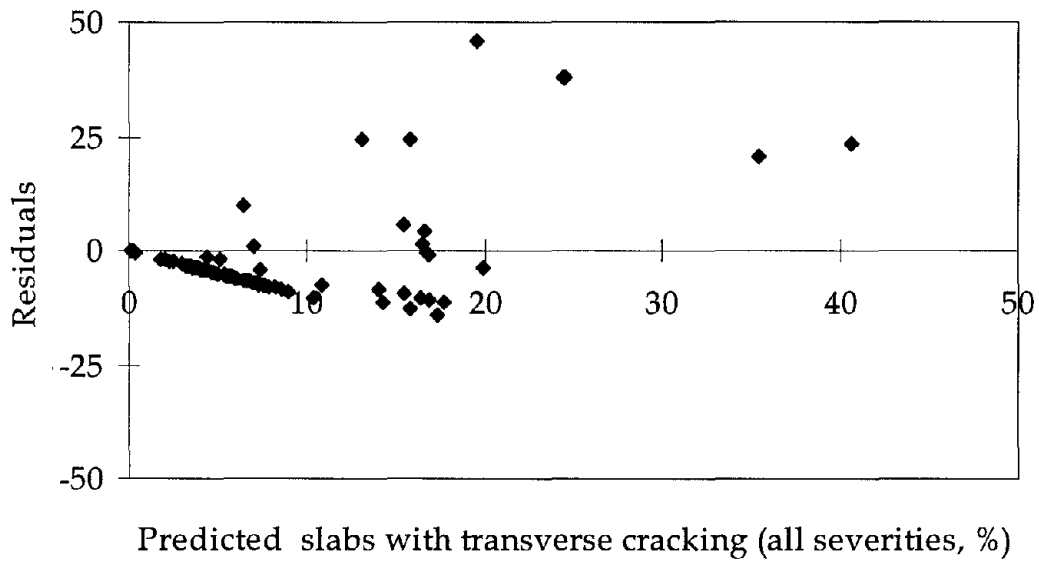


Figure 44. Plot of residuals versus predicted percentage of slabs with transverse cracking.

The results show that all the parameter estimates had values other than zero; therefore, the variables in the model were significant. Prediction accuracy of transverse cracking in absolute units is reflected by the standard error of estimate (SEE = 12 percent). The overall effectiveness of the model should be judged on all the diagnostic statistics, the residual plots, and the results from the sensitivity analysis to follow. The diagnostic statistics obtained for the transverse cracking model show that the model can predict transverse cracking with reasonable accuracy for the LTPP data utilized.

### **Sensitivity Analysis**

The mechanistic-empirical models developed for predicting corner breaks and transverse cracking were evaluated to determine trends predicted by the models and engineering plausibility of the results obtained. The models were also checked against previous empirical and theoretical observations.

### **Corner Breaks Model**

The effects of the significant variables that influence the occurrence of corner breaks according to the mechanistic-empirical model developed are discussed in the next few sections.

#### *Effect of Age and Traffic*

The number of temperature stress cycles the pavement is subjected to directly relates to the age of the pavement. Also, the number of 80-kN ESAL's applied to the pavement gives an estimate of the traffic stress cycles the pavement has undergone. An increase in both of these stress cycles, which can occur separately or simultaneously, increases both damage to the pavement and the amount of distress on the pavement. Figures 45 and 46 confirm this trend.

#### *Effect of PCC Thickness*

Figure 47 is a plot of percentage of slabs with corner breaks versus cumulative ESAL's for different slab thicknesses. The plot shows a rapid increase in the amount of corner breaks in a pavement as the slab thickness decreases. This is in agreement with the fact that it will take longer for a microcrack to propagate from the bottom to the top of a PCC slab as the slab thickness increases.

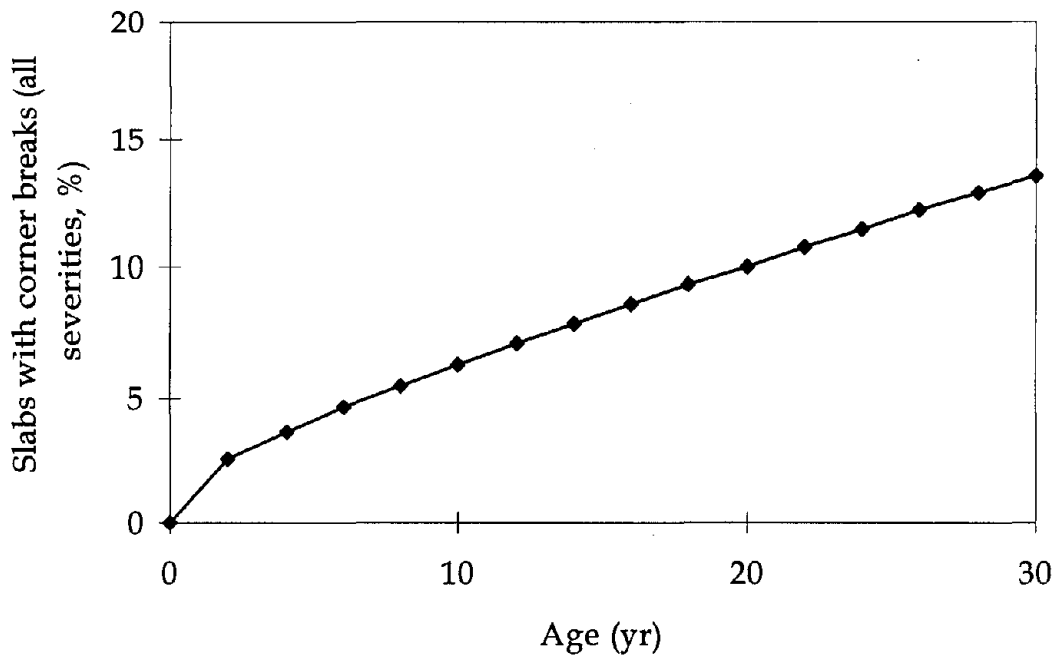


Figure 45. Plot of percentage of slabs with corner breaks versus pavement age.

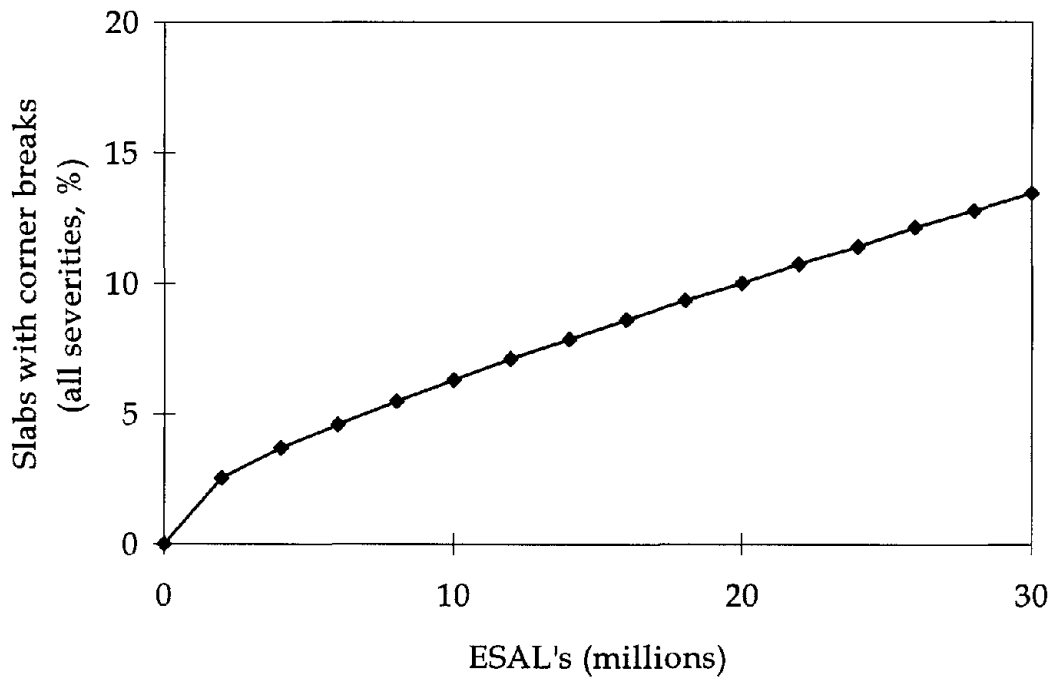


Figure 46. Plot of percentage of slabs with corner breaks versus cumulative ESAL's.

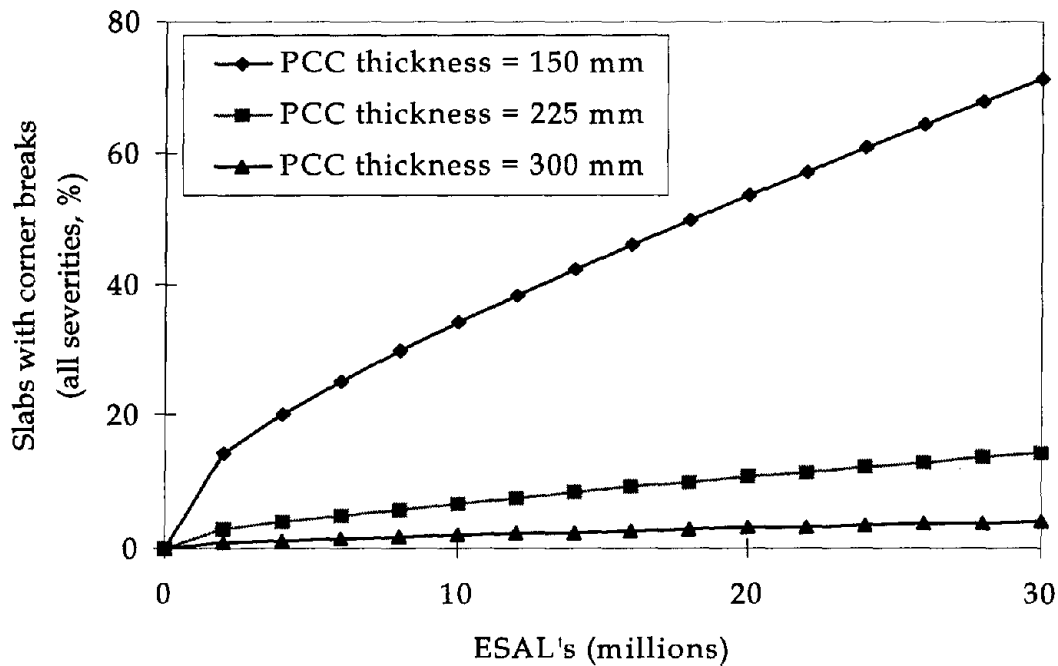


Figure 47. Plot of percentage of slabs with corner breaks versus cumulative ESAL's for different slab thicknesses.

#### *Effect of Freeze-Thaw Cycles*

Figure 48 is a plot of percentage of slabs with corner breaks versus cumulative ESAL's for different levels of freeze-thaw cycles. The plot shows that there is a rapid increase in the amount of corner breaks in a pavement as the level of freeze-thaw cycles increases. This is in agreement with empirical data that show that subjecting concrete to freezing and thawing weakens the concrete material and makes it susceptible to distress.

#### *Effect of Joint Spacing*

Figure 49 is a plot of percentage of slabs with corner breaks versus cumulative ESAL's for different PCC joint spacing. The plot shows that there is an increase in the amount of corner breaks in a pavement as the joint spacing increases. This is in agreement with engineering principles.

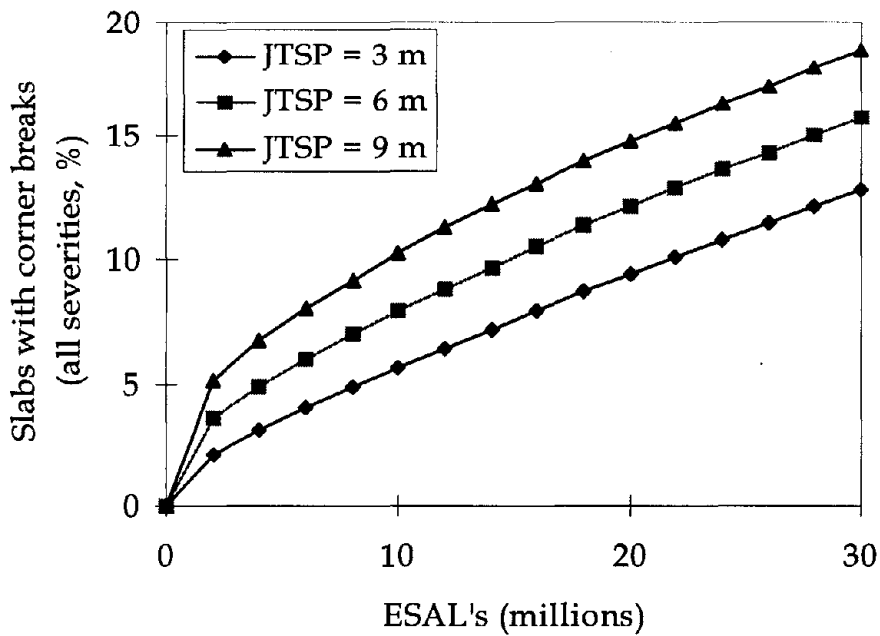


Figure 48. Plot of percentage of slabs with corner breaks versus cumulative ESAL's for different levels of joint spacing.

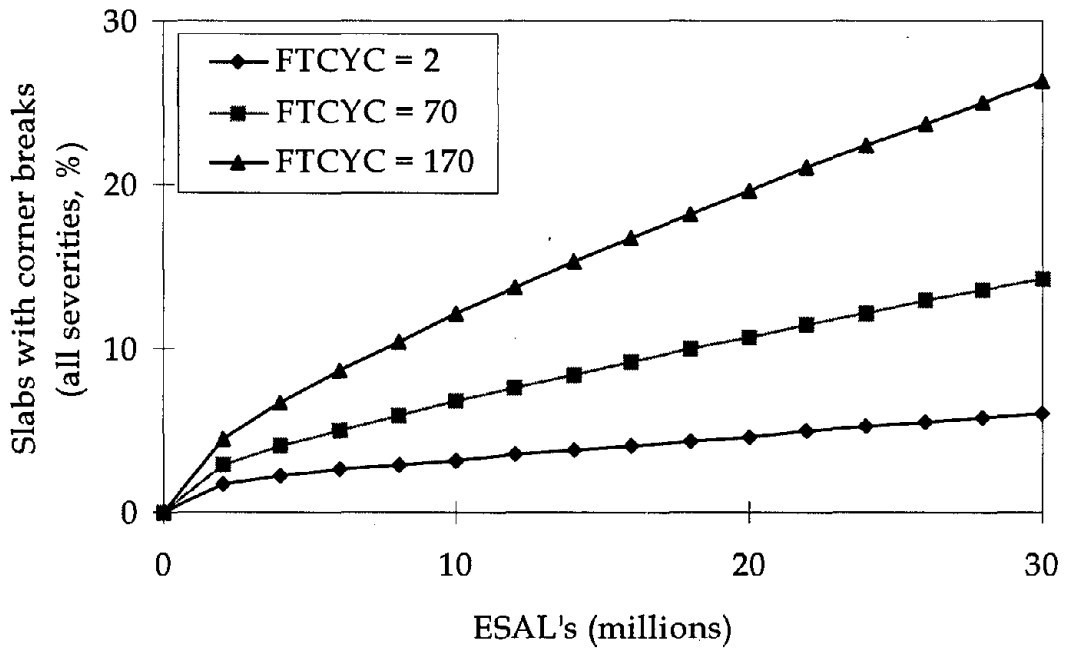


Figure 49. Plot of percentage of slabs with corner breaks versus cumulative ESAL's for different levels of freeze-thaw cycles.

## Transverse Cracking Model

The significant variables that influence the occurrence of transverse cracks, according to the mechanistic-empirical model developed, are discussed in the next few sections.

### *Effect of Age and Traffic*

This is similar to the trends obtained for the transverse cracking model. The number of temperature stress cycles to which the pavement is subjected directly relates to the age of the pavement. Also, the number of 80-kN ESAL's applied to the pavement gives an estimate of the traffic stress cycles the pavement has undergone. An increase in both of these stress cycles, which can occur separately or simultaneously, increases damage to the pavement and therefore increases the amount of distress on the pavement. Figures 50 and 51 confirm this trend.

### *Effect of PCC Thickness*

Figure 52 is a plot of percentage of slabs with transverse cracks versus cumulative ESAL's for different slab thicknesses. The plot shows a rapid increase in the amount of transverse cracking in a pavement as the slab thickness decreases. This is in agreement with the fact that it takes longer for a microcrack to propagate from the bottom to the top of a PCC slab as the slab thickness increases.

### *Effect of Freeze-Thaw Cycles*

Figure 53 is a plot of percentage of slabs with transverse cracking versus cumulative ESAL's for different levels of freeze-thaw cycles. The plot shows that there is a rapid increase in the number of corner breaks in a pavement as the level of freeze-thaw cycles increases. This is in agreement with empirical data that show that subjecting concrete to freezing and thawing weakens the concrete material and makes it susceptible to distress.

### *Effect of the Number of Wet Days and Days with Temperature Above 32°C*

Figures 54 and 55 are plots of percentage of slabs with transverse cracking versus cumulative ESAL's for different levels of wet days and days with temperature above 32 °C. Both plots indicate that with more wet days and higher temperatures there are corresponding higher levels of transverse cracking. This is in agreement with empirical data because pavements in wet environments tend to have weaker and eroded foundations as the pavement structure ages, and higher temperatures generate higher stresses in the pavement slab.

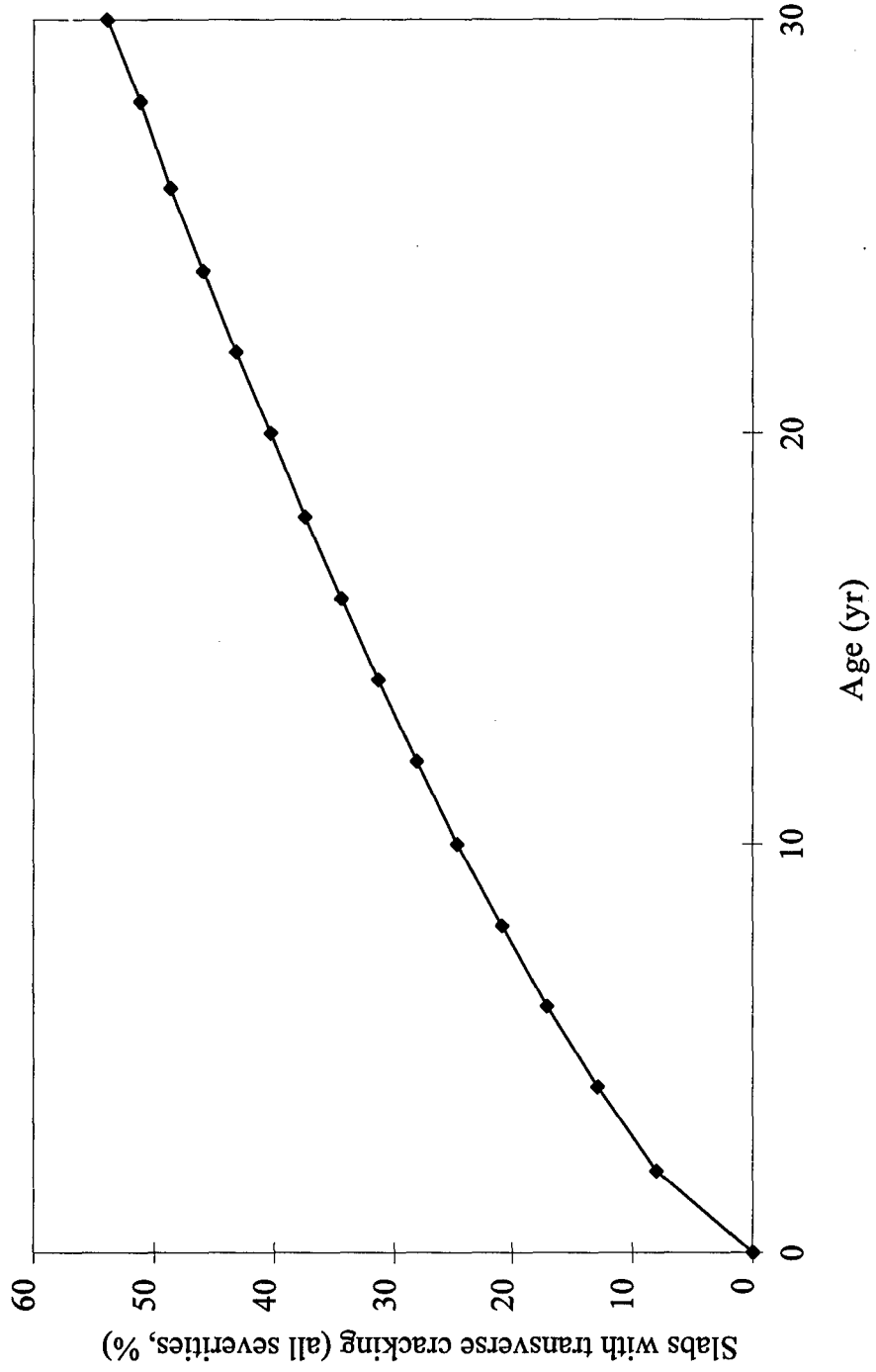


Figure 50. Plot of percentage of slabs with transverse cracking versus pavement age.



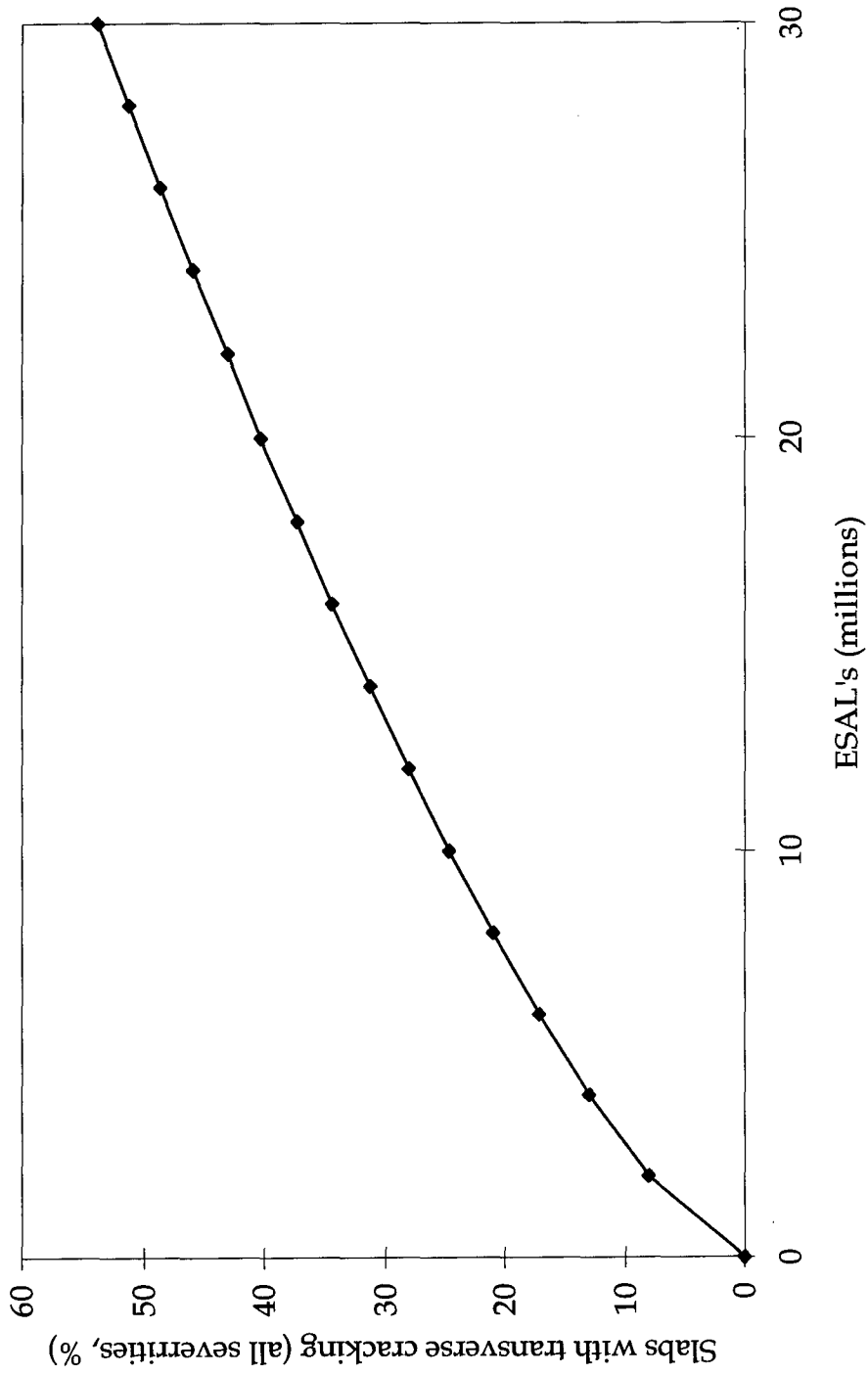


Figure 51. Plot of percentage of slabs with transverse cracking versus cumulative ESAL's.

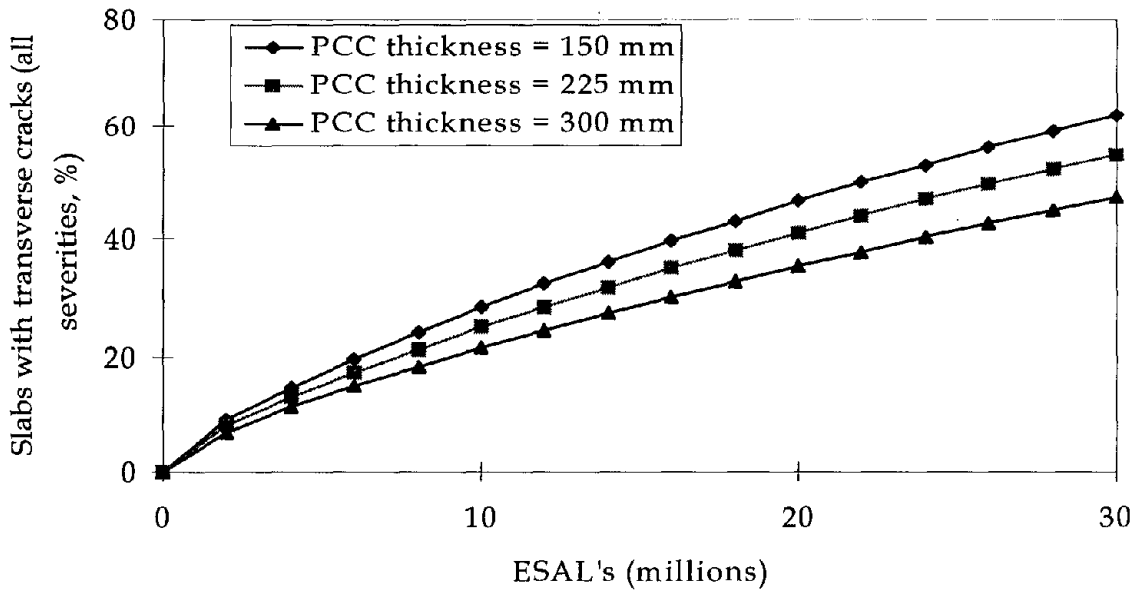


Figure 52. Plot of percentage of slabs with transverse cracking versus cumulative ESAL's for different slab thicknesses.

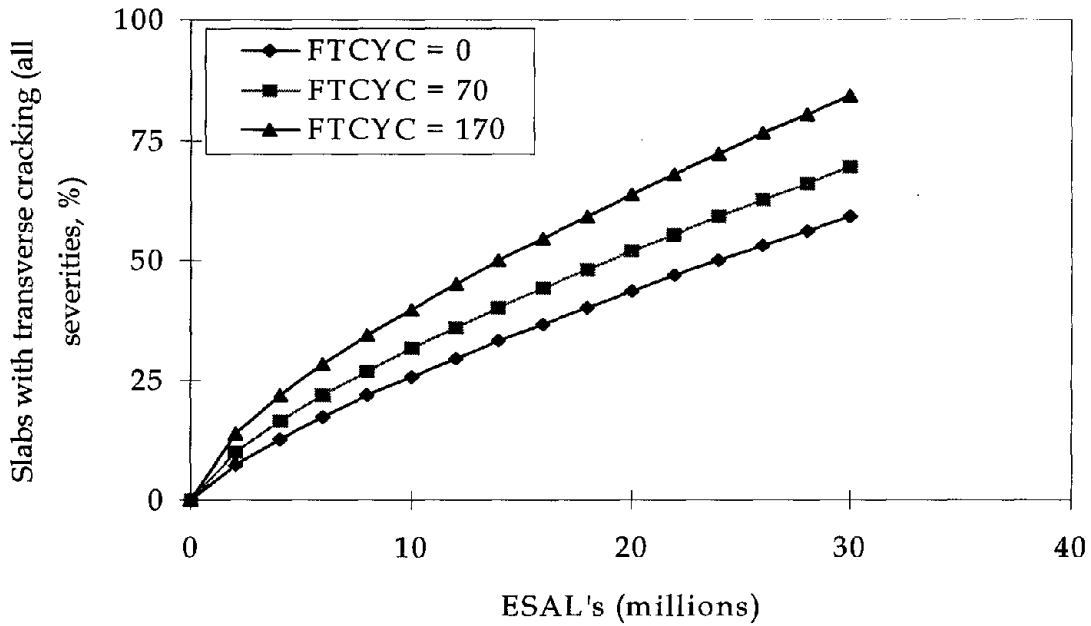


Figure 53. Plot of percentage of slabs with transverse cracking versus cumulative ESAL's for different levels of freeze-thaw cycles.

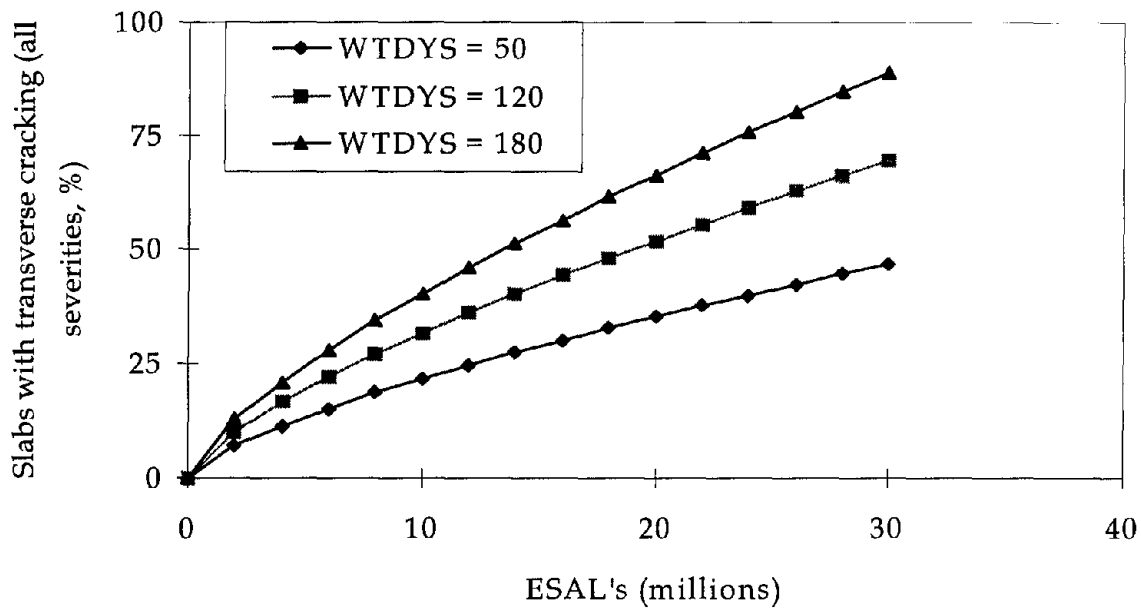


Figure 54. Plot of percentage of slabs with transverse cracking versus cumulative ESAL's for different annual number of wet days.

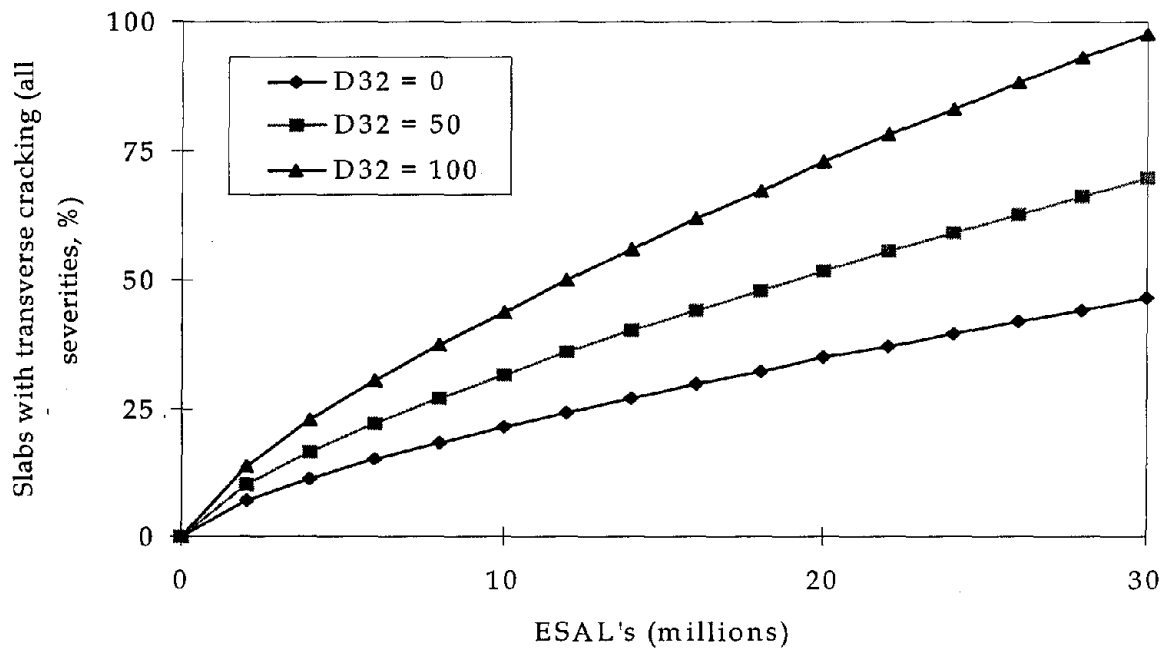


Figure 55. Plot of percentage of slabs with transverse cracking versus cumulative ESAL's for different number of days with temperatures above 32 °C.

## Summary

### Corner Breaks

The following can be summarized about the JPCP corner breaks model:

- Sixty-nine percent of the total variation of corner breaks can be explained by the included variables.
- Some of the unexplained variation is caused by errors in the independent variables used to develop the model, such as the traffic estimates.
- The “average” error in predicting corner breaks is 9 percent.
- There are no discernible patterns in the residuals.
- Data from 92 pavement sections from all over the United States were used to develop the model (N = 92).
- Each independent variable and the overall model was significant at a level of significance of 5 percent.
- The sensitivity analysis shows that all of the explanatory variables have a plausible effect on corner breaks that agrees with theoretical expectations and previous empirical field results.

### Transverse Cracking

The following can be summarized about the JPCP transverse cracking model:

- Sixty-four percent of the total variation of transverse cracking can be explained by the included variables.
- Some of the unexplained variation is caused by errors in the independent variables used to develop the model, such as the traffic estimates.
- The “average” error in predicting transverse cracking is 12 percent.
- There are no discernible patterns in the residuals.
- Data from 92 pavement sections from all over the United States were used to develop the model (N = 92).
- Each independent variable and the overall model was significant at a level of significance of 5 percent.

- The sensitivity analysis shows that all of the explanatory variables have a plausible effect on transverse cracking that agrees with theoretical expectations and previous empirical field results.

### **Implications and Recommendations**

The procedure used to develop the models used fracture mechanics principles for analysis of crack propagation within a PCC slab at both the center and edge positions. Using a modified version of ILLISLAB, a two-dimensional finite element model was used to analyze crack propagation in PCC slabs. Several mathematical expressions were developed for calculating the integral of the stress intensity factor across the thickness of the PCC slab. The equations can be used to estimate the allowable number of applications of temperature and traffic stresses that it takes for the crack to propagate across the slab thickness using Paris's crack growth law.

Using the LTPP database, the number of load applications to failure and the total damage caused by traffic and temperature loading were determined. Damage to the pavement was determined using Miner's cumulative damage hypothesis. Statistical and optimization techniques were then used to obtain mechanistic-empirical models that can be used to predict the percentage of slabs with transverse cracks or corner breaks in JPCP. The models were partially verified by conducting comprehensive sensitivity analyses. The fracture mechanics approach resulted in models that reasonably predict transverse cracks and corner breaks.



## 7. ROUGHNESS MODELS

### Introduction

Roughness is the irregularity of the surface of a pavement. Road users, in general, consider roughness the most important criterion when evaluating the condition of a road. Rough roads lead to user discomfort, increased travel times, and higher vehicle operating costs that can lead to millions of dollars in losses to the general economy. Although the structural performance of a pavement is most important to highway designers, the complaints generated by rough roads often contribute to a large part of the rehabilitation decisions that are made by State highway agencies.

The importance of roughness dates back many decades. The AASHO Road Test introduced the concept of serviceability as a measure of a pavement's ability to serve the traveling public, essentially the primary purpose of roadways.<sup>(18)</sup> The present serviceability rating (PSR) concept was adopted as a subjective measure of the ability of a pavement to serve the traveling public on the basis of panel ratings. The history of the serviceability of the pavement in relation to the loads applied was also used to represent the performance of the pavement.

For practical purposes, an objective measure of performance based on the serviceability concept, called the present serviceability index (PSI), was developed as a means of determining performance from physical measurements on the pavement.<sup>(53)</sup> Although the physical measurements used in computing PSI included distresses such as cracking and patching, it was the longitudinal profile or roughness of the pavement that provided the major correlation variable. Several studies since the AASHO Road Test have confirmed roughness as a strong indicator of the serviceability of a pavement, and most State highway agencies rely on roughness to estimate serviceability.<sup>(54, 55, 56, 57)</sup> Therefore, models for predicting roughness of pavements are very important as design checks and in pavement management systems. This chapter describes the development of such models for predicting the roughness of concrete pavements using the LTPP database.

### Roughness Measure

Road roughness can be defined as "the variation in surface elevation that induces vibrations in traversing vehicles."<sup>(58)</sup> Although there are various methods for measuring the roughness of pavements, one of the most common indices used is the International Roughness Index (IRI).<sup>(57)</sup> In 1982, the World Bank initiated the International Road Roughness Experiment (IRRE) in Brazil to study and serve as a reference for all profilic and response type systems that are used to measure roughness.<sup>(59, 60, 61)</sup> The experiment resulted in the evolution of the IRI.

IRI is a mathematical summary of the longitudinal surface profile of the road in the wheel path and is representative of the typical vibrations induced in a passenger car by the roughness of the road. IRI was adopted as a standard measure of roughness for the following reasons:

- It is time stable and can be reproduced easily from elevation data, since it is just a summary of the road profile.

- It gives consistently high correlations with the outputs of other roughness measuring devices at different speeds.

Following the World Bank study, the FHWA adopted IRI as a standard for measuring roughness and, since 1989, has been requiring all States to report pavement roughness in terms of IRI units for paved rural arterials and urban freeways, including Interstates.<sup>(57)</sup> As a result, IRI, computed from roughness measurements using the K. J. Law profilometer, is also used in the LTPP database as a measure of roughness. This profilometer uses a noncontact light sensor system to measure the distance between the vehicle frame and the road surface. It also measures the vertical motion of the vehicle. The difference between the displacement and vehicle motion is computed and is the raw road profile output stored in the database.

### **Progression of Roughness**

No one fundamental mechanism can be attributed to the development of roughness on pavements. A key factor is the initial smoothness (or roughness) of the pavement when it is constructed. Results from a recent extensive evaluation of several projects showed that initial smoothness is significantly related to future smoothness for all pavement types.<sup>(57)</sup> For PCC pavements, the study found that the initial smoothness was significant to the future smoothness for over 80 percent of the projects evaluated.

An evaluation of the LTPP IRI data for GPS 3, 4, and 5 pavement sections also found similar results.<sup>(62)</sup> Plots of the IRI over time for different pavement designs for the different pavement types are illustrated in figures 56, 57, and 58. In general, a comparison of the plots shows a remarkable stability in the development of roughness for the individual pavements. This suggests that pavements that are constructed smoother will typically stay smoother, and pavements that are rougher initially will tend to get rougher with time. Therefore, the initial smoothness of a pavement is very important to the prediction of the future progression of roughness for all pavements.

For a given pavement with a particular initial smoothness, several factors combine to contribute to the progression of roughness. Chief among them are the occurrence and progression of distress on the pavement. Increasing distress on the pavement will contribute to an increase in the roughness.



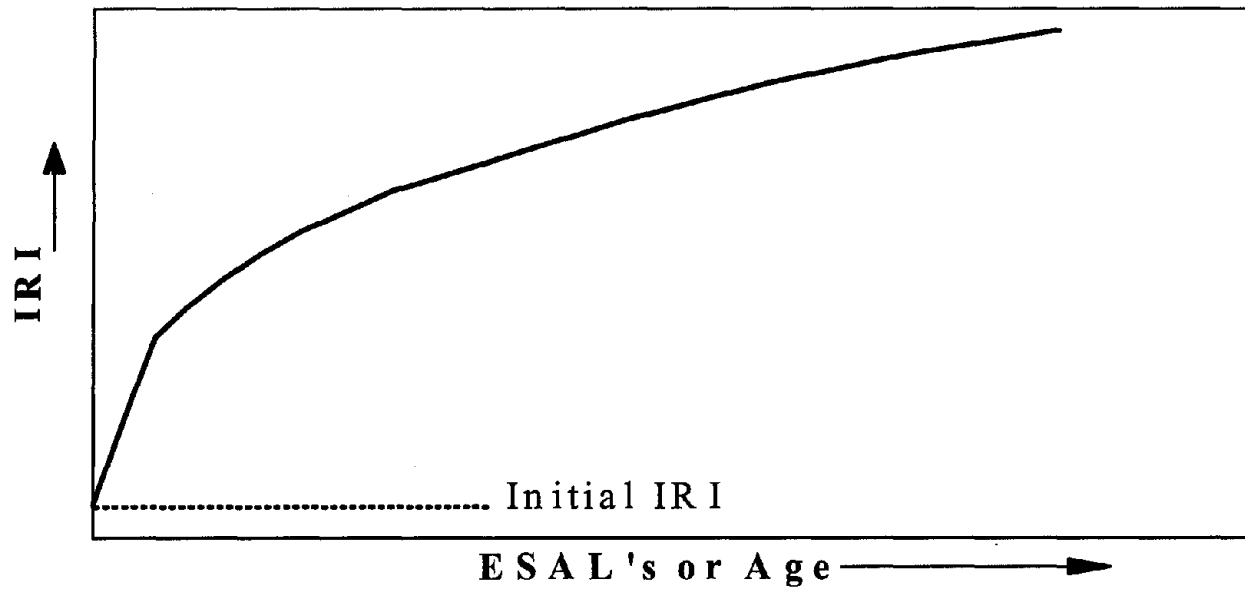


Figure 56. IRI model form A.

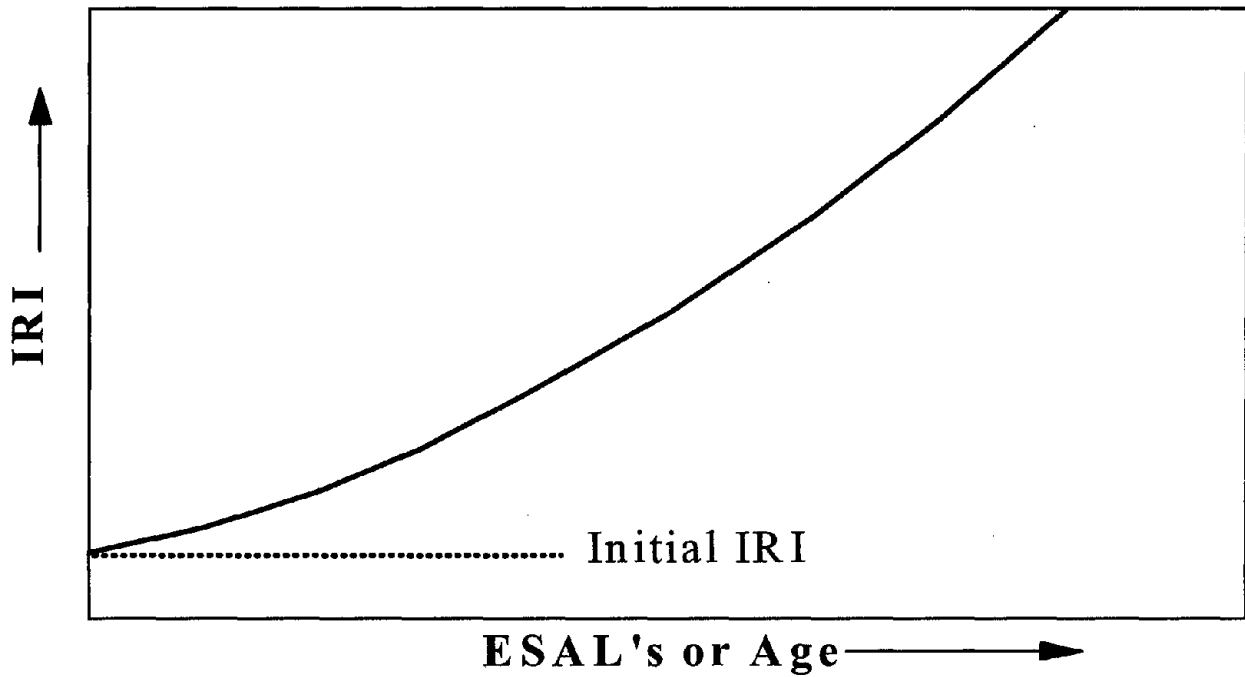


Figure 57. IRI model form B.<sup>(62)</sup>

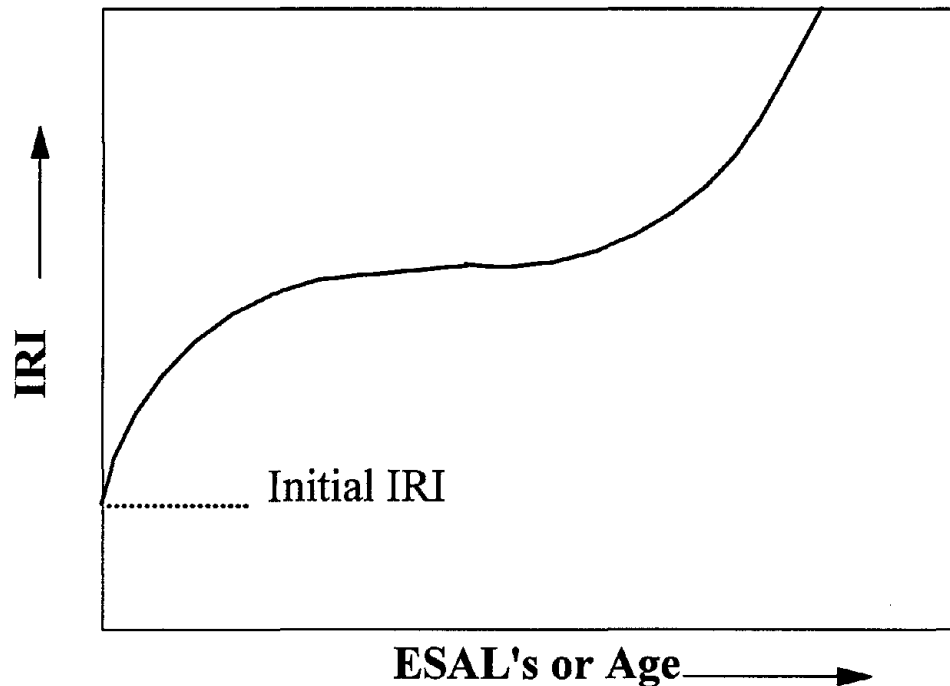


Figure 58. IRI model form C.<sup>(11)</sup>

The occurrence and progression of the distresses are directly related to the deterioration caused by the application of traffic loads, the environment, the support provided by the foundation, and the effects of aging of the pavement materials. Therefore, these factors also play an important part in the progression of roughness. The ability of the design features incorporated into the pavement to mitigate the deterioration of the pavement also has an important effect on the progression of roughness.

### **Evaluation of Existing Roughness Models**

To determine the significant variables associated with the various factors that contribute to the progression of roughness, previous models developed for predicting roughness were evaluated. The models evaluated were mainly empirical models that related IRI to pavement and environmental variables.

#### SHRP P-020 Study

In the SHRP P-020 study, models were developed for predicting the IRI of doweled JPCP, nondoweled JPCP, JRCP, and CRCP.<sup>(4)</sup>

### *IRI Model for Doweled JPCP*

The model developed for doweled JPCP is as follows:

$$\begin{aligned} \text{IRI} = & 105.9 + 159.1 \left[ \frac{\text{AGE}}{\text{KSTATIC}} \right] + 2.16\text{JTSP} \\ & + 7.13h_{\text{PCC}} + 13.5\text{EDGESUP} \end{aligned} \quad (93)$$

where

|                  |   |  |
|------------------|---|--|
| AGE              | = | pavement age, yr   |
| KSTATIC          | = | modulus of subgrade reaction, psi/in                       |
| JTSP             | = | joint spacing, ft  |
| $h_{\text{PCC}}$ | = | PCC slab thickness, in                                     |
| EDGESUP          | = | edge support; 1= tied PCC shoulder, 0= other shoulder type |

In this model, IRI is related to the age of the pavement and basic pavement design factors. According to the model, IRI is positively correlated to age and increases with age. This is reasonable because pavement distresses that increase the roughness of the pavement generally tend to increase with age. The pavement design features that were found to be significant to IRI were the modulus of subgrade reaction, joint spacing, PCC slab thickness, and the type of edge support.

### *IRI Model for Nondoweled JPCP*

The SHRP P-020 model developed for nondoweled JPCP is as follows:

$$\text{IRI} = 38.85 + 12.89\text{CESAL} + 0.2217\text{FT} + 1.5\text{PRECIP} - 10.96\text{BASE} - 13.7\text{SUBG} \quad (94)$$

where

|        |   |  |
|--------|---|--|
| CESAL  | = | cumulative number of ESAL's  |
| FT     | = | number of freeze-thaw cycles   |
| PRECIP | = | precipitation, in  |
| BASE   | = | base type; 1=treated (asphalt treated or lean concrete), 0=untreated |
| SG     | = | subgrade type; 1= coarse-grained, 0=fine-grained                     |

The most significant variables in this model were the cumulative number of ESAL's and amount of precipitation. Traffic loading, high number of freeze-thaw cycles, and increased precipitation were all found to increase roughness. The type of base and subgrade were also found to influence roughness, with treated bases and coarse-grained soils decreasing roughness. All these trends indicate a reasonable model.

### *IRI Model for JRCF*

The model developed for JRCF is as follows:

$$\text{IRI} = 0.85\text{AGE} + 0.347\text{PRECIP} + 1390/\text{KSTATIC} + 21.2h_{\text{PCC}} + 15.1 \text{ EDGESUP} - 141 \quad (95)$$

where

|                  |   |                                       |
|------------------|---|---------------------------------------|
| AGE              | = | pavement age, yr                      |
| KSTATIC          | = | modulus of subgrade reaction, psi/in  |
| $h_{\text{PCC}}$ | = | PCC slab thickness, in                |
| EDGESUP          | = | edge support; 1 = tied PCC, 0 = other |
| PRECIP           | = | precipitation, in                     |

The model predicts IRI as a function of basic pavement properties, climatic data, and age. Age is positively correlated to IRI with an increase in age increasing the predicted IRI. This is similar to the trend observed for JPCP pavements. The other pavement material and design features that influenced the predicted IRI include the modulus of subgrade reaction, the PCC slab thickness, precipitation, and the PCC slab edge support condition.

### *IRI Model for CRCP*

The SHRP P020 model developed for CRCP is as follows:

$$\text{IRI} = 262 + 1.47\text{CESAL} - 2.94h_{\text{PCC}} - 232.2\text{PSTEEL} - 29.8\text{WIDENED} - 16.8\text{SUBG} \quad (96)$$

where

|                  |   |  |
|------------------|---|--|
| $h_{\text{PCC}}$ | = | PCC slab thickness, in                           |
| CESAL            | = | cumulative number of ESAL's                      |
| SUBG             | = | subgrade type; 1= coarse-grained, 0=fine-grained |
| PSTEEL           | = | percentage of steel in PCC slab                  |
| WIDENED          | = | presence of widened lanes                        |

The CRCP model also predicts IRI as a function of basic pavement properties and climatic data. CESAL is positively correlated to IRI; that is, an increase in the number of 80-kN ESAL applications increases IRI. The pavement subgrade type and design features such as widened lanes, percentage of steel in PCC slab, and PCC slab thickness were all shown to have an influence on the predicted IRI.

### RIPPER Study

In the FHWA jointed concrete pavement research study commonly referred to as the RIPPER study, a model for predicting IRI of JPCP was developed that is based on pavement distresses such as faulting, spalling, and cracking.<sup>(10)</sup> The final model developed for predicting IRI is as follows:

$$IRI^2 = 99.6 + 2.6098\text{FaultT} + 1.84\text{Spall} + 2.28 \cdot 10^{-6} \text{T-crack}^3 \quad (97)$$

where

FaultT = total joint faulting per mile, in  
T-crack = total number of transverse cracks  
Spall = percentage of spalled joints

This model presents another approach to developing roughness models. It is based on the philosophy that IRI should be directly correlated to the pavement distresses that lead to roughness.

### Other LTPP-Based IRI Models

There have been two recent efforts to develop models for predicting IRI on concrete pavements using the LTPP data.<sup>(11, 62)</sup> Both of these efforts resulted in the development of models for predicting IRI for JPCP, JRCP, and CRCP. This followed an extensive evaluation of the LTPP data, and they showed that IRI is correlated to a host of pavement design and climatic variables.<sup>(11, 62)</sup>

### Roughness Model Forms

The models reviewed show that a variety of methods can be used to develop models for predicting IRI. They include models that relate IRI to pavement design features and climatic variables, as well as those that predict IRI directly from distresses. However, the most common IRI models are those that include a wide range of pavement design and climatic variables that potentially, through their influence on the occurrence and progression of distress, influence roughness. Another important observation common to most of the models is that they include an estimate of an average initial IRI. In spite of the difficulty in determining the actual initial IRI values for the pavements in the databases used, the results obtained are quite consistent when the estimated average initial IRI values are compared. An examination of the models shows that three main forms have been used in past studies to model roughness.<sup>(4, 10, 11, 62)</sup> The model forms are shown in figures 56, 57, and 58, and the mathematical expressions for the models are given by equations 98, 99, and 100, respectively:

Model Form A:

$$IRI = \text{DET}^n (IRI_0 + a_1 X_1 + a_2 X_2 + \dots + a_n X_n) \quad (98)$$

where

IRI = International Roughness Index, m/km  
DET = age or cumulative ESAL's  
IRI<sub>0</sub> = initial IRI, m/km  
X<sub>i</sub> = various pavement and climatic variables  
a<sub>i</sub> = regression constants

Model Form B.<sup>(62)</sup>

$$IRI(t) = e^{r_0 t} \left[ \frac{IRI_{max} * IRI_0}{IRI_0(e^{r_0 t} - 1) + IRI_{max}} \right] \quad (99)$$

where

- IRI (t) = IRI at time t, m/km
- IRI<sub>0</sub> = estimated initial IRI, m/km
- IRI<sub>max</sub> = estimated long-term IRI, m/km
- r (t) = growth rate constant
- t = time in years

Model Form C.<sup>(11)</sup>

$$IRI = IRI_0 + \frac{\rho}{\left[ \ln \left( \frac{t_0}{t} \right) \right]^{\frac{1}{\beta}}} \quad (100)$$

where

- IRI<sub>0</sub> = initial IRI, m/km
- t<sub>0</sub> = pavement age or cumulative ESAL's at failure
- t = pavement age or cumulative ESAL's
- β, ρ = regression parameters that are correlated to pavement structural and climatic properties

All three models are similar at the initial stages of the pavement's life, in the sense that they agree on the existence of an initial IRI value at the traffic opening date of the pavement that influences the future IRI. However, the progression of roughness over time is different for each of the model forms.

Model A assumes a rapid increase in roughness in the initial stages of aging or deterioration of the pavement. The rate of increase decreases appreciably thereafter and approaches a maximum value asymptotically. Conversely, model form B assumes that in the initial stages of the pavement's life the increase in roughness is slow. However, later in life the rate increases appreciably and IRI continues to increase as the pavement gets rougher. Model C is a combination of the previous two model forms. It assumes that, for the most part, IRI follows the trend similar to that described for model form A; however, instead of the IRI approaching a maximum value asymptotically, after some point in time the rate of increase in roughness once again increases rapidly with no maximum IRI value.

### Preliminary Data Analysis

The procedure outlined previously for developing prediction models was followed to determine the explanatory variables and model forms for the development of IRI prediction models.

### Data Assembly, Cleaning, and Exploration

This included the assembly of the data required for the development of the models for predicting IRI of JPCP, JRCP, and CRCP; the data were obtained from the GPS 3, 4, and 5 experiments, respectively. The variables included in the databases were those identified from the review of literature and existing models for predicting roughness. Table 19 shows the variables that were included in the investigation. The databases were evaluated thoroughly to check for missing and erroneous data, cleaned, and prepared for analysis.

The databases were then explored to learn more about their suitability for model development. This included a comprehensive statistical analysis of the cleaned data to evaluate the preliminary relationships between the measured roughness and the explanatory variables. Univariate statistical analyses were conducted to learn about the distribution of the IRI for each of the pavement types and the explanatory variables. In addition, the data exploration consisted of evaluation of bivariate plots of IRI for the different pavement types versus potential independent variables and correlation studies.

Table 19. Variables identified for use in the development of roughness models.

| Symbol   | Explanatory Variable                                     |
|----------|--|
| FI       | Freezing index   |
| FTCYC    | Mean annual number of freeze-thaw cycles                 |
| PRECIP   | Mean annual precipitation, mm                            |
| WTDYS    | Mean annual number of wet days                           |
| TEMP     | Mean annual temperature, °C                              |
| JTSP     | Joint spacing, m   |
| $C_d$    | Drainage coefficient                                     |
| k value  | Modulus of subgrade reaction, kPa/mm                     |
| D90      | Mean annual days with temperature above 90 °C            |
| BASE     | Base type, 0 = erodible, 1 = nonerodible                 |
| DTYPE    | Presence of edge drains, 0 = not present, 1 = present    |
| PSTEEL   | Percentage of steel reinforcement in PCC slab            |
| BTHICK   | Base thickness, mm                                       |
| BTYPE    | Base material type, 0 = fine, 1 = coarse                 |
| PCCthick | PCC layer thickness, mm                                  |
| MAXTEMP  | Average daily maximum temperature, °C                    |
| MINTEMP  | Average daily minimum temperature, °C                    |
| TRANGE   | Difference in daily maximum and minimum temperatures, °C |
| SGTYPE   | Subgrade type, 0 = fine, 1 = coarse                      |
| AGE      | Pavement age since construction, yr                      |
| KESAL    | Cumulative number of 80-kN axle loads, thousands         |
| IRI      | International Roughness Index, m/km                      |

A key part of the data evaluation was examination of the trends between the various independent variables and IRI. Figures 59, 60, and 61 show bivariate plots that relate the IRI of JPCP, JRCP, and CRCP, respectively, to several individual variables. In all cases, an increase in age and traffic loading results in an increase in IRI. Increases in most of the climatic variables, such as precipitation, number of freeze-thaw cycles, and freezing index, also tend to increase IRI. Stronger base and subgrade materials, such as nonerodible bases and granular subbases, tend to decrease IRI. Other pavement design variables, such as the thickness of the PCC concrete layer,



increase or decrease roughness depending on pavement type. The correlation tables that show the strength of the relationships between the potential independent variables and IRI for JPCP, JRCP, and CRCP, as well as the relationships between the independent variables themselves, are shown in tables 20 through 22.

### Selection of Model Form

On the basis of results obtained from the preliminary evaluation of the databases assembled for development of the IRI models, and an evaluation of several model forms, the final model form that was selected for consideration is as follows:

$$IRI = IRI_0 + ESAL^\alpha(a_1X_1 + a_2X_2 + \dots + a_nX_n) + AGE^\beta(b_1Z_1 + b_2Z_2 + \dots + b_nZ_n) \quad (101)$$

where

|  |   |  |
|--|---|--|
| IRI                                    | = | International Roughness Index, m/km            |
| IRI <sub>0</sub>                       | = | initial IRI, m/km                              |
| ESAL                                   | = | cumulative ESAL's                              |
| X <sub>i</sub> , Z <sub>i</sub>        | = | various pavement design and climatic variables |
| a <sub>i</sub> , b <sub>i</sub> , α, β | = | regression constants                           |

The basic philosophy behind this model form is that the future IRI is dependent on the initial IRI after construction. The model then assumes that the progression of roughness is dependent on two major factors, namely, the effect of traffic loading on the pavement and the effect of aging on the pavement. These effects are accounted for by including the interactions between traffic loading and pavement and climatic variables that influence roughness, and the interactions between age and pavement and climatic variables that influence roughness in the model. The model agrees with the results of several earlier studies on the effect of initial IRI.<sup>(4, 10, 11, 62)</sup> In addition, it is reasonable to assume that the progression of roughness is a function of the interaction between traffic loading and age on one side and pavement and climatic variables on the other. However, because of the errors associated with estimating the initial IRI for all the pavements in the LTPP database used for this analysis, it was decided to obtain an average IRI<sub>0</sub> for each of the pavement types from regression analysis, included in the model as an intercept.

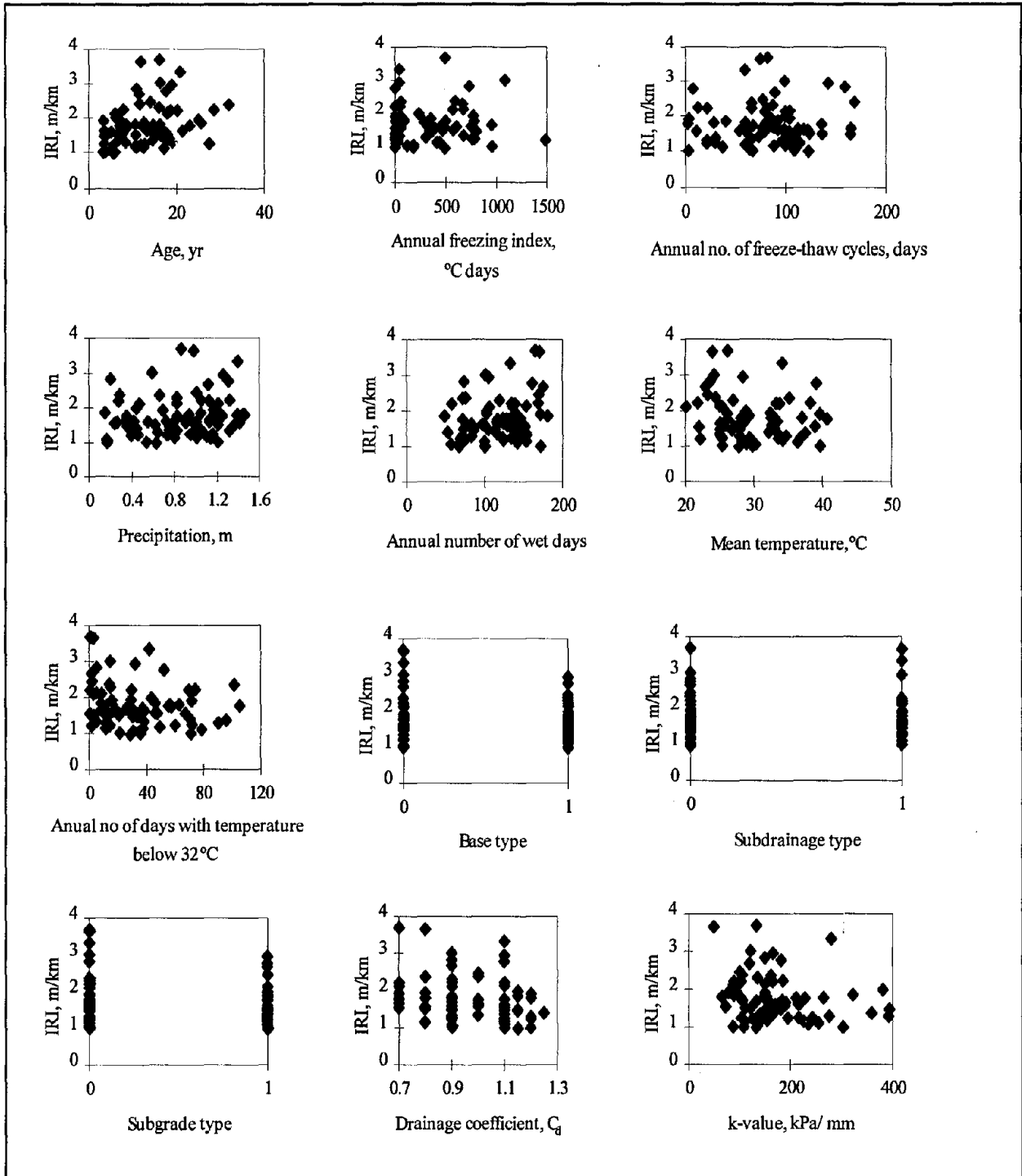


Figure 59. Plots of IRI versus significant variables for JPCP.

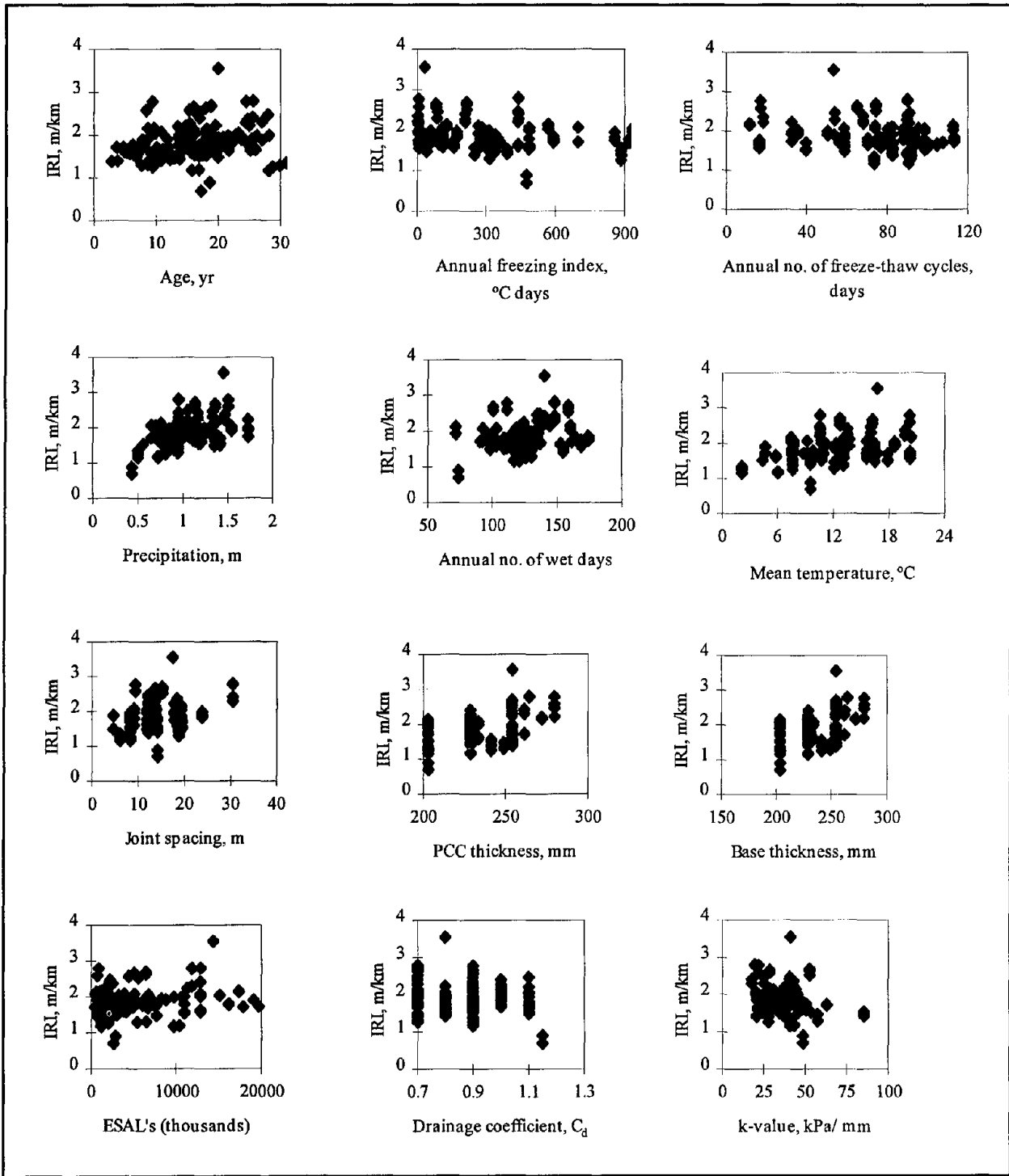


Figure 60. Plots of IRI versus significant variables for JRCP.

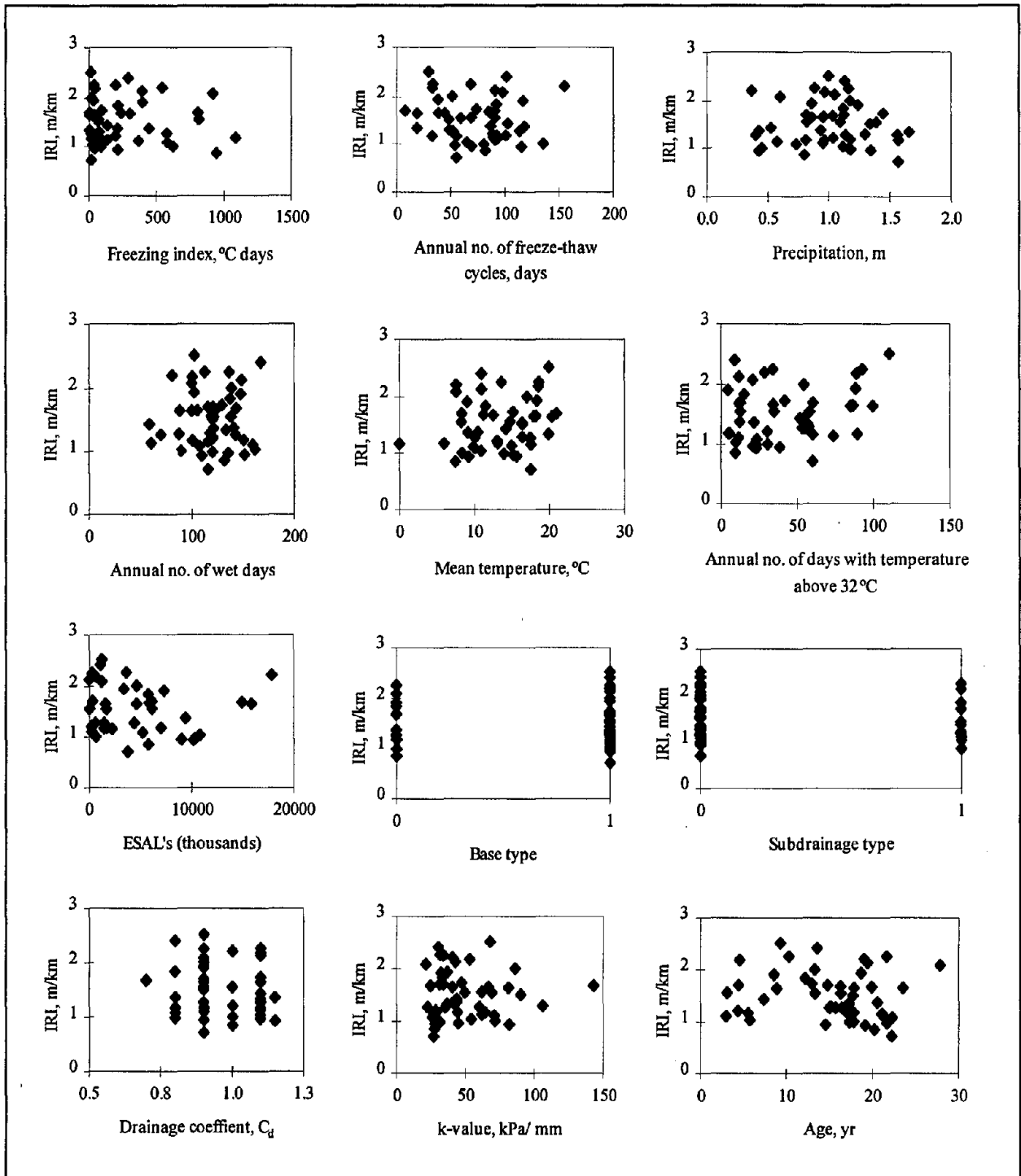


Figure 61. Plots of IRI versus significant variables for CRCP.

Table 20. Summary of correlation analysis for significant variables versus IRI for JPCP.

|         | AGE    | FI     | FTCYC  | PRECIP | WTDYS  | TEMP   | D32    | BTYPE  | DTYPE  | Cd     | k-value | KESAL  | IRI    |         |
|---------|--------|--------|--------|--------|--------|--------|--------|--------|--------|--------|---------|--------|--------|---------|
| AGE     | 1      | -0.031 | -0.163 | 0.215  | 0.166  | 0.057  | -0.038 | -0.179 | 0.001  | -0.204 | -0.114  | 0.438  | 0.340  | AGE     |
| FI      | -0.031 | 1      | 0.096  | -0.038 | 0.206  | -0.549 | -0.399 | -0.282 | -0.028 | -0.290 | -0.350  | -0.204 | 0.269  | FI      |
| FTCYC   | -0.163 | 0.096  | 1      | -0.516 | -0.396 | -0.738 | -0.540 | -0.114 | -0.045 | -0.169 | -0.047  | -0.139 | 0.050  | FTCYC   |
| PRECIP  | 0.215  | -0.038 | -0.516 | 1      | 0.803  | 0.461  | 0.106  | 0.123  | 0.231  | -0.137 | -0.081  | 0.095  | 0.169  | PRECIP  |
| WTDYS   | 0.166  | 0.206  | -0.396 | 0.803  | 1      | 0.134  | -0.232 | -0.037 | 0.283  | -0.256 | -0.153  | -0.091 | 0.229  | WTDYS   |
| TEMP    | 0.057  | -0.549 | -0.738 | 0.461  | 0.134  | 1      | 0.837  | 0.405  | 0.072  | 0.407  | 0.322   | 0.254  | -0.148 | TEMP    |
| D32     | -0.038 | -0.399 | -0.540 | 0.106  | -0.232 | 0.837  | 1      | 0.451  | 0.002  | 0.548  | 0.418   | 0.216  | -0.181 | D90     |
| BTYPE   | -0.179 | -0.282 | -0.114 | 0.123  | -0.037 | 0.405  | 0.451  | 1      | 0.230  | 0.594  | 0.452   | 0.070  | -0.173 | BTYPE   |
| DTYPE   | 0.001  | -0.028 | -0.045 | 0.231  | 0.283  | 0.072  | 0.002  | 0.230  | 1      | 0.171  | 0.137   | 0.223  | 0.022  | DTYPE   |
| Cd      | -0.204 | -0.290 | -0.169 | -0.137 | -0.256 | 0.407  | 0.548  | 0.594  | 0.171  | 1      | 0.499   | 0.083  | -0.224 | Cd      |
| k-value | -0.114 | -0.350 | -0.047 | -0.081 | -0.153 | 0.322  | 0.418  | 0.452  | 0.137  | 0.499  | 1       | -0.004 | -0.215 | k-value |
| KESAL   | 0.438  | -0.204 | -0.139 | 0.095  | -0.091 | 0.254  | 0.216  | 0.070  | 0.223  | 0.083  | -0.004  | 1      | 0.156  | KESAL   |
| IRI     | 0.340  | 0.269  | 0.050  | 0.169  | 0.229  | -0.148 | -0.181 | -0.173 | 0.022  | -0.224 | -0.215  | 0.156  | 1      | IRI     |

Table 21. Summary of correlation analysis for significant variables versus IRI for JRCF.

|         | FI       | FTCYC    | PRECIP   | WTDYS    | TEMP     | JTSP     | HPCC     | BTHICK   | KESAL    | AGE      | Cd       | k-value  | IRI      |
|---------|----------|----------|----------|----------|----------|----------|----------|----------|----------|----------|----------|----------|----------|
| FI      | 1        | 0.09345  | -0.45447 | -0.04821 | -0.25457 | -0.32615 | -0.34355 | -0.13245 | -0.11539 | 0.30547  | -0.01839 | 0.01059  | -0.28991 |
| FTCYC   | 0.09345  | 1        | -0.7146  | 0.20345  | -0.22403 | -0.05634 | -0.26593 | 0.06205  | -0.03748 | -0.17301 | -0.19912 | 0.08984  | -0.30063 |
| PRECIP  | -0.45447 | -0.7146  | 1        | 0.13559  | 0.12159  | 0.32848  | 0.34467  | 0.30223  | 0.11636  | 0.17202  | 0.20329  | -0.09988 | 0.44008  |
| WTDYS   | -0.04821 | 0.20345  | 0.13559  | 1        | -0.11206 | 0.25538  | 0.28804  | 0.44631  | 0.11165  | 0.06847  | -0.22195 | 0.16088  | 0.2318   |
| TEMP    | -0.25457 | -0.22403 | 0.12159  | -0.11206 | 1        | 0.09631  | 0.07509  | 0.00394  | 0.00728  | -0.13732 | 0.26433  | -0.05527 | 0.16051  |
| JTSP    | -0.32615 | -0.05634 | 0.32848  | 0.25538  | 0.09631  | 1        | 0.26412  | 0.28814  | 0.35098  | 0.28078  | -0.22819 | -0.22984 | 0.34608  |
| HPCC    | -0.34355 | -0.26593 | 0.34467  | 0.28804  | 0.07509  | 0.26412  | 1        | 0.07091  | 0.10401  | -0.16212 | -0.12534 | 0.23021  | 0.40374  |
| BTHICK  | -0.13245 | 0.06205  | 0.30223  | 0.44631  | 0.00394  | 0.28814  | 0.07091  | 1        | 0.21768  | 0.18112  | -0.06467 | 0.22079  | 0.09112  |
| KESAL   | -0.11539 | -0.03748 | 0.11636  | 0.11165  | 0.00728  | 0.35098  | 0.10401  | 0.21768  | 1        | 0.42592  | -0.22965 | -0.1783  | 0.21929  |
| AGE     | 0.30547  | -0.17301 | 0.17202  | 0.06847  | -0.13732 | 0.28078  | -0.16212 | 0.18112  | 0.42592  | 1        | -0.0225  | -0.30201 | 0.24155  |
| Cd      | -0.01839 | -0.19912 | 0.20329  | -0.22195 | 0.26433  | -0.22819 | -0.12534 | -0.06467 | -0.22965 | -0.0225  | 1        | -0.02382 | -0.15156 |
| k-value | 0.01059  | 0.08984  | -0.09988 | 0.16088  | -0.05527 | -0.22984 | 0.23021  | 0.22079  | -0.1783  | -0.30201 | -0.02382 | 1        | -0.25426 |
| IRI     | -0.28991 | -0.30063 | 0.44008  | 0.2318   | 0.16051  | 0.34608  | 0.40374  | 0.09112  | 0.21929  | 0.24155  | -0.15156 | -0.25426 | 1        |

Table 22. Summary of correlation analysis for significant variables versus IRI for CRCP.

|         | FI       | FTCYC    | PRECIP   | WTDYS    | TEMP     | D32      | KESAL    | BTYPE    | DTYPE    | Cd       | k-value  | AGE      | IRI      |         |
|---------|----------|----------|----------|----------|----------|----------|----------|----------|----------|----------|----------|----------|----------|---------|
| FI      | 1        | 0.63806  | -0.53522 | -0.10866 | -0.83279 | -0.57413 | 0.05743  | -0.43926 | 0.16635  | -0.17619 | -0.21588 | 0.32686  | -0.06188 | FI      |
| FTCYC   | 0.63806  | 1        | -0.51159 | 0.0611   | -0.89745 | -0.74752 | 0.16812  | -0.3434  | 0.17454  | -0.1757  | -0.1082  | 0.24905  | -0.11489 | FTCYC   |
| PRECIP  | -0.53522 | -0.51159 | 1        | 0.46404  | 0.53244  | 0.11391  | -0.03543 | 0.09119  | 0.08404  | -0.18431 | -0.03479 | -0.16405 | -0.07238 | PRECIP  |
| WTDYS   | -0.10866 | 0.0611   | 0.46404  | 1        | -0.14247 | -0.54119 | 0.22258  | -0.12269 | 0.46103  | -0.22013 | 0.00223  | -0.15962 | -0.0417  | WTDYS   |
| TEMP    | -0.83279 | -0.89745 | 0.53244  | -0.14247 | 1        | 0.84365  | -0.15855 | 0.4299   | -0.3025  | 0.12834  | 0.0971   | -0.21393 | 0.1826   | TEMP    |
| D32     | -0.57413 | -0.74752 | 0.11391  | -0.54119 | 0.84365  | 1        | -0.22817 | 0.41421  | -0.45313 | 0.26423  | 0.11748  | -0.15332 | 0.25191  | D32     |
| KESAL   | 0.05743  | 0.16812  | -0.03543 | 0.22258  | -0.15855 | -0.22817 | 1        | 0.07539  | 0.26156  | 0.23042  | 0.05881  | 0.24008  | 0.1521   | KESAL   |
| BTYPE   | -0.43926 | -0.3434  | 0.09119  | -0.12269 | 0.4299   | 0.41421  | 0.07539  | 1        | -0.24196 | 0.50606  | 0.14997  | -0.27279 | -0.05728 | BTYPE   |
| DTYPE   | 0.16635  | 0.17454  | 0.08404  | 0.46103  | -0.3025  | -0.45313 | 0.26156  | -0.24196 | 1        | -0.04748 | -0.18992 | -0.13788 | -0.07511 | DTYPE   |
| Cd      | -0.17619 | -0.1757  | -0.18431 | -0.22013 | 0.12834  | 0.26423  | 0.23042  | 0.50606  | -0.04748 | 1        | 0.01158  | -0.05897 | -0.15216 | Cd      |
| k-value | -0.21588 | -0.1082  | -0.03479 | 0.00223  | 0.0971   | 0.11748  | 0.05881  | 0.14997  | -0.18992 | 0.01158  | 1        | -0.22884 | 0.02666  | k-value |
| AGE     | 0.32686  | 0.24905  | -0.16405 | -0.15962 | -0.21393 | -0.15332 | 0.24008  | -0.27279 | -0.13788 | -0.05897 | -0.22884 | 1        | -0.09549 | AGE     |
| IRI     | -0.06188 | -0.11489 | -0.07238 | -0.0417  | 0.1826   | 0.25191  | 0.1521   | -0.05728 | -0.07511 | -0.15216 | 0.02666  | -0.09549 | 1        | IRI     |

## Development of Final Models

The final step was to perform multiple linear regression analysis using the most suitable variables and interactions to obtain the final model parameter estimates for the model form selected. The relevant diagnostic statistics to be used to verify the suitability and stability of the model were also obtained. In each case, several models were developed and evaluated for each pavement type. The most suitable model was selected based on both engineering judgment and diagnostic statistics. The diagnostic statistics used included the coefficient of determination,  $R^2$ , and standard error of estimate (SEE). The relevance of these statistics is discussed in appendix A.

For each pavement type, the model that was in accordance with engineering principles and also had the best combination of diagnostic statistics was selected as the final model for predicting IRI. A primary goal was to select the model that best describes the progression of IRI but includes just the appropriate number of explanatory variables and parameters. Including too many variables in the model will not necessarily improve its predictive capability. A model's  $R^2$  will always increase with an increasing number of independent variables, but the standard error of estimate may also increase and compromise the accuracy of the model.

### Final IRI Prediction Models

The final models developed for predicting IRI of JPCP, JRCP, and CRCP are presented in this section.

#### JPCP IRI Prediction Model

The model developed for predicting IRI of JPCP pavements is as follows:

$$\begin{aligned} \text{IRI} = & 1.3033 + \text{KESAL}^{0.4}(1.578\text{WETDAYS} + 113.6\text{FREEZE}) \\ & * 10^{-4} + \text{AGE}^{0.4}(1.4437\text{FI} + 3.6*10^{-5}\text{E}_{\text{PCC}} - 552 \text{SUGTYP} \\ & - 19.08\text{DOWDIA}) * 10^{-4} \end{aligned} \quad (102)$$

where

|                  |   |   |
|------------------|---|---|
| IRI              | = | International Roughness Index, m/km                           |
| KESAL            | = | cumulative 80-kN equivalent single axle loads, thousands      |
| WETDAYS          | = | number of days precipitation is greater than 12.7 mm          |
| FREEZE           | = | LTPP climatic zone, 1=freezing climate, 0=nonfreezing climate |
| AGE              | = | pavement age, yr  |
| FI               | = | freezing index, °C days                                       |
| $E_{\text{PCC}}$ | = | PCC elastic modulus, kPa                                      |
| SUGTYP           | = | subgrade type, 1=coarse-grained, 0=fine-grained               |
| DOWDIA           | = | Dowel diameter, mm  |



Statistics:

|                |   |                               |
|----------------|---|-------------------------------|
| N              | = | 155                           |
| R <sup>2</sup> | = | 0.50                          |
| SEE            | = | 0.328 m/km                    |
| p-value        | < | 0.005 (significance of model) |

A plot of the predicted and measured JPCP IRI is shown in figure 62. A plot of the residuals (predicted - actual IRI) against the predicted IRI is shown in figure 63. The overall accuracy of the JPCP IRI model is reflected by the R<sup>2</sup> of 0.50, which is the proportion of variation of IRI explained by the variables included in the model. A test of hypothesis was performed to determine the significance of the variables used in the model for predicting IRI. The null and alternate hypotheses were as follows:

- H<sub>0</sub>: all model parameters are zero (variables are not significant)  
H<sub>A</sub>: all model parameters are not zero

The F-test statistic used for the hypothesis test was calculated as the ratio of the mean square for the model divided by the mean square of the error. For this study the null hypothesis will be rejected if the level of significance is less than 5 percent (0.05). A level of significance (p-value) of less than 0.005 implies a rejection of the null hypothesis. This shows that the variables in the model are highly significant. Also, individual t-tests were conducted to test if the individual parameter estimates are equal to zero. The p-values for this test ranged from 0.0001 to 0.004. The results show that all the parameter estimates had values other than zero; therefore, the variables in the model were significant. Prediction accuracy of IRI in absolute units is reflected by the standard error of estimate (SEE = 0.328 m/km). The overall effectiveness of the model should be judged on all the diagnostic statistics, the residual plots, and the results from the sensitivity analysis to follow. The diagnostic statistics obtained for the JPCP IRI model show that the model can predict JPCP IRI with reasonable accuracy for the current LTPP database utilized.

JRCP IRI Prediction Model

The model developed for predicting IRI of JRCP pavements is as follows:

$$\text{IRI} = 1.272 + 0.00866*\text{PSTEEL}*\text{KESAL}^{0.4} + 0.00742*\text{AGE}^{0.7}(5.78 + 0.0106\text{PRECIP} - 1.95\text{DRAIN} - 3.73\text{SUGTYP}) \quad (103)$$

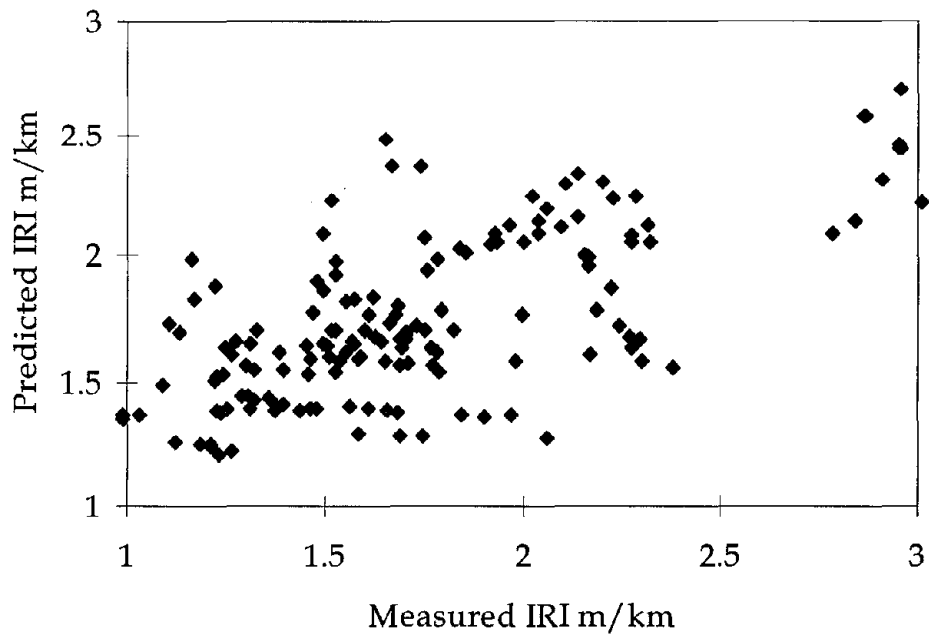


Figure 62. Plot of predicted versus actual IRI for JPCP.

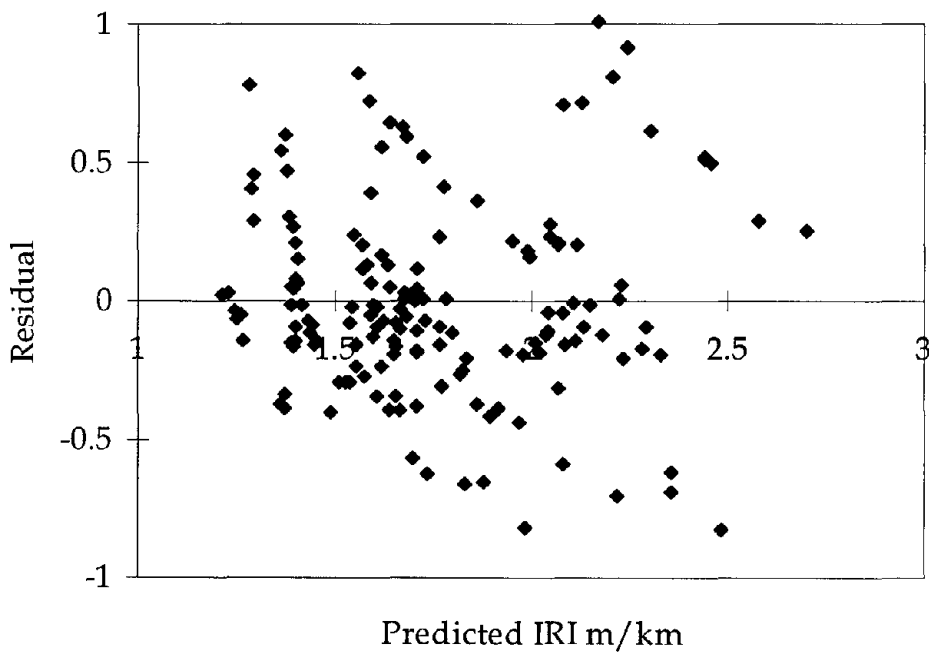


Figure 63. Plot of residual versus predicted IRI for JPCP.

where

|        |   |   |
|--------|---|---|
| IRI    | = | International Roughness Index, m/km                       |
| KESAL  | = | cumulative 80-kN equivalent single axle loads, thousands  |
| PSTEEL | = | percentage of steel                                       |
| AGE    | = | pavement age, yr  |
| PRECIP | = | average annual precipitation, mm                          |
| DRAIN  | = | presence of edge drain, 1 = edge drain 0 = no edge drains |
| SUGTYP | = | subgrade type, 1=coarse-grained, 0=fine-grained           |

Statistics:

|                |   |                                |
|----------------|---|--------------------------------|
| N              | = | 93                             |
| R <sup>2</sup> | = | 0.50                           |
| SEE            | = | 0.246 m/km                     |
| p-value        | < | 0.0001 (significance of model) |

A plot of the predicted and measured JRCP IRI is shown in figure 64. A plot of the residuals (predicted - actual IRI) against the predicted IRI is shown in figure 65. The overall accuracy of the JRCP IRI model is reflected by the R<sup>2</sup> of 0.50, which is the proportion of variation of IRI explained by the variables included in the model. A test of hypothesis was performed to determine the significance of the variables used in the model for predicting IRI. The null and alternate hypotheses were as follows:

- H<sub>0</sub>: all model parameters are zero (variables are not significant)  
H<sub>A</sub>: all model parameters are not zero

The F-test statistic used for the hypothesis test was calculated as the ratio of the mean square for the model divided by the mean square of the error. For this study the null hypothesis will be rejected if the level of significance is less than 5 percent (0.05). A level of significance (p-value) of less than 0.0001 implies a rejection of the null hypothesis. This shows that the variables in the model are highly significant. Also, individual t-tests were conducted to test if the individual parameter estimates are equal to zero. The p-values for this test ranged from 0.0001 to 0.01. The results show that all the parameter estimates had values other than zero; therefore, the variables in the model were significant. Prediction accuracy of IRI in absolute units is reflected by the standard error of estimate (SEE = 0.246 m/km). The overall effectiveness of the model should be judged on all the diagnostic statistics, the residual plots, and the results from the sensitivity analysis to follow. The diagnostic statistics obtained for the JRCP IRI model show that the model can predict JRCP IRI with reasonable accuracy for the current LTPP database utilized.

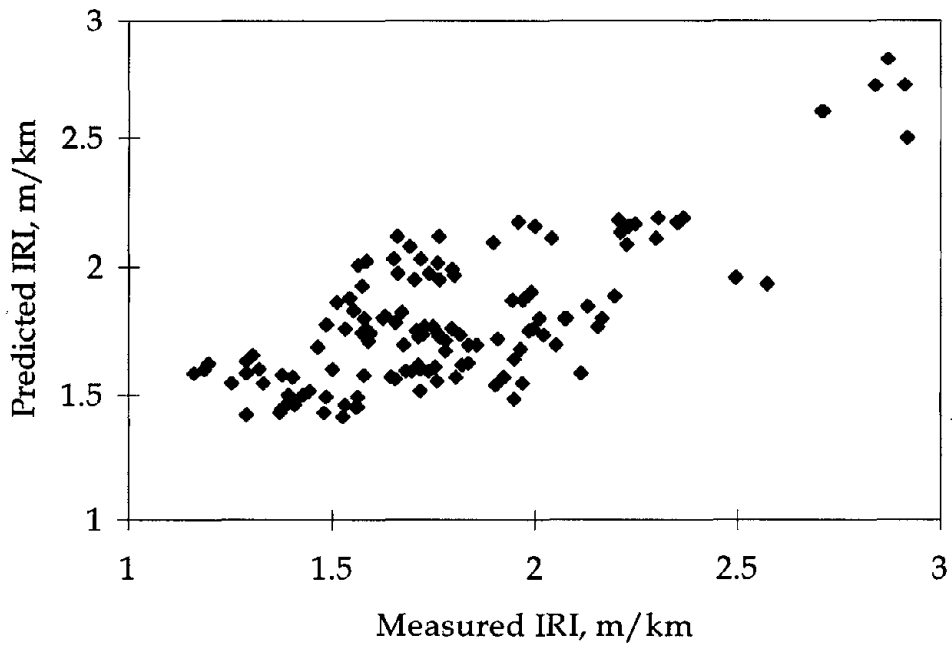


Figure 64. Plot of predicted versus actual IRI for JRCP.

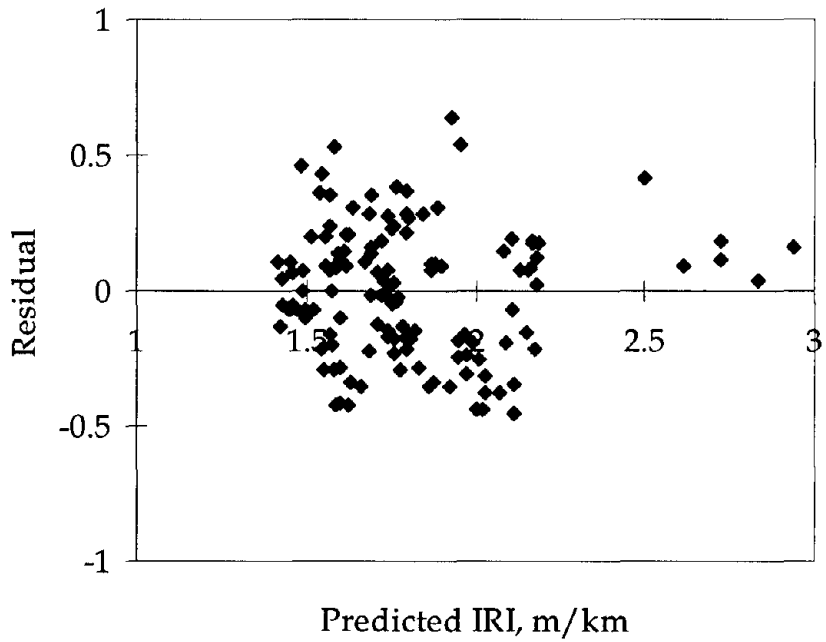


Figure 65. Plot of residual versus predicted IRI for JRCP.

## CRCP IRI Prediction Model

The model developed for predicting IRI for CRCP pavements is as follows:

$$\text{IRI} = 1.118 + \text{KESAL}^{0.3}(0.0142 - 9.787 \times 10^{-3} \text{PSTEEL}) + \text{AGE}^{0.4}(3.157 \times 10^{-3} \text{D32} - 0.054 \text{DRY} + 0.293 \text{FREEZE} - 4.65 \times 10^{-4} \text{KVAL} + 0.1203) \quad (104)$$

where

|        |   |   |
|--------|---|---|
| IRI    | = | International Roughness Index, m/km                               |
| KESAL  | = | cumulative 80-kN equivalent single axle loads, thousands          |
| PSTEEL | = | percentage of steel   |
| EPCC   | = | PCC elastic modulus, kPa  |
| AGE    | = | pavement age, yr  |
| D32    | = | average annual number of days with temperatures above 32 °C       |
| DRY    | = | LTPP climatic zone, 1 = dry climate, 0 = wet climate              |
| FREEZE | = | LTPP climatic zone, 1 = freezing climate, 0 = nonfreezing climate |
| KVAL   | = | modulus of subgrade reaction, kPa/mm                              |

Statistics:

|                |   |                                |
|----------------|---|--------------------------------|
| N              | = | 156                            |
| R <sup>2</sup> | = | 0.51                           |
| SEE            | = | 0.277 m/km                     |
| p-value        | < | 0.0007 (significance of model) |

A plot of the predicted and measured CRCP IRI is shown in figure 66. A plot of the residuals (predicted - actual IRI) against the predicted IRI is shown in figure 67. The overall accuracy of the CRCP IRI model is reflected by the R<sup>2</sup> of 0.51, which is the proportion of variation of IRI explained by the variables included in the model. A test of hypothesis was performed to determine the significance of the variables used in the model for predicting IRI. The null and alternate hypotheses were as follows:

|                  |   |
|------------------|---|
| H <sub>0</sub> : | all model parameters are zero (variables are not significant) |
| H <sub>A</sub> : | all model parameters are not zero                             |

The F-test statistic used for the hypothesis test was calculated as the ratio of the mean square for the model divided by the mean square of the error. For this study the null hypothesis will be rejected if the level of significance is less than 5 percent (0.05). A level of significance (p-value) of less than 0.0007 implies a rejection of the null hypothesis. This shows that the variables in the model are highly significant. Also, individual t-tests were conducted to test if the individual parameter estimates are equal to zero. The p-values for this test ranged from 0.0001 to 0.012. The results show that all the parameter estimates had values other than zero, so the variables in the

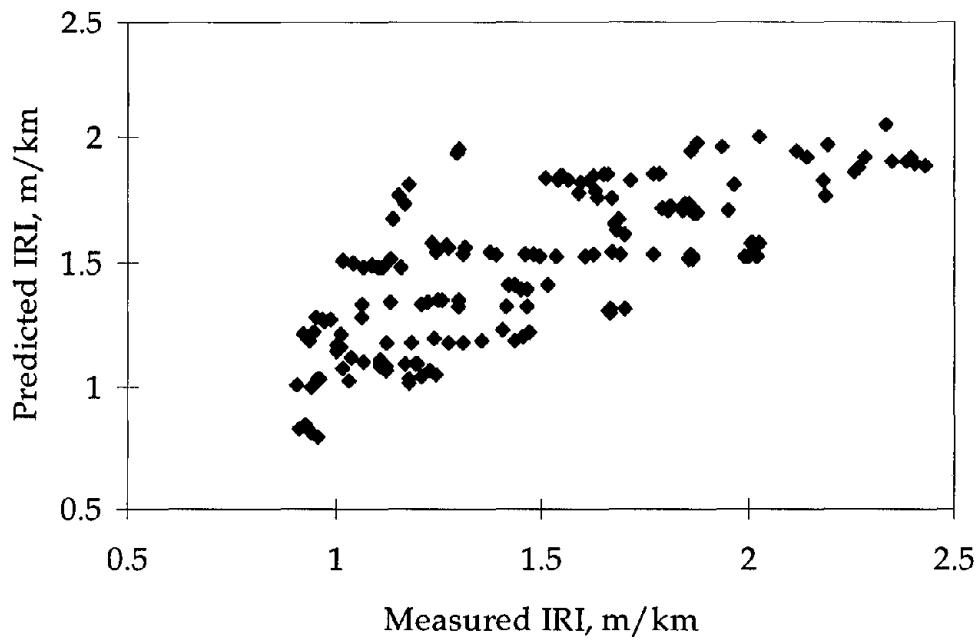


Figure 66. Plot of predicted versus actual IRI for CRCP.

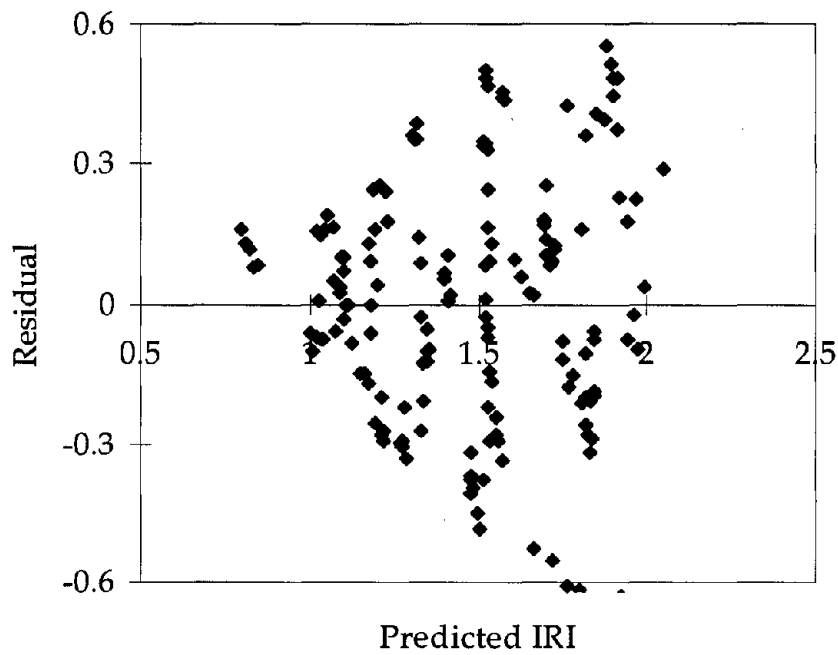


Figure 67. Plot of residual versus predicted IRI for CRCP.

model were significant. Prediction accuracy of CRCP IRI in absolute units is reflected by the standard error of estimate ( $SEE = 0.276$  m/km). The overall effectiveness of the model should be judged on all of the diagnostic statistics, the residual plots, and the results from the sensitivity analysis to follow. The diagnostic statistics obtained for the CRCP IRI model show that the model can predict CRCP IRI with reasonable accuracy for the current LTPP database.

### **Sensitivity Analysis**

A final and important step in the development of the models for predicting IRI was sensitivity analysis to check the engineering plausibility of the models. This was accomplished by studying the effects of the various input parameters on the output generated by the roughness models and comparing the results to theoretical and empirical observations. By virtue of the model form selected, traffic loading and pavement age automatically have a significant influence on the progression of IRI.

#### **JPCP IRI Model**

In addition to traffic loading and age, the variables that were found to be significant in the model developed for predicting IRI of JPCP include several climatic and pavement design variables. The climatic variables include the number of wet days, whether the pavement is in the LTPP freeze or no-freeze zone, and the freezing index.

The pavement design variables that were significant include the modulus of elasticity of the PCC slab, dowel diameter, and the type of subgrade. The influence of these factors on the progression of the IRI predicted with the model are discussed below.

#### *Effect of Climate*

Figure 68 is a plot of cumulative ESAL's versus IRI for different number of wet days (i.e., days with precipitation greater than 12.7 mm), and figure 69 is a plot of IRI versus cumulative ESAL's for pavements in different climatic zones. Both plots and the parameter estimate associated with freezing index in the model show that harsher climatic conditions will cause an increase in IRI. This is reasonable, since harsher climatic conditions in general increase the rate of progression of most of the distresses associated with JPCP pavements. The precipitation associated with the number of wet days will tend to saturate, weaken, and erode the pavement support layers. This weakens the pavement structure as a whole and reduces its ability to withstand traffic and environmental loads. For pavements that experience freezing conditions, freezing and thawing cycles will lead to further weakening of the pavement structure and increase roughness.

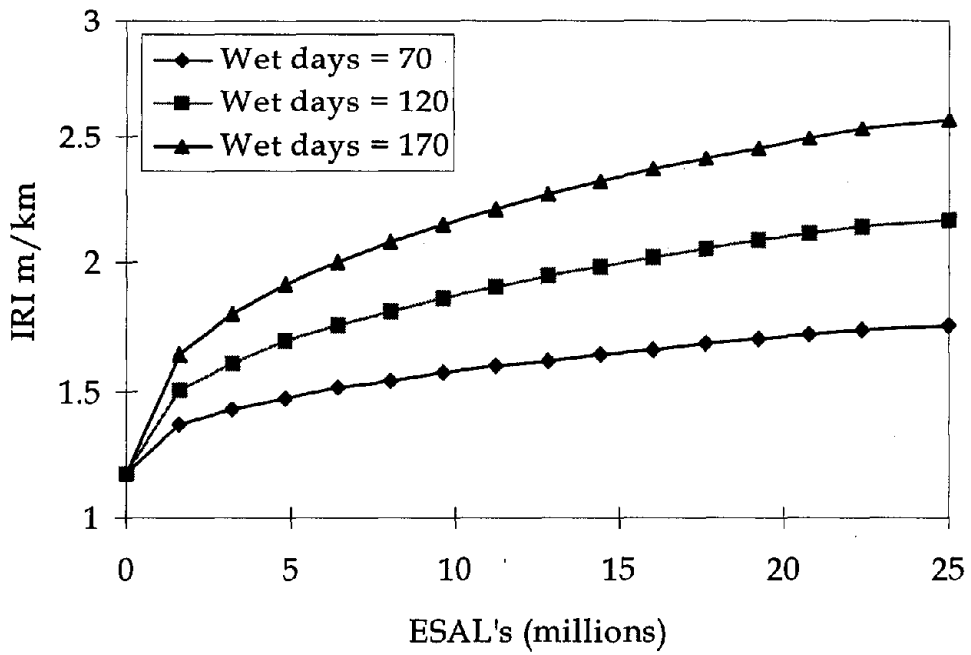


Figure 68. Influence of annual number of wet days on IRI of JPCP.

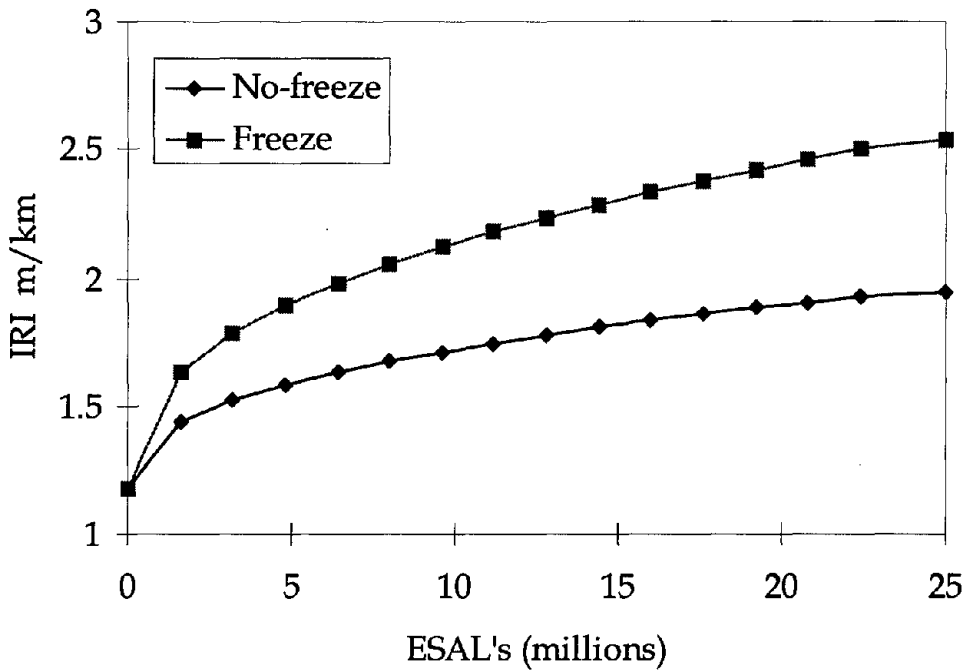


Figure 69. Influence of climate (freeze or no-freeze) on IRI of JPCP.



### *Effect of Pavement Design Features*

Figure 70 shows the influence of subgrade type on the predicted IRI. The influence of dowel diameter on IRI is illustrated in figure 71. According to figure 70, pavements with fine-grained subgrades will be more prone to an increased progression of roughness. Fine-grained soils provide less support because they are more sensitive to moisture effects. An interesting observation about the model is the influence of dowel diameter on roughness. According to the model, increasing dowel diameter will reduce the progression of roughness. This can be explained by the influence of dowels on faulting. The model clearly shows the importance of using dowels and also shows that, the larger the dowel diameter, the more it reduces the progression of distress. The model also confirmed that increasing traffic loading and age will increase the progression of roughness.

### JRCP IRI Model

The model for predicting IRI on JRCP confirmed that increasing traffic loading and age will increase the progression of roughness. The other variables that were found to be significant to the progression of roughness of JRCP included the design steel content, amount of precipitation, the presence of edge drains, and the subgrade type. The effects of the factors for increasing traffic load applications were examined by comparing the results predicted by the model to empirical and theoretical observations.

### *Effect of Pavement Design Features*

The design features that were found to be significant to roughness of JRCP are the design steel content, the presence of edge drains, and subgrade type. Figure 72 shows the effect of the design steel content on the progression of distress. According to the model, the higher the design steel content, the higher the predicted IRI. There is no obvious explanation for this trend. The influence of subgrade type is shown in figure 73. Because coarse-grained subgrades are less susceptible to moisture, they provide better support to the PCC slab. Therefore, pavements with coarse-grained soils can be expected to experience less distress and less roughness. Figure 74 shows that the provision of an edge drain will reduce the progression of roughness. This is a reasonable trend, since the positive drainage will improve the overall performance of JRCP.

### *Effect of the Climate*

The only climatic variable that turned out to be significant to roughness was the amount of precipitation. According to the model, more precipitation will result in increased progression of roughness, as illustrated in figure 75. Again, this is a reasonable trend, as more precipitation generally results in more pavement distress because of the higher chance of moisture-related distress, such as faulting.

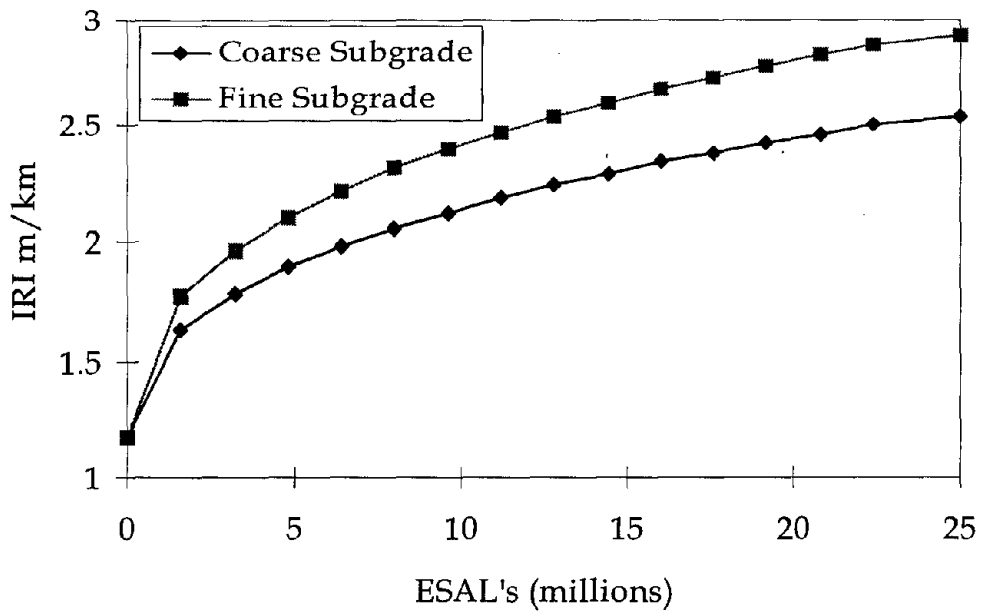


Figure 70. Influence of subgrade type on IRI of JPCP.

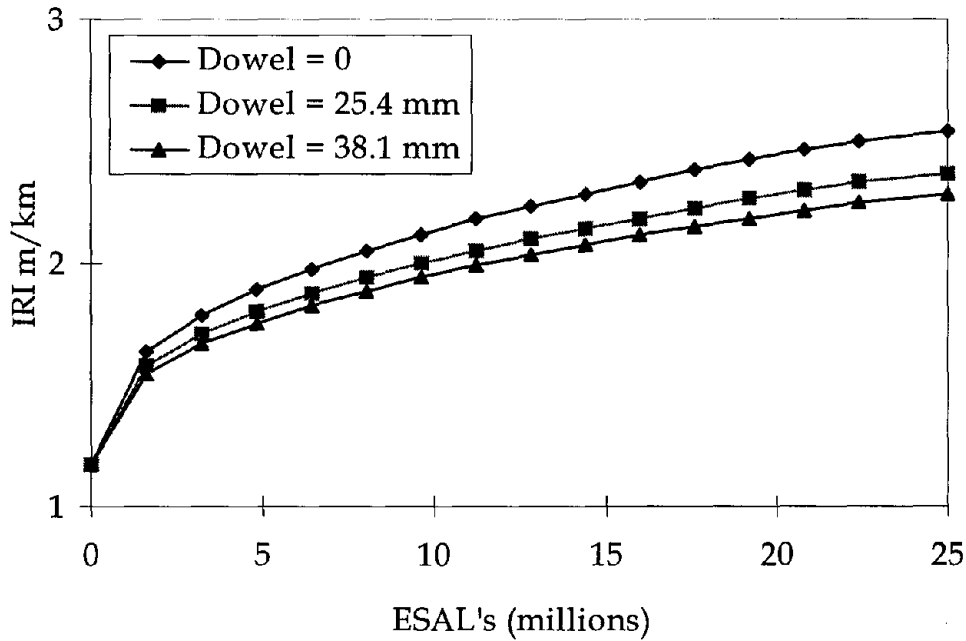


Figure 71. Influence of dowels and dowel diameter on IRI of JPCP.

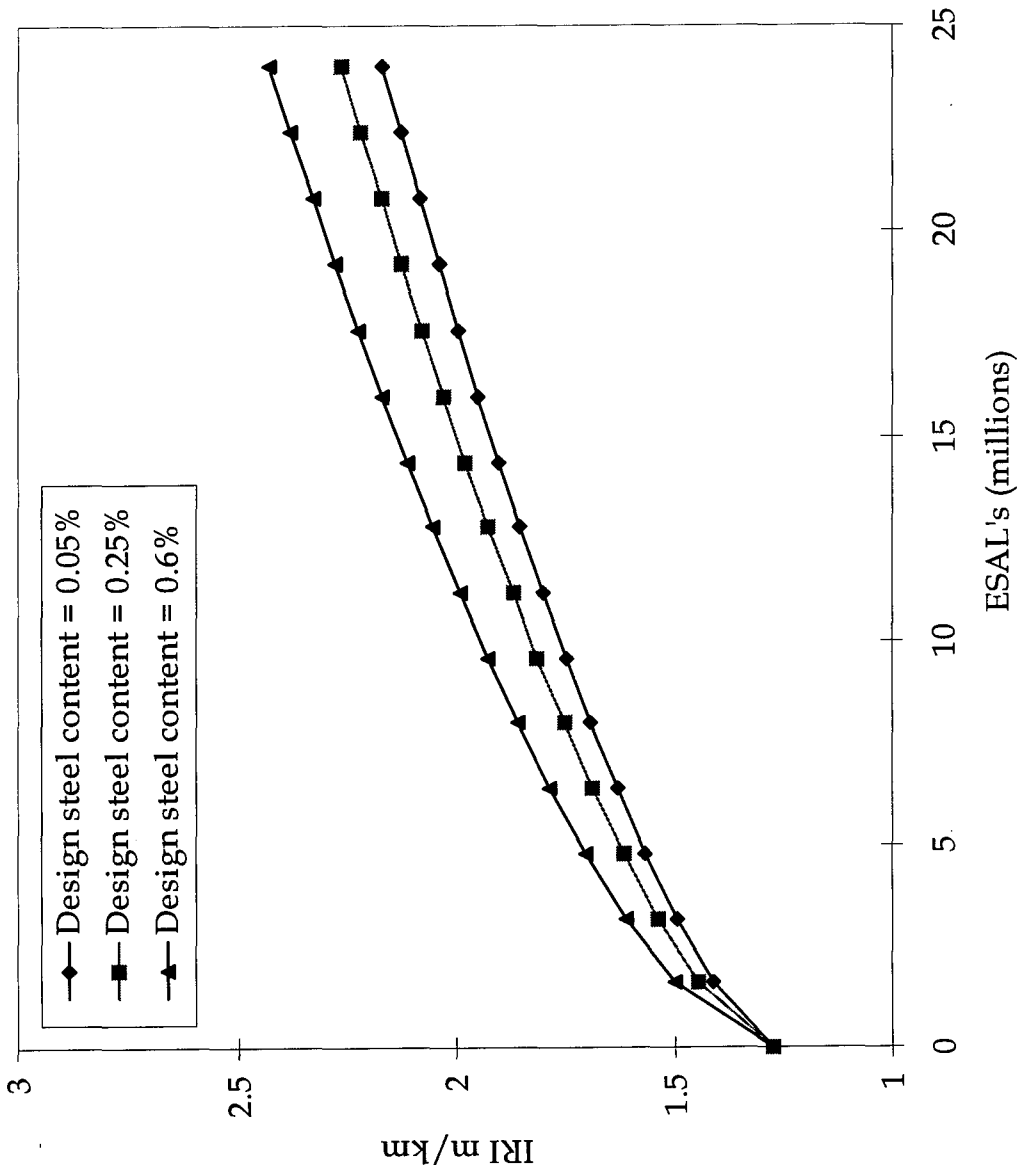


Figure 72. Influence of design steel content on JRCP IRI.

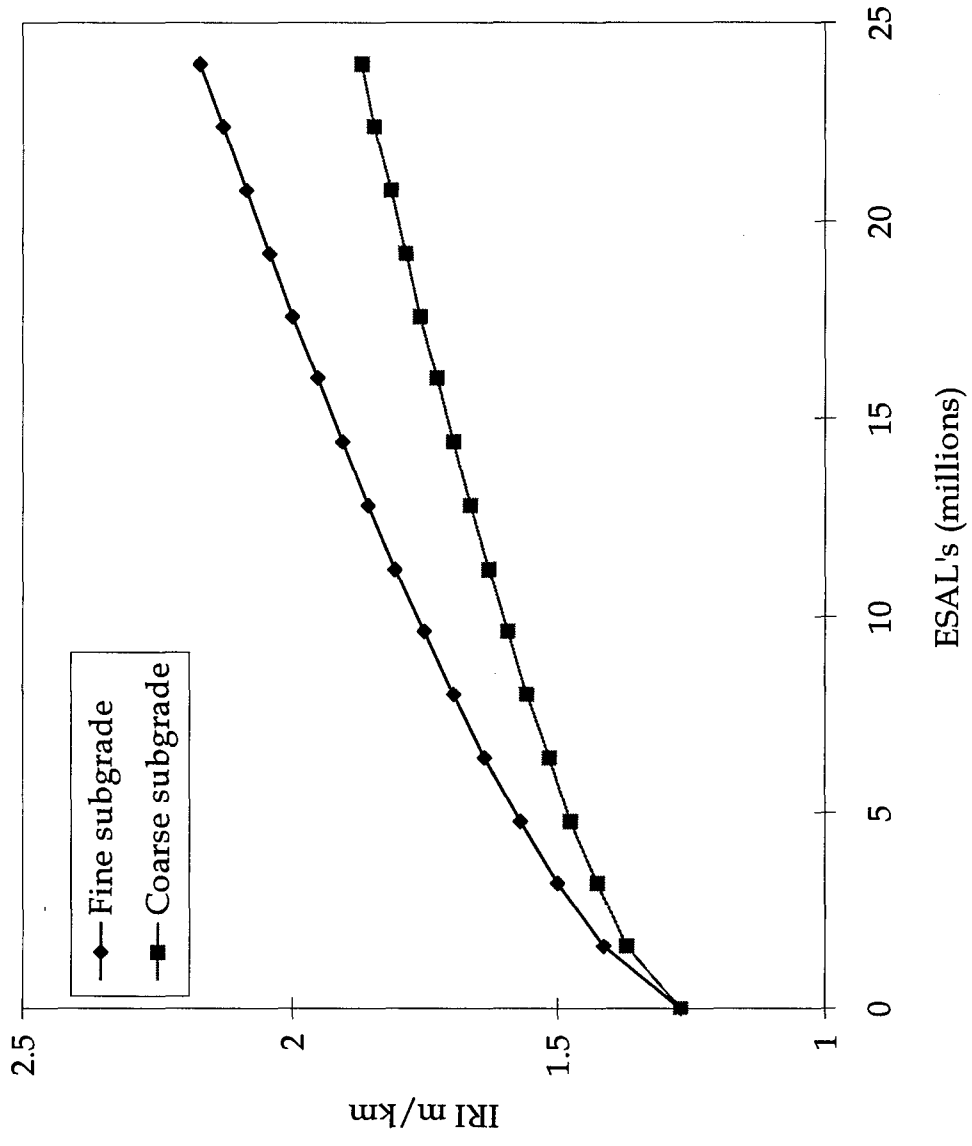


Figure 73. Influence of subgrade type on JRCF IRI.

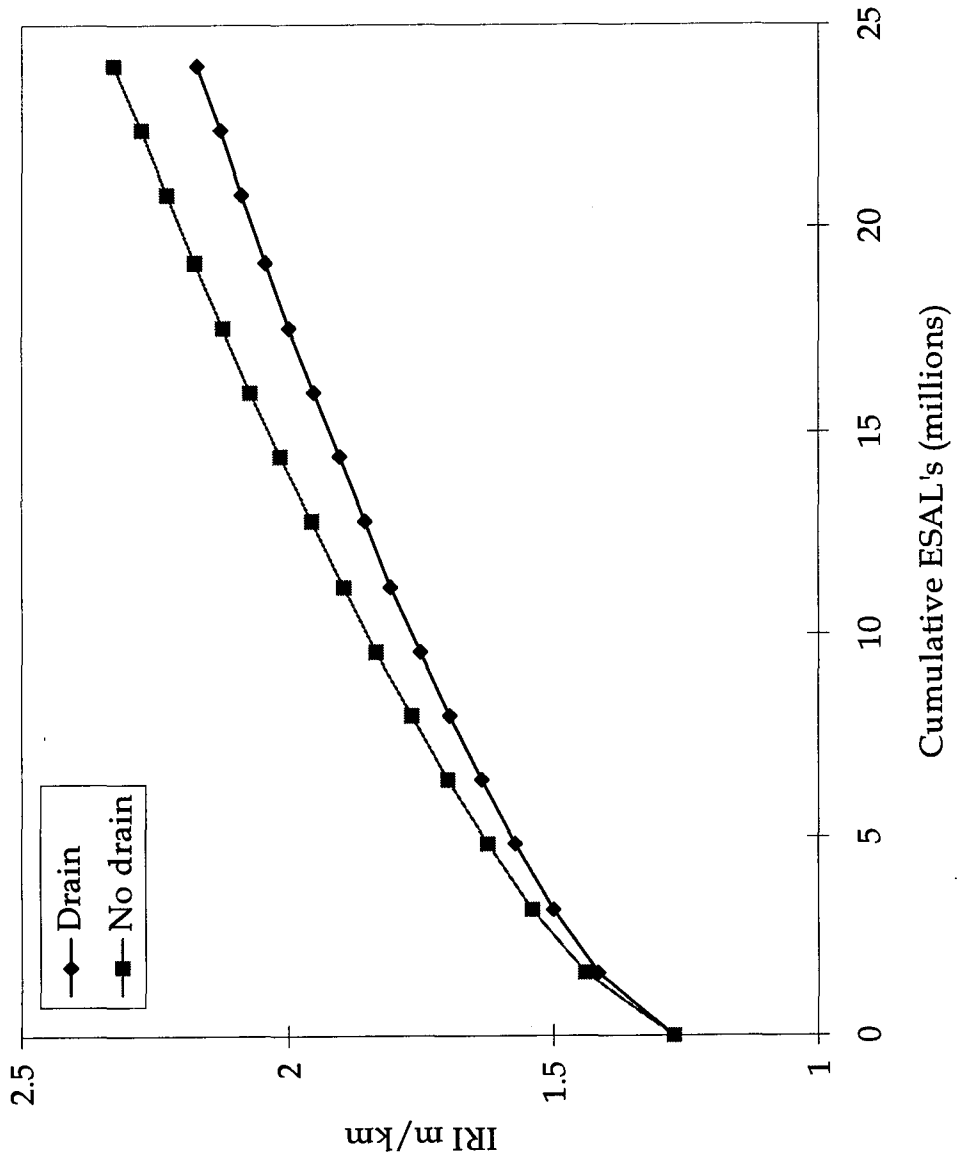


Figure 74. Influence of edge drains on JRCF IRI.

## CRCP IRI Model

As with the other IRI models, an increase in traffic loading and age was found to increase the progression of roughness. In addition, several other variables were found to be significant to roughness. They include pavement design variables such as the design steel content, the modulus of elasticity of the PCC slab, and the modulus of subgrade reaction. The climatic variables that were found to be significant to roughness include the climatic region in which the pavement is located and the number of days with the highest temperature exceeding 32 °C.

### *Effect of Pavement Design Features*

Figures 76 and 77 are plots of IRI versus the CRCP design steel content and the modulus of subgrade reaction, respectively. According to the model, the predicted IRI decreases with increasing steel content, as illustrated in figure 76. This result is reasonable and is in agreement with recent observations in Illinois and Belgium that indicate that higher steel contents for CRCP are beneficial, as they keep the cracks that form tight and reduce punchouts.<sup>(63, 64)</sup> Although the higher steel contents induce more closely spaced cracks in CRCP, this does not appear to cause a problem as long as they are kept tight.

Another design variable that was found to influence roughness is the modulus of subgrade reaction. As shown in figure 77, the better the support provided by the subgrade, the less the roughness predicted by the model. The greater support will mean that the pavement can withstand more traffic loading before experiencing the typical distresses that are associated with CRCP and the increase in pavement roughness.

### *Effect of the Climate*

The climatic variables found to be significant to the roughness of CRCP all show reasonable trends. The model obtained shows an interesting influence of the climatic region of a pavement on the progression of roughness. According to the model, pavements located in freezing regions will experience more roughness than those in the no freeze region. Less roughness will be experienced by pavements located in a drier region. Therefore, as illustrated in figure 78, in terms of reducing the progression of roughness, the best location for CRCP pavements is in the dry-no freeze region. This is not unexpected, since that is the region within which a pavement will experience the least distress (all things being equal). The influence of the number of days when the maximum temperature exceeds 32 °C, as illustrated in figure 79, is interesting. CRCP slabs that experience a higher number of days when the temperature exceeds 32 °C are more prone to expansive forces that can lead to more spalling and blowups.

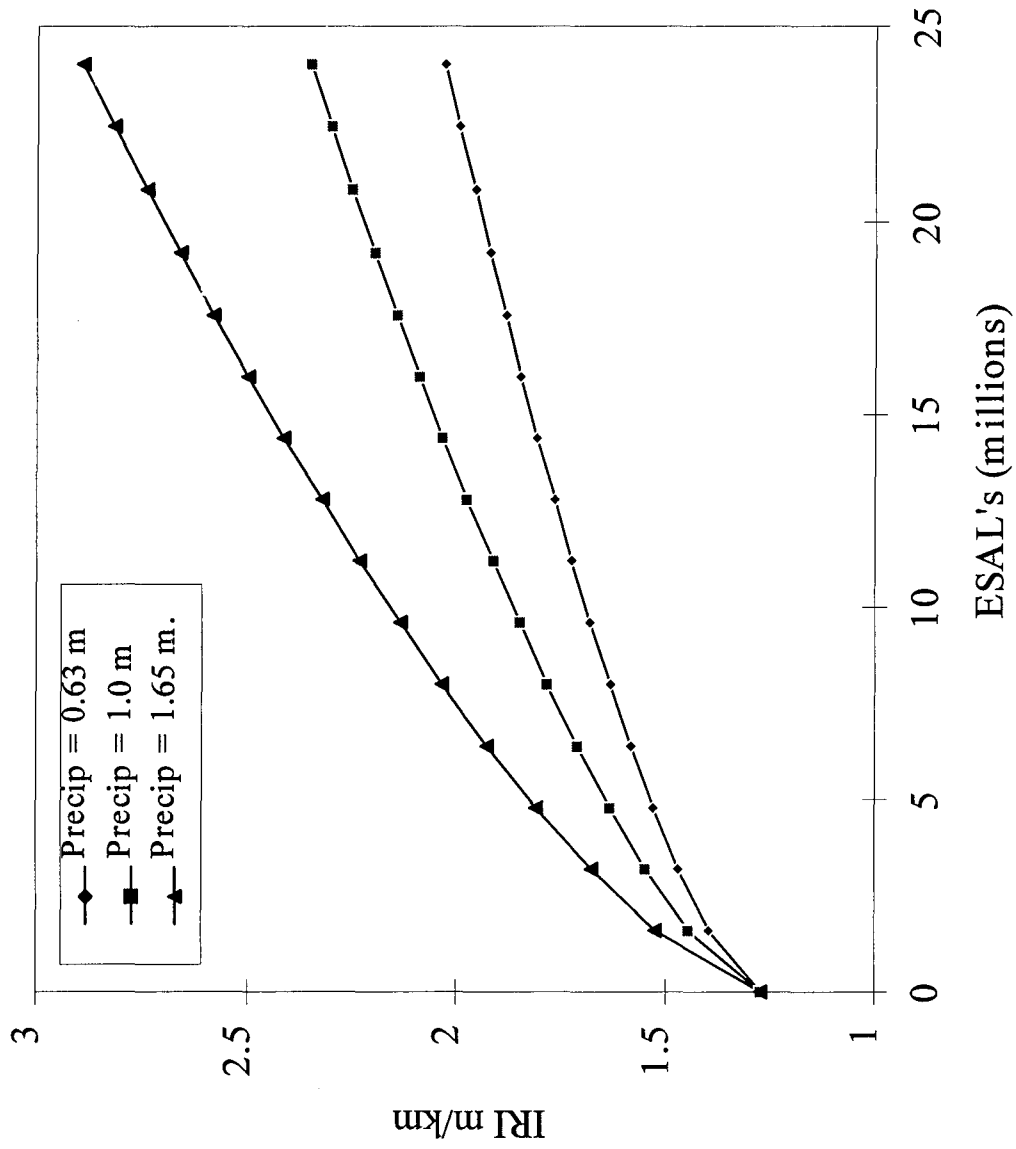


Figure 75. Influence of precipitation on JRCP IRI.

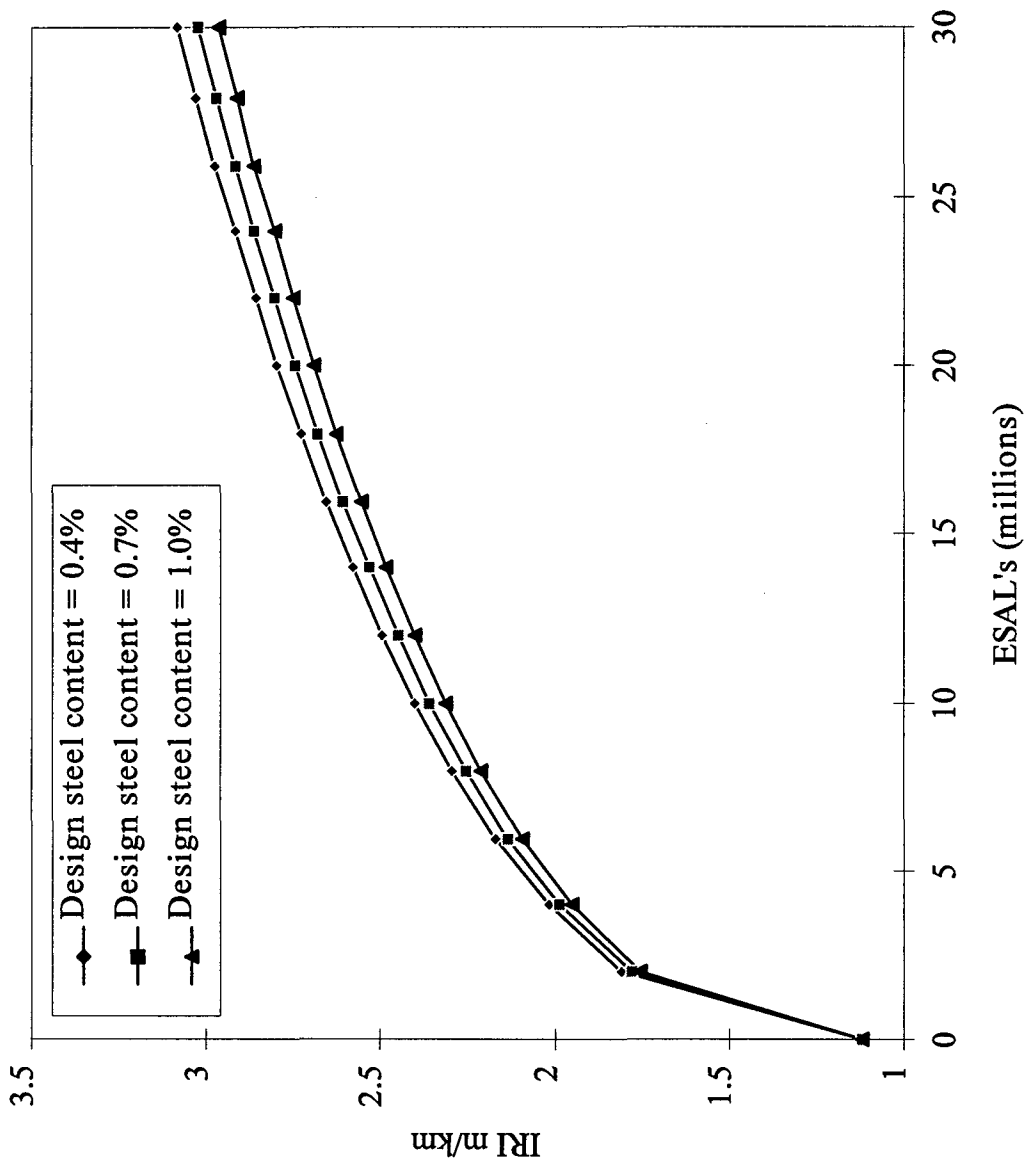


Figure 76. Influence of design steel content on CRCP IRI.



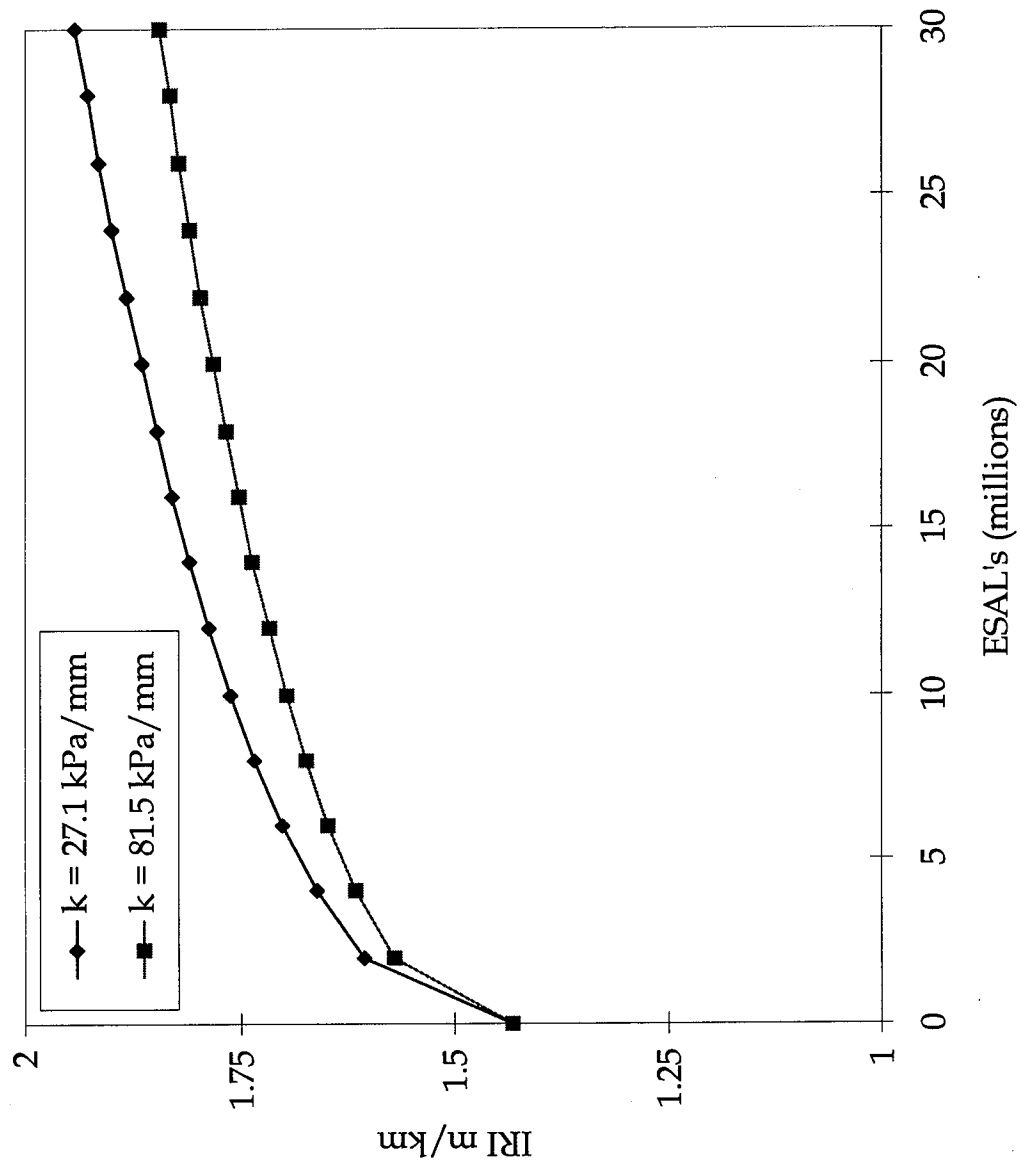


Figure 77. Influence of subgrade support on CRCP IRI.

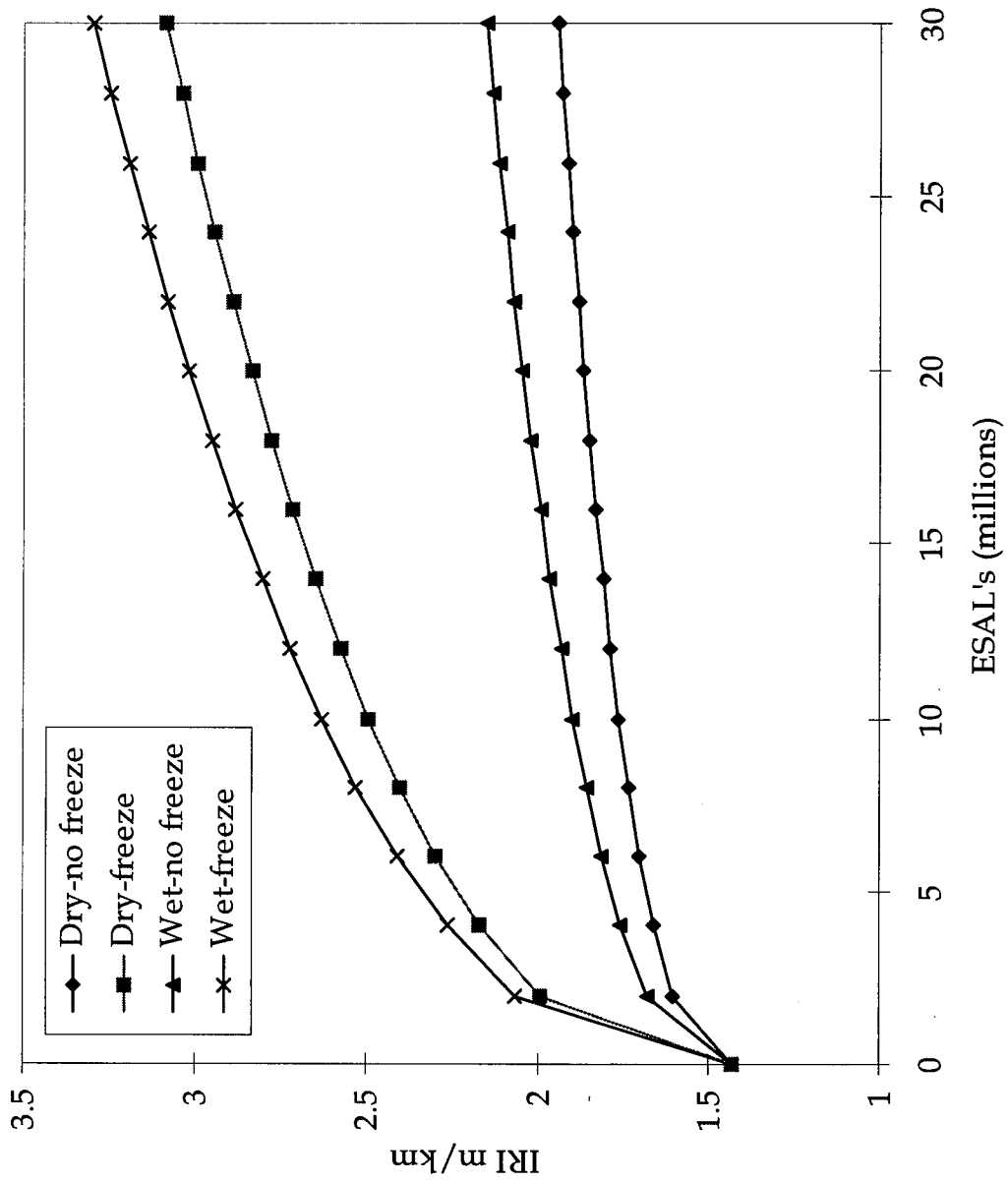


Figure 78. Influence of climatic region on CRCP IRI.

## Summary

### JPCP IRI

The following can be summarized about the JPCP IRI model:

- Fifty percent of the total variation of roughness can be explained by the included variables.
- Some of the unexplained variation may be due to errors in the independent variables used to develop the model, such as the traffic estimates.
- The “average” error in predicting JPCP IRI is 0.328 m/km.
- There are no discernible patterns in the residuals.
- Data from a large number of pavement sections from all over the United States were used to develop the model (N = 155).
- Each independent variable and the overall model were significant at a level of significance of 5 percent.
- The sensitivity analysis shows that all of the explanatory variables have a plausible effect on roughness that agrees with theoretical expectations and previous empirical field results.

### JRCP IRI

The following can be summarized about the JRCP IRI model:

- Fifty percent of the total variation of roughness can be explained by the included variables.
- Some of the unexplained variation may be due to errors in the independent variables used to develop the model, such as the traffic estimates.
- The “average” error in predicting JRCP IRI is 0.246 m/km.
- There are no discernible patterns in the residuals.
- Data from a large number of pavement sections from all over the United States were used to develop the model (N = 93).
- Each independent variable and the overall model was significant at a level of significance of 5 percent.

- The sensitivity analysis shows that all of the explanatory variables have a plausible effect on roughness that agrees with theoretical expectations and previous empirical field results.

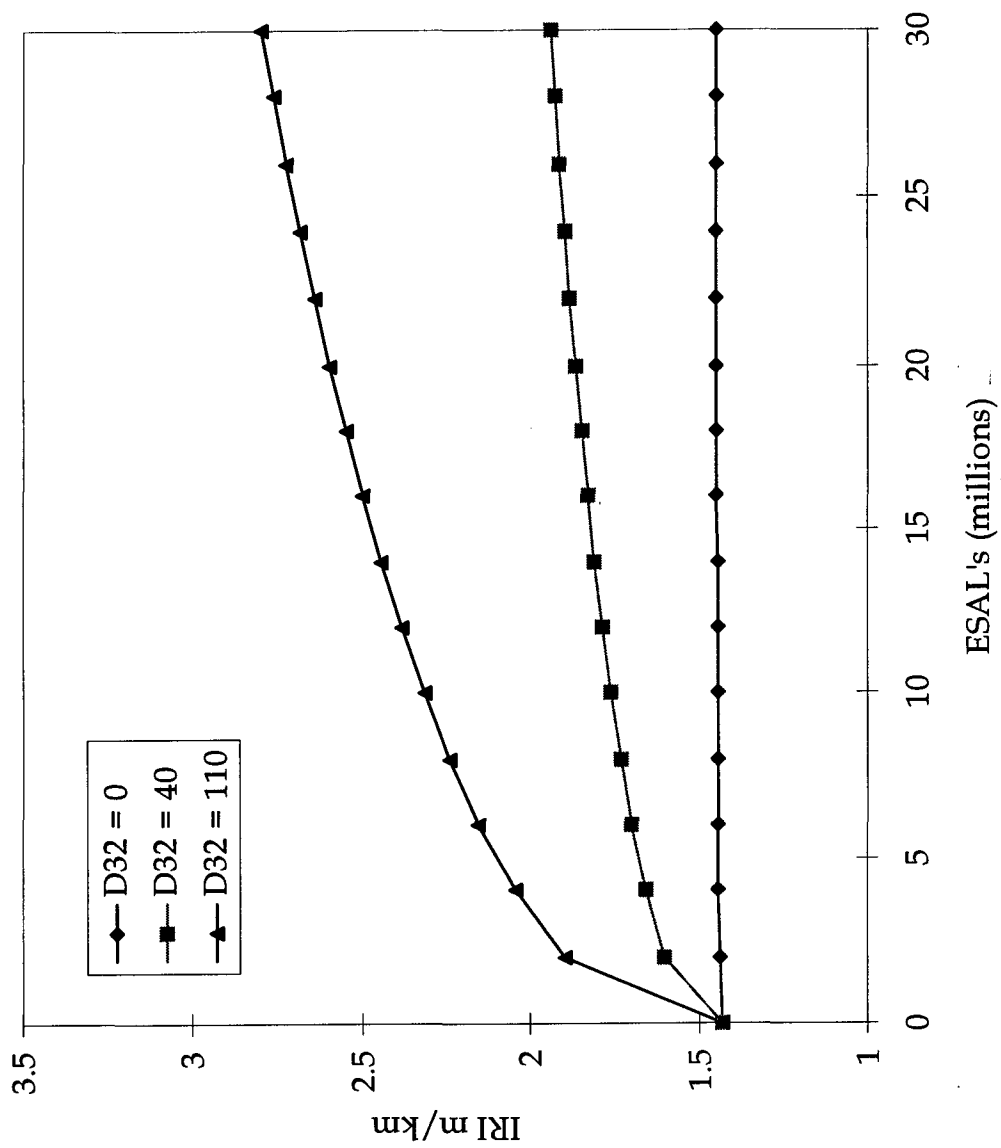


Figure 79. Influence of hot weather on CRCP IRI.

## CRCP IRI

The following can be summarized about the CRCP IRI model:

- Fifty-one percent of the total variation of roughness can be explained by the included variables.
- Some of the unexplained variation may be due to errors in the independent variables used to develop the model, such as the traffic estimates.
- The “average” error in predicting CRCP IRI is 0.277 m/km.
- There are no discernible patterns in the residuals.
- Data from a large number of pavement sections from all over the United States were used to develop the model (N = 93).
- Each independent variable and the overall model was significant at a level of significance of 5 percent.
- The sensitivity analysis shows that all of the explanatory variables have a plausible effect on roughness that agrees with theoretical expectations and previous empirical field results.

## Implications and Recommendations

The models developed for predicting IRI of JPCP, JRCP, and CRCP were based on basic principles. The model forms selected are backed by results that have been obtained from an extensive evaluation of the LTPP data and recent studies on IRI.<sup>(57, 62)</sup> Although reasonable results were obtained, the models had some limitations. The major limitation was the inability to include the initial IRI for a majority of the pavement sections in the LTPP database. Thus, the effect of initial IRI on the future roughness was not considered.

In spite of these limitations, the models obtained provide reasonable predictions and show the influence of several significant pavement design and climatic variables on roughness. An interesting result from these studies, confirmed and reported by other LTPP studies, is the values of the estimated initial IRI for JPCP, JRCP, and CRCP.<sup>(62)</sup> According to the models developed, the average initial IRI for the JPCP, JRCP, and CRCP sections from the GPS studies were approximately 1.3, 1.2, and 1.1 m/km. Recent LTPP studies investigating the development of pavement roughness, which involved the evaluation of data from newly constructed pavement sections, have reported similar initial IRI results, with the actual and estimated initial IRI ranging from about 0.63 to more than 1.6 m/km.<sup>(62)</sup>

## 8. APPLICATION OF DISTRESS PERFORMANCE MODELS

### Introduction

The performance prediction models developed in this study can be used to determine whether a given pavement design will meet certain performance criteria. Mechanistic-empirical models are recommended because they more realistically consider the mechanism of distress formation. The critical checks recommended for concrete pavements include the following:

- Faulting for doweled and nondoweled JPCP.
- Transverse joint spalling for JPCP and JRCP.
- Transverse cracking of JPCP.
- Corner breaks for JPCP.
- Roughness for JPCP, JRCP, CRCP.

Each of the models should be used to predict distress over the design period for the applicable PCC pavement design, and the results should be checked against the performance criteria of the agency. The models can also be used for analysis of the cost effectiveness of design alternatives.

This chapter presents a summary of the variables required as inputs and examples of the models' applications. The methods of model formulation, calibration, and limitations identified in the model development process are discussed in previous chapters of this report.

### Faulting of JPCP

Faulting is the most critical distress related to JPCP ride quality. The faulting model developed as part of this study using data from the GPS 3 pavement sections in the LTPP database is recommended for checking design. A summary of the input variables required for use in the model is presented in table 23, and the procedure to determine faulting follows. The actual faulting model and procedure for calculating faulting are given in chapter 4.

1. Calculate Load Transfer Factor (Chapter 4, equation 39).

$$\frac{AGG}{k\ell} = 0.25 e^{\left(1 + 0.0992D^{0.1} - 99.93 \frac{L}{\ell}\right)}$$

where

|             |   |  |
|-------------|---|--|
| $AGG/k\ell$ | = | nondimensional load transfer factor                    |
| $D$         | = | dowel diameter, mm ( $D = 0$ , if nondoweled pavement) |
| $L$         | = | slab length, m   |
| $\ell$      | = | radius of relative stiffness, mm                       |

Table 23. Summary of variables required for estimating faulting.

| Dependent Variable            | Independent Variables                                  | Effect on Joint Faulting* |
|-------------------------------|--|---------------------------|
| Transverse joint faulting, mm | Cumulative number of 80-kN ESAL applications           | +                         |
|                               | PCC elastic modulus, kPa                               | -                         |
|                               | PCC thickness, mm                                      | -                         |
|                               | Modulus of subgrade reaction, kPa/mm                   | -                         |
|                               | Dowel diameter, mm                                     | -                         |
|                               | Drainage coefficient                                   | -                         |
|                               | Annual number of wet days                              | +                         |
|                               | BASE, Base, or subbase type, 0=erodible, 1=nonerodible | -                         |

\* Positive indicates that an increase in this variable results in an increase in faulting.

2. Calculate Load Transfer Efficiency (Chapter 4, equations 30 and 31).

$$LTE_{x=0} = 1 / [1 + 1.2*(AGG/K\ell)^{-0.849}]$$

$$LTE_{x=915} = 1 / [1 + 0.3483*(AGG/K\ell)^{-1.13677}]$$

where

LTE = load transfer efficiency  
 x = distance of load from corner, mm  
 AGG/kℓ = nondimensional load transfer factor

Interpolate to obtain the load transfer efficiency for wheel loads placed between 0 and 915 mm from the slab corner.

3. Calculate Free Edge Corner Deflection, assuming no load transfer, (Chapter 4, equations 28 and 29).

$$w_{fe, x=0} = (0.10514\ell^2 + 87.18\ell + 231473)/k\ell^2$$

$$w_{fe, x=915} = (0.0784\ell^2 + 123.6\ell - 19993)/k\ell^2$$



where

- $w_{fe}$  = free edge corner deflection, mm
- $k$  = modulus of subgrade reaction, kPa/mm
- $l$  = radius of relative stiffness, mm

Interpolate to obtain the free edge corner deflection for wheel loads placed between 0 and 915 mm from the slab corner.

4. Calculate Loaded and Unloaded Corner Deflection, assuming load transfer, (Chapter 4, equations 32 and 33).

$$w_{UL,x} = w_{fe,x} * (LTE_x) / (1 + LTE_x)$$

$$w_{L,x} = w_{UL,x} / LTE_x$$

where

- $w_{fe}$  = free edge corner deflection, mm
- $x$  = distance between wheel load and slab corner (less than 915 mm)
- $LTE$  = load transfer efficiency

5. Calculate Differential Elastic Deformation Energy (Chapter 4, equation 20).

$$DE = 1.84k (w_L + w_{UL})(w_L - w_{UL})$$

where

- $k$  = modulus of subgrade reaction, kPa/mm
- $w_L$  = deflection of loaded slab, mm
- $w_{UL}$  = deflection of unloaded slab, mm

6. Calculate Allowable Number of ESAL Repetitions (Chapter 4, equation 40).

$$\text{Log}_e N_f = 5.50 - \text{Log}_{10} (0.005706 DE + 1)$$

where

- $N_f$  = allowable number of 80-kN ESAL's to failure, in thousands
- $DE$  = differential elastic deformation energy

7. Calculate Faulting Damage.

$$FDAM = \sum n/N_f$$

where

n = actual number of 80-kN ESAL's, in thousands  
 $N_f$  = allowable number of 80-kN ESAL's to failure, in thousands

8. Calculate Transverse Joint Faulting (Chapter 4, equation 41).

$$\text{Fault} = \text{FDAM}^{0.3} [1.25 + 0.00102 \text{WETDAYS} - 2.5 \cdot 10^{-3} \text{DOWDIA} - 0.625 C_d (0.5 + \text{BASE})]$$

where

FDAM = faulting damage =  $n/N_f$   
n = number of 80-kN ESAL applications, in thousands  
 $N_f$  = allowable number of 80-kN ESAL applications, in thousands  
WETDAYS = number of wet days in the year  
DOWDIA = dowel diameter, mm  
 $C_d$  = drainage coefficient  
BASE = base or subbase type, 0=erodible, 1=nonerodible

**Transverse Joint Spalling for JPCP and JRCP**

The mechanism of spalling is yet to be fully understood; however, it is believed to be caused by several interacting mechanisms, including stresses imposed by traffic and environmental forces, as well as inadequate quality control during construction. Although traffic may have some effect on spalling, environmental factors constitute the largest contributor to development of the distress.

Two models were developed for estimating the percentage of transverse joints with spalling (all severities) for JPCP and JRCP, and they are recommended for design checking. A summary of the input variables required for use in the models is presented in tables 24 and 25, and the procedure for calculating spalling is presented below. The actual spalling models are given in chapter 5.

1. Calculate Traffic Load Tensile Stress (Chapter 5, equation 49).

$$\sigma_{tr} = 305.5 + 48.563 h_s - 23.62 k_v + 0.000757 k_s - 0.17728 h_p h_s + 0.0888 h_p k_v - 1.89 \cdot 10^{-6} h_p k_s - 1.889 \cdot 10^{-7} h_s E_p + 1.98 \cdot 10^{-6} h_s k_s - 1.32 \cdot 10^{-6} k_v k_s$$

where

$\sigma_{tr}$  = maximum tensile stress at crack or joint surface from traffic loading, kPa  
 $h_s$  = depth of sealant, mm  
 $k_v$  = modulus of subgrade reaction, kPa/mm  
 $k_s$  = modulus of sealant material, kPa  
 $h_p$  = PCC slab thickness, mm

$E_p$  = modulus of PCC slab, kPa

2. Calculate Thermal Load Tensile Stress (Chapter 5, equation 47).

$$\sigma_{js} = k_{js} CL(\alpha\Delta T + e)/2t$$

where

$k_{js}$  = spring coefficient of joint sealant or incompressibles in the joint, kPa

$u$  = displacement of spalled concrete, m

$t$  = depth of spall delamination (= 1)

$C$  = subbase friction factor

$L$  = joint spacing, m

$\alpha$  = concrete thermal expansion, per °C

$\Delta T$  = thermal gradient in the slab, °C

$e$  = concrete drying shrinkage strain

3. Calculate Allowable Number of Traffic ( $N_T$ ) and Environment ( $N_E$ ) Load Applications for JPCP (Chapter 5, equations 56 and 57).

The equations for calculating  $N_T$  and  $N_E$  are as follows:

$$N_T = 199252 \left( \frac{1}{\sigma_t} \right)^{0.15}$$

where

$\sigma_t$  = tensile stress, kPa (calculated from chapter 5, equation 49)

Table 24. Summary of variables required for predicting JPCP joint spalling.

| Predicted Variable  | Dependent Variables   | Effect on Joint Spalling |
|---|---|--------------------------|
| JPCP transverse joint spalling (percentage of joints spalled) | Cumulative number of 80-kN ESAL applications                        | +                        |
|   | Joint spacing, m  | +                        |
|   | PCC coefficient of thermal expansion                                | +                        |
|   | Thermal gradient within the PCC slab                                | +                        |
|   | PCC drying shrinkage strain   | +                        |
|   | Subbase friction factor   | +                        |
|   | Depth of sealant, mm  | +                        |
|   | Modulus of sealant or incompressibles, kPa/mm                       | +                        |
|   | PCC elastic modulus, kPa  | -                        |
|   | PCC thickness, mm   | -                        |
|   | Modulus of subgrade reaction, kPa/mm                                | -                        |
|   | Pavement age in years   | +                        |
|   | Average daily temperature range, °C                                 | +                        |
|   | Average daily relative humidity range for the month of construction | -                        |
|   | Average annual freeze-thaw cycles                                   | +                        |

\* Positive indicates that an increase in this variable results in an increase in joint spalling.

Table 25. Summary of variables required for estimating JRCP joint spalling.

| Predicted Variable  | Dependent Variables                           | Effect on Joint Spalling |
|---|---|--------------------------|
| JRCP transverse joint spalling (percentage of joints spalled) | Cumulative number of 80-kN ESAL applications  | +                        |
|   | Joint spacing, m                              | +                        |
|   | PCC coefficient of thermal expansion          | +                        |
|   | Thermal gradient within the PCC slab          | +                        |
|   | PCC drying shrinkage strain                   | +                        |
|   | Subbase friction factor                       | +                        |
|   | Depth of sealant, mm                          | +                        |
|   | Modulus of sealant or incompressibles, kPa/mm | +                        |
|   | PCC elastic modulus, kPa                      | -                        |
|   | PCC thickness, mm                             | -                        |
|   | Modulus of subgrade reaction, kPa/mm          | -                        |
|   | Pavement age in years                         | +                        |
|   | Average annual freezing index, °C days        | +                        |

\* Positive indicates that an increase in this variable results in an increase in joint spalling.

$$N_E = 650162 \left( \frac{t}{k_{js} \text{ ELONG}} \right)^{0.85}$$

where

- $k_{js}$  = modulus of the sealant material or incompressibles, kPa
- $\text{ELONG}$  = a factor estimating the horizontal movement of the slab, m
- =  $3.28CL(3.24\alpha\Delta T + e)$
- $L$  = slab length or joint spacing, m
- $\Delta T$  = thermal gradient in the slab, °C
- $e$  = concrete drying shrinkage strain
- $\alpha$  = concrete thermal expansion, per °C
- $C$  = subbase friction factor
- $t$  = 1 mm

4. Calculate Damage Accumulation for JPCP (Chapter 5, equation 58).

The model for calculating the total damage from traffic and environmental loading for JPCP is as follows:

$$\text{Damage} = \frac{\text{KESAL}}{N_T} + \frac{\text{AGE}^{0.145}}{N_E}$$

where ,

|       |   |  |
|-------|---|--|
| KESAL | = | 80-kN ESAL's, in thousands                               |
| AGE   | = | pavement age in years                                    |
| $N_T$ | = | allowable number of cycles due to traffic stresses       |
| $N_E$ | = | allowable number of cycles due to environmental stresses |

5. Calculate JPCP Transverse Joint Spalling (Chapter 5, equation 59).

The final model for predicting the percentage of spalled joints for JPCP is as follows:

$$\text{Spall}_{\text{JPCP}} = \frac{100 \text{Damage}^{2.1}}{1 + \text{Damage}^{2.5}} (0.344\text{TRANGE} - 0.042\text{RH} + 0.0318\text{FTCYC})$$

where

|                              |   |  |
|------------------------------|---|--|
| $\text{Spall}_{\text{JPCP}}$ | = | percentage of JPCP joints with spalling of all severities  |
| TRANGE                       | = | average daily temperature range, °C  |
| RH                           | = | average daily range of relative humidity during the month of construction<br>(can be obtained from NOAA tables), percent |
| FTCYC                        | = | annual number of freeze-thaw cycles  |
| Damage                       | = | total damage (chapter 5, equation 58)  |

6. Calculate Allowable Number of Traffic ( $N_T$ ) and Environment ( $N_E$ ) Load Applications for JRCP (Chapter 5, equations 60 and 61).

The equations for calculating  $N_T$  and  $N_E$  for JRCP obtained are as follows:

$$N_T = \frac{26841k^2 + 28.9kh_{\text{PCC}}}{\sigma_t}$$

$$N_E = \frac{868 h_{\text{PCC}}^2 + 83800 kh_{\text{PCC}}}{k_{js}\text{ELONG}}$$

where

|            |   |  |
|------------|---|--|
| $\sigma_t$ | = | tensile stress, kPa (calculated from chapter 5, equation 49) |
| $K_{js}$   | = | modulus of the sealant material or incompressibles, kPa      |
| ELONG      | = | an estimate of the horizontal movement, mm                   |
| k          | = | modulus of subgrade reaction, kPa/mm                         |
| $h_{pcc}$  | = | PCC thickness, mm  |

The recommended values for elastic moduli of the sealants or incompressibles,  $K_{js}$ , for JRCPC are given in chapter 5, table 16.

7. Calculate Damage Accumulation for JRCPC (Chapter 5, equation 62).

The model for calculating the total damage to JRCPC from traffic and environmental loading is as follows:

$$\text{Damage} = \frac{0.0667 * \text{KESAL}}{N_T} + \frac{5.667 * \text{AGE}}{N_E}$$

where

|       |   |  |
|-------|---|--|
| KESAL | = | number of 80-kN ESAL's, in thousands                     |
| AGE   | = | pavement age in years                                    |
| $N_T$ | = | allowable number of cycles due to traffic stresses       |
| $N_E$ | = | allowable number of cycles due to environmental stresses |

8. Calculate JRCPC Transverse Joint Spalling (Chapter 5, equation 63).

The final model for predicting the percentage of spalled joints for JRCPC is as follows:

$$\text{Spall}_{\text{JRCPC}} = 100\text{DAM}^{0.85} (1.764 * 10^{-5} \text{FI} + 6.3478 * 10^{-8} E_{\text{PCC}} - 0.0271k)$$

where

|                               |   |  |
|-------------------------------|---|--|
| $\text{Spall}_{\text{JRCPC}}$ | = | percentage of joints with spalling of all severities |
| DAM                           | = | damage due to traffic and environmental stresses     |
| FI                            | = | mean annual freezing index, °C days                  |
| $E_{\text{PCC}}$              | = | PCC elastic modulus, kPa                             |
| k                             | = | modulus of subgrade reaction, kPa/mm                 |

### **Transverse Cracking for JPCPC**

Transverse cracks are a major cause of structural failure of JPCPC. They develop from the repeated application of heavy axle loads and as the slab responds to drying shrinkage, thermal curling, and thermal contractions. Medium- and high-severity transverse cracks in JPCPC cause increased roughness and user discomfort and trigger the need for rehabilitation. A model was developed as part of this study for estimating the percentage of slabs with transverse cracks (all severities), and it is recommended for design checking. A summary of the input variables

required for use in the model developed is presented in table 26. The actual transverse cracking model and the procedure for calculating the percentage of slabs with transverse cracking for a given pavement section are given in chapter 6.

1. Calculate Allowable Number of Load Repetitions (Chapter 6, equations 90 and 91).

The final model for estimating  $N_i$  for traffic and temperature stresses are as follows:

$$N_{TRTC} = \frac{(-2.0 \cdot 10^4 + 5.507 \cdot 10^{-3} E_{PCC} + 150.63 h_{PCC} + 4.564 \cdot 10^{-6} E_{PCC} h_{PCC} + 0.744 h_{PCC}^2)^{1.33}}$$

$$N_{TETC} = \frac{(-2.0 \cdot 10^4 + 5.507 \cdot 10^{-3} E_{PCC} + 150.63 h_{PCC} + 4.564 \cdot 10^{-6} E_{PCC} h_{PCC} + 0.744 h_{PCC}^2)^2}$$

where

- $N_{TRTC}$  = allowable number of 80-kN ESAL applications
- $N_{TETC}$  = allowable number of temperature stress applications
- $E_{PCC}$  = PCC slab modulus, kPa
- $h_{PCC}$  = PCC slab thickness, mm

2. Calculate Damage Due to Temperature and Traffic (Chapter 6, equations 88 and 89).

The damage to the pavement from the imposed stresses can be calculated using a modified form of Miner's cumulative damage equation. The modified damage equations for estimating both traffic and temperature stresses are as follows:



Table 26. Summary of variables required for estimating JPCP transverse cracking.

| Dependent Variable                                   | Independent Variables                                      | Effect on Transverse Cracking* |
|--|--|--------------------------------|
| Transverse cracking<br>(percentage of slabs cracked) | Cumulative number of 80-kN ESAL applications               | +                              |
|  | PCC elastic modulus, kPa                                   | -                              |
|  | PCC thickness, mm  | -                              |
|  | Pavement age in years                                      | +                              |
|  | Average annual number of freeze-thaw cycles                | +                              |
|  | Annual number of wet days                                  | +                              |
|  | Average annual number of days with temperature above 32 °C | +                              |

\* Positive indicates that an increase in this variable results in an increase in transverse cracking.

$$DAM_{TRTC} = \left( \frac{KESAL}{N_{TRTC}} \right)^{0.5}$$

$$DAM_{TETC} = \left( \frac{AGE}{N_{TETC}} \right)^{0.75}$$

where

KESAL = cumulative number of ESAL's, thousands  
 AGE = pavement age, years  
 N<sub>i</sub> = allowable number of load repetitions

3. Calculate Percentage of Slabs with Transverse Cracking (Chapter 6, equation 92).

The model for predicting transverse cracking is given as follows:

$$TC = 100*(50.8FTCYC - 3.2*10^{-5}E_{PCC}) DAM_{TETC} + 100*(0.274WTDYS + 0.432D32) DAM_{TRTC}$$

where

TC = percentage of slabs with transverse cracks

|              |   |  |
|--------------|---|--|
| FTCYC        | = | annual number of freeze-thaw cycles                |
| $E_{PCC}$    | = | elastic modulus of PCC, kPa                        |
| $DAM_{TETC}$ | = | damage caused by temperature stresses              |
| WTDYS        | = | annual number of wet days                          |
| D32          | = | annual number of days with temperature above 32 °C |
| $DAM_{TRTC}$ | = | damage caused by traffic stresses                  |

### Corner Breaks for JPCP

Corner breaks also are a major cause of structural failure in JPCP with inadequate load transfer or weak underlying material. They develop as the slab corners are subjected to repeated application of heavy axle loads. Corner breaks in JPCP cause increased roughness and user discomfort, and they trigger the need for rehabilitation. A model was developed as part of this study for estimating the percentage of slabs with corner breaks (all severities), and it is recommended for design checking. A summary of the input variables required for use in the model developed is presented in table 27. The actual corner breaks model and the procedure for calculating the percentage of slabs with corner breaks for a given pavement section are given in chapter 6.

1. Calculate Allowable Number of Traffic and Temperature Load Repetitions Model (Chapter 6, equations 85 and 86).

The final model for estimating  $N_i$  for traffic was as follows:

$$N_{TRCB} = \left( (5.6 + 8.7 \cdot 10^{-8} E_{PCC} - 4.724 \cdot 10^{-2} h_{PCC} - 1.7 \cdot 10^{-10} E_{PCC} h_{PCC} + 1.056 \cdot 10^{-3} h_{PCC}^2) \right)^{2.93}$$

The final model for estimating  $N_i$  for temperature was as follows:

$$N_{TECB} = \left( (5.6 + 8.7 \cdot 10^{-8} E_{PCC} - 4.724 \cdot 10^{-2} h_{PCC} - 1.7 \cdot 10^{-10} E_{PCC} h_{PCC} + 1.056 \cdot 10^{-3} h_{PCC}^2) \right)^{8.8}$$

where

|           |   |                        |
|-----------|---|------------------------|
| $E_{PCC}$ | = | PCC slab modulus, kPa  |
| $h_{PCC}$ | = | PCC slab thickness, mm |

2. Calculate Damage Due to Temperature and Traffic Loading (Chapter 6, equations 83 and 84).

Damage for traffic and temperature stresses was calculated as follows:

$$DAM_{TRCB} = \left( \frac{KESAL}{N_{TRCB}} \right)^{0.75}$$

$$DAM_{TECB} = \left( \frac{AGE}{N_{TECB}} \right)^{0.25}$$

where

KESAL = cumulative number of ESAL's, thousands  
 AGE = pavement age in years  
 N<sub>i</sub> = allowable number of load repetitions

3. Calculate Percentage of Slabs With Corner Breaks (Chapter 6, equation 87).

The model for predicting the occurrence of corner breaks is as follows:

$$SWCB = 100 * (24.26JTSP + 2.236AGE - 9.95 * 10^{-7} E_{PCC}) DAM_{TECB} + 100 * (3.08 * 10^{-3} FTCYC - 3.78 * 10^{-3} C_d) DAM_{TRCB}$$

where

SWCB = percentage of slabs with corner breaks  
 JTSP = pavement joint spacing, m  
 AGE = pavement age, yr  
 E<sub>PCC</sub> = elastic modulus of PCC, kPa  
 DAM<sub>TECB</sub> = damage due to temperature stresses  
 FTCYC = annual number of freeze-thaw cycles  
 C<sub>d</sub> = drainage coefficient  
 DAM<sub>TRCB</sub> = damage due to traffic stresses

**Roughness for JPCP, JRCP, and CRCP**

Roughness is the irregularity of the pavement surface. In general, road users consider roughness the most important criterion when deciding on the state or condition of a road. Rough roads lead to user discomfort, increased travel times, and higher vehicle operating costs that can lead to millions of dollars in losses to the general economy. Although the structural performance of a pavement is most important to highway designers, the complaints generated by rough roads often contribute to a large part of the rehabilitation decisions made by State highway agencies. Three models were developed as part of this study for estimating roughness for JPCP, JRCP, and CRCP, and they are recommended for design checking. A summary of the input variables required for use in the roughness models developed is presented in table 28. The actual roughness models are given in chapter 7.

Table 27. Summary of variables required for estimating JPCP corner breaks.

| Dependent Variable                                | Independent Variables                            | Effect on Corner Breaks* |
|---|--|--------------------------|
| Corner breaks<br>(percentage of slabs<br>cracked) | Cumulative number of 80-<br>kN ESAL applications | +                        |
|   | PCC elastic modulus, kPa                         | -                        |
|   | PCC thickness, mm                                | -                        |
|   | Drainage coefficient, $C_d$                      | -                        |
|   | Joint spacing, m                                 | +                        |
|   | Pavement age in years                            | +                        |
|   | Average annual number of<br>freeze-thaw cycles   | +                        |

\* Positive indicates that an increase in this variable results in an increase in corner breaks.

1. Calculate JPCP Roughness (Chapter 7, equation 102).

$$\text{IRI} = 1.3033 + \text{KESAL}^{0.4}(1.578\text{WETDAYS} + 113.6\text{FREEZE}) \\ * 10^{-4} + \text{AGE}^{0.4}(1.4437\text{FI} + 3.6*10^{-5}\text{E}_{\text{PCC}} - 552 \text{SUGTYP} \\ - 19.08\text{DOWDIA}) * 10^{-4}$$

where

|                  |   |   |
|------------------|---|---|
| IRI              | = | International Roughness Index, m/km                           |
| KESAL            | = | cumulative 80-kN equivalent single axle loads, thousands      |
| WETDAYS          | = | number of days precipitation is greater than 12.7 mm          |
| FREEZE           | = | LTPP climatic zone, 1=freezing climate, 0=nonfreezing climate |
| AGE              | = | pavement age, yr  |
| FI               | = | freezing index, °C days                                       |
| $E_{\text{PCC}}$ | = | PCC elastic modulus, kPa                                      |
| SUGTYP           | = | subgrade type, 1=coarse-grained, 0=fine-grained               |
| DOWDIA           | = | dowel diameter, mm  |

Table 28. Variables required for predicting IRI for JPCP, JRCP, and CRCP.

| Predicted Variable | Dependent Variables   | Effect on Roughness* |
|--------------------|---|----------------------|
| JPCP IRI (m/km)    | Cumulative number of 80-kN ESAL applications  | +                    |
|                    | Dowel diameter, mm  | -                    |
|                    | Elastic modulus of PCC slab, kPa  | +                    |
|                    | Pavement age since construction, yr   | +                    |
|                    | Freezing index in degree days (°C days)   | +                    |
|                    | FREEZE (pavements located in climates with average mean temperature less than 12.75 °C) | +                    |
|                    | Subgrade type, 1=coarse-grained, 0=fine-grained   | -                    |
|                    | Average annual number of wet days   | +                    |
| JRCP IRI (m/km)    | Cumulative number of 80-kN ESAL applications  | +                    |
|                    | Percentage of steel per area for PCC slab   | +                    |
|                    | Presence of edge drain, 1 = edge drain, 0 = no edge drains                              | -                    |
|                    | Pavement age since construction, yr   | +                    |
|                    | Average annual precipitation, mm  | +                    |
|                    | Subgrade type, 1=coarse-grained, 0=fine-grained   | -                    |
| CRCP IRI (m/km)    | Cumulative number of 80-kN ESAL applications  | +                    |
|                    | Percentage of steel per area for PCC slab   | -                    |
|                    | Pavement age since construction, yr   | +                    |
|                    | Average annual number of days with temperature above 32 °C                              | +                    |
|                    | DRY (pavements located in climates with average precipitation less than 0.6 m)          | -                    |
|                    | FREEZE (pavements located in climates with average mean temperature less than 12.75 °C) | +                    |
|                    | Modulus of subgrade reaction, kPa/mm  | -                    |

\* Positive indicates that an increase in this variable results in an increase in roughness.

2. Calculate JRCR Roughness (Chapter 7, equation 103).

$$\text{IRI} = 1.272 + 0.00866 * \text{PSTEEL} * \text{KESAL}^{0.4} + 0.00742 * \text{AGE}^{0.7} (5.78 + 0.0106 \text{PRECIP} - 1.95 \text{DRAIN} - 3.73 \text{SUGTYP})$$

where

|        |   |   |
|--------|---|---|
| IRI    | = | International Roughness Index, m/km                       |
| KESAL  | = | cumulative 80-kN equivalent single axle loads, thousands  |
| PSTEEL | = | percent steel, percent                                    |
| AGE    | = | pavement age, yr  |
| PRECIP | = | average annual precipitation, mm                          |
| DRAIN  | = | presence of edge drain, 1 = edge drain 0 = no edge drains |
| SUGTYP | = | subgrade type, 1 = coarse-grained, 0 = fine-grained       |

3. Calculate CRCP Roughness (Chapter 7, equation 104).

The model developed for predicting IRI for CRCP is as follows:

$$\text{IRI} = 1.118 + \text{KESAL}^{0.3} (0.0142 - 9.787 * 10^{-3} \text{PSTEEL}) + \text{AGE}^{0.4} (3.157 * 10^{-3} \text{D32} - 0.054 \text{DRY} + 0.293 \text{FREEZE} - 4.65 * 10^{-4} \text{KVAL} + 0.1203)$$

where

|        |   |   |
|--------|---|---|
| IRI    | = | International Roughness Index, m/km                               |
| KESAL  | = | cumulative 80-kN equivalent single axle loads, thousands          |
| PSTEEL | = | percent steel   |
| AGE    | = | pavement age, yr  |
| D32    | = | annual number of days with temperature below 32 °C                |
| DRY    | = | LTPP climatic zone, 1 = dry climate, 0 = wet climate              |
| FREEZE | = | LTPP climatic zone, 1 = freezing climate, 0 = nonfreezing climate |
| KVAL   | = | modulus of subgrade reaction, kPa/mm                              |

### Suitability of Prediction Models

The models presented in this report have all been checked using both diagnostic statistics and sensitivity analyses. In all cases, the models were found to be in agreement with sound engineering principles and judgment. These models can therefore be used for checking new pavement design. Detailed procedures for using these models and discussions on their limitations are presented in chapters 4 through 7.

### Examples of Application of Performance Models

The assessment of PCC pavement performance and failure is based on critical levels of the common distresses that occur. The distress and roughness prediction equations developed under this study may be used for a variety of applications, including:

- Evaluation of a pavement design obtained through a standard procedure.
- Evaluation of the cost-effectiveness of designs.

The application of these models can be best explained by use of examples. Example 1 uses prediction models to check and evaluate a new pavement design. Example 2 uses prediction models to evaluate the cost-effectiveness of alternative pavement designs.

### Checking the Design of New Pavements with Prediction Models

The inputs to each of the prediction models must be obtained first. If the predicted distress at the end of the initial performance period exceeds some defined critical level, the pavement design will be considered inadequate, and modifications to certain design inputs may be appropriate. Table 29 provides suggested critical distress levels. An example of using the models for checking concrete pavement design is as follows:

#### Example 1

##### *Pavement Design Features*

|                                 |   |  |
|---------------------------------|---|--|
| Pavement type                   | = | JPCP without dowels                              |
| Modulus of subgrade reaction, k | = | 20.4 kPa/mm                                      |
| Joint spacing                   | = | 6.1 m  |
| Standard lane slab width        | = | 3.65 m   |
| Joint sealant type              | = | Silicone joint sealant (modulus = 2,520,000 kPa) |
| Drainage coefficient            | = | 0.7 (poor)                                       |
| PCC elastic modulus             | = | 24,150,000 kPa                                   |
| PCC thickness                   | = | 200 mm   |
| Dowel diameter                  | = | 0 mm (no dowels)                                 |
| Base type                       | = | erodible (untreated aggregate)                   |
| Sealant depth                   | = | 50.8 mm  |

##### *Climatic Variables*

|                                   |   |                              |
|-----------------------------------|---|------------------------------|
| Wet climate, annual precipitation | = | 1.016 m                      |
| Freezing Index, FI                | = | 278 °C days (cold climate)   |
| Annual air freeze-thaw cycles     | = | 70                           |
| Temperature range                 | = | 11 °C                        |
| Annual number of wet days         | = | 50 (precipitation > 12.7 mm) |
| Relative humidity                 | = | 30 percent                   |
| Days with temperature above 32 °C | = | 40                           |

Table 29. Suggested critical values for key performance indicators.

| Performance Indicator | JPCP                 | JRCP                                 |
|-----------------------|----------------------|--------------------------------------|
| Joint faulting        | 3.05 mm              | 6.1 mm                               |
| Transverse cracking   | 40 percent           | 30 deteriorated transverse cracks/km |
| Corner breaks         | 10 percent           | 10 percent                           |
| Joint spalling        | 40 percent of joints | 25 percent of joints                 |
| IRI                   | 2.7 m/km             | 2.7 m/km                             |

*Design Period*

Design age = 20 yr  
 Design ESAL applications = 20 million

*Evaluation of Design*

*Iteration No. 1 - Initial pavement design*

Predicted mean transverse joint faulting = 4.06 mm (high)  
 Predicted mean transverse joint spalling = 41 percent (high)  
 Percentage of slabs with transverse cracking = 43 percent (high)  
 Percentage of slabs with corner breaks = 11 percent (high)  
 Predicted IRI = 2.64 m/km (rough)

The design is not adequate because the levels of all five distresses are above acceptable or too close to the acceptable values to ensure an adequate safety factor. Some design features should be modified to obtain more acceptable levels of distress.

*Iteration No. 2*

The following inputs are used in the next iteration:

Drainage coefficient  $C_d$  = 1.2 (permeable treated base with edge drain)  
 Base type = Nonerodible  
 Dowel diameter = 25.4 mm  
 Depth of sealant = 12.7 mm  
 Elastic modulus of PCC = 31,000,000 kPa  
 PCC thickness = 300 mm

The revised design results in the following projected distress levels after 20 yr and with 20 million ESAL applications:



|                                |   |              |
|--------------------------------|---|--------------|
| Predicted faulting             | = | 0.42 mm      |
| Predicted spalling             | = | 31 percent   |
| Slabs with transverse cracking | = | 28.5 percent |
| Slabs with corner breaks       | = | 1.8 percent  |
| Predicted IRI                  | = | 2.56 mm/km   |

### *Summary*

The distress levels are reduced considerably in all cases (refer to iteration 1) and, based on the results of this final iteration, the revised design is reasonable. The acceptability of the distress levels is based on the values in table 17, which presents recommendations for critical levels of pavement distress at which some form of rehabilitation is required. The critical distress levels are subjective and depend on an agency's performance standards or the local experience of the design and maintenance engineer. The evaluation of this design illustrates the use of distress and roughness equations and shows that distress and roughness models are very important tools in pavement design and evaluation.

### **Comparing Cost-Effectiveness of Alternative Designs**

Good management of pavements can provide several benefits for highway agencies at both the network and project levels. Foremost among these benefits is the selection of cost-effective design alternatives. Whether new construction, rehabilitation, or maintenance is concerned, an evaluation of cost-effectiveness can help management achieve the best possible performance value for the public dollar.

At the project level, detailed consideration is given to alternative designs, construction, maintenance, or rehabilitation activities for a particular roadway section or project within the overall program. By comparing the costs and benefits among alternative designs, an optimum strategy is identified that will provide the desired benefits and service levels at the least total cost over the analysis period. Figure 80 presents a flow chart of a procedure for selecting alternative designs based on performance models. The process is further explained with the following example.

#### Example 2

##### *Design Features for Design Alternative 1*

|                                       |   |                         |
|---------------------------------------|---|-------------------------|
| Pavement type                         | = | JPCP                    |
| Modulus of subgrade reaction, k-value | = | 54.33 kPa/mm            |
| Joint spacing                         | = | 4.6 m                   |
| Joint sealant type                    | = | preformed joint sealant |
| Depth of sealant                      | = | 50.8 mm                 |
| Drainage coefficient                  | = | 1.1                     |
| PCC elastic modulus                   | = | 31,000,000 kPa          |
| PCC thickness                         | = | 300 mm                  |
| Base type                             | = | nonerodible             |
| Dowel diameter                        | = | 25.4 mm                 |

*Climatic Variables for Design Alternative 1*

|  |   |             |
|--|---|-------------|
| Annual precipitation                               | = | 1.1 m       |
| Annual number of wet days                          | = | 50          |
| Freezing Index                                     | = | 555 °C days |
| Annual number of air freeze-thaw cycles            | = | 75          |
| Annual number of days with temperature above 32 °C | = | 45          |
| Climate  | = | freeze      |
| Relative humidity                                  | = | 40 percent  |

*Design Features for Design Alternative 2*

|                      |   |                        |
|----------------------|---|------------------------|
| Pavement type        | = | JPCP                   |
| Granular base, k     | = | 20.4 kPa/mm            |
| Joint spacing        | = | 9.15 m                 |
| Joint sealant type   | = | silicone joint sealant |
| Drainage coefficient | = | 0.7                    |
| PCC elastic modulus  | = | 24,150,000 kPa         |
| PCC thickness        | = | 200 mm                 |
| Base type            | = | erodible               |
| Dowel diameter       | = | 0 mm                   |

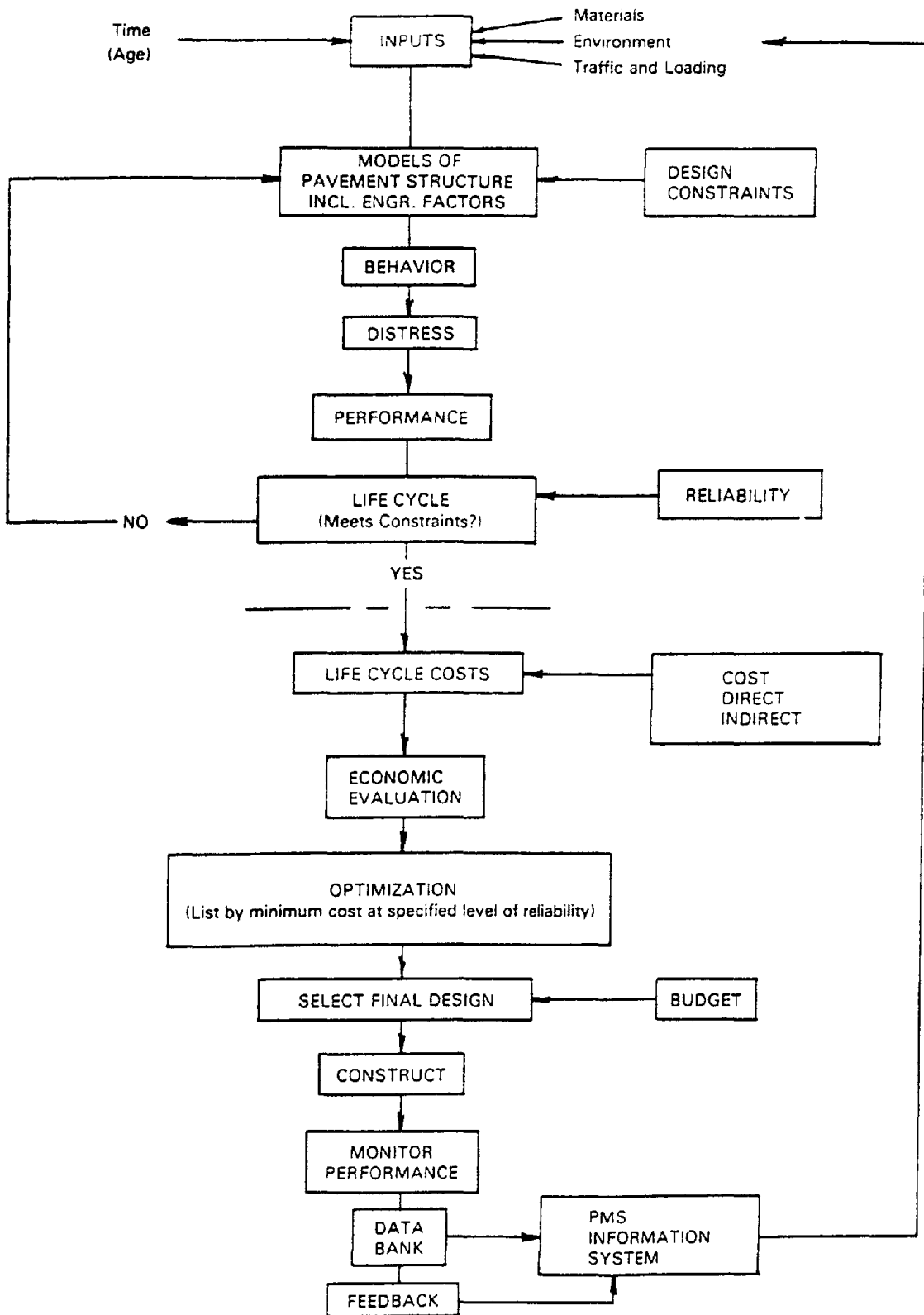


Figure 80. Schematic diagram of pavement design practice with emphasis on cost-effectiveness.<sup>(33)</sup>

### *Climatic Variables for Design Alternative 2*

All the climate variables remain the same as those for alternative 1.

### *Performance Criteria*

|                     |   |  |
|---------------------|---|--|
| Performance period  | = | determined based on critical distress values in table 28 |
| Maximum IRI         | = | 2.7 m/km   |
| Maximum faulting    | = | 3.05 mm  |
| Maximum spalling    | = | 40 percent of joints with low, medium, and high severity |
| Transverse cracking | = | 40 percent   |
| Corner breaks       | = | 10 percent   |

A comparison of the two design alternatives is given in table 29. The percent cost and life are calculated as follows:

$$\text{Percent Cost} = 100 * \frac{\text{Cost of Alternative 1}}{\text{Cost of Alternative 2}} - 1 \quad (105)$$

$$\text{Percent Life} = 100 * \frac{\text{ESAL 's 1}}{\text{ESAL 's 2}} - 1 \quad (106)$$

If the percent increase in life is greater than the percent increase in cost, then Alternative 1 is more cost-effective. However, if the percent increase in life is less than the percent increase in cost, then this design alternative is not more cost-effective. It is obvious from the analysis presented in table 30 that Alternative 1 is more cost-effective. Performance equations are used in this manner by design engineers to evaluate different pavement design alternatives and strategies.

### **Summary**

This chapter has presented two different ways performance models are used. The models were used in the evaluation of pavements designed using standard design procedures and in selecting between alternative pavement designs. These are just a couple of the wide variety of ways in which performance models can be used. However, these models must be used with care and should not extend beyond the inference space for which they were developed.

Table 30. Comparison of cost-effectiveness of two alternate pavement designs.

|   | Alternate Design 1 | Alternate Design 2 |
|---|--------------------|--------------------|
| Faulting (ESAL's/millions to reach critical)            | 30 +               | 8                  |
| Spalling (ESAL's/millions to reach critical)            | 28.5               | 21                 |
| Transverse cracking (ESAL's/millions to reach critical) | 28                 | 16                 |
| Corner breaks (ESAL's/millions to reach critical)       | 30 +               | 6                  |
| IRI (ESAL's/millions to reach critical)                 | 23                 | 20.5               |
| Cost of design  | \$2.0 million      | \$1.6 million      |
| Lifespan of design (ESAL's)                             | 20*10 <sup>6</sup> | 7*10 <sup>6</sup>  |
| Percent cost  | 124 percent        |                    |
| Percent life  | 380 percent        |                    |
| More cost-effective design                              | ✓                  |                    |



## 9. CONCLUSIONS AND RECOMMENDATIONS

### Conclusions

Models that are used to predict the occurrence and amount of distress and roughness are important tools in pavement engineering. They can be used to check the adequacy of new designs or to predict the distress of existing pavements for use in pavement management systems. Prediction models also provide information on the design features and practices that influence the long-term performance of pavements.

A major objective of this study was to use the LTPP database to develop improved prediction models for PCC pavements. An important goal was to use innovative analytical techniques and mechanistic principles to develop state-of-the-art prediction models that are practical for application by State highway agencies.

This report presents several mechanistic-empirical and empirical models that have been developed for predicting the following key types of distress and roughness of PCC pavements:

- Transverse joint faulting.
- Transverse joint spalling.
- Transverse cracking and corner breaks.
- Roughness.

The models for transverse joint faulting, transverse spalling, transverse cracking, and corner breaks are based on mechanistic clusters derived from mechanistic analysis. For each distress type, this required the identification of a primary mechanistic response parameter that could be related to the damage accumulation in the pavement that leads to distress. Using a combination of pavement analysis techniques, this was successfully accomplished, and several mechanistic clusters were developed for the key distress types. Distress model forms including the mechanistic clusters were then calibrated with LTPP data to obtain the models presented. Because of this approach, the models obtained take into consideration many of the significant factors that have an influence on pavement performance.

Each of the models was evaluated and verified using statistical techniques and by performing comprehensive sensitivity analyses. This was to ensure the ability of each model to predict distress within reasonable accuracy and within the limits of the LTPP database. The sensitivity analyses also confirmed that the pavement distress models are in agreement with sound engineering principles and judgment. The roughness models developed in this study were also checked in a similar manner. As an illustration, examples of the application of the models are presented in chapter 8 of this report. Recommendations on the design and construction of PCC pavements developed using the models presented in chapters 4 through 7 are presented in volume I of this report.

### Recommendations

The main products developed in this study are the improved mechanistic-empirical and empirical models for predicting PCC pavement distress and roughness. Extensive checks of the models

indicate that they provide reasonably accurate results and can be used in pavement design and management. The innovative techniques used also provide evidence that mechanistic principles can be applied successfully to develop mechanistic-based models that provide more accurate predictions. This report presents an example that future analysts can follow to improve on the results obtained. Examination of the models provides several insights and recommendations that are immediately useful to State highway agencies for improving the long-term performance of PCC pavement. As indicated previously, recommendations that include specific information on the design features and practices for the design and construction of long-lived PCC pavements are presented in volume I. Tables 18 through 25 in the present volume provide a summary of the effects of significant pavement design and climatic variables on the distress types and roughness, based on the models developed. The tables present useful information for designers and analysts on the design and construction of PCC pavements.

Tables 31 through 38 confirm the importance of the interacting effect of climate, traffic, and pavement design features on pavement performance. In most instances, the climate cannot be controlled and traffic can only be controlled to a certain extent; therefore, designers need to pay attention to those design features that affect the occurrence and progression of distress. The most practical way to minimize the onset and severity of distress is to take these effects into account during the design process.

### **Recommendations for Future Research**

The results presented in this report are based on a comprehensive analysis of the LTPP data and the use of innovative analytical techniques to develop improved models for predicting key PCC distress and roughness. To a large extent, the attempt to use mechanistic principles to develop mechanistic-empirical models was successful. However, because of a variety of limitations, a number of improvements are warranted in future efforts. Future research is necessary to address some of the limitations that were faced in this effort. For example, the traffic loading data used in this research were historical ESAL estimates. For most of the pavements in the LTPP database, ESAL data were not available for several years. Therefore, projections were necessary to obtain the cumulative and yearly ESAL's used in the analysis. Improved traffic loading data that include load spectra data for investigating the effect of different load levels, type, and configuration on distresses will greatly improve the accuracy of the models presented.<sup>(12)</sup>

The lack of pavement-specific environmental data (e.g., thermal gradients in the PCC slab) made it difficult to estimate accurately the effect of environmental stresses within the scope of this study. Environmental data from the LTPP Seasonal Monitoring Program (SMP) should be obtained in future studies for the development of models that can be used to estimate such data.

Finally, the techniques applied in this study provided an opportunity for application of mechanistic principles to the development of prediction models for pavement distress. However, in several cases, because of the current scope of the project and limitations in the data available (in particular, traffic loading and materials data), an in-depth application of mechanistic principles was not possible. These innovative analytical techniques should be explored further in future research to improve on the models.



Table 31. Effect of key pavement design features and site condition factors on transverse joint faulting.

| Key Design Feature or Site Condition Factor           | Effect on JPCP Joint Faulting   |
|---|---|
| Traffic loading                                       | Significantly increases the progression of faulting.  |
| Load transfer or dowels                               | Dowels of at least 25.4 mm diameter reduce faulting by at least half. The larger the dowel diameter, the more the reduction in faulting. Thus, dowel diameter can be determined for a given pavement design.  |
| PCC slab thickness                                    | Thicker PCC slabs reduce the progression of faulting.   |
| Base type   | A nonerodible base (e.g., lean concrete) appreciably decreases faulting in comparison to erodible bases, such as untreated materials. There is a strong interaction between the base type and the drainage coefficient. Coarse, permeable, and nonerodible bases increase the drainage coefficient of the pavement and reduce faulting. |
| Modulus of subgrade reaction, k-value                 | A stiffer support reduces faulting, but not as effectively as a nonerodible base placed on the subgrade.  |
| Joint spacing   | Pavements with shorter slabs fault less than those with longer joint spacing.   |
| Drainage coefficient, $C_d$                           | Increasing the drainage coefficient by improving drainage reduces the propensity of the pavement to be saturated for long periods. This results in reduced faulting.  |
| Number of wet days (i.e., frequency of precipitation) | A high frequency of precipitation will result in more faulting.   |

Table 32. Effect of key pavement design features and site condition factors on transverse joint spalling.

| Key Design Feature or Site Condition Factor      | Effect on JPCP Joint Spalling  |
|--|--|
| Traffic loading/age                              | Both traffic loading and aging increase spalling of JPCP.  |
| Climatic conditions during construction          | The relative humidity and temperature range during construction influence spalling. A high relative humidity, probably caused by improving the curing process and reducing the formation of early microcracks, reduces spalling in later years. On the other hand, a high daily temperature range, probably caused by an increase in restrained temperature stresses, increases microcrack formation and spalling. |
| Annual freeze-thaw cycles                        | Pavements located in areas with a high number of freeze-thaw cycles will experience more spalling.   |
| Average daily temperature range                  | The higher the average daily temperature range during the life of a pavement, the higher the chance of spalling.   |
| Joint sealant characteristics                    | In general, pavements with sealants experience less spalling than those without. Among the different sealants, preformed sealants perform best in terms of reduction in joint spalling. Stiffer sealants cause more spalling.  |
| PCC slab thickness                               | Pavements with thicker PCC slabs experience less spalling in general.  |
| PCC slab elastic modulus and material properties | Stiffer PCC slabs (i.e., higher elastic modulus) experience less spalling. Material properties that cause less horizontal expansion or elongation of the PCC slab will also reduce spalling.   |
| Modulus of subgrade reaction                     | Pavements with higher subgrade and, therefore, better support experience less spalling.  |

Table 33. Effect of key pavement design features and site condition factors on JRCP transverse joint spalling.

| Key Design Feature or Site Condition Factor      | Effect on JRCP Joint Spalling   |
|--|---|
| Traffic loading/age                              | Traffic loading and aging both increase spalling of JRCP.   |
| Freezing index                                   | A higher freezing index will cause more spalling in JRCP.   |
| Annual freeze-thaw cycles                        | Pavements located in areas with a high number of freeze-thaw cycles will experience more spalling.  |
| Joint sealant characteristics                    | In general, JRCP pavements with sealants will experience less spalling than those without. Among the different sealants, silicone and asphalt sealant perform best in terms of reduction in joint spalling. Stiffer sealants cause more spalling. |
| PCC slab thickness                               | Pavements with thicker PCC slabs experience less spalling in general.   |
| PCC slab elastic modulus and material properties | For JRCP, stiffer PCC slabs (i.e., higher elastic modulus) will cause more spalling. Material properties that cause less horizontal expansion or elongation of the PCC slab will reduce spalling.   |
| Modulus of subgrade reaction                     | Pavements with higher subgrade modulus and, therefore, better support will experience less spalling.  |

Table 34. Effect of key pavement design features and site condition factors on JPCP corner breaks

| <b>Key Design Feature or Site Condition Factor</b> | <b>Effect on JPCP Corner Breaks</b>   |
|--|---|
| Traffic loading/age                                | Traffic loading and aging increase the occurrence of corner breaks.   |
| Joint spacing                                      | Longer joint spacing will increase the occurrence of corner breaks. This may be attributable to the higher levels of curling that occur over longer joint spacing and the loss of support at the corner that is associated with it. |
| PCC slab thickness                                 | Thicker slabs will experience less corner breaks.   |
| PCC elastic modulus                                | Stiffer PCC slabs will experience less corner breaks.   |
| Number of freeze-thaw cycles                       | More freeze-thaw cycles will increase corner breaking.  |
| Drainage coefficient                               | A higher drainage coefficient will reduce the occurrence of corner breaks.  |

Table 35. Effect of key pavement design features and site condition factors on JPCP transverse cracking.

| Key Design Feature or Site Condition Factor | Effect on JPCP Transverse Cracking  |
|---|---|
| Traffic loading/age                         | Traffic loading and aging will increase transverse cracking of JPCP.                                    |
| PCC slab thickness                          | JPCP with thicker PCC slabs will experience less transverse cracking.                                   |
| PCC slab elastic modulus                    | A stiffer PCC slab will reduce the occurrence of transverse cracking.                                   |
| Number of freeze-thaw cycles                | More freeze-thaw cycles will increase the occurrence of transverse cracks.                              |
| Frequency of precipitation                  | A higher frequency of precipitation will increase the occurrence of transverse cracks.                  |
| Number of days temperature exceeds 32 °C    | A higher number of days during which the temperature exceeds 32 °C will cause more transverse cracking. |

Table 36. Effect of key pavement design features and site condition factors on JPCP roughness.

| <b>Key Design Feature or Site Condition Factor</b> | <b>Effect on JPCP Roughness</b>  |
|--|--|
| Traffic loading/age                                | Both traffic loading and aging will increase roughness.  |
| Climatic conditions                                | Harsher climatic conditions, probably because of the higher levels of distress associated with them, increase roughness. Specifically, a higher frequency of precipitation and the location of a pavement in a freezing climate (i.e., higher freezing index) will cause more roughness. |
| PCC slab elastic modulus                           | Pavements with higher PCC elastic moduli seem to get rougher with time.  |
| Dowel diameter                                     | Use of dowels in JPCP pavements reduces roughness. Increasing the dowel diameter, probably by reducing joint distress such as faulting, further reduces the roughness.   |
| Subgrade type                                      | Coarse-grained subgrade types will cause less roughness.   |

Table 37. Effect of key pavement design features and site condition factors on JRCP roughness.

| <b>Key Design Feature or Site Condition Factor</b> | <b>Effect on JRCP Roughness</b>  |
|--|--|
| Traffic loading/age                                | Traffic loading and aging increase the roughness of all pavements.                               |
| Steel content                                      | JRCP with a higher steel content exhibited more roughness.                                       |
| Precipitation                                      | JRCP pavements that experience more rainfall will get rougher with time.                         |
| Drainage   | An edge drain will reduce the progression of roughness on a JRCP by promoting positive drainage. |
| Subgrade type                                      | Coarse-grained subgrades will cause less roughness of JRCP.                                      |

Table 38. Effect of key pavement design features and site condition factors on CRCP roughness.

| <b>Key Design Feature or Site Condition Factor</b> | <b>Effect on CRCP Roughness</b>  |
|--|--|
| Traffic loading/age                                | Traffic loading and aging increase the roughness of all pavements.   |
| Steel content                                      | A higher steel content in CRCP will reduce roughness.  |
| Climatic conditions                                | A freezing climate will cause more roughness. Pavements located in drier climates will experience less roughness, but a large number of days during which the maximum temperature exceeds 32 °C will increase roughness. |
| Modulus of subgrade reaction                       | CRCP pavement with better support (i.e., higher modulus of subgrade reaction) will experience less roughness.  |





## APPENDIX A. CALIBRATION OF PREDICTION MODELS

This appendix provides information on the process that was used to calibrate the prediction models presented in this study. The process is the culmination of the research team's many years of experience. It involves application of modern statistical techniques, combined with a large dose of engineering theory, to obtain models for predicting the distress and performance of pavements. Figure 81 is a flow chart that provides an overview of the process, which can be divided into the following:

- Data preparation and selection of independent variables.
- Tentative model development and verification.
- Model evaluation, verification, and validation.

### **Data Preparation and Selection of Independent Variables**

An important part of the process for calibrating or developing regression models is the collection and preparation of the data needed and selection of the independent variables that should be considered. The following are the steps taken to accomplish this:

#### Literature Review

A comprehensive literature search and review is required to determine the most appropriate variables, clusters, and mechanistic equations that could be used to develop the model. In model development efforts that use observational data, the information from past studies and the experience of the researcher are necessary for selecting the independent variables that should be considered. For studies with observational data, this step is more important than is often recognized. Theory can often provide guidance on the variables that should be selected, as well as the model form that will provide good models. Accordingly, in this study, considerable effort was spent to review past studies.

#### Identify and Define Potential Variables and Clusters

This is an important follow-up to the literature review process. The goal is to identify which variables are relevant to the model and need to be included in the final analysis data set. Not all the variables identified in the literature search may be relevant; however, it provides a starting point for identifying potential variables and clusters to look at more closely.

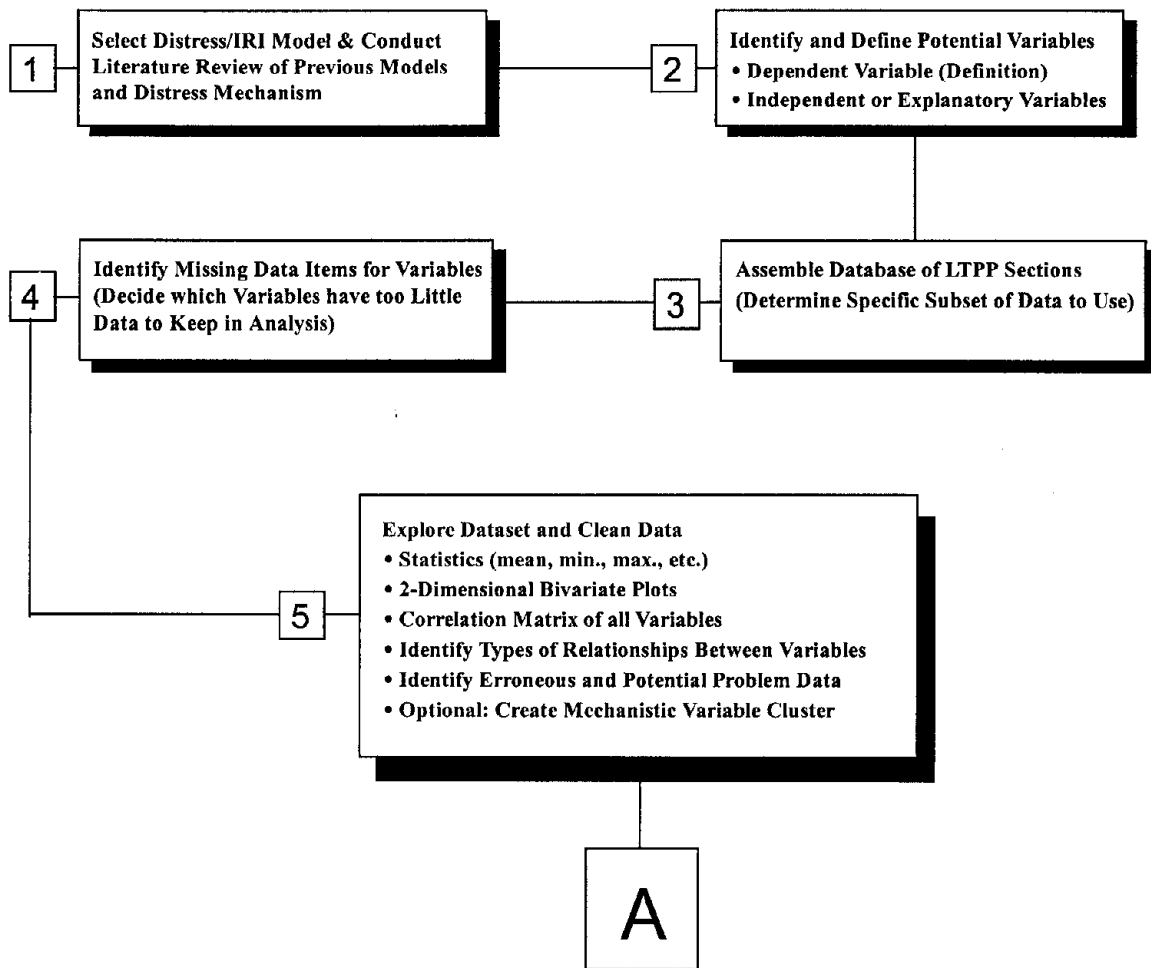


Figure 81. Flow chart for developing distress models.

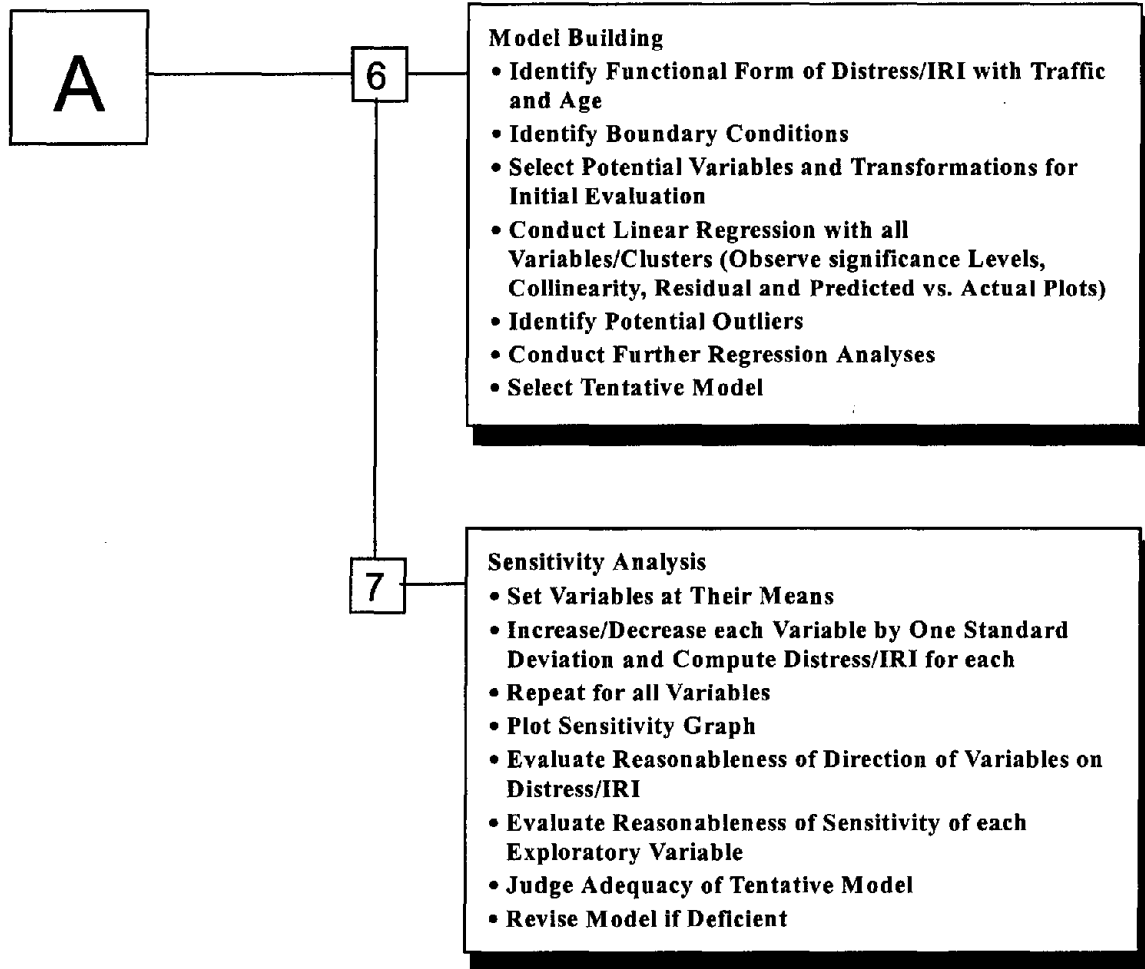


Figure 81. Flow chart for developing distress models (continued).

## Assemble Analysis Database

This involves assembly of the data set to be used for model development on the basis of the information on potential variables and clusters obtained from literature review and preliminary statistical analysis. In this study, the LTPP database was the source of data used for developing all models.

## Explore Data Set and Clean Data

A thorough evaluation of the analysis data set is always necessary to identify any missing data elements and possible problem spots in the database. Attempts should be made to obtain replacements for missing data where possible. The analysis data set should also be checked closely for anomalies and gross data error. Data determined to be outliers were cleaned out of the data set used in the analysis.

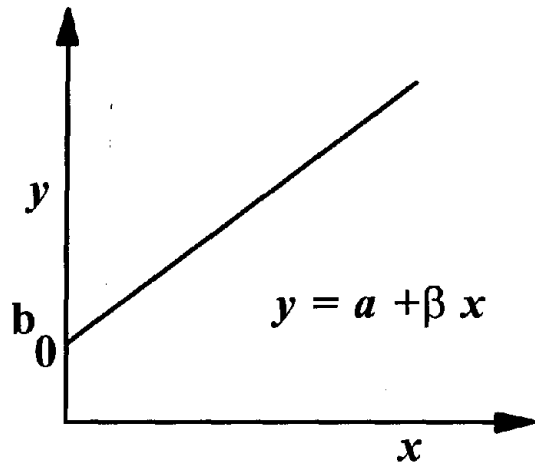
Basic univariate analyses are required to provide information on the distribution of each variable being considered, as well as the dependent variable. Bivariate analyses should be conducted to identify relationships between independent variables and between the independent variables and the dependent variable. Exploration of the data set will also provide insights into possible model forms. Univariate and bivariate analyses are also good methods for determining whether the data include outliers, errors, potential problem sources, and the possibility of creating interactions and mechanistic clusters. These analyses should provide useful information for further reducing the number of independent variables to subsets that contain only those that are known to be essential to the model.

## **Model Development and Verification**

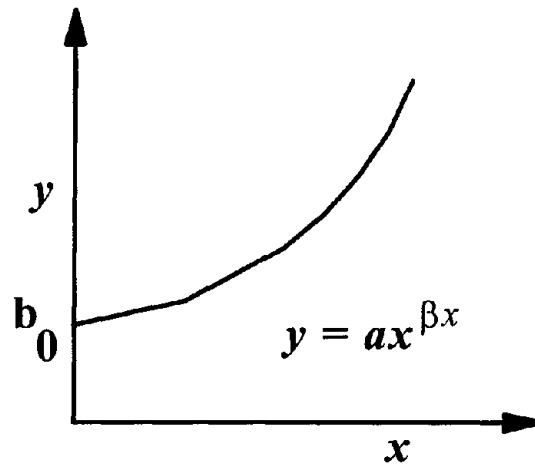
### Development of Tentative Model

The first step in model building is the identification of suitable mathematical model forms for evaluation. For pavements, deterioration or distress progression varies for different pavement types and distresses. Figure 82 shows common mathematical models that have been used successfully to develop models for the progression of pavement distress.

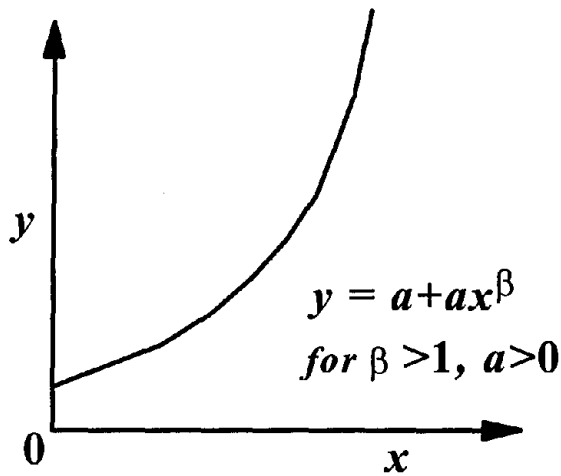
Selecting the most suitable model form is the key to developing a sound and stable model. Most statistical packages available provide the capability of using multiple regression analyses to identify the model forms that fit the data well. The procedures are also very useful for narrowing down the variables that should be included in the final models. However, for observational data (such as pavement performance data), it is very important to conduct such analyses with care to ensure that essential independent variables are not eliminated.



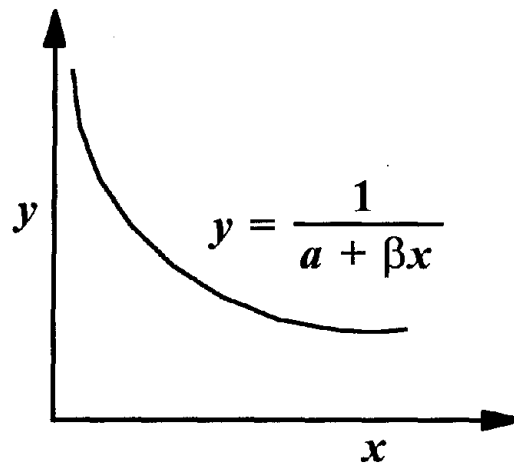
(a) Linear



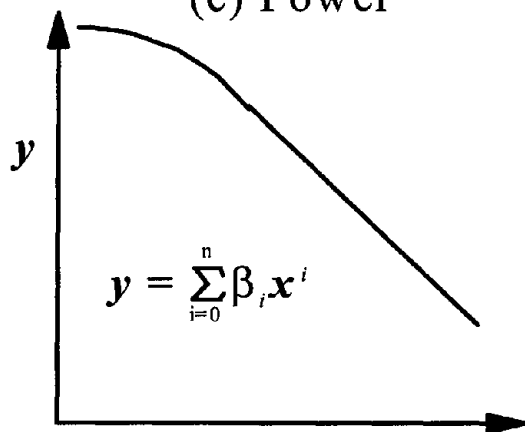
(b) Exponential



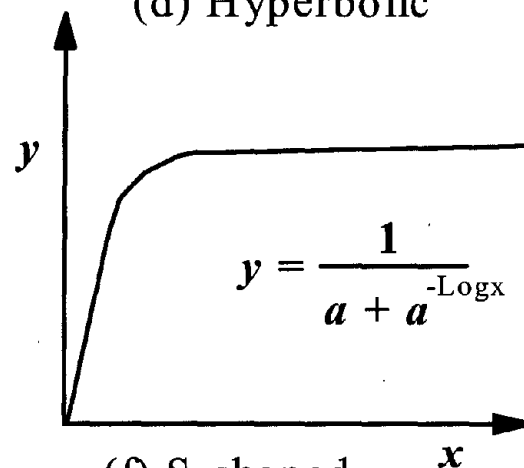
(c) Power



(d) Hyperbolic



(e) Polynomial  $x$



(f) S-shaped  $x$

Figure 82. Typical functional forms used for pavement distress modeling.

Standard mathematical model forms, such as linear, quadratic, log-transformed, and other nonlinear model forms, can be used to fit the independent data to the dependent variable once the final list of variables has been selected. Model forms that work well for pavement distresses are given in Figure 82. The following are the mathematical equations that describe these model forms:

Linear Model (figure 82(a))

$$y = a_0 + a_1X_1 + a_2X_2 + \dots + a_nX_n$$

Exponential Model (figure 82(b))

$$y = a_0 + a_1^{\beta x}$$

Power Model (figure 82(c))

$$y = a_0 + a_1X^\beta$$

Hyperbolic Model (figure 82(d))

$$y = \frac{1}{a_0 + a_1X}$$

Polynomial Model (figure 82(e))

$$y = \sum_{i=0}^n a_i X^i$$

S-Shaped Model (figure 82(f))

$$y = \frac{1}{a_0 + a_1 C_1^{-\text{Log}X_1}}$$

The advantage of the linear regression model is its simplicity in development and use, as well as its relative insensitivity to the “noise” in the database. The main drawback is that the deterioration of pavements and the progression of distresses exhibit a more complex relationship with other independent pavement properties or parameters. The polynomial functional form permits the most flexibility in modeling; however, polynomial regression does not guarantee that the resulting model will decrease or increase in the entire interval of the inference space, as could be required by engineering judgment.

The diagnostic statistics listed in table 39, which are part of the output for multiple regression, must be analyzed to establish the suitability and stability of the model under consideration. The critical values of the diagnostic statistics are also given in table 39 and are explained in greater detail in the subsequent section.

#### Coefficient of Determination ( $R^2$ )

The coefficient of determination is an indication of how much variation is explained by the model. It is defined as follows:

$$R^2 = 1 - SSE/TSS \quad (107)$$

where

$R^2$  = coefficient of determination  
 SSE = sum of squares for error  
 TSS = corrected sum of squares error

A good model that fits the data should have the maximum possible coefficient of determination.

#### Variance Inflation Factor

Variance inflation factors measure the strength of interrelationships among regressor or independent variables in the model. If all variables are independent of each other, the variance inflation factor is equal to 1.0. If a variable is closely related to other variables, its tolerance goes to zero as the variance inflation factor gets very large. Tolerance (TOL) and variance inflation factor (VIF) are defined as follows:

$$TOL = 1 - R^2 \quad (108)$$

where

$R^2$  = coefficient of determination

$$VIF = 1/TOL \quad (109)$$

Table 39. Diagnostic statistics and corresponding critical values.

| Diagnostic Statistic                           | Diagnostic Objective                             | Critical Values  |
|--|--|--|
| Coefficient of determination (R <sup>2</sup> ) | Goodness of fit                                  | Maximize   |
| Variance inflation factor (VIF)                | Multicollinearity                                | < 10   |
| Durbin-Watson test statistic (d)               | Serial correlation and independence of variables | 1.5 < d < 2.5  |
| Mallow's C <sub>p</sub>                        | Optimum number of independent variables          | Approximately equal to number of independent variables |
| Mean square error (MSE)                        | Goodness of fit                                  | Minimize   |
| Press statistic (Press <sub>p</sub> )          | Ability to predict outside of current data set   | Minimize   |
| Test of significance (Prob>F-statistic)        | Significance of parameter estimate               | < 0.05   |

For model development, the effect of correlations between independent variables or multicollinearity should be minimized to obtain a model that will be adequate and robust for different databases. A tolerance level of 0.1 or a maximum VIF value of 10 should ensure this.

#### Durbin-Watson Test Statistic (d)

The Durbin-Watson test statistic (d) is a measure of the independence of errors in time-series data used in the model. As noted in earlier sections of this report, one of the key assumptions made in model development is the independence of the variables. With most data, especially time-series data, the errors are autocorrelated, that is, e<sub>i</sub> is correlated with e<sub>i-1</sub> just before it. Autocorrelation is a symptom of systematic lack of fit. The Durbin-Watson test statistic is defined as follows:

$$d = \frac{\sum_{i=2}^n (e_i - e_{i-1})}{\sum_{i=2}^n e_i^2} \quad (108)$$

where

e<sub>i</sub> = error (y<sub>measured</sub> - y<sub>predicted</sub>) for data i

The value of d is close to 2.0 if the errors are uncorrelated. A value of d ranging from 1.5 to 2.5 is reasonable for most models.



## Mallow's $C_p$

To choose a model that provides the best prediction using the sample estimates, there is the need to guard against the use of more independent variables than can be reliably used with the given sample size.  $C_p$  is a criterion for selecting the optimum number of independent variables in a model.  $C_p$  is defined as:

$$C_p = \frac{SSE_p}{s^2} - (N - 2p) \quad (111)$$

where

- $SSE_p$  = sum of squares error for a model with  $p$  number of independent variables
- $s$  = mean square error for the full model
- $N$  = total number of independent variables in the full model
- $p$  = number of parameters in a given model, including the intercept

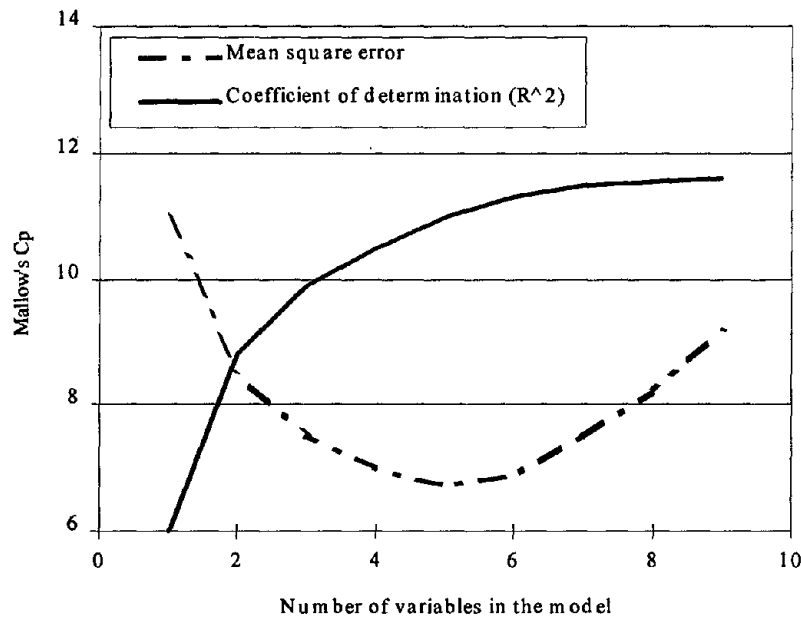


Figure 83. Variation in  $C_p$  with MSE and  $R^2$ .

Mallow suggests that the model where  $C_p$  first approaches  $p$  is the optimum model with parameter estimates unbiased. Figure 83 shows the variation of  $C_p$  with the mean square error (MSE) and the coefficient of determination ( $R^2$ ) of a model.

### Mean Square Error and Test for Significance

The mean square error is an estimate of the absolute difference between the actual and predicted dependent variable. It is calculated as follows:

$$\text{MSE} = \text{SSE}/(n - p) \quad (112)$$

where

SSE = sum of squares error  
n = number of data points in database  
p = number of variables in the model

MSE should be minimized for all models. The test of significance or p-values do not necessarily measure the importance of a variable. They do, however, give an indication of the contribution the variable makes to predicting the dependent variable. This test statistic is used to eliminate variables that contribute little to the model. A significance level of less than 5 percent is satisfactory.

### PRESS<sub>p</sub> Statistic

The predicted residual for observation  $j$  is defined as the residual for the  $k$ th observation that results from dropping the  $j$ th observation from the parameter estimates. The sum of squares of the predicted residual errors is called the PRESS<sub>p</sub> statistic. The PRESS<sub>p</sub> statistic gives an indication of the ability of the model to be used outside the database that was used in model development. PRESS<sub>p</sub> should be minimized.

### Model Evaluation and Verification

Each model was verified to check its predictive accuracy and whether it made engineering sense. Model validation is the process of checking the ability of the model to predict distress when used with independent data. Attempts were made to validate the models with independent data, but this was not possible. However, a variety of statistical approaches were used to evaluate the predictive capability of the models, including the following:

- Sensitivity analyses.
- Statistical diagnostic tests.

The sensitivity analyses involved using the model to evaluate the effect of various inputs on the predicted distress and comparing the results with empirical and theoretical observations. It involved setting all other variables at their means and varying the inputs of interest. Plots of the results obtained were evaluated to check the engineering plausibility of the models and whether

the models provided predictions that made sense. The tentative model was selected on the basis of the results of this process and the acceptable diagnostic statistic results.



## REFERENCES

1. Rowshan, S. and S. Harris. *Long Term Pavement Performance Information Management System*. Report No. FHWA-RD-93-094. Federal Highway Administration, Washington, DC, July 1993.
2. Crovetti, J.A. *Evaluation of Jointed Concrete Pavement Systems Incorporating Open-Graded Permeable Bases*. Ph.D. dissertation. University of Illinois at Urbana-Champaign, 1994.
3. Owusu-Antwi, E.B. and M.I. Darter. "Early Results of the LTPP Concrete Pavement Data Analysis." Third International Workshop on the Design and Evaluation of Concrete Roads, Vienna, Austria, 1994.
4. Simpson, A.L., J.B. Rauhut, P.R. Jordahl, E.B. Owusu-Antwi, M.I. Darter, and R. Ahmad. *Early Analysis of LTPP General Pavement Studies Data, Volume 3: Sensitivity Analyses for Selected Pavement Distresses*. Report No. SHRP-P-393. Strategic Highway Research Program, Washington, DC, 1994.
5. Federal Highway Administration. *Program Reference Guide—Version 1.0*. Federal Highway Administration, LTPP Division, Washington, DC, March 1996.
6. Federal Highway Administration. *Data Collection Guide for Long-Term Pavement Performance Studies*. Operational Guide No. SHRP-LTPP-OG-001. Strategic Highway Research Program, Washington, DC, January 1990 (Revised October 1993, FHWA-LTPP Division).
7. Strategic Highway Research Program. *SHRP Database Structure Reference Manual*. Washington, DC, April 1992.
8. Darter M.I., J.M. Beck, M.B. Snyder, and R.E. Smith, *Portland Cement Concrete Pavement Evaluation System-COPES*. National Cooperative Highway Research Program Report No. 277. Transportation Research Board, Washington, DC, 1985.
9. Smith, K.D., D.G. Peshkin, M.I. Darter, and A.L. Mueller, *Performance of Jointed Concrete Pavements, Volume III: Summary of Research Findings*. Report No. FHWA-RD-89-138. Federal Highway Administration, Washington, DC, November 1990.
10. Yu, H.T., M.I. Darter, K.D. Smith, J. Jiang, and L. Khazanovich. *Performance of Concrete Pavements, Volume III - Improving Concrete Pavement Performance*, Final Report. Contract No. DTFH61-91-C-00053. Federal Highway Administration, McLean, VA, 1996.
11. Wilde, W.J., D.G. Zollinger, E.D. Moody, R.O. Rasmussen, and D.K. Rozycki. *Long Term Pavement Performance Data Analysis: Model Development for Prediction of Distress and Roughness in PCC Pavements*, Draft Final Report. Contract No. DTFH61-94-C-00208. Federal Highway Administration, McLean, VA, 1996.

12. Owusu-Antwi, E.B., L. Titus-Glover, L. Khazanovich, and J.R. Roesler. *Development and Calibration of Mechanistic-Empirical Distress Models for Cost Allocation*. Preliminary Draft Final Report. Federal Highway Administration, Washington, DC, March 1997.
13. Permanent International Association of Road Congresses. *Combating Concrete Pavement Slab Pumping by Interface Drainage and Use of Low-Erodibility Materials: State of the Art and Recommendations*, Paris, France, 1987.
14. Christory, J.P. "Assessment of PIARC Recommendations on the Combatting of Pumping in Concrete Pavements." Sixth International Symposium on Concrete Roads. Madrid, Spain, 1990.
15. Highway Research Board. *Research Reports No. 1D, Special Papers on the Pumping Action of Concrete Pavements*, 1945.
16. Highway Research Board. *Research Reports No. 1D, Special Papers on the Pumping Action of Concrete Pavements, Supplement*, 1946.
17. Highway Research Board. *Current Road Problems No. 4R, Maintenance Methods for Preventing and Correcting the Pumping Action of Concrete Pavement Slabs*, 1947.
18. Highway Research Board. *Research Reports No. 1D, A Survey of Pumping in Illinois*, 1948.
19. Highway Research Board. *The AASHO Road Test—Report 5, Pavement Research*. Special Report 61E. Highway Research Board, Washington, DC, 1962.
20. Phu, N.C., J.P. Christory, and J. Ray, "The Hydromechanics of Pumping in Concrete Pavements: Modeling and Prevention, Appendix I, Combating Concrete Pavement Pumping: State-of-the-Art and Recommendations," PIARC Technical Committee on Pavements, 1986.
21. Gulden, W. "Experience with Drainage of Jointed Concrete Pavements." Permanent International Association of Road Congresses, International Seminar on Drainage and Erodibility at the Concrete Slab-Subbase-Shoulder Interface, March 1983.
22. Larralde, J. "Structural Analysis of Rigid Pavements With Pumping." Ph.D. dissertation. Purdue University, West Lafayette, IN, 1984.
23. Hansen, E., R. Johannesen, and J.M. Armaghani. "Field Effects of Water Pumping Beneath Concrete Pavement Slabs," ASCE, *Journal of Transportation Engineering*, Vol. 117, No. 6, Nov-Dec 1991.
24. Poblete, M. "Informe Anual 1986," Control y Seguimiento de Pavimentos de Hormigon, IDIEM-Direccion de Vialidad, Universidad de Chile, 1986.

25. Neal, B.F. *Evaluation of Design Changes and Experimental PCC Construction Features*. Report No. FHWA/CA/TL-85/07. Caltrans, Sacramento, CA, 1987.
26. Wu, C.L., J.W. Mack, P.A. Okamoto, and R.G. Packard. "Prediction of Faulting of Joints in Concrete Pavements," *Proceedings, Fifth International Conference on Concrete Pavement Design and Rehabilitation*, Vol. 2., Purdue University, West Lafayette, IN, April 1993.
27. Yao, Z. "Design Theory and Procedure of Concrete Pavements in China," Second International Workshop on the Theoretical Design of Concrete Pavements, Siguenza, Spain, 1990.
28. Yoder, E.J., and M.W. Witczak. *Principles of Pavement Design*. John Wiley & Sons, Inc., New York, NY, 1975.
29. Van Wijk, A.J., J. Larralde, C.W. Lovell, and W.F. Chen. "Pumping Prediction Model for Highway Concrete Pavements," ASCE, *Journal of Transportation Engineering*, Vol. 115, No. 2, 1989, pp. 161-175.
30. Bhatti, M.A., J.A. Barlow, and J.W. Stoner. "Modeling Damage to Rigid Pavements Caused by Subgrade Pumping," ASCE, *Journal of Transportation Engineering*, Vol. 122, No. 1, Jan.-Feb. 1996, pp. 12-21.
31. Westergaard, H.M. "Analysis of Stresses in Concrete Pavements Due to Variations of Temperature," *Proceedings, Sixth Annual Meeting, Highway Research Board*, Washington, DC, 1926.
32. Benekohal, R.F., K.T. Hall, and H.W. Miller "Effects of Lane Widening on Lateral Distribution of Truck Wheels," *Transportation Research Record 1286*, Transportation Research Board, Washington, DC, 1990.
33. American Association of State Highway and Transportation Officials. *AASHTO Guide for Design of Pavement Structures — 1993*. Washington, DC, 1993.
34. Dempsey, B.J., S.H. Carpenter, and M.I. Darter. *Improving Subdrainage and Shoulders of Existing Pavements*, Final Report. Federal Highway Administration, Washington, DC, 1980.
35. Dempsey, B.J. "Laboratory and Field Studies of Channeling and Pumping," Transportation Research Board, *Transportation Research Record 849*, 1982, pp. 1-12.
36. Raad, L. "Pumping Mechanisms of Foundation Soils Under Rigid Pavements," Transportation Research Board, *Transportation Research Record 849*, 1982, pp. 29-37.
37. Raad, L., G.H. Miniassian, and J.L. Hulsey. "Mechanistic Evaluation of Saturated Bases Under Concrete Pavements," ASCE, *Journal of Transportation Engineering*, Vol. 121, No. 6, Nov.-Dec. 1995, pp. 495-501.

38. Van Wijk, A.J. "Rigid Pavement Pumping: (1) Subbase Erosion and (2) Economic Modeling." Ph.D. dissertation. Purdue University, West Lafayette, IN, 1985.
39. Phu, N.C. "Hydraulique du pompage des chaussées en béton et érodabilité des matériaux de couche de fondation et de couche de forme." Ph.D. dissertation. Université Paris VI, LCPC, March 1979.
40. Huang, Y.H. *Pavement Design and Analysis*. Prentice Hall, Englewood Cliffs, NJ, 1993.
41. *Distress Identification Manual for the Long-Term Pavement Performance Project*. Report No. SHRP-P-338. Strategic Highway Research Program/National Research Council, Washington, DC, 1993.
42. McCullough, B.F. and G.E. Elkins. *CRC Pavement Design Manual*, Austin Research Engineers, 1979.
43. Tayabji, S.D. and B.E. Colley. *Improved Rigid Pavement Joints*. Report No. FHWA-RD-86-040. Federal Highway Administration, Washington, DC, 1986.
44. Darter, M.I. and E.J. Barenberg. *Design of Zero-Maintenance Plain Jointed Concrete Pavements, Vol. 1*. Report No. FHWA-RD-77-111. Federal Highway Administration, Washington, DC, January 1993.
45. Guiterriz de Veiasco, M. and B.F. McCullough. *Summary Report for 1978 CRCP Condition Survey in Texas*. Research Report 177-20. Center for Transportation Research, University of Texas, Austin, Texas, 1981.
46. Zollinger, D.G. and E.J. Barenberg. *Continuously Reinforced Pavements: Punchouts and Other Distresses and Implications for Design*. Report No. FHWA/IL/UI/227. Illinois Department of Transportation, Springfield, IL, 1990.
47. Sanadheera, S.P. and D.G. Zollinger. *Influence of Coarse Aggregate in Portland Cement Concrete on Spalling of Concrete Pavements*. Research Report 1244-11. Texas Transportation Institute, College Station, TX, 1995.
48. Hibbit, Karlson, and Sorenson, Inc. *ABAQUS/Standard Example Problems Manual*, 1996.
49. Miner, M.A. "Cumulative Damage in Fatigue," ASME, *Transactions*, Volume 67, 1945.
50. Pell, P.S. "Characterization of Fatigue Behavior." In Special Report 140: *Structural Design of Asphalt Concrete Pavement Systems to Prevent Fatigue Cracking*, Highway Research Board, National Research Council, Washington, DC, 1973.
51. Anderson, T.L. *Fracture Mechanics Fundamentals and Applications*. CRC Press, Inc., Boca Raton, FL, 1991.



52. Roesler, J.R. and L. Khazanovich. "Finite-Element Analysis of Portland Cement Concrete Pavements With Cracks," *Transportation Research Record 1568*, Transportation Research Board, Washington, DC, 1997.
53. Carey, W.N. and P.E. Irick. "The Pavement Serviceability–Performance Concept." *Highway Research Bulletin 250*. Highway Research Board, Washington, DC, 1990.
54. American Association of State Highway and Transportation Officials. *Summary Results of 1987 AASHTO Rideability Survey*. Washington, DC, 1987.
55. Janoff, M.S. *Pavement Smoothness*. Information Series 111. National Asphalt Pavement Association, Lanham, MD, 1991.
56. Al-Omari, B. and M.I. Darter. *Relationships Between IRI and PSR*. Report No. UILU-ENG-92-2013. Illinois Department of Transportation, Springfield, IL, 1992.
57. Smith, K.L., K.D. Smith, L.D. Evans, T.E. Hoerner, and M.I. Darter. *Smoothness Specifications for Pavements*. Final Report. National Cooperative Highway Research Program, Washington, DC, March 1997.
58. Sayers, M.W. and T.D. Gillespie. "The International Road Roughness Experiment: A Basis for Establishing a Standard Scale for Road Roughness Measurements." *Transportation Research Record 1084*. Transportation Research Board, Washington, DC, 1986.
59. Queiroz, C.A.V. and W.R. Hudson. "A Stable, Consistent, and Transferable Roughness Scale for Worldwide Standardization." *Transportation Research Record 997*. Transportation Research Board, Washington, DC, 1984.
60. Sayers, M.W., T.D. Gillespie, and W.D.O. Paterson. *Guidelines for Conducting and Calibrating Road Roughness Measurements*. Technical Paper 46. The World Bank, Washington, DC, 1986.
61. Sayers, M.W., T.D. Gillespie, and C.A.V. Queiroz. *The International Road Roughness Experiment: Establishing Correlation and a Calibration Standard for Measurements*. Technical Paper 45. The World Bank, Washington, DC, 1986.
62. Perera, M. *Long Term Pavement Performance Data Analysis: Study to Investigate the Development of Pavement Roughness*. Draft Final Report. Contract No. DTFH61-95-C-00124. Federal Highway Administration, McLean, VA, 1996.
63. Larson, R.M., S. Vanikar, and S. Forster. *Summary Report—U.S. Tour of European Concrete Highways (U.S. TECH)—Follow-Up Tour of Germany and Austria*, Report No. FHWA-SA-93-080. Federal Highway Administration, Washington, DC, October 1993.
64. Darter, M.I. *Report on the 1992 U.S. Tour of European Concrete Highways*. Report No. FHWA-SA-93-012., Federal Highway Administration, Washington, DC, January 1993.

